This electronic thesis or dissertation has been downloaded from the King's Research Portal at https://kclpure.kcl.ac.uk/portal/

Astrophysical and cosmological consequences of string-inspired models.

Elghozi, Thomas André Claude

Awarding institution:
King's College London

The copyright of this thesis rests with the author and no quotation from it or information derived from it may be published without proper acknowledgement.

END USER LICENCE AGREEMENT

Unless another licence is stated on the immediately following page this work is licensed

under a Creative Commons Attribution-NonCommercial-NoDerivatives 4.0 International

licence. https://creativecommons.org/licenses/by-nc-nd/4.0/

You are free to copy, distribute and transmit the work

Under the following conditions:

- Attribution: You must attribute the work in the manner specified by the author (but not in any way that suggests that they endorse you or your use of the work).
- Non Commercial: You may not use this work for commercial purposes.
- No Derivative Works - You may not alter, transform, or build upon this work.

Any of these conditions can be waived if you receive permission from the author. Your fair dealings and other rights are in no way affected by the above.

Take down policy

If you believe that this document breaches copyright please contact librarypure@kcl.ac.uk providing details, and we will remove access to the work immediately and investigate your claim.

Download date: 20. May. 2021

Astrophysical and cosmological consequences of string-inspired models

King's College London, University of London

Thomas Elghozi

A thesis submitted for the degree of *Doctor of Philosophy*

July 2016

Abstract

The standard model of cosmology, namely the ΛCDM model, is based on Einstein's theory of General Relativity (GR) with a Cold Dark Matter (CDM) content and a positive cosmological constant Λ, in addition to ordinary matter and radiation components. While it provides a paradigm in very good agreement with many observations, from Big Bang Nucleosynthesis (BBN) to Cosmic Microwave Background (CMB), several questions remain open and various theoretical extensions seem necessary in order to address them.

An extensively studied ingredient of the ΛCDM model is the inflationary scenario, which solves some of the issues associated with the initial conditions that the original hot Big Bang model cannot address, such as the homogeneity and flatness problems. Furthermore, it fits very well with current data, in particular, the spectrum of temperature anisotropies in the CMB. As we recall in Chapter 2, in some scenarii, the end of inflation may lead to the formation of Cosmic Strings (CS) or Cosmic SuperStrings (CSS), which can have a significant impact on some observables, even though they have been proven not to be the main source of CMB anisotropies. We focus on a particular phenomenological consequence of C(S)S, Gravitational Waves (GWs), which are becoming an important tool to gather new information on our universe. More specifically, energetic high frequency GW Bursts (GWB) are thought to be emitted by cusps, which are points on C(S)S temporarily reaching the speed of light. We investigate the occurrence of such phenomena in a particular setup where a light string is stretched between two heavy, almost fixed strings, as could appear in a C(S)S network. First, an analytical study allows us to draw simplifying hypotheses, such as the periodicity of the non-interacting movement of the string, and yields an effective rule to identify cuspy strings. In addition, we implement these assumptions in a numerical simulation, which settles the free parameter of this criterion. Also, the string and the network parameters are found to influence strongly the average number of cusps and thus the amount of energy released in the form of GWB. In particular, both the analytical and numerical studies demonstrate that the smaller the correlation length is (that is, the wavier the string

is), the more cusps the string holds.

String/M-theory yields a large variety of scenarii and thus a large phenomenological diversity, from inflation to Dark Matter (DM) candidates. It generally implies additional dimensions and additional ingredients, such as scalar fields (often involved with inflation) or extended objects (such as Cosmic SuperStrings). It can also provide a description of our universe, on which we focus in Chapter 3, in which all fields but the graviton live on a (3+1) brane, itself embedded in a larger-dimensional bulk. We consider a model where the bulk is populated with a gas of punctual, effectively 0-dimensional defects, which interact with our brane universe. Their collisions with open strings attached to the brane generate a recoil velocity of such D0-branes, later called D-particles. This additional vector field acts as a new content of the universe, which from the low energy point of view behaves as a Dark Matter/Dark Energy (DE) mixture. The modifications of the graviton equations of motion are related to its squared field strength, which under certain circumstances condensate and plays the rôle of an extra scalar field. This model, called the D-material universe, can not only give a mechanism for the growth of large scale structure but, as we show here, can also lead to a successful inflationary scenario, the condensate appearing as the slowly rolling inflaton. Moreover, it provides an effective DM fluid which fits restricted — by our model's hypotheses — lensing data, thus diminishing the need of conventional DM without overclosing the universe. Finally, this supplementary ingredient alters the graviton propagation as it brings in an effective mass term and affects the refractive index experienced by radiations. This study, which spans several cosmological eras and covers several length scales, leads to constraints on the free parameters of the model including the number density of D-particles and the string scale.

Such analyses of models beyond the ΛCDM model may provide important information — alternative exploration routes as well as additional possible bounds on the parameters — that would help us understand the dynamics of our universe.

Acknowledgements

Foremost, I would like to thank my supervisor, Mairi Sakellariadou, who has been guiding me through all these years. You have been gladly sharing your thoughts and ideas, sometimes in challenging arguments. You remained hopeful and confident when things (codes) went wrong, helping me out in these more difficult moments. You provided relevant comments and wise insights — on the core work, from physics to numerics, but also on presentation and communication ingredients of this thesis — as well as dedicated and helpful collaborators. It has been an extremely valuable experience, full of creativity, knowledge, and challenges. For all this time devoted to me, caring about my work and bolstering my success, thank you so much!

I would also like to thank those, in addition to Mairi, who shared in the creation of this work, those who examined in much details every line of our papers, published or not, those who spent so many hours to check, rethink, push forward our ideas, those who discussed so many times on Skype, questioning and answering, always with the same rigour, namely Will Nelson, Nick Mavromatos, Furqaan Yusaf and Matt Stott. Similarly, thanks to Dimitri Skliros for his insights on cusps and gravity waves.

A special thank you goes to Julia Kilpatrick, our dedicated superadmin, without whom my life at King's would have been a lot more complicated. I have always felt I owe Julia my grant, which may be incorrect, but I do owe Julia so much over the years. I hope you enjoyed being the angel saving us from the burning hell that is administrative paperwork or financial troubles.

Thanks as well to the whole Department of Physics, admin, students and staff, for the great atmosphere which made these years a lot easier, funnier, nicer. Especially, a big thank you to John, Rob, Phil, Tevong, Tom and all the other PhDs who started before and with me; similarly to Katy, Andreas and all those who started after me. Thanks as well to Jean for so many beers, Katy for such a fun Pub Quiz, Marcello for the invitation to speak at Pint of Science, and many more. In addition, I would like to warmly thank those who proofread this large amount of words called a thesis, namely Mairi, Phil, Andreas, Katy, Aurelia and Marine.

I have been driven on the track of this great scientific life experience by inspiring lecturers and professors. They led me through the joys and challenges of mathematics, physics, chemistry and more generally of the scientific reasoning, highlighting both its requirements of rigour and the amazement of wonder if brings. Thank you to Damien Jurine and Alexis Fagebaume, Marie-Noëlle Sanz and the professors of $PC_2^\star$, the great Roland Lehoucq, Jean Dalibard, David Langlois, Marios Petropoulos and many more at Ecole Polytechnique, Jerome Gauntlett, Daniel Waldram, Amihay Hanany and again many more at Imperial College. Let me also point out the extraordinary power and importance that Wikipedia has had in my leaning over the years, so thank you to those making this great project possible.

I would also like to thank those outside work who shared my happy thoughts and despair, my issues and my joys, those who made my time off so enjoyable and who gave me the energy to start, pursue and finish this thesis. Aude from the first days; Mathew and Captain Morgan; Aurelia and your wines; Marine, Jouda and Juliette, our walks, drinks, nights out, and so much more; Clem for your good inspiring words and parties; Pau et Co, in France but always there; Pen, for so many discussions on physics, for so long; David, always supportive, always there; and again, many more.

Similarly, I would like to thank my parents for the time they spent on me, with me, for the encouragements, from day 1 (literally), on this PhD but mainly on all these steps that lead me here. I would like to thank my brothers and sister for the time they spent on trying to understand what I dedicated so many years on. A special mention to David, who introduced me to complex numbers and started questioning my scientific brain way before the beginning of my PhD.

Finally, to Solène, the love of my life, to the one who managed to support me every day with ever more energy and less hesitation, managing to bear with me in the long and sometimes painful and unsatisfactory process that is a PhD, sharing and highlighting the happy days of success, and who enlightened my days, one after the other, with so much passion. From the bottom of my heart.

Declaration

I hereby declare that the contents and organisation of this thesis, titled "Astrophysical and cosmological consequences of string-inspired models", constitute my own original work and effort. Where other sources of information have been used, they have been acknowledged for and duly referenced. This thesis has not been submitted, in whole or in part, for any other degree.

Thomas Elghozi
July 2016

Contents

List of Figures

List of Tables

Notations and conventions

We summarise here all the choices in notations, signs and other conventions used throughout this thesis unless stated otherwise.

Latin indices refer to spatial components $a, b, i, j... = 1, 2, 3$ while greek indices refer to space-time components $\alpha, \beta, \mu, \nu... = 0, 1, 2, 3$. If needed, additional dimensions (above the usual $3 + 1$ spacetime denoted by x_μ) are referred to as y_A using capital letters $A, B, C... = 4, 5, 6...10$. When a specific coordinate basis is used, the numbers referring to space-time components $0, 1, 2, 3$ might be replaced by the explicit coordinate considered, for instance (t, x, y, z) for cartesian coordinates or (t, r, θ, ϕ) for spherical coordinates — where θ is the polar angle and ϕ the azimuthal angle.

The space-time metric signature is chosen to be $(-, +, +, +)$, with all (additional) space dimensions (also) associated to a $+$ sign; we use Einstein summation convention.

Three-vectors are written in boldface $\mathbf{x}$ while their components are written using regular characters x^i. Their norm is denoted as $|\mathbf{x}|$ and one has $|\mathbf{x}|^2 \equiv x_i x^i$. Four-vectors are only written without any explicit index when obviouly contracted with another neighbouring four-vector. In such case, both are in regular font and the contraction is made explicit using a dot, for instance $k \cdot x \equiv k_\mu x^\mu = g^{\mu\nu} k_\mu x_\nu$. Note that one could also find $\mathbf{k} \cdot \mathbf{x} \equiv k^i x_i$.

$\partial_\mu \equiv {}^{\partial}/_{\partial x^\mu}$ denote (usual) derivatives with respect to the coordinates x^μ, while covariant derivatives are denoted using D_μ. Alternatively, $A_{\mu,\nu} \equiv \partial_\nu A_\mu$ while $A_{\mu;\nu} \equiv D_\nu A_\mu$.

An overdot denotes the derivative with respect to (the most obvious) time, usually specified; for instance, $\dot{a} \equiv {}^{\mathrm{d}a}/_{\mathrm{d}t}$ or $\dot{X}_\mu(\sigma, t) \equiv {}^{\mathrm{d}X_\mu}/_{\mathrm{d}t}$. A dash denotes the derivative with respect to a (non-time) coordinate or parameter, when there is only one or no ambiguity; for instance, $V'(\varphi) \equiv {}^{\mathrm{d}V}/_{\mathrm{d}\varphi}$ or $X'_\mu(\sigma, t) \equiv {}^{\mathrm{d}X_\mu}/_{\mathrm{d}\sigma}$.

The Riemann curvature tensor is defined as $R^\mu{}_{\nu\rho\sigma} = \partial_\sigma \Gamma^\mu_{\nu\rho} - \partial_\rho \Gamma^\mu_{\nu\sigma} + \Gamma^\alpha_{\nu\rho}\Gamma^\mu_{\alpha\sigma} - \Gamma^\alpha_{\nu\sigma}\Gamma^\mu_{\alpha\rho}$ while the Ricci tensor is $R_{\mu\nu} = R^\beta{}_{\mu\nu\beta} = \partial_\beta \Gamma^\beta_{\mu\nu} - \partial_\nu \Gamma^\beta_{\mu\beta} + \Gamma^\alpha_{\mu\nu}\Gamma^\beta_{\alpha\beta} - \Gamma^\alpha_{\mu\beta}\Gamma^\beta_{\alpha\nu}$.

$\langle\langle \xi \rangle\rangle$ is the average (over time, position, population...) of the quantity ξ. When

a quantity ξ is complex, ξ^* denotes its complex conjugate and $|\xi|^2 \equiv \xi\xi^*$.

A subscript 0 (on a quantity which is not a 4-vector) often refers to today's value of a parameter, while a sub- or superscript c is usually denoting a critical value.

Unless stated otherwise, (reduced) Planck units are considered, following $c = \hbar = k_{\rm B} = 8\pi\, G = 1$. The mass scale is thus the (four dimensional) reduced Planck mass $M_{\rm Pl} \simeq 2.4 \times 10^{18}$ GeV.

Chapter 1

Cosmology

1.1 Introduction

Cosmology is a comparatively new natural philosophy, a new science, compared to others such as chemistry or astronomy. Its key questions remained metaphysical for thousands of years before data could be collected that would make them a matter of physics: a matter of numbers rather than images, a matter of theories rather than myths, a matter of doubts rather than beliefs. Of course, many questions remain unanswered, and some will potentially remain outside the reach of physics and mathematics forever, but our collective intelligence has begun to lift the veil on a tiny part of what the universe is.

Our story begins when stars are no longer considered as the remains of our ancestors, when our galaxy is no longer seen as a spray of celestial milk across the sky, and when explanations are found to interpret the nature of motion in the cosmos. One could start with the Ptolemaic system or with Newton's law of gravity but here we will fast forward to the 20^{th} century. The first tool needed to grasp the nature of our universe is General Relativity (GR), for three key reasons. First, GR explains what gravity really is, namely a consequence of the elasticity of spacetime, and provides a means by which to quantify it. This is fundamental because gravity is the main force acting at large scales. Secondly, GR suggests that spacetime could expand or shrink and that it could have a shape and a curvature. It suggests that the universe could start and begin, be open or closed, and that it could have boundaries or be embedded into something larger. This was, of course, a difficult idea to accept for almost everybody at the time it was proposed, Einstein included, but ultimately the universe was unavoidably shown to be 'not everlasting' and 'unsettled'. Finally, GR imposes a speed limit, the speed of light in vacuum, for everything that exists but, in particular, for any information travelling through the universe. This is the

basis of causality but also allows us to see further back in the past when looking further away from us. Space thus stores the memories of time.

Armed with this underlying theory, data has led to an exponential increase of our understanding of the universe. The first set of data was composed of direct observations of the sky using visible light, to which Galileo made a notable contribution. Still, the most important advance may be that by Lemaître and Hubble in the late 1920s [1, 2]. Their observations suggested that galaxies further from us receded faster than those closer to us, which in turn led to the idea of an expanding (and thus, contrary to the prevailing belief, non-static) universe. This was probably the first time that the universe, as a whole, was the physical system being experimentally studied. Thermodynamics implies that the universe, cold and diluted as it is today, used to be warm and dense, so much so that it was nothing more than a kind of a plasma of highly energetic particles. Then, during the expansion, cooling and dilution of the universe, its contents became organised, first as atoms, then as clouds of gas, and today as stars, galaxies, clusters, filaments and voids.

The second essential dataset for our current cosmology is the Cosmic Microwave Background (CMB) radiation and the myriad information which has been extracted from it in the last fifty years or so. When the universe was dense and filled with highly energetic charged particles, photons were intensely interacting, being scattered, absorbed, and reemitted almost continuously in their attempts to travel. When the universe cooled down and diluted sufficiently for electrons and nuclei to recombine into neutral atoms, radiation-matter interactions became significantly less intense, so much so that the universe became transparent, freeing the photons for an unfettered journey through space. The analysis of these photons shows that the universe was almost exactly homogeneous and isotropic at that time, with its temperature varying only by one part in 10^5. It also helps one to infer the energy budget of the universe, i.e. what the content of the universe is. Currently, cosmologists consider space to be filled with about $68 - 70\,\%$ Dark Energy (DE), $25 - 27\,\%$ Dark Matter (DM) and around $5\,\%$ ordinary matter, with a pinch of radiation. The age of the universe (13.7 billion years old) and its overall curvature (the universe is flat with a $0.4\,\%$ error range) can also be deduced from CMB analysis [3].

Today's most promising directions come from precision measurements, gravitational waves and neutrinos. The first of these requires the statistical analysis of huge amounts of data (mostly in the infrared, visible and ultraviolet parts of the electromagnetic spectrum) that is either currently available or soon to be. Years of

observations give us an incredible amount of information to work with. The second direction is the detection of vibrations of spacetime itself. These were predicted by GR and only very recently directly observed [4] (although indirect evidence has been obtained by studying compact objects inspirals). Their weak interactions with matter and other kinds of radiation make them both extremely difficult and extremely interesting to detect, the latter because they would carry information which would otherwise be unavailable. Similarly, neutrinos are extremely light, weakly interacting particles of the Standard Model of particle physics and are produced in many processes such as nuclear reactions occurring in stars. They remain for the most part unaltered during their journey through space and thus would yield new information were we able to detect them more efficiently and more accurately.

This detailed information is building up a story of the universe in which we live, which is commonly (but wrongly) referred to as the Big Bang model, or more appropriately as the ΛCDM model. The former is due to the journalist Fred Hoyle who chose it for popularisation in radio programmes in the 1950s. It portrays the universe as hot and dense at the beginning (whatever this means), then rapidly expanding. This Big Bang picture is misleading as the universe did not make any noise, did not occur in an explosion and probably did not even start as a singularity, or "primordial atom" (as Lemaître, who first mentioned such a theory, named it). Still, it is catchy and thus the image has endured. The latter description, even though less fancy, describes more accurately the reality we observe and adds several hypotheses on top of the Big Bang model. The Λ refers to the cosmological constant or DE, which today drives the expansion of the universe, acting as a negative pressure or vacuum pressure (counting as $68 - 70\,\%$ of the energy content of the universe), while CDM stands for Cold Dark Matter. Everyday matter and, more generally, any (massive) particle of the Standard Model of particle physics may interact not only gravitationally but also through the weak and the strong nuclear forces and, more importantly here, via the electromagnetic force; it is thus (directly) visible. On the other hand, so-called *Dark* Matter interacts mainly gravitationally rather than strongly or electromagnetically, rendering it difficult to observe directly. Gravitational and CMB analyses suggest, however, that DM contributes to somewhat more than a fourth of the energy content of the universe, making it the second most important ingredient, and leading to the denomination of what is considered as the standard model of cosmology, as will be discussed later.

1.1.1 Cosmological solutions of General Relativity

As mentioned previously, GR is the underlying theory of most cosmological and astrophysical models. Developed in the late 1900s and the 1910s, mainly by Albert Einstein, but with early inputs from mathematicians and physicists such as Marcel Grossmann, Tullio Levi-Civita, David Hilbert, Hendrik Lorentz and Willem de Sitter, its field equation, named after Einstein, was published in November 1915 as[1]

$$R_{\mu\nu} - \frac{1}{2} R\, g_{\mu\nu} = T_{\mu\nu} \tag{1.1}$$

where $R_{\mu\nu} = R^{\alpha}_{\ \mu\nu\alpha}$ is the Ricci tensor, defined from the Riemann tensor[2] and containing the information about the local curvature of spacetime, $R = g^{\mu\nu} R_{\mu\nu}$ is the Ricci scalar, $g_{\mu\nu}$ is the local metric of spacetime used to compute the Christoffel symbols $\Gamma^{\alpha}_{\beta\gamma}$, while $T_{\mu\nu}$ is the stress energy (or energy momentum) tensor containing the information about the energy distribution in spacetime. The constant factor, ${}^{8\pi G}/_{c^4}$, has been omitted as we here use (reduced) Planck units.

Soon after, the cosmological hypothesis of a homogeneous, isotropic, expanding universe was described by the Friedmann-Lemaître-Robertson-Walker (FLRW) metric

$$\mathrm{d}s^2 = -\mathrm{d}t^2 + a(t)^2\, \mathrm{d}\Sigma^2 \tag{1.2}$$

where $a(t)$ is the scale factor and $\mathrm{d}\Sigma^2$ is the time-independent 3-dimensional uniformly-curved space interval. It is often expressed using hyperspherical coordinates

$$\mathrm{d}\Sigma^2 = \mathrm{d}r^2 + S_k(r)^2\, \mathrm{d}\Omega^2 \tag{1.3a}$$

$$\text{where} \quad S_k(r) = \begin{cases} |k|^{-1/2}\ \sin(|k|^{1/2}\, r) & \text{for} \quad k > 0 \\ r & \text{for} \quad k = 0 \\ |k|^{-1/2}\ \sinh(|k|^{1/2}\, r) & \text{for} \quad k < 0 \end{cases} \tag{1.3b}$$

with $\mathrm{d}\Omega^2 = \mathrm{d}\theta^2 + \sin^2\theta\, \mathrm{d}\phi^2$ and k is the (dimension $[L^{-2}]$) Gaussian curvature. The use of this metric within the Einstein equations yields the Friedmann equations

$$\frac{\dot{a}^2}{a^2} = \frac{8\pi G}{3}\, \rho - \frac{k}{a^2} + \frac{\Lambda}{3} \tag{1.4a}$$

$$\frac{\ddot{a}}{a} = -\frac{4\pi G}{3}\, (\rho + 3p) + \frac{\Lambda}{3} \tag{1.4b}$$

[1] Remark that the cosmological constant term, $\frac{1}{2}\Lambda\, g_{\mu\nu}$, was only introduced two years later.
[2] $R^{\alpha}_{\ \beta\gamma\delta} = \partial_\delta\, \Gamma^{\alpha}_{\beta\gamma} + \Gamma^{\lambda}_{\beta\gamma}\, \Gamma^{\alpha}_{\lambda\delta} - (\gamma \leftrightarrow \delta)$.

where G, Newton's constant, has been reintroduced (while c is still taken to be 1), the overdot denotes a derivative with respect to time t, p and ρ respectively denote the pressure and density of the fluid(s) filling the universe and Λ is the cosmological constant. Note that while the second is often called the acceleration equation, the first will sometimes be referred to as the Friedmann equation. The continuity equation, given by

$$\dot{\rho} = -3\,\frac{\dot{a}}{a}\,(\rho + p) \tag{1.5}$$

and also often used in cosmological computations, can be derived from the Friedmann equations. It can also be found using the first law of thermodynamics if one assumes adiabatic expansion of the universe, which is actually equivalent to homogeneity in the cosmological principle.

In all these equations, ρ and p can be split into different components of the energy content of the universe such as radiation (ρ_r and p_r) and dust or cold (non-relativistic) matter (ρ_m and p_m). In addition, the cosmological constant term can be rewritten as a DE density term using $\rho_\Lambda = (8\pi G)^{-1}\,\Lambda$. The main difference between these components lies in their equation of state, that is, the equation relating ρ and p, often parametrised by a dimensionless number w as

$$p = w\,\rho \tag{1.6}$$

where $w = 1/3$ for radiation, $w = 0$ for dust and $w = -1$ for DE (that is, an effective cosmological constant fluid). Putting this equation of state into the continuity equation and the Friedmann equation leads to the time evolution of the density and the scale factor. Excluding the case $w = -1$, one gets

$$\rho = \rho_0\; a^{-3(1+w)} \tag{1.7a}$$

$$a(t) = a_0 \left(\frac{t}{t_0}\right)^{\frac{2}{3(1+w)}} \tag{1.7b}$$

where the index 0 refers to the present day value of a quantity and it is usually chosen that $a_0 = 1$. This yields the usual dependence of the density of dust on the scale factor $\rho_\mathrm{m} \propto a^{-3}$ while due to redshift the radiation density scales as $\rho_\mathrm{r} \propto a^{-4}$. The time dependence of the scale factor thus reads, respectively, $a \propto t^{2/3}$ and $a \propto t^{1/2}$ for a universe dominated by such components. Alternatively, with the case $w = -1$, DE exhibits a constant density and yields $a \propto e^{Ht}$, that is, a de Sitter accelerated

expansion, where $H \equiv \dot{a}/a$ is the Hubble parameter.

One can also express the density parameters in terms of the critical density. The latter is defined as the density of a flat $k = 0$ universe, all components being accounted for. The Friedmann equation yields

$$\rho_{\mathrm{c}} \equiv \frac{3H^2}{8\pi G} \tag{1.8}$$

while its current numerical value is about 5 atoms per cubic metre. Note that the word 'atom' here refers to the hydrogen atom, that is roughly a proton. Density parameters are dimensionless quantities defined, for each component or group of components of the universe, as the ratio of its energy density to the critical density ρ_{c}. They allow us to rewrite the Friedmann equation as

$$\Omega_{\mathrm{tot}} - 1 = \frac{k}{H^2 a^2} \tag{1.9a}$$

where $\Omega_{\mathrm{tot}} = \Omega_{\mathrm{r}} + \Omega_{\mathrm{m}} + \Omega_{\Lambda}$, or

$$\frac{H^2}{H_0^2} = \Omega_{\mathrm{r}0}\, a^{-4} + \Omega_{\mathrm{m}0}\, a^{-3} + \Omega_{k0}\, a^{-2} + \Omega_{\Lambda 0} \tag{1.9b}$$

where $\Omega_k = 1 - \Omega_{\mathrm{tot}}$ is the spatial curvature density parameter, from the energy density due to global space curvature, and again the subscript 0 refers to today's universe.

1.1.2 The concordance model of cosmology

The knowledge that our universe is expanding, coupled with an understanding of how a universe filled with such ingredients would expand depending on the relative abundance of each component, gives us the ability to rewind the history of the universe from today's observations. The models made by Lemaître and Hubble in the late 1920s [1, 2] showed, as mentioned earlier, that the universe was not static as Einstein and some of his contemporaries would have thought and preferred, but, rather, was expanding. Indeed, Lemaître and Hubble's measurements proved, by observing many extragalactic objects and in particular their redshift, that they follow an empirical law known as Hubble's law, stating that the receding velocity is proportional to the distance. The proportionality constant is H, the Hubble parameter, whose value today is about $H_0 \simeq 70\,\mathrm{km\,s^{-1}\,Mpc^{-1}}$ [5, 6], meaning that a galaxy

at a distance of 1 Mpc has a radial centrifugal velocity of around 70 km/s. Rather than us occupying a special point at the centre of an expansion, it is understood that a uniformly expanding universe would produce such an effect, the observed velocity being due to spacetime between us and the galaxy being constantly stretched. This leads to the definition of a cosmological redshift z, as the consequence of the expansion of the universe on photon energy, following $1 + z \equiv {}^{a_0}/_{a}$; that is, $z = 0$ today ($a_0 = 1$) and z grows for smaller a, for older times.

The behaviours described above lead to the following results: an expanding universe filled with any amount of radiation and dust will eventually be dominated by matter (since radiation is diluted more efficiently), and an expanding universe also containing DE will eventually be dominated by this last component, which gives a constant density regardless of the expansion. This is very important as the rewinding of time starting from the current state of our universe, filled with a mixture of all three, will give rise to eras dominated by one fluid dictating the expansion rate, separated by eras of codominance, during which one component slowly takes over another. The presence of matter, naively considered as the most abundant ingredient of today's universe, as well as radiation, yields to a matter-radiation equality point somewhere around a redshift $z \simeq 3300$ [5, 6].

Unexpectedly, today's data points to a universe filled with about 68.3 % of its energy budget in DE, slightly less than 31.7 % in dust and about 0.01 % in CMB photons. This means that the cosmological constant of our universe has *recently*[3] become dominant, ending a matter dominated era (MDE) which lasted most of the universe's history and started after a radiation dominated era (RDE), itself lasting about 6×10^4 years. This knowledge comes from the analysis of the matter present around us (in stars and galaxies, but actually mainly in the gas in between), giving us a rough estimate of the matter density, as well as the detection and analysis of the Cosmic Microwave Background (CMB). Its photons represent a major fraction of the photons of today's universe, allowing for an estimation of the radiation energy density and thus of the baryon to photon ratio, currently estimated to $N_{\mathrm{b}}^{(0)} \simeq 6 \times 10^{-10}\, N_{\gamma}^{(0)}$.

Predominantly, the CMB is the relic radiation emitted by the last scattering surface which travelled almost without interaction and thus without alteration since then — apart from the redshift due to cooling. When the universe cooled down

[3] 'Recently' might sound slightly misleading since the equivalence between matter and DE occurred about 3.5 to 4.5 billion years ago, but this corresponds to a redshift of only $z = 0.4$, which is small on cosmological timescales.

enough so that electrons and protons were able to bind and recombine as neutral hydrogen (and helium) atoms, photons were able to travel roughly unscattered in a now quasi-transparent medium. The CMB thus yields all the information about the content of the universe at that time. First, the CMB is a uniform blackbody spectrum (up to an extremely high accuracy), giving the temperature of the universe today to be $T_0 = 2.7255$ K [3, 6] and confirming the general idea of an expanding universe which was originally filled mainly with high energy radiation. Since the temperature of an expanding universe filled with radiation[4] is inversely proportional to its scale factor and thus proportional to $1 + z$, one can infer that the decoupling occurred at a redshift $z \simeq 1100$ and a temperature $T_{\text{dec}} \simeq 3000$ K. The ratio of baryons to photons obtained through CMB observations can also be used to compute the abundance of primordial elements. Indeed, Big Bang Nucleosynthesis (BBN) analysis shows that this ratio is the only parameter needed to predict a 4-helium mass fraction of about 0.25, for deuterium and tritium about 10^{-3} and 10^{-4} respectively, and for lithium about 10^{-9}. Current observations yield very good agreement with these estimations, especially regarding deuterium.

In addition, the CMB exhibits anisotropies whose amplitude is roughly a part in 10^5 and whose angular size peaks for angles around $\theta \simeq 1^\circ$ or multipole moments around $\ell \simeq 220$ (where ℓ is the multipole moment in the spherical harmonics decomposition[5] of the signal), as can be seen in Fig. 1.1. Two main effects drive the shape of the CMB power spectrum: Baryon Acoustic Oscillations (BAO) and diffusion damping. The first is driven by the fact that the pressure of radiation, which tends to erase overdensities, is in conflict with dust gravitational instability, which tends to amplify overdensities. This conflict generates oscillations at various scales, creating several peaks in the power spectrum. The fact that the universe did not become instantaneously transparent is at the origin of the second effect, which blurs the small scale anisotropies and results in an exponential damping in the large multipole moment of the power spectrum.

A detailed analysis of the anisotropies and the power spectrum of the CMB yields information on many aspects of our universe, in addition to a more accurate

[4]Indeed, Maxwell's relations of thermodynamics tell us that $\left(\frac{\partial S}{\partial V}\right)_T = \left(\frac{\partial P}{\partial T}\right)_V$ (where S is the entropy, P the pressure, T the temperature and V the volume). For radiation, the equation of state is given by $P = \frac{1}{3}\rho$, where ρ is the energy density, which yields $\rho \propto a^{-4}$ but also $U = \rho V$ and $S = \frac{U+PV}{T} = \frac{4}{3}\frac{V}{T}\rho(T)$. Using the aforementioned Maxwell's relation, one gets $\frac{\mathrm{d}\rho}{\mathrm{d}T} = \frac{4\rho(T)}{T}$, leading to $\rho \propto T^4$ and hence $T \propto a^{-1}$.

[5]The coefficients $\mathcal{C}_\ell$ of such decomposition are related to the plotted $\mathcal{D}_\ell$ of Fig. 1.1 by $\mathcal{D}_\ell \propto \ell(\ell+1)\,\mathcal{C}_\ell$.

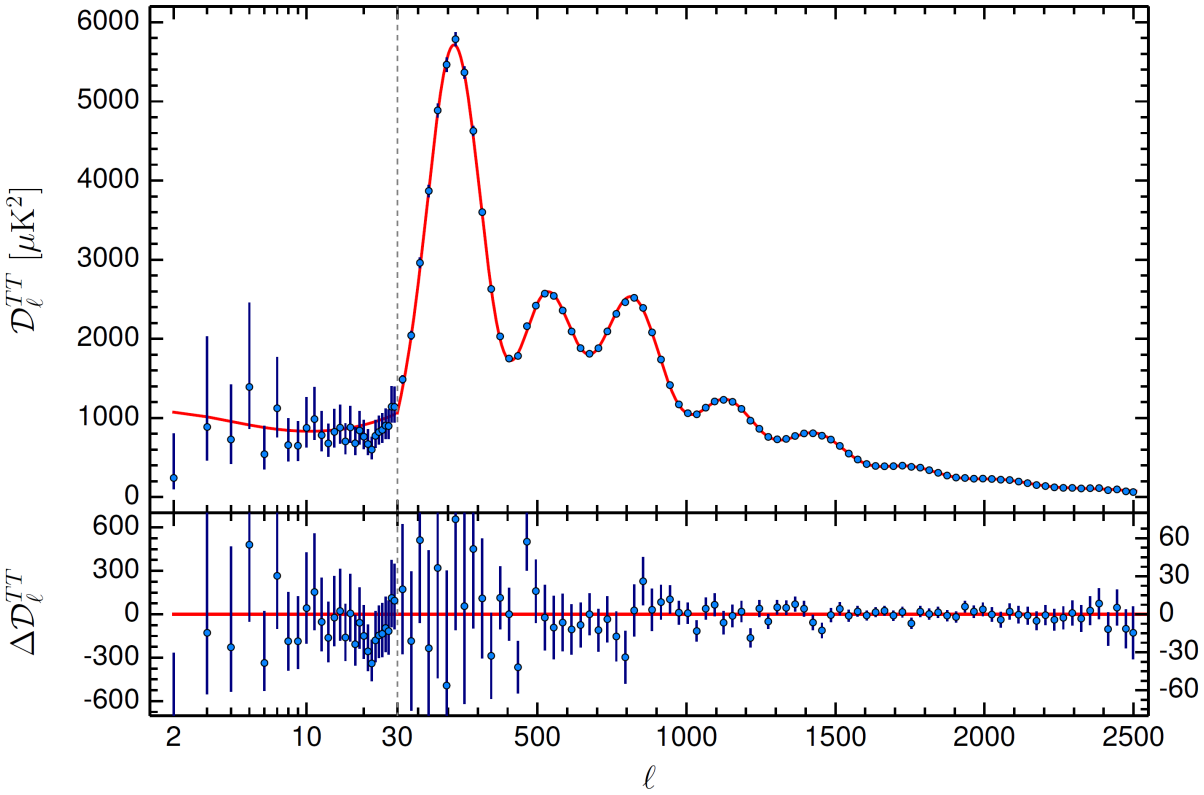

Figure 1.1: CMB temperature power spectrum. The red line shows the best fit ΛCDM theoretical spectrum while the blue dots and error bars give the actual measurements and uncertainties (at 1σ). The lower panel shows residual with respect to the best fit model. From the Planck Collaboration [6, Figure 1].

value of the Hubble constant, $H_0 \simeq 67.74 \pm 0.46$ km s^{-1} Mpc^{-1} [6]. The first peak's angular scale gives the curvature of the universe, which is flat up to 0.4 %, and thus the total density parameter of the universe is constrained to 1.00 ± 0.02 [7]. The second and third peaks determine, respectively, the baryon density and the DM density. Indeed, dust is actually divided into two components, one being the usual Standard Model particles, well known and studied, while the other remains largely unknown. This indefinite DM component can be inferred as being massive, probably weakly interacting, stable or quasi-stable over billions of years, electrically and colour neutral (no electromagnetic or strong interaction) and cold, meaning non-relativistic — hence not carrying much kinetic or thermal energy compared to its mass energy. The presence of DM is suggested by many other different and independent experiments, at all scales and eras (for instance galactic rotation curves and galactic dynamics, bullet cluster and gravitational lensing, structure formation or BAO). It also emerges naturally from many 'beyond the Standard Model' theories

of particle physics (such as axions, in supersymmetry or string theories).

Finally, the pattern in the angular scale of the peaks is influenced by the type of density perturbations. Any perturbation can be decomposed into a sum of adiabatic modes — where the overdensity is evenly spread between components — and isocurvature modes — where a specific component overdensity is overall compensated by other components under or overdensities. More explicitly, for each component of the universe, say radiation and matter for simplicity, one can define the number density N_{X} in addition to the energy density ρ_{X}, with $\mathrm{X} \in (\mathrm{r}, \mathrm{m})$, and the linear (first order) perturbations with respect to their averaged value, $\delta N_{\mathrm{X}} \equiv N_{\mathrm{X}} - \langle N_{\mathrm{X}} \rangle$ and $\delta\rho_{\mathrm{X}} \equiv \rho_{\mathrm{X}} - \langle \rho_{\mathrm{X}} \rangle$. An adiabatic one is such that the ratios of each component remain unchanged, thus leading to a perturbation of the total energy density and thus of the curvature. This yields

$$\delta\left(\frac{N_{\mathrm{m}}}{N_{\mathrm{r}}}\right) = 0 \qquad \Leftrightarrow \qquad \frac{\delta N_{\mathrm{m}}}{\delta N_{\mathrm{r}}} = \frac{N_{\mathrm{m}}}{N_{\mathrm{r}}} \ , \tag{1.10a}$$

leading, for the energy density, to

$$\frac{\delta\rho_{\mathrm{m}}}{\rho_{\mathrm{m}}} = \frac{3}{4}\frac{\delta\rho_{\mathrm{r}}}{\rho_{\mathrm{r}}} \ , \tag{1.10b}$$

the prefactor coming out of the components' equations of state. In contrast, isocurvature modes leave the geometry unchanged, that is, the total energy density unchanged, and thus implies in our two-component example[6]

$$\delta\rho_{\mathrm{m}} + \delta\rho_{\mathrm{r}} = 0 \qquad \Leftrightarrow \qquad \frac{\delta N_{\mathrm{m}}}{\delta N_{\mathrm{r}}} = -\frac{4}{3}\frac{\rho_{\mathrm{r}}}{\rho_{\mathrm{m}}}\frac{N_{\mathrm{m}}}{N_{\mathrm{r}}} \ . \tag{1.11}$$

The first peak has been measured to be around $\ell \simeq 220$, indicating mostly adiabatic initial perturbations, and in addition allows us to infer the flatness of the universe. Indeed, all other things being equal, initial isocurvature modes would yield a peak at $\ell \simeq 330$ and subsequent peaks similarly shifted towards smaller angles, with their amplitude also being modified. This rules out cosmic strings as the main source of anisotropies — as they would mostly produce isocurvature modes — and supports inflation — which is a de Sitter expansion period generating almost adiabatic perturbations. Furthermore, scale invariant expansion (such as de Sitter) lead to a flat primordial power spectrum, as has been roughly measured in the CMB. One can

[6] In a case with n components, one can define $n-1$ isocurvature modes with respect to each but one component, which serves as reference.

define the scalar spectral index n_s as in $\mathcal{P}_s(k) \propto k^{n_s-1}$, where $\mathcal{P}_s(k)$ is the scalar power spectrum and k is the wave number (related to the multipole moment ℓ). It has been constrained to $n_s \simeq 0.968 \pm 0.006$ [6], where a perfectly flat spectrum would yield $n_s = 1$.

It is important to note that many additional effects have distorted or blurred the spectrum anisotropies after the CMB photons were emitted. Three are worth mentioning: the reionisation of the intergalactic medium, the Sunyaev-Zel'dovich (SZ) effect and the Sachs-Wolfe (SW) effect. As mentioned previously, decoupling occurred because the universe became neutral via the recombination of electrons and nuclei, but today's universe is mainly ionised. This reionisation occurred, according to CMB analysis, around $z \simeq 10$ [5] at which point intergalactic space started scattering the CMB photons, as well as altering the polarisation. This effect is not significant anymore due to the very low baryon density but would have been quite substantial in the past. The SZ effect is due to inverse Compton scattering, in which high energy electrons of a hot cloud locally boost the CMB photons. The SW effect is the redshift or blueshift of the CMB photons due to gravitational potentials on their path. In fact, this effect would have also occurred on the last scattering surface due to uneven distribution of energy, and this is called the non-integrated SW effect. In contrast, the Integrated SW (ISW) effect occurred after $z \simeq 1100$, on the line of sight, mostly in late eras. When the universe is dominated by DE[7], large enough gravitational wells may evolve significantly while photons are travelling through them, since they are damped by the acceleration of the expansion of the universe. Thus, photons are more blueshifted (respectively redshifted) when entering an overdense (underdense) region than they are redshifted (blueshifted) when they exit the same region, which has been smoothed out.

Careful analysis of CMB data has made it possible to tightly constrain the main parameters of our model of the universe within the most concordant one, the ΛCDM model. These parameters include H_0, and thus the age of the universe, $t_0 \simeq 13.799 \pm 0.021 \times 10^9$ years [6], the energy budget of the universe, and the type of primordial anisotropies, which are found to be mainly adiabatic.

[7]The effect is also happening when the universe is still affected in its evolution by radiation, just after decoupling, but its effect is smaller and often integrated into the primordial CMB anisotropies, that is, those imprinted on the CMB photons initially.

1.2 Inflation

So naively, the story is complete: the universe, which started as a hot dense patch of spacetime, started to rapidly expand and thus cool down and dilute, until its contents organised themselves into atoms and stars to form what we know today. But more questions are raised from these answers. The first one that one could ask is about what was before that. What led to what we see today? How come the universe is so homogeneous? And flat? Is it naturally evolving towards such state? These questions all boil down to what is known as the initial conditions problem(s): if one can use the laws of physics to rewind back through time and explain the state of the universe at some instant using knowledge about it at some later instant, when do we stop doing so, why and what was the universe like back then?

1.2.1 Initial conditions

There are several unanswered questions ("problems") which are connected to the initial conditions of our cosmological history. Indeed, rewinding the history of the universe following the known laws of physics in their validity limits, one might run back up to a very small, very dense, very warm and surprisingly homogeneous, isotropic universe. For instance looking at the CMB, which yields an almost unaltered photonic image of the early universe about 380 000 years after the so-called "Big Bang", one notes that our universe is homogeneous and isotropic with an accuracy of about 10^{-5}. Even though we do not know all the details of the laws governing the evolution of the early universe, it seems — considering General Relativity as a valid background — that no phenomenon can reduce inhomogeneities in a decelerating expanding universe, meaning that the further back in time one looks at, the more homogeneous and isotropic it should be.

One can also assume that quantum effects (especially quantum fluctuations) do not occur at scales below Planck scale, or at least do not have a dramatic role. Above Planck scales, one can only say that it is likely they do have a large impact on the physical properties and evolution of the universe. One can thus set the "initial" time scale at around $t_{\mathrm{ini}} \sim t_{\mathrm{Pl}} \sim 10^{-43}$ s. The key question now is: how was the universe at that time? [8, Chapter 5]

A complete description of the early universe, that is, a complete set of initial conditions, is given by two pieces of information, the energy density field and the velocity (or energy flow) field. The issue with the first one comes out when looking

at the size of today's horizon $ct_0 \sim 10^{28}$ cm and trying to compare it with the "initial" horizon. Today's universe is a patch of homogeneous, isotropic and causally connected spacetime — it might even be a part of a larger homogeneous, isotropic patch. It is the result of the expansion of a smaller (homogeneous, isotropic) patch, smaller by a factor a_i/a_0, thus at least as large as

$$l_h \sim ct_0 \frac{a_i}{a_0} \,. \tag{1.12}$$

When compared with the size of the causal region at the time $l_c \sim ct_i$, one obtains the ratio

$$\frac{l_h}{l_c} \sim \frac{t_0}{t_i} \frac{a_i}{a_0} \tag{1.13}$$

that we would like to evaluate. Considering that primordial radiation dominates the initial universe, its temperature is given by the Planck temperature $T_{\mathrm{Pl}} \sim 10^{32}$ K. This leads to

$$\frac{l_h}{l_c} \sim \frac{t_0}{t_i} \frac{T_0}{T_{\mathrm{Pl}}} \sim \frac{10^{17}}{10^{-43}} \frac{1}{10^{32}} \sim 10^{28} \tag{1.14}$$

which one should understand as the fact that the homogeneous, isotropic patch that expanded into our current universe was at least 10^{28} times larger (in length) than the causally connected patch at the time. This involves about 10^{84} causally disconnected patches whose energy density was equal, up to $10^{-3}\,\%$. This is called the homogeneity, isotropy problem.

To understand why this problem is also often called the horizon problem, one needs to assume in addition that the scale factor follows a power law in time, that is, that $\dot{a} \sim a/t$. It yields

$$\frac{l_h}{l_c} \sim \frac{\dot{a}_i}{\dot{a}_0} \,. \tag{1.15}$$

Since we assumed that the universe has always been expanding with a decelerating expansion — which ultimately means that gravity has always been attractive — the ratio of rates of expansion has always been larger than 1, meaning that the scale of the homogeneous isotropic patch has always been larger than the scale of the causality patch.

Similarly, assuming that matter is evenly distributed and that its velocity follows Hubble law (otherwise the matter distribution would quickly be spoiled), one can evaluate the total energy of matter in a patch of spacetime. It is the sum of the kinetic energy due to Hubble expansion E_{K} and the (negative) gravitational potential energy E_{P}, and it is conserved. The kinetic energy is related to the square of the

velocity, which itself is related to the expansion rate, leading to

$$E_{\mathrm{K}}^{i} = E_{\mathrm{K}}^{0} \left(\frac{\dot{a}_i}{\dot{a}_0} \right)^2 . \tag{1.16}$$

Evaluating now the proportion of the total energy which lays in the kinetic form, one has

$$\frac{E_{\mathrm{tot}}^{i}}{E_{\mathrm{K}}^{i}} = \frac{E_{\mathrm{tot}}^{0}}{E_{\mathrm{K}}^{0} \left(\frac{\dot{a}_i}{\dot{a}_0} \right)^2} = \frac{E_{\mathrm{tot}}^{0}}{E_{\mathrm{K}}^{0}} \left(\frac{\dot{a}_0}{\dot{a}_i} \right)^2 \lesssim 10^{-56} \tag{1.17}$$

where we used the matter homogeneity and isotropy found previously to set a bound $\frac{\dot{a}_0}{\dot{a}_i} \lesssim 10^{-28}$. One should understand this as the fact that, in the early universe at least, the absolute value of the gravitational potential energy of matter is almost exactly equal to the kinetic energy of matter due to Hubble expansion, up to a precision of $10^{-54}\,\%$. Note as well that deviating from this cancellation would produce either a rapid collapse of matter or a rapid dilution of matter. This problem is known as the initial velocities problem or the flatness problem. To understand this, one can use the Friedmann equation expressed in terms of the total cosmological parameter: recall cosmological parameters are parameters of the ΛCDM model defined as the energy density (total or of a certain component of the universe) scaled by the critical energy density, where the critical energy density is the one such that the universe is flat; it yields

$$\Omega_{\mathrm{tot}} - 1 = \frac{k}{H^2 a^2} \tag{1.18}$$

where k is a measure of curvature and $H \equiv {}^{\dot{a}}/_{a}$ is the Hubble rate. One thus has

$$\Omega_{\mathrm{tot}}^{i} - 1 = \left(\Omega_{\mathrm{tot}}^{0} - 1 \right) \frac{H_0^2 a_0^2}{H_i^2 a_i^2} = \left(\Omega_{\mathrm{tot}}^{0} - 1 \right) \frac{\dot{a}_0^2}{\dot{a}_i^2} \lesssim 10^{-56} \tag{1.19}$$

which in turn should be understood as the fact that the initial universe had to be extremely flat (up to, again, $10^{-54}\,\%$) in order to obtain today's flat universe.

Finally, one can also consider the (less dramatic) problem of the initial perturbations. Indeed, even though the universe at the time of the CMB was very homogeneous and isotropic, one cannot avoid the fact that today's universe contains large scale structures, that are galaxies, clusters, filaments and large voids. During the matter dominated era, though, the temperature anisotropies grow and lead to density anisotropies. The problem is that they are too small, of the order $\Delta T \simeq 10^{-5}\, T$, to explain the structures observed, which are such that $\Delta\rho \simeq \rho$.

Said differently, to explain the density anisotropies, one needs larger temperature anisotropies than those observed or additional ingredients. These structures must have been sourced by some inhomogeneities and anisotropies which are thus yet to be explained in details by future models.

1.2.2 Inflationary phase

These two different problems, the horizon and the flatness problems, are thus driven by the same ratio, that is, the ratio of the initial expansion rate by the present one. For a universe where gravity is attractive, the expansion rate decreases unavoidably leading to this ratio being larger than one. We estimated it at 10^{28}, see Eqs. (1.14) and (1.15). A necessary condition to solve these issues is to set up a period of time where gravity is repulsive: it would allow for an accelerated expansion of spacetime, opening the possibility of a smaller ratio of expansion rates, to order unity, allowing the universe to grow from a fully causally connected patch. It would also explain the Big Bang by generating large velocities from small ones. As already well-understood phenomena — such as nucleosynthesis and CMB — should be maintained, this period of repulsive gravity and accelerated expansion, called inflation, has to occur very early in the history of the universe and has to end up smoothly into a decelerating phase.

Starting with a small patch of causally connected, homogeneous and isotropic spacetime and inflating it, one can first look at the event horizon. Recall the event horizon of an observer at time t is the set of points whose light emissions will ever reach the observer in the future; its physical size is defined as

$$d_{\mathrm{e}}(t) \equiv a(t) \int_t^{t_\infty} \frac{\mathrm{d}\tilde{t}}{a(\tilde{t})} \tag{1.20a}$$

where t_∞ is either finite or infinite. Proceeding to a change of coordinates $t \to a(t)$, $\mathrm{d}t \to {}^1\!/_{\dot{a}(t)}\, \mathrm{d}a$, one obtains

$$d_{\mathrm{e}}(t) = a(t) \int_{a(t)}^{a_\infty} \frac{\mathrm{d}\alpha}{\dot{\alpha}\, \alpha} \,. \tag{1.20b}$$

During inflation, this integral always converges — the event horizon always exists — even if $a_\infty \equiv a(t_\infty) \to \infty$, because $\dot{a}$ grows with a, thus $\dot{a}\, a \propto a^{1+\epsilon}$ with $\epsilon > 0$. This is very important as it implies that whatever happens outside a patch of spacetime of radius $2d_{\mathrm{e}}(t)$ — for instance inhomogeneities — will never influence what happens

in the (concentric) patch of spacetime of radius $d_\mathrm{e}(t)$.

Let us now study the particle horizon, which is the set of points from which an observer can receive information at a given time t and whose physical size is given by

$$d_\mathrm{p}(t) \equiv a(t) \int_{t_\mathrm{i}}^{t} \frac{\mathrm{d}\tilde{t}}{a(\tilde{t})} = a(t) \int_{a_\mathrm{i}}^{a(t)} \frac{\mathrm{d}\alpha}{\dot{\alpha}\,\alpha} \tag{1.21a}$$

where t_i is the origin of time, the time of initial state, and $a_\mathrm{i} \equiv a(t_\mathrm{i})$. In the case of an accelerated expansion where a and $\dot{a}$ grow (quickly), one can roughly approximate the integral's upper bound to infinity (as the additional bit is very small) and obtain

$$d_\mathrm{p}(t) \simeq a(t) \int_{a_\mathrm{i}}^{a_\infty} \frac{\mathrm{d}\alpha}{\dot{\alpha}\,\alpha} = \frac{a(t)}{a_\mathrm{i}}\, d_\mathrm{e}(t_\mathrm{i}) \ . \tag{1.21b}$$

Interestingly, the radius of the homogeneous patch $r_\mathrm{h}(t)$, which at the beginning of inflation is given by $d_\mathrm{e}(t_\mathrm{i})$ as seen above, grows by a factor ${a_\mathrm{f}}/{a_\mathrm{i}}$ (the subscript f referring to the end of inflation) such that

$$r_\mathrm{h}(t_\mathrm{f}) = \frac{a_\mathrm{f}}{a_\mathrm{i}}\, d_\mathrm{e}(t_\mathrm{i}) \simeq d_\mathrm{p}(t_\mathrm{f}) \ . \tag{1.22}$$

Thus again homogeneity and isotropy are preserved on the patch throughout inflation; its size matches the event horizon at the beginning of inflation and the particle horizon at the end of it.

One could argue that inflation only simplifies the problem (by making the size of the initial homogeneous patch smaller) but does not fully solve it. First, one should recall that this homogeneous patch is now causally connected, which could explain the homogeneity and isotropy. In fact, the hypothesis of homogeneity and isotropy can be relaxed as inflation smoothes down inhomogeneities. Indeed, the physical wavelength of a perturbation mode grows with a during inflation while the curvature scale or Hubble radius, given by H^{-1}, is approximately constant. Therefore, large perturbation modes are getting larger than the Hubble radius and exit it, thus making it more and more homogeneous — even though the perturbation amplitude remains the same. Said differently, the contribution of the inhomogeneities to the variation of energy density on the Hubble radius dims, their amplitude being roughly constant. One would simply need to assume that the rate of expansion before inflation $\dot{a}_i$ is small compared to today's $\dot{a}_0$, so that these modes which exited the Hubble radius at the beginning of inflation would not come back in today. CMB analyses suggest a bound on the ratio ${\dot{a}_\mathrm{i}}/{\dot{a}_0} < 10^{-5}$.

Finally, this last bound has interesting consequencies for the total cosmological parameter $\Omega_{\rm tot}$. Equation (1.19) yields

$$\Omega^0_{\rm tot} = 1 + \left(\Omega^{\rm i}_{\rm tot} - 1\right) \frac{\dot{a}_{\rm i}^2}{\dot{a}_0^2} \tag{1.23}$$

meaning that flatness is no longer a problem as inflation also flattens the patch of spacetime. Indeed, any initial deviation of $\Omega^{\rm i}_{\rm tot}$ from unity is strongly suppressed today, by a factor $\left({}^{\dot{a}_{\rm i}}/_{\dot{a}_0}\right)^2 < 10^{-10}$ — instead of any deviation being amplified, meaning that one would need very fine tuned $\Omega^i_{\rm tot}$ to fit today's observations. $\Omega \to 1$ becomes a future attractor instead of being a past attractor. Note though that quantum effects lead to very small deviations from this simplified behaviour.

Accelerated expansion via repulsive gravity thus solves both our initial value issues, the horizon problem and the flatness problem. Let us review now quickly the main ideas to achieve such acceleration.

1.2.3 Negative pressure

According to the second Friedmann equation (the acceleration equation), which reads[8]

$$\frac{\ddot{a}}{a} = -\frac{4\pi G}{3}\left(\rho + 3p\right) \ , \tag{1.24}$$

one requires $\rho + 3p < 0$ in order to observe accelerated expansion $\ddot{a} > 0$. De Sitter spacetime for instance, which is filled with a (DE) fluid following the equation of state $\rho = -p$ and thus satisfying $\rho + 3p = -2\rho < 0$, yields an exponential expansion but no smooth exit. Indeed, one always has

$$\dot{H} = \frac{\ddot{a}}{a} - H^2 \qquad \Leftrightarrow \qquad \frac{\ddot{a}}{a} = H^2 + \dot{H} \tag{1.25}$$

but the Hubble parameter H is constant in de Sitter universe ($\dot{H} \sim 0$), leading to a constant positive acceleration of the expansion. To achieve a smooth exit from inflation where $\ddot{a}$ becomes progressively negative, one needs a varying decreasing H ($\dot{H} < 0$) and the ratio ${}^{|\dot{H}|}/_{H^2}$ progressively becoming of order unity. Before this exit, assuming a is almost exponential, one can safely suppose that H is approximately constant during inflation and $|\dot{H}| \ll H^2$. We shall denote the Hubble parameter during inflation by $H_{\rm I} \simeq H_{\rm i} \simeq H_{\rm f}$. One can also assume $|\ddot{H}| < 2H|\dot{H}|$ (meaning

[8] We here consider DE, absorbed in the total density ρ and pressure p, rather than a cosmological constant term; hence formally $\Lambda = 0$.

that H^2 is varying more rapidly than $|\dot{H}|$) and thus the duration of inflation can be approximately given by

$$t_f \sim \frac{H_\mathrm{I}}{|\dot{H}_\mathrm{I}|} \tag{1.26}$$

where the subscript I refers to inflationary era.

To evaluate t_f, let us recall the constraints for a successful inflation are ${}^{\dot{a}_\mathrm{f}}/_{\dot{a}_0} \gtrsim 10^{28}$ (to obtain a homogeneous, isotropic patch) and ${}^{\dot{a}_\mathrm{i}}/_{\dot{a}_0} < 10^{-5}$ (to avoid large perturbation modes spoiling the homogeneity), yielding

$$\frac{a_\mathrm{f}}{a_\mathrm{i}} = \frac{H_\mathrm{i}}{H_\mathrm{f}}\frac{\dot{a}_\mathrm{f}}{\dot{a}_\mathrm{i}} \simeq \frac{\dot{a}_\mathrm{f}}{\dot{a}_0}\frac{\dot{a}_0}{\dot{a}_\mathrm{i}} > 10^{33} \tag{1.27a}$$

An almost exponential expansion gives

$$\frac{a_\mathrm{f}}{a_\mathrm{i}} \sim e^{H_\mathrm{I} t_\mathrm{f}} \tag{1.27b}$$

which, combined with the previous equation, leads to $t_\mathrm{f} \gtrsim 75\, H_\mathrm{I}^{-1}$. This means that inflation must last for at least 75 Hubble times, also called e-folds, in order to produce a suitable universe. Using the estimation of t_f given earlier on, one has ${}^{|\dot{H}_\mathrm{I}|}/_{H_\mathrm{I}^2} < {}^{1}/_{75}$. To express this in the form of an equation of motion, one has Friedmann equations

$$H^2 + \frac{k}{a^2} = \frac{8\pi G}{3}\,\rho \tag{1.28a}$$

$$\dot{H} - \frac{k}{a^2} = -4\pi G\,(\rho + p) \tag{1.28b}$$

whose ratio (in the flat case $k = 0$) yield

$$\frac{\rho_\mathrm{I} + p_\mathrm{I}}{\rho_\mathrm{I}} < 10^{-2}\ . \tag{1.28c}$$

This leads to the approximate equation of state

$$p_\mathrm{I} \simeq -\rho_\mathrm{I}\ . \tag{1.28d}$$

1.2.4 Slow-roll inflation

To realise this equation of state, the simplest model is to consider a scalar field φ (named the inflaton) whose energy density and pressure can, in general, be written

in terms of kinetic and potential terms as

$$\rho = \frac{1}{2}\dot{\varphi}^2 + V(\varphi) \tag{1.29a}$$

$$p = \frac{1}{2}\dot{\varphi}^2 - V(\varphi)\ . \tag{1.29b}$$

In order to satisfy the equation of state, this inflaton field must satisfy $1/2\,\dot{\varphi}^2 \ll V(\varphi)$, which in fact is a condition on the potential. Indeed, recall the conservation of energy, which in relativistic cases reads $\mathrm{d}E = -p\,\mathrm{d}V$ (with E the total energy, p the pressure and V the volume), leads to a form of the continuity equation which yields

$$\dot{\rho} = -3H\,(\rho + p)\ . \tag{1.30a}$$

This, using Eq. (1.29), leads to

$$\ddot{\varphi} + 3H\dot{\varphi} + V' = 0 \tag{1.30b}$$

where $V' \equiv {}^{\mathrm{d}V}/_{\mathrm{d}\varphi}$. Note that this is the equation of motion of a damped harmonic oscillator. Assuming a large damping term, this leads to small velocities and a slow-rolling regime, as in Ref. [9], characterised by a small kinetic energy compared to potential energy, as required, and by a negligible acceleration term compared to the damping term. The equation of motion thus reads

$$3H\dot{\varphi} + V' \simeq 0 \tag{1.30c}$$

Similarly, Friedmann equation (setting $k = 0$ and $8\pi G = 1$) gives

$$H^2 = \frac{1}{3}\left(\frac{1}{2}\dot{\varphi}^2 + V(\varphi)\right) \simeq \frac{1}{3}\,V(\varphi)\ . \tag{1.31}$$

These two last equations, obtained under the approximations that $1/2\,\dot{\varphi}^2 \ll V$ and $\ddot{\varphi} \ll 3H\dot{\varphi}$, can lead us to two conditions on the potential. First, isolating $\dot{\varphi}$ from Eq. (1.30c) and using Eq. (1.31) to remove H, one obtains

$$\dot{\varphi}^2 \simeq \left(\frac{V'}{3H}\right)^2 \qquad \Leftrightarrow \qquad \frac{\dot{\varphi}^2}{V} \simeq \frac{1}{3}\left(\frac{V'}{V}\right)^2\ . \tag{1.32}$$

Enforcing $(\frac{V'}{V})^2 \ll 1$ thus results in the desired equation of state. Secondly, deriving the equation of motion with respect to time and using again Eq. (1.31) leads to

$$|V''| \simeq \left|3H\frac{\ddot{\varphi}}{\dot{\varphi}} + 3\dot{H}\right| \quad \Leftrightarrow \quad \left|\frac{V''}{V}\right| \simeq \frac{1}{3H^2}\left|3H\frac{\ddot{\varphi}}{\dot{\varphi}} + 3\dot{H}\right| = 3\left|\frac{\ddot{\varphi}}{3H\dot{\varphi}} + \frac{\dot{H}}{3H^2}\right| \tag{1.33a}$$

where $V'' \equiv {}^{\mathrm{d}^2V}/_{\mathrm{d}\varphi^2}$. In the last equality, the first term (of the right hand side) is small compared to 1 — since the acceleration of the scalar field is negligible compared to the damping term. Concerning the second term, deriving Eq. (1.31) and reorganising it gives

$$\frac{\dot{H}}{H} \simeq \frac{V'\dot{\varphi}}{2V} \qquad \Leftrightarrow \qquad \frac{\dot{H}}{3H^2} \simeq \frac{1}{3H}\frac{V'\dot{\varphi}}{2V} \simeq \frac{V'}{3H\dot{\varphi}}\frac{{}^1\!/_2\,\dot{\varphi}^2}{V} \ . \tag{1.33b}$$

Since ${}^1\!/_2\,\dot{\varphi}^2 \ll V$ and $|V'| \simeq |3H\dot{\varphi}|$, this second term is small as well compared to unity. Thus, enforcing $|\frac{V''}{V}| \ll 1$ implies that our slow-roll assumptions are satisfied: ${}^1\!/_2\,\dot{\varphi}^2 \ll V$ and $\ddot{\varphi} \ll 3H\dot{\varphi} \simeq V'$.

One can thus look for potentials satisfying

$$\epsilon \equiv \frac{1}{2}M_{\mathrm{Pl}}^2\left(\frac{V'}{V}\right)^2 \ll 1 \tag{1.34a}$$

$$\eta \equiv M_{\mathrm{Pl}}^2\left|\frac{V''}{V}\right| \ll 1 \tag{1.34b}$$

where ϵ and η are called the slow-roll parameters and M_{Pl} is the (reduced) Planck mass. Another constraint comes from N the number of e-foldings which, as mentioned previously, satisfies $N \gtrsim 75$ (or rather 60 following different model-dependent approximations). Using Eq. (1.27b), one has

$$N \equiv \int H\,\mathrm{d}t = -\frac{1}{M_{\mathrm{Pl}}}\int_{\varphi_i}^{\varphi_e}\frac{V}{V'}\,\mathrm{d}\varphi \ . \tag{1.35}$$

Finally, two constraints commonly used on the inflaton potential are given by experimental bounds from CMB experiments in particular. The first one is a requirement on n_{s} the (scalar) spectral index. This parameter measures the deviation from scale invariance ($n_{\mathrm{s}} = 1$), which is only achieved in exact de Sitter expansion. Theoretical computations lead to the relation

$$n_{\mathrm{s}} = 1 - 6\epsilon + 2\eta \tag{1.36a}$$

while current experimental bounds [10] yield

$$n_{\mathrm{s}} = 0.968 \pm 0.006 \ . \tag{1.36b}$$

The second one is constraining the ratio of the energy scale to the slope and is given by the WMAP experiment [5, 11] as

$$\left(\frac{V}{\epsilon}\right)^{\frac{1}{4}} = 0.0275\, M_{\mathrm{Pl}} \ . \tag{1.37}$$

Finally, some scenarii predict a non-vanishing tensor to scalar ratio r, which is defined as the ratio of the tensor power spectrum to the scalar one, and is given in the slow-roll approximation by

$$r \equiv \frac{\mathcal{P}_t}{\mathcal{P}_{\mathrm{s}}} = -8 n_{\mathrm{t}} = 16\epsilon \tag{1.38}$$

where $\mathcal{P}_t$ is the tensor power spectrum and n_{t} is the tensor spectral index.[9] After some controversy [6], the tensor to scalar ratio is constrained to $r_{0.002} < 0.09$,[10] disfavouring models of inflation providing large tensor component participation to the universe energy budget such as quadratic ($V \sim \varphi^2$) potential.

A scenario or a potential achieving $\epsilon \ll 1$, $\eta \ll 1$, $N \sim 60$, $n_{\mathrm{s}} \simeq 0.968$ and ${}^{V}\!/_{\epsilon} \simeq (0.0275\, M_{\mathrm{Pl}})^4$ is thus a valid, successful inflation scenario. Note that a small ϵ will almost immediately confer a small enough r.

1.2.5 Some successful scenarii

Several generations of models have achieved, partially or fully, the general requirements of producing a universe which satisfies the data constraints. These include, as a first motivation, the resolution of the horizon and flatness problem, that is, the issue of initial conditions. As we have seen, this can be realised with a single scalar field in a potential, but alternative models suggested several scalar fields or vector and higher rank fields. In addition, inflation should end and should produce a hot universe filled with today's components, mainly matter particles and dark fluids. Indeed, the energy in the form of the inflaton should be converted into hot particles in a successful process called reheating.

[9] Similarly to the scalar spectral index, one has $\mathcal{P}_t(k) \propto k^{n_{\mathrm{t}}-1}$ or $n_{\mathrm{t}} - 1 \equiv \frac{\mathrm{d}\ln \mathcal{P}_t}{\mathrm{d}\ln k}$.

[10] Since the power spectrum is a function of the wavenumber k, one has to fix a scale to use data constraints, which has been chosen in some analysis to be $k_0 = 0.002$ Mpc^{-1}.

At first, the steepening of the potential due to the presence of a minimum $V = 0$ managed an exit and the oscillations of the inflaton led to its decay into other fields. Note that its incomplete decay could interestingly lead to the inflaton participating to the dark sector. Still, assuming the universe had to be in thermal equilibrium at very high temperature previously to the inflationary era did not fully solved the initial condition problem. Chaotic inflation, on the contrary, considered a field which did not lay necessarily in the minimum of its potential and thus a universe out of thermal equilibrium, but rather a random initial state which should lead to the same post inflation universe. Very often remained the so-called η-problem,[11] which was then solved by introducing a second scalar field or a phase transition to end inflation. A first order phase transition, initially considered [12] for instance by tunnelling from a false vacuum, generates bubble nucleation of true vacuum universe, whose coalescence and collision can reheat the universe, but would either not manage a graceful exit or generate different types of anisotropies. A second order phase transition with a second scalar field (as in hybrid inflation) avoids the bubble nucleation and may succeed in conforming with the data. More recently, supersymmetric or string theory inspired models emerged, suggesting modifications of General Relativity (GR) in higher energy scales within an effective theory of gravity [13], and providing many possible scalar fields. On a different note, the shape of the potential (namely exponential, power-law or any other specific description) can be used to describe which specific model of inflation is considered.

The interest of an effective theory framework is double. First, one can ignore the incompleteness of a theory and thus derive valid corrections to the known low energy theory. This is what is done when quantising GR to obtain quantum corrections, but also when modifying the Einstein-Hilbert action by hand, adding a priori some terms. The many possibilities resulting from such modifications may well be invalid or cause problems at higher energies, this does not affect the pragmatic, effective reasoning leading to valid corrections at current energies. Indeed, no one really expects such theories to consistently describe our universe up to the Planck scale, so the possible phenomenological manifestations of the theory can be used to constrain it or rule it out. The most well-studied set of such theories, known as $f(R)$ theories in which the linear Ricci scalar R is replaced in the action by any function f of it,

[11] The η-problem is due to chaotic inflation requiring large inflaton field values, (way) above the Planck scale $M_{\rm Pl}$. This can be seen as a large mass term for the inflaton and implies that the quantum corrections from renormalisation procedures might disrupt the inflation process itself, by introducing large yet ignored terms in the potential. The slow-roll is spoiled, generating a large value for the parameter η.

leads to a plethora of models, more or less constrained [14].

The second use lies in top-down approaches, where one knows a more UV complete theory and builds up a low energy version of it to confront it to phenomenology. The underlying theory, which may or may not be entirely formalised and well described, leads to an action, which can then be expanded in the low energy limit or simplified using additional assumptions. One can thus exploit this new effective action to study some observables, regardless of the fact that it does not encompass the whole theory or all the effects included in it. In this respect, a lot of work is done these days to derive string theory low energy effective actions, in particle physics. The point is to predict the future detections at the Large Hadron Collider if such theory is valid, and in particular the properties of superpartners that could soon be discovered. Similarly, string-inspired models of modified gravity are studied in order to explain or predict the cosmological phenomenology, from inflation to DM, as we will see further on.

One of the first attempts to realise all the features of successful inflation was Starobinsky's proposal [15], in which both the graceful exit and the initial condition issue were satisfactorily addressed, as we will explore in some more details further on. In addition, the realisation of hybrid models in extended theories, such as Grand Unified Theories (GUTs), Supersymmetric (SUSY) GUTs and brane inflation, produce some interesting features and will thus be also addressed here.

Starobinsky inflation

In order to obtain a theoretically motivated source for our scalar field potential, one may start from a modified Einstein-Hilbert action, treating GR and its extensions as an effective theory. These so-called $f(R)$-models, where the Ricci scalar R is replaced by any function f of R [16], yield

$$S_f = \int \mathrm{d}^4x \sqrt{-g}\, \frac{1}{2} M_{\mathrm{Pl}}^2 f(R) \ , \tag{1.39}$$

where $g = \det(g_{\mu\nu})$ and f is an arbitrary function of R. One can then perform the transformation $g_{\mu\nu} \to g^{\mathrm{E}}_{\mu\nu} = (1/f'(R))\, g_{\mu\nu}$, with $f'(R) = \mathrm{d}f(R)/\mathrm{d}R$. In this frame, the

Einstein frame,[12] the action reads

$$S_f^{\mathrm{E}} = \int \mathrm{d}^4x \, \sqrt{-g^{\mathrm{E}}} \left(\frac{1}{2} M_{\mathrm{Pl}}^2 \, R^{\mathrm{E}} - \frac{1}{2} g^{\mathrm{E}\,\alpha\beta} \, \partial_\alpha \chi \partial_\beta \chi - V(\chi) \right) \, , \tag{1.40}$$

where the subscript E refers to the Einstein frame and the scalar field[13] χ and its potential $V(\chi)$ are defined as

$$\chi = \sqrt{\frac{3}{2}} \, M_{\mathrm{Pl}} \, \ln(f'(R)) \tag{1.41}$$

$$V(\chi) = \frac{1}{2} M_{\mathrm{Pl}}^2 \, \frac{R \, f'(R) - f(R)}{f'^2(R)} \, . \tag{1.42}$$

One thus retrieves an action for the metric and a coupled scalar field, which can lead to an inflationary phase.

A specific example of such modified gravity induced inflation is called Starobinsky inflation and follows from adding in the action a higher order term of the Ricci scalar R, following quantum corrections considerations, yielding

$$S_{\mathrm{Staro}} = \int \mathrm{d}^4x \, \sqrt{-g} \, \frac{1}{2} M_{\mathrm{Pl}}^2 \left(R + \frac{R^2}{6M^2} \right) \, , \tag{1.43}$$

where M is an additional mass scale. One obtains

$$\chi = \sqrt{\frac{3}{2}} \, M_{\mathrm{Pl}} \, \ln \left(1 + \frac{R}{3M^2} \right) \tag{1.44}$$

$$V(\chi) = \frac{3}{4} M^2 M_{\mathrm{Pl}}^2 \left(1 - e^{-\sqrt{\frac{2}{3}} \frac{\chi}{M_{\mathrm{Pl}}}} \right)^2 \, . \tag{1.45}$$

One can notice that the effective potential is thus flat for large fields $\chi \gg M_{\mathrm{Pl}}$, with value $V \sim 3/4 \, M^2 M_{\mathrm{Pl}}^2$, allowing for a long enough inflation era. The number of e-folds is indeed $N \simeq 3/4 \, e^{\sqrt{\frac{2}{3}} \frac{\chi}{M_{\mathrm{Pl}}}} \sim 10^2$ for χ of the order of a few M_{Pl}. Similarly, one can compute the slow-roll parameters, obtaining $\epsilon \simeq 3/4N^2 \ll 1$ and $\eta \simeq -1/N \ll 1$, thus yielding $n_{\mathrm{s}} \simeq 1 - 2/N$. More accurately, $N \simeq 60$ implies $\chi \simeq 3.6 \, M_{\mathrm{Pl}}$ and leads to $n_{\mathrm{s}} \simeq 0.967$, $r \simeq 0.0033$. Starobinsky inflation thus passes all the theoretical and experimental tests.

[12] The phenomenology of the two frames, namely the Jordan and the Einstein frames, are identical since inflation in one frame is inflation in the other and the power spectra would be equivalent [17, 18].

[13] This χ is a field as long as f is not a linear function of R.

Note that several models with theoretical motivations lead to a Starobinsky-like inflation, the most well known of which being the Higgs inflation. In this case, the inflaton field is played by the Standard Model Higgs doublet and the action yields the usual "Mexican hat" Higgs potential as well as Higgs kinetic terms and a coupling term between the Higgs field and the curvature R in the form $h^2\,R$. The main issue is that this coupling has to be unexpectedly large to obtain successful inflation.

Hybrid and brane inflation

As mentioned, another type of inflation emerges from the use of several features from different independent models, called hybrid inflation. The first attempt [19] was to bring another scalar field in order to extend chaotic inflation, which remained unsatisfactory due to its so-called η-problem, as well as solve the issue of the graceful exit from first order phase transition. Indeed, one scalar field is slow-rolling, determining the duration of the inflationary era, to reach the bottom of its potential. This modifies the landscape for the second scalar field, which in turn rolls (most naturally rapidly) down its new potential. This triggering mechanism allows one scalar field to be responsible for the energy scale at which inflation takes place and thus for the expansion rate, while the other is determining the time scales. Said differently, the dominant contribution to the potential comes from a field, which is not slow-rolling but whose dynamics is set up by its interaction with the slow-rolling field.

Keeping Einstein's General Relativity as the background, one thus introduces two scalar fields, here denoted as φ and σ, and the potential

$$V(\sigma,\varphi) = \frac{1}{4\lambda}\left(M^2 - \lambda\sigma^2\right)^2 + \frac{1}{2}m^2\,\varphi^2 + \frac{1}{2}g^2\,\varphi^2\sigma^2 \tag{1.46}$$

where one might want to consider σ as the (Standard Model) Higgs field. In the rest of this section, we will thus call σ the Higgs while φ will be called the inflaton.

Interestingly, the effective mass of the Higgs is given here by $(-M^2 + g^2\varphi^2)$ while the quartic term $^1/_4\ \lambda\sigma^4$ keeps the field from rolling to infinite values. The symmetry is intact if $\varphi > \varphi_c = {}^M/_g$ as the only minima for the Higgs field is attained for $\sigma = 0$ (effective positive mass squared). Alternatively, if $\varphi < \varphi_c = {}^M/_g$, the potential exhibits its well known 'Mexican hat' shape, the symmetry is broken and the Higgs field lies in its symmetry breaking minimum at $\sigma = \sqrt{{}^1/_\lambda\,(M^2 - g^2\varphi^2)} > 0$.

Dynamically, in the symmetric case ($\varphi > \varphi_c$), because the acceleration of the Higgs is much greater than the inflaton's (due to the quartic term), the Higgs will quickly roll down to its minimum while the inflaton could remain large for a longer time. Under the assumption that $1/2\ m^2\varphi^2 \ll 1/4\lambda\ M^4$ (at least for $\varphi \lesssim \varphi_c$), the evolution of the fields in the intact symmetry potential is driven by the vacuum energy density term $1/4\lambda\ M^4$ rather than by the inflaton field (at least at the end of this phase, some time before the phase transition). Friedmann equation and the slow-roll assumptions (especially the form of ρ) imply that the Hubble parameter is given by

$$H^2 \simeq \frac{V}{3\,M_{\rm Pl}^2} \simeq \frac{M^4}{12\lambda\,M_{\rm Pl}^2} \tag{1.47}$$

and the universe in the symmetric phase exhibits an inflationary era (as in quadratic chaotic inflation).

Once the inflaton reaches its critical value φ_c, a phase transition occurs since the Higgs now has a negative mass term and should thus roll from $\sigma = 0$ to its new minimum. The equation of motion for the inflaton, given by Eq. (1.30c), allows to compute how φ varies from φ_c during one e-folding H^{-1} and thus the effective mass of the Higgs. The latter thus rolls rapidly towards its minimum while the effective potential for the inflaton is now becoming steep, allowing φ to rapidly roll down its potential in a time small compared to an e-folding, under additional assumptions such as $M \gg 12m$ and $\sqrt{\lambda} \sim g$. Inflation thus ends very quickly after the inflaton field reaches its critical value.

Interestingly, so-called brane inflation is very similar to hybrid inflation but gives a theoretical motivation for it. Indeed, string theory usually produces plenty of scalar fields called moduli fields from geometrical considerations on the extra dimensions, whether compactified or extended. These can play the role of the needed fields for inflation, which would acquire a theoretical backing as well as providing some knowledge on their evolution. One specific case of interest is realised by a brane-brane system, that are (usually) $3 + 1$ dimension objects evolving in a larger dimension universe referred to as the bulk. The interactions lead to a potential parametrised by the distance, in the extra dimension, between the branes, which plays the role of the slow-rolling inflaton field. Inflation ends with the collision of the branes, whose energy is then released and reheats the universe.

As we will see in more details in the following chapter, an interesting feature of these sceanarii lies in the production of extended one-dimensional topological defects called cosmic strings, whose cosmological consequences have been limited by

the observation of adiabatic anisotropies but whose astrophysical phenomenology exhibits several promising features.

1.3 Gravitational waves

Although some additional ingredients are needed to hold together all data on our universe, General Relativity (GR) remains, so far, the backbone of cosmology. It has been tested on local (Earth and Solar system) scales and in the weak limit up to high accuracy, as well as less precisely on the high velocities and stronger curvature limits, though not together. Still, one of the main predictions of GR which remained without any direct evidence until very recently is Gravitational Waves (GW). Fortunately, even before the extraordinary September, 14^{th} 2015 and December, 26^{th} 2015 direct detections [4], compact binaries inspirals and period shortening accounted for indirect proof of their existence, in particular since the discovery and measurements of PSR 1913+16 by Hulse and Taylor[14] from 1974 onwards [20]. In the decades to come, GW observations may provide remarkable new insights of our universe.

1.3.1 The weak-field approximation

Recall [21, Chapter 10] the Einstein-Hilbert action yields the Einstein equations

$$G_{\mu\nu} = 8\pi G\, T_{\mu\nu} \tag{1.48}$$

where the gravitational constant $8\pi G$ has been reintroduced, and the Einstein tensor and the stress energy tensor are defined as

$$G_{\mu\nu} \equiv R_{\mu\nu} - \frac{1}{2}\, g_{\mu\nu} R \tag{1.49a}$$

$$T_{\mu\nu} \equiv -2\frac{1}{\sqrt{-g}}\,\frac{\delta S_m}{\delta g^{\mu\nu}} \tag{1.49b}$$

with S_m the action describing matter.

Let us consider a perturbed metric $g_{\mu\nu} = \eta_{\mu\nu} + h_{\mu\nu}$ with $\eta_{\mu\nu}$ the flat metric and

[14] They received the Nobel Prize in 1993 for their discovery.

$|h_{\mu\nu}| \ll 1$ the perturbation of this flat metric. To first order in h, one thus has

$$\Gamma^{\lambda}_{\mu\nu} \simeq \frac{1}{2}\eta^{\lambda\alpha}\left(\partial_\mu h_{\alpha\nu} + \partial_\nu h_{\alpha\mu} - \partial_\alpha h_{\mu\nu}\right) \tag{1.50a}$$

$$\begin{aligned} R_{\mu\nu} &\simeq \partial_\alpha \Gamma^{\alpha}_{\mu\nu} - \partial_\nu \Gamma^{\alpha}_{\alpha\mu} \\ &\simeq \frac{1}{2}\left(\partial_\alpha \partial_\mu h^{\alpha}_{\ \nu} + \partial_\alpha \partial_\nu h^{\alpha}_{\ \mu} - \partial_\alpha \partial^\alpha h_{\mu\nu} - \partial_\mu \partial_\nu h^{\alpha}_{\ \alpha}\right) \end{aligned} \tag{1.50b}$$

$$R \simeq \partial_\alpha \partial_\beta h^{\alpha\beta} - \partial_\alpha \partial^\alpha h^{\beta}_{\ \beta} \tag{1.50c}$$

since the terms in $\Gamma\Gamma$ would yield subleading terms, of order h^2. Recall also that for consistent expansions to first order in h, one has to raise and lower indices using the zeroth order metric $\eta_{\mu\nu}$.

Now as in the electromagnetic case, one has some gauge freedom which needs to be fixed. Considering the coordinate transformation

$$x^\mu \to x'^\mu = x^\mu + \xi^\mu(x) \tag{1.51}$$

where $\partial_\mu \xi_\nu = \mathcal{O}(h_{\mu\nu})$ is the only restriction, the perturbation of the metric is transformed following

$$h'_{\mu\nu} = h_{\mu\nu} - \partial_\mu \xi_\nu - \partial_\nu \xi_\mu \ . \tag{1.52}$$

To fix this gauge freedom, let us choose the harmonic gauge

$$g^{\mu\nu}\Gamma^{\lambda}_{\mu\nu} = 0 \tag{1.53a}$$

leading to

$$\partial_\mu h^{\mu}_{\ \nu} = \frac{1}{2}\partial_\nu h^{\mu}_{\ \mu} \ . \tag{1.53b}$$

It is important to note here that if $h_{\mu\nu}$ does not satisfy Eq. (1.53b), one can consider the coordinate transformation with ξ_ν such that $\partial_\alpha \partial^\alpha \xi_\nu = \partial_\mu h^{\mu}_{\ \nu} - \frac{1}{2}\partial_\nu h^{\mu}_{\ \mu}$, which leads to a field $h'_{\mu\nu}$ satisfying the gauge constraint. One can safely consider from now on that the field $h_{\mu\nu}$ satisfies Eq. (1.53b). It yields

$$R_{\mu\nu} = -\frac{1}{2}\,\partial_\alpha \partial^\alpha h_{\mu\nu} \tag{1.54a}$$

$$R = -\frac{1}{2}\partial_\alpha \partial^\alpha h^{\beta}_{\ \beta} \tag{1.54b}$$

and hence to the field equation

$$\partial_\alpha \partial^\alpha h_{\mu\nu} - \frac{1}{2}\,\eta_{\mu\nu}\partial_\alpha \partial^\alpha h^\beta{}_\beta = -16\pi G\, T_{\mu\nu}\ . \tag{1.55a}$$

Equivalently, one can work with a traceless field, constraining $h^\beta{}_\beta = 0$. Then, the harmonic gauge is equivalent to the temporal gauge $\partial_\mu h^\mu{}_\nu = 0$. It leads to $R = 0$ and to the field equation

$$\partial_\alpha \partial^\alpha h_{\mu\nu} = -16\pi G\, T_{\mu\nu}\ , \tag{1.55b}$$

which is a wave equation sourced by $T_{\mu\nu}$. One important solution is given by the retarded potential

$$h_{\mu\nu}(\mathbf{x}, t) = 4G \int \frac{\mathrm{d}^3\tilde{\mathbf{x}}}{|\mathbf{x} - \tilde{\mathbf{x}}|}\, T_{\mu\nu}(\tilde{\mathbf{x}}, t - |\mathbf{x} - \tilde{\mathbf{x}}|)\ . \tag{1.56}$$

1.3.2 Polarisation modes

Let us first study the unsourced solutions, solutions of the equation

$$\partial_\alpha \partial^\alpha h_{\mu\nu} = 0\ , \tag{1.57}$$

interpreted as the plane waves coming in from infinity. They have the general form

$$h_{\mu\nu}(x^\alpha) = e_{\mu\nu}\, e^{ik_\alpha x^\alpha} + e^*_{\mu\nu}\, e^{-ik_\alpha x^\alpha} \tag{1.58}$$

where $e_{\mu\nu}$ is the symmetric polarisation tensor and k_μ is the wave vector. They must satisfy

$$k_\mu k^\mu = 0 \tag{1.59a}$$

$$k_\mu e^\mu{}_\nu = 0 \tag{1.59b}$$

for $h_{\mu\nu}$ to satisfy both the wave equation and the gauge constraint. Even with this constraint, there is still some gauge freedom. Indeed, let us consider a coordinate transformation with

$$\xi_\mu(x^\alpha) = i\xi_\mu\, e^{ik_\alpha x^\alpha} - i\xi^*_\mu\, e^{-ik_\alpha x^\alpha}\ . \tag{1.60a}$$

This leads to a change of the perturbation field $h_{\mu\nu}$ and the polarisation tensor $e_{\mu\nu}$ as in

$$h'_{\mu\nu}(x^\alpha) = e'_{\mu\nu}\, e^{ik_\alpha x^\alpha} + e'^{*}_{\mu\nu}\, e^{-ik_\alpha x^\alpha} \tag{1.60b}$$

$$e'_{\mu\nu} = e_{\mu\nu} + k_\mu \xi_\nu + k_\nu \xi_\mu \tag{1.60c}$$

with the gauge constraint still satisfied since $k^\mu e'_{\mu\nu} = k^\mu e_{\mu\nu} + k^\mu k_\mu \xi_\nu + k^\mu k_\nu \xi_\mu = 0$ (with the first term being null due to the gauge constraint, the second one due to the wave equation and the third one due to $e'_{\mu\nu}$ remaining traceless[15]).

One thus has different polarisation tensors, that is, different fields $h_{\mu\nu}$, representing the same physical situation whatever the value taken by the field ξ^μ. Of the $10 - 4 = 6$ degrees of freedom left so far by the symmetry and gauge constraints, 4 are again to be removed due to this remaining gauge freedom. This leads to only 2 physical degrees of freedom.

To illustrate this, let us consider a wave travelling along the z-axis with a wave vector

$$k^\mu = \begin{pmatrix} k \\ 0 \\ 0 \\ k \end{pmatrix} \tag{1.61}$$

which immediately satisfies Eq. (1.59a). Equation (1.59b) yields

$$e_{00} + e_{30} = e_{10} + e_{13} = e_{20} + e_{23} = e_{30} + e_{33} = 0 \tag{1.62a}$$

leading to only six independent degrees of freedom, chosen to be

$$e_{00}, \quad e_{10}, \quad e_{20}, \quad e_{11}, \quad e_{12}, \quad e_{22} \tag{1.62b}$$

while the four redundant components are given by $e_{33} = -e_{30} = e_{00}$, $e_{13} = -e_{10}$, $e_{23} = -e_{20}$. In addition, using the coordinate transformation mentioned in Eq. (1.60a) gives

$$e'_{00} = e_{00} - 2k\,\xi_0 \qquad e'_{01} = e_{01} - k\,\xi_1 \qquad e'_{02} = e_{02} - k\,\xi_2 \tag{1.62c}$$

$$e'_{11} = e_{11} \qquad e'_{12} = e_{12} \qquad e'_{22} = e_{22} \tag{1.62d}$$

[15] Indeed, $e^\mu{}_\mu = 0$ and $e'^\mu{}_\mu = e^\mu{}_\mu + 2k^\mu \xi_\mu$, leading to $k^\mu \xi_\mu = 0$ if one still requires a traceless field $h_{\mu\nu}$.

where $e'_{\mu\nu}$ and $e_{\mu\nu}$ should describe the same physical situation. This means that only e_{11}, e_{12} and e_{22} have a physical relevance. In other words, one can fix ξ_μ to cancel out all the $e'_{0\mu}$ components, leaving only three non-null components.

Finally, recalling we choose $h_{\mu\nu}$ traceless, one has $e_{11} = -e_{22}$, yielding two physically significant components, here e_{11} and e_{12}. They are the two polarisation modes of gravitational waves. One has just

$$e_{\mu\nu} = \begin{pmatrix} 0 & 0 & 0 & 0 \\ 0 & e_{11} & e_{12} & 0 \\ 0 & e_{12} & -e_{11} & 0 \\ 0 & 0 & 0 & 0 \end{pmatrix} . \tag{1.63}$$

To characterise these two modes in more detail, let us perform a rotation about the propagation direction. This leads to

$$e'_{\mu\nu} = R_\mu{}^\alpha R_\nu{}^\beta e_{\alpha\beta} \tag{1.64a}$$

$$\text{with} \quad R_\mu{}^\nu = \begin{pmatrix} 1 & 0 & 0 & 0 \\ 0 & \cos\theta & \sin\theta & 0 \\ 0 & -\sin\theta & \cos\theta & 0 \\ 0 & 0 & 0 & 1 \end{pmatrix} \tag{1.64b}$$

Considering only the significant components of $e_{\mu\nu}$, this rotation yields

$$\begin{cases} e'_{11} = \cos 2\theta\, e_{11} + \sin 2\theta\, e_{12} \\ e'_{12} = \cos 2\theta\, e_{12} - \sin 2\theta\, e_{11} \end{cases} \tag{1.64c}$$

$$\text{or} \quad \begin{cases} e'_+ = e^{+2i\theta}\, e_+ \qquad \text{where} \quad e_+ = e_{11} - ie_{12} \\ e'_- = e^{-2i\theta}\, e_- \qquad \text{where} \quad e_- = e_{11} + ie_{12} \end{cases} \tag{1.64d}$$

which means that one has two polarisation modes e_+ and e_-, of helicity ± 2.

The energy carried away by these waves can be computed using Einstein field equation Eq. (1.48), which we expand with respect to h up to order 2, yielding

$$T^h_{\mu\nu} \simeq \frac{1}{8\pi G}\left(\frac{1}{2}\eta_{\mu\nu}\, h^{\alpha\beta} R^{(1)}_{\alpha\beta} + R^{(2)}_{\mu\nu}\right) \tag{1.65a}$$

where again $R \equiv \eta^{\mu\nu} R_{\mu\nu} = 0$ (to all orders in h) and where $R^{(i)}_{\mu\nu}$ denotes the i^{th} order term in the expansion of $R_{\mu\nu}$ with respect to h. The first order equation is already satisfied by the full metric $g_{\mu\nu} = \eta_{\mu\nu} + h_{\mu\nu}$ (leading to the gravitational

waves), leaving only

$$T^h_{\mu\nu} \simeq \frac{1}{8\pi G} R^{(2)}_{\mu\nu} \tag{1.65b}$$

In order to compute $R^{(2)}_{\mu\nu}$ in its simplest form, the easiest is to average it over a spacetime volume of typical dimension large compared to the wavelength, or similarly to k^{-1}, removing all terms proportional to $e^{\pm 2ik_\mu x^\mu}$. In addition, one can use the gauge constraints without any loss of generality,[16] yielding the simple form

$$\langle\langle R^{(2)}_{\mu\nu} \rangle\rangle = \frac{1}{2} k_\mu k_\nu \, e^*_{\alpha\beta} e^{\alpha\beta} \tag{1.66}$$

and leading to

$$\langle\langle T^h_{\mu\nu} \rangle\rangle = \frac{1}{16\pi G} k_\mu k_\nu \, e^*_{\alpha\beta} e^{\alpha\beta} \ . \tag{1.67}$$

Performing again the coordinate transformation given in Eq. (1.60a), one obtains

$$e'^*_{\alpha\beta} e'^{\alpha\beta} = e^*_{\alpha\beta} e^{\alpha\beta} + 2|k^\alpha \xi_\alpha|^2 \tag{1.68}$$

describing again the same physical system and thus the same stress-energy tensor $\langle\langle T^h_{\mu\nu} \rangle\rangle$. This confirms that the energy and momentum of the gravitational waves are also determined by only two polarisation modes. One thus finally obtains the stress energy tensor of a gravitational wave with wave vector k^μ

$$\langle\langle T^h_{\mu\nu} \rangle\rangle = \frac{1}{16\pi G} k_\mu k_\nu \left(|e_+|^2 + |e_-|^2 \right) \ . \tag{1.69}$$

1.3.3 Generation of gravitational waves

Let us now compute the energy emitted in gravitational waves from a system whose energy-momentum tensor is known and can be decomposed in one Fourier component, in a sum of Fourier components or in a continuum of Fourier components (and

[16] Indeed, if one performs a coordinate transformation which would give a field configuration not satisfying the gauge constraint, the additional terms would actually cancel out in $\langle\langle R^{(2)}_{\mu\nu} \rangle\rangle$, leading to an unaltered $\langle\langle T^h_{\mu\nu} \rangle\rangle$.

thus expressed as a Fourier integral)

$$T_{\mu\nu}(\mathbf{x},t) = T_{\mu\nu}(\mathbf{x},\omega)\, e^{-i\omega t} + \text{c.c.} \tag{1.70a}$$

$$= \sum_{\omega} T_{\mu\nu}(\mathbf{x},\omega)\, e^{-i\omega t} + \text{c.c.} \tag{1.70b}$$

$$= \int_0^\infty \mathrm{d}\omega\, T_{\mu\nu}(\mathbf{x},\omega)\, e^{-i\omega t} + \text{c.c.} \tag{1.70c}$$

where c.c. represents the complex conjugate. In the first case (only one Fourier mode), the retarded potential takes the form

$$h_{\mu\nu}(\mathbf{x},t) = 4G \int \frac{\mathrm{d}^3\tilde{\mathbf{x}}}{|\mathbf{x}-\tilde{\mathbf{x}}|}\, T_{\mu\nu}(\tilde{\mathbf{x}},\omega)\, e^{-i\omega(t-|\mathbf{x}-\tilde{\mathbf{x}}|)} + \text{c.c.} \tag{1.71}$$

Let us now consider that the observer sits in the wave-zone, which is defined by a distance to the source $|\mathbf{x}|$ large compared to the typical size of the source R, to the (reduced) wavelength[17] of the gravitational wave $\frac{1}{\omega} = \frac{T}{2\pi}$ and to the mass angular momentum[18] ωR^2. One can thus perform the following approximation

$$|\mathbf{x}-\tilde{\mathbf{x}}| \simeq |\mathbf{x}| - \frac{\mathbf{x}\cdot\tilde{\mathbf{x}}}{|\mathbf{x}|} \tag{1.72}$$

which, up to first order, yields

$$h_{\mu\nu}(\mathbf{x},t) = 4G \int \frac{\mathrm{d}^3\tilde{\mathbf{x}}}{|\mathbf{x}|}\; T_{\mu\nu}(\tilde{\mathbf{x}},\omega)\, e^{-i\omega\left(t-|\mathbf{x}|+\frac{\mathbf{x}\cdot\tilde{\mathbf{x}}}{|\mathbf{x}|}\right)} + \text{c.c.} \tag{1.73a}$$

$$= 4G\, \frac{e^{i\omega(|\mathbf{x}|-t)}}{|\mathbf{x}|} \int \mathrm{d}^3\tilde{\mathbf{x}}\; T_{\mu\nu}(\tilde{\mathbf{x}},\omega)\, e^{-i\omega\left(\frac{\mathbf{x}\cdot\tilde{\mathbf{x}}}{|\mathbf{x}|}\right)} + \text{c.c.} \tag{1.73b}$$

$$= e_{\mu\nu}(\mathbf{x},\omega)\, e^{ik_\alpha x^\alpha} + \text{c.c.} \tag{1.73c}$$

where we used the fact that $|\mathbf{x}| \gg \frac{1}{\omega}$ to recognise the form of a plane wave, with a wave vector

$$k^0 = \omega\ , \qquad \mathbf{k} \equiv \omega\hat{\mathbf{n}} = \omega\, \frac{\mathbf{x}}{|\mathbf{x}|} \tag{1.74a}$$

[17] Here it is rather the (reduced) period, but since $c = 1$, these are equal.

[18] This simply relates to the typical angular velocity of the system being smaller than $c = 1$. Indeed, we already have $|\mathbf{x}| \gg R$, so assuming $|\mathbf{x}| \gg \omega R^2$ is equivalent to assuming $\omega R < 1$.

and a polarisation tensor

$$e_{\mu\nu}(\mathbf{x},\omega) \equiv \frac{4G}{|\mathbf{x}|} \int \mathrm{d}^3\tilde{\mathbf{x}}\ \ T_{\mu\nu}(\tilde{\mathbf{x}},\omega)\, e^{-i\mathbf{k}\cdot\tilde{\mathbf{x}}} \tag{1.74b}$$

$$\equiv \frac{4G}{|\mathbf{x}|}\, T_{\mu\nu}(\mathbf{k},\omega)\ . \tag{1.74c}$$

Note that since the stress-energy tensor $T_{\mu\nu}$ satisfies a conservation equation

$$\partial_\mu T^\mu_{\ \nu}(x^\alpha) = 0 \quad \Leftrightarrow \quad k_\mu T^\mu_{\ \nu}(k^\alpha) = 0\ , \tag{1.75}$$

the polarisation tensor defined above in Eq. (1.74b) satisfies the gauge constraint Eq. (1.59b).

In order to compute the emitted power in the form of gravitational waves per unit solid angle around the direction $\hat{\mathbf{n}}$, we can use the spacetime averaged value of the energy flux vector in gravitational waves $\langle\langle T^h_{i0}\rangle\rangle$, thus obtaining

$$\frac{\mathrm{d}P}{\mathrm{d}\Omega} = |\mathbf{x}|^2\ \hat{\mathbf{n}}_i \langle\langle T^{h\,i0}\rangle\rangle\ . \tag{1.76a}$$

This stress-energy tensor of gravitational waves can be expressed, using Eq. (1.67), in terms of the wave vector and polarisation tensor of the gravitational waves themselves, which in turn we can express in terms of the stress-energy tensor of the system generating the gravitational waves, following Eqs. (1.74). This yields

$$\frac{\mathrm{d}P}{\mathrm{d}\Omega} = \frac{|\mathbf{x}|^2}{16\pi G}\ \hat{\mathbf{n}}_i\, k^i k^0\, e^*_{\alpha\beta} e^{\alpha\beta} \tag{1.76b}$$

$$= \frac{G\omega^2}{\pi}\, T^*_{\alpha\beta}(\mathbf{k},\omega) T^{\alpha\beta}(\mathbf{k},\omega)\ . \tag{1.76c}$$

where the power emitted is expressed directly in terms of the stress-energy tensor of the source of gravitational waves.

In the more general case, that is, when the emitting system's stress-energy tensor is made up of a sum of Fourier components, one has to consider the most stringent, restrictive definition of the wave zone. This implies for instance that the longest period has to be considered when assuming $|\mathbf{x}| \gg \frac{1}{\omega}$. In addition, the perturbation field $h_{\mu\nu}$ will be a sum of plane waves, each with its own frequency. Consequently, the power emitted is a double sum over the pulsation ω, but due to the average over large spacetime volumes — large compared to the longest period — only the square terms remain while the cross terms vanish. One obtains a sum, for each ω, of terms

such as in Eq. (1.76c).

Similarly, in the case where the stress-energy tensor of the emitting system is a Fourier integral, the perturbation field $h_{\mu\nu}$ is an integral over ω of a continuum of plane waves while the power emitted in gravitational waves is a double integral over, say, ω and ω'. Given that the definition of the wave zone becomes slightly more difficult, due to ω running from 0 to ∞, let us compute the total energy emitted by integrating over time. One has a term in

$$\int_{-\infty}^{\infty} \mathrm{d}t\, e^{-i\omega t} e^{i\omega' t} \tag{1.77a}$$

which is exactly the Dirac delta function; it is thus replaced by

$$2\pi\, \delta(\omega - \omega') \ . \tag{1.77b}$$

We obtain

$$\frac{\mathrm{d}E}{\mathrm{d}\Omega} = 2G \int_0^{\infty} \mathrm{d}\omega\, \omega^2\, T^*_{\alpha\beta}(\mathbf{k}, \omega) T^{\alpha\beta}(\mathbf{k}, \omega) \ . \tag{1.78}$$

Before going further, one might want to rewrite $T^*_{\alpha\beta}(k^\mu)T^{\alpha\beta}(k^\mu)$ using only the spatial components of the stress-energy tensor. One would need relations between its various components, such as in the momentum space version of Eq. (1.75) which yields

$$T_{0i} = -\hat{k}^j\, T_{ji} \tag{1.79a}$$

$$T_{00} = \hat{k}^i \hat{k}^j\, T_{ji} \tag{1.79b}$$

where $\hat{\mathbf{k}} \equiv {}^1\!/\!_\omega\, \mathbf{k}$ is the normalised wave vector. One obtains

$$T^*_{\alpha\beta}(\mathbf{k}, \omega) T^{\alpha\beta}(\mathbf{k}, \omega) = \Lambda_{ijlm}(\hat{\mathbf{k}})\ T^{ij*}(\mathbf{k}, \omega) T^{lm}(\mathbf{k}, \omega) \tag{1.80a}$$

$$\text{with} \qquad \Lambda_{ijlm}(\hat{\mathbf{k}}) = \hat{k}_i \hat{k}_j \hat{k}_l \hat{k}_m + \delta_{ij}\delta_{lm} - 2\hat{k}_j \hat{k}_m \delta_{il} \tag{1.80b}$$

which can then be used in Eq. (1.76c) and (1.78), and in what follows.

1.3.4 Quadrupole moment

Let us now use another approximation, namely that the angular velocities (so far only assumed to be physical, that is, $\omega R < 1$) are small $\omega R \ll 1$. This is equivalent to assuming that the typical radius of the source R is small compared to the

wavelength of the gravity waves $\frac{1}{\omega}$.

This approximation allows us to simplify the Fourier transform of the stress-energy tensor $T_{\mu\nu}(\mathbf{k},\omega)$, defined in Eq. (1.74c), by a $\mathbf{k}$-independent integral, yielding

$$T_{\mu\nu}(\mathbf{k},\omega) \equiv \int \mathrm{d}^3\tilde{\mathbf{x}}\ \ T_{\mu\nu}(\tilde{\mathbf{x}},\omega)\, e^{-i\mathbf{k}\cdot\tilde{\mathbf{x}}} \simeq \int \mathrm{d}^3\tilde{\mathbf{x}}\ \ T_{\mu\nu}(\tilde{\mathbf{x}},\omega)\ , \tag{1.81}$$

since $\mathbf{k}\cdot\tilde{\mathbf{x}} \lesssim \omega R \ll 1$. The Fourier transform of the conservation law given in Eq. (1.79b) is

$$\partial_i\partial_j T^{ij}(\mathbf{x},\omega) = -\omega^2 T^{00}(\mathbf{x},\omega)\ . \tag{1.82}$$

Recall the quadrupole moment is defined by

$$D_{ij}(\omega) \equiv \int \mathrm{d}^3x\, x^i x^j\, T^{00}(\mathbf{x},\omega) \tag{1.83a}$$

$$D_{ij}(t) \equiv \int \mathrm{d}^3x\, x^i x^j\, T^{00}(\mathbf{x},t) = \int_0^\infty \mathrm{d}\omega\, D_{ij}(\omega)\, e^{-i\omega t} + \text{c.c.} \tag{1.83b}$$

After multiplying the conservation law by $x^i x^j$, integrating over space and using the approximation given in Eq. (1.81), one obtains the following spatial part of the stress energy tensor

$$T_{ij}(\mathbf{k},\omega) \simeq -\frac{\omega^2}{2}\, D_{ij}(\omega)\ . \tag{1.84}$$

This is very useful since the quadrupole moment of a system is quite simple to evaluate as it depends only on the energy density of the system (not on the flux or strain) and on the frequency mode ω (not on the wave vector).

The power per solid angle emitted for a single frequency is thus given by

$$\frac{\mathrm{d}P}{\mathrm{d}\Omega} = \frac{G\omega^6}{4\pi}\, \Lambda_{ijlm}(\hat{\mathbf{k}})\ D^*_{ij}(\omega) D_{lm}(\omega) \tag{1.85a}$$

which can be integrated over solid angle since the quadrupole moment is direction independent. Using spatial symmetries, one obtains the power emitted for a monochromatic source

$$P = \frac{2G\omega^6}{5}\left(D^*_{ij}(\omega)D_{ij}(\omega) - \frac{1}{3}\left|D_{ii}(\omega)\right|^2\right)\ . \tag{1.85b}$$

For a source which is a sum of discrete Fourier components, these are summed over all the discrete modes to obtain the full power radiated. Similarly, for a source which

is a Fourier integral, the energy emitted per solid angle is given by

$$\frac{\mathrm{d}E}{\mathrm{d}\Omega} = \frac{G}{2}\,\Lambda_{ijlm}(\hat{\mathbf{k}}) \int_0^\infty \mathrm{d}\omega\,\omega^6\, D^*_{ij}(\omega) D_{lm}(\omega)\ . \tag{1.86a}$$

which can in turn be integrated over solid angle to yield

$$E = \frac{4\pi G}{5} \int_0^\infty \mathrm{d}\omega\,\omega^6 \left(D^*_{ij}(\omega) D_{ij}(\omega) - \frac{1}{3}\left|D_{ii}(\omega)\right|^2 \right)\ . \tag{1.86b}$$

Note that even though we can choose $h_{\mu\nu}$ to be traceless, which leads to $T_{\mu\nu}$ traceless as well, we cannot say anything about T_{ii} nor D_{ii}. One should then be careful when using the formulae above as they might be sensitive to specific choices.

1.4 Gravitational lensing

One might also want to look at lensing, which provides information about DM, inhomogeneities of the universe and gravity itself.

Gravity, by deflecting trajectories or by bending spacetime, allows lensing effects by massive objects. Even Newton's law of gravity can explain the deviation of a photon, allowing its mass to be infinitely small but not null. Indeed, the equivalence principle, which states that the inertial mass and the gravitational mass are the same, holds in both Newton's and Einstein's laws. It implies that the trajectory of a test particle within the gravitational potential of a massive object does not depend on this test particle's mass, with the caveat that this mass should not be zero in Newton's formulation. Still, the two theories differ here on the angle of deflection caused by a static mass, as we will quickly explain below to review the physical processes at stake.

1.4.1 According to Newton

Recall Newton's law of gravity

$$\mathbf{F}_\mathrm{G} = -G\,\frac{Mm}{r^3}\,\mathbf{r} \tag{1.87}$$

where $\mathbf{F}_\mathrm{G}$ is Newton's gravitational force, G is (Newton's) gravitational constant, being here reintroduced, M and m are the masses of the static (heavy) object and of the test particle travelling in the former's gravitational potential, r is the radial

distance and $\mathbf{r}$ the radial centrifugal vector between the centres of mass. Associated with the Newton's second law of motion, which states

$$\Sigma\,\mathbf{F}_{\text{ext}} = m\mathbf{a}\ , \tag{1.88}$$

one obtains the acceleration of the test particle

$$\mathbf{a} = -G\,\frac{M}{r^3}\,\mathbf{r} \tag{1.89}$$

which, again, does not depend on its own mass and is thus valid in the limit of an almost massless photon. In spherical coordinates (r, θ, ϕ)[19] and assuming — with no loss of generality — that $\phi = \pi/2$, the kinematics give

$$\mathbf{a} = (\ddot{r} - r\dot{\theta}^2)\,\mathbf{u}_r + (r\ddot{\theta} + 2\dot{r}\dot{\theta})\,\mathbf{u}_\theta \tag{1.90a}$$

where the dot is a shorthand for derivation with respect to time and $(\mathbf{u}_r, \mathbf{u}_\theta, \mathbf{u}_\phi)$ is the direct orthonormal basis associated with the spherical coordinates (r, θ, ϕ). These yield

$$r\ddot{\theta} + 2\dot{r}\dot{\theta} = 0 \qquad \Leftrightarrow \qquad \frac{\mathrm{d}}{\mathrm{d}t}\big(r^2\dot{\theta}\big) = 0 \tag{1.90b}$$

$$\ddot{r} - r\dot{\theta}^2 = -G\,\frac{M}{r^2} \tag{1.90c}$$

The first equation implies that $r^2\dot{\theta}$, the angular momentum, is a constant. Its value can be determined at the closest approach to the heavy mass, denoted by r_0, recalling that $\dot{r} = 0$ at this point, meaning that the velocity is simply $r\dot{\theta}$. Assuming that the velocity at the closest approach is equal to c (and neglecting all relativistic considerations for now), one has $L = r^2\dot{\theta} = r_0 c$.

For the second equation, performing the change of coordinates $u = 1/r$ gives $\dot{\theta} = L\,u^2$ and $\ddot{r} = -L^2\,u^2\,\frac{\mathrm{d}^2u}{\mathrm{d}\theta^2}$.[20] Hence the second of the above equations, Eq. (1.90c)

[19] Spherical coordinates with r the radial distance, θ the azimuthal angle and ϕ the polar angle.

[20] Using $\frac{\mathrm{d}^2u}{\mathrm{d}\theta^2} = \frac{\ddot{u}}{\dot{\theta}^2} - \frac{\dot{u}\ddot{\theta}}{\dot{\theta}^3}$, $\dot{u} = -\frac{\dot{r}}{r^2}$ and $\ddot{u} = -\frac{\ddot{r}}{r^2} + \frac{2\dot{r}^2}{r^3}$, and $\dot{L} = 2\dot{r}r\dot{\theta} + r^2\ddot{\theta} = 0$, one has $-L^2u^2\frac{\mathrm{d}^2u}{\mathrm{d}\theta^2} = -r^2\dot{\theta}^2\left(\frac{\ddot{u}}{\dot{\theta}^2} - \frac{\dot{u}\ddot{\theta}}{\dot{\theta}^3}\right) = -r^2\left(\frac{-\ddot{r}}{r^2} + \frac{2\dot{r}^2}{r^3} - \left(\frac{-\dot{r}}{r^2}\right)\frac{\ddot{\theta}}{\dot{\theta}}\right) = \ddot{r} - \frac{\dot{r}}{L}\frac{\mathrm{d}L}{\mathrm{d}t} = \ddot{r}$.

yields

$$\frac{\mathrm{d}^2u}{\mathrm{d}\theta^2} + u = \frac{GM}{(r_0c)^2} \tag{1.91a}$$

$$\Rightarrow \quad u(\theta) = \left(\frac{1}{r_0} - \frac{GM}{(r_0c)^2}\right)\cos\theta + \frac{GM}{(r_0c)^2} \tag{1.91b}$$

where the cosinus prefactor has been determined using again the closest approach since at this point $u = 1/r_0$ and $\theta = 0$. The resulting trajectory, given by

$$r(\theta) = \frac{(r_0c)^2}{GM}\,\frac{1}{1 + \left(\frac{r_0c^2}{GM} - 1\right)\cos\theta}\ , \tag{1.92}$$

is, as anticipated, a conic section which in most cases turns out to be a hyperbola. Note that parabolic and elliptic path can be obtained if the eccentricity, here equal to $\frac{r_0c^2}{GM} - 1$, becomes respectively equal to or smaller than 1, that is, for very large mass M.

The deflection angle $\Delta\theta$ is thus given by the difference of direction of the two infinite limits of this hyperbolic path, up to π the angle obtained in case of no deviation. Denoting by $\theta_\pm$ the angles such that

$$\lim_{\theta\to\theta_\pm} r(\theta) = \pm\infty \tag{1.93a}$$

$$\Rightarrow \quad \theta_\pm = \pm\arccos\left(\frac{1}{1 - \frac{r_0c^2}{GM}}\right) \simeq \pm\left(\frac{\pi}{2} + \frac{GM}{r_0c^2} + ...\right) \tag{1.93b}$$

This gives the (Newtonian first order approximation of the) total deflection angle

$$\Delta\theta = (\theta_+ - \theta_-) - \pi \simeq \frac{2GM}{r_0c^2}\ . \tag{1.94}$$

1.4.2 Following Einstein's law

In Einstein's description of gravity in which deflection is due to the deformation of spacetime around the massive static object, the formalism is quite different and one should consider the Schwarzschild metric. Note that here, an exactly massless test particle behaves identically as an approximately massless one, such as the one used in Newton's description, and no discontinuity in the deflection angle occurs at $m = 0$. Here too we will assume — without loss of generality — that $\phi = \pi/2$. The

metric is thus given by

$$\mathrm{d}s^2 = g_{\mu\nu}\mathrm{d}x^\mu \mathrm{d}x^\nu = -\left(1 - \frac{2GM}{rc^2}\right) c^2\,\mathrm{d}t^2 + \left(1 - \frac{2GM}{rc^2}\right)^{-1} \mathrm{d}r^2 + r^2\,\mathrm{d}\theta^2 \tag{1.95}$$

yielding the null geodesic equation describing the path of a massless particle

$$0 = -\left(1 - \frac{2GM}{rc^2}\right) c^2\,\dot{t}^2 + \left(1 - \frac{2GM}{rc^2}\right)^{-1} \dot{r}^2 + r^2\,\dot{\theta}^2 \tag{1.96}$$

where the dot is a shorthand for derivation with respect to the affine parameter of the trajectory τ.

The conserved quantities that are energy and angular momentum, respectively associated with the coordinates t and θ (and with the respective Killing vectors), can be expressed as

$$E = \left(1 - \frac{2GM}{rc^2}\right) c^2\dot{t} \tag{1.97a}$$

$$L = r^2\dot{\theta}\ . \tag{1.97b}$$

Rewriting the geodesic equation using these quantities, one obtains

$$\frac{\dot{r}^2}{\dot{\theta}^2} = \frac{E^2 r^4}{c^2 L^2} - \left(1 - \frac{2GM}{rc^2}\right) r^2 \tag{1.98a}$$

$$\Rightarrow \quad \mathrm{d}\theta = \left[\frac{E^2 r^4}{c^2 L^2} - \left(1 - \frac{2GM}{rc^2}\right) r^2\right]^{-1/2} \mathrm{d}r\ . \tag{1.98b}$$

In order to obtain the deflection angle by integrating this out, one needs to evaluate the ratio $(L/E)^2$. First, one can use their definition, yielding

$$\frac{L^2}{E^2} = \frac{r^4}{\left(1 - \frac{2GM}{rc^2}\right)^2} \frac{\dot{\theta}^2}{c^4\dot{t}^2}\ . \tag{1.99a}$$

Using again the point of closest approach r_0, for which $\dot{r} = 0$, and the geodesic equation, which in such case states

$$0 = -\left(1 - \frac{2GM}{r_0 c^2}\right) c^2\,\dot{t}^2 + r_0^2\,\dot{\theta}^2\ , \tag{1.99b}$$

one gets

$$\frac{L^2}{E^2} = \frac{r_0^2}{\left(1 - \frac{2GM}{r_0 c^2}\right) c^2} \ . \tag{1.99c}$$

This can be introduced in Eq. (1.98b), which can also be rewritten using the parity of the path with respect to r (the path from $r \to -\infty$ to $r = r_0$ is the symmetric as the path from $r = r_0$ to $r \to +\infty$) and a change of variable $u = {}^{r_0}/_{r}$, yielding

$$\Delta\theta + \pi = 2 \int_0^1 \left[\left(1 - \frac{2GM}{r_0 c^2}\right) - u^2 \left(1 - \frac{2GM}{r_0 c^2}\, u\right) \right]^{-1/2} \mathrm{d}u \ . \tag{1.100}$$

One can first integrate the limit for $M \to 0$, which yields $\Delta\theta = 2\arcsin(1) - \pi = 0$ as expected; indeed, this is the deflection angle around a massless point, that is, in flat spacetime. For a massive central object, one can expand the integrand for small mass, that is, considering $\frac{2GM}{r_0 c^2} \ll 1$. It yields

$$\Delta\theta + \pi \simeq 2 \int_0^1 \left[\frac{1}{\sqrt{1-u^2}} + \frac{GM}{r_0 c^2} \frac{1-u^3}{\left(1-u^2\right)^{3/2}} + \mathcal{O}\left(\frac{G^2 M^2}{r_0^2 c^4}\right) \right]^{-1/2} \mathrm{d}u \tag{1.101}$$

$$\simeq 2 \left(\frac{\pi}{2} + \frac{2GM}{r_0 c^2} \right) \tag{1.102}$$

$$\Rightarrow \quad \Delta\theta \simeq \frac{4GM}{r_0 c^2} \ . \tag{1.103}$$

The General Relativistic (first order approximation of the) deflection angle is thus twice that from Newtonian's law.

Note that it is again only depending on the ratio of the Schwarzschild radius of the massive object $\frac{2GM}{c^2}$ by the closest approach distance r_0, which is at least equal to the size of the object. Following Newton's law, the assumption that this ratio would be small compared to 1 was *de facto* holding as otherwise General Relativistic corrections would be needed. In the GR case, one could argue that this ratio could approach 1 as the lensing object could *a priori* be anything and as r_0 tend to be close to the physical size of the object. In practice, this is not an issue since the lenses are often clusters or galaxies which, even if they could host a black hole or a very compact region in their centre, are surrounding this central densest region with dust and gas, which prevent photons from reaching us unaltered.

1.4.3 Another Dark Matter motivation

This deflection from a straight line was first verified, with some controversy on the accuracy of the measurement, in 1919 during a Solar eclipse and subsequently in multiple occasions with greater and greater accuracy. It is a very often used tool to measure the mass of lensing objects which alter the position, the shape and the number of images we receive from more distant objects, often galaxies or clusters. It is also more recently used in microlensing, that is, the use of weaker deformations of spacetime by lighter objects to detect and study them, which can be exoplanets, dwarf stars, neutron stars or black holes for instance. Finally, current more extensive surveys use lensing to measure, for different redshifts, the amount of massive cold matter in space, providing maps of the universe that surrounds us.

Lensing is also a very useful tool regarding some still ongoing controversies on DM and modified gravity models. Indeed, the measure of the rotation velocity of stars in galaxies showed a discrepancy with what one would expect considering the amount of visible matter (mainly stars but also hot gas) and the gravitational field it exerts. The suggestion, first made by Fritz Zwicky in 1933 and then a lot more accurately by Vera Rubin and Kent Ford from the 1960s, that some missing, invisible but massive matter would generate the observed acceleration lasted, in different forms, over the years. As in the search for an explanation of the irregular trajectory of Mercury,[21] alternatives, such as MOdified Newtonian Dynamics (MOND), suggested that the laws of dynamics and gravity have to be modified, at least on these scales. Studies on larger scales, such as galaxy clusters, proved the presence of additional matter to be able to explain at once these different phenomena, while lensing analyses helped to measure with greater accuracy the gravitational presence.

The best example in this battle on DM and on the power of lensing is the Bullet Cluster, a cluster of galaxies formed by the collision of two smaller ones. Indeed, this kind of objects can be observed in three independent ways: the internal dynamics of galaxies shows, using the Virial theorem,[22] how much mass is gravitationally bound; X-ray emissions by hot gas informs about the temperature and thus the pressure,

[21] At the end of the first half of the 19^{th} century, both Uranus and Mercury had unaccounted trajectories. In 1846, Urbain Le Verrier calculated the deviations of Uranus' path and deduced the position of Neptun, so far unknown, thus allowing its immediate discovery. He also thought some missing matter, some missing mass was perturbing Mercury and looked for it for decades, unsuccessfully. Indeed, the explanation was to be given by Albert Einstein who modified Newton's law of gravity with relativistic corrections, thus avoiding the need of a hidden mass.

[22] The Virial theorem states that, for a stable mechanical system made of many identical objects interacting via conservative forces, the (average of the) kinetic energy is related to the (average of

which, by balancing gravitational collapse, yields information about the mass there; gravitational lensing studies on different scales allow to measure again the mass profile, but assuming no prior knowledge on the dynamics. Interestingly, the Bullet Cluster, because of its collision history, seems to exhibit a case where DM and galaxies on one side, and baryonic matter in gas clouds on the other, split, due to the almost non-self-interacting nature of the former and to the efficient electromagnetic interactions in the latter. The (strong) lensing found two gravitational wells centred around the galaxies, even though most of the visible matter lies in the gas, supporting the presence of DM surrounding the galaxies. In addition, weak lensing analysis on the substructure of the cluster proved that the DM lies on the outskirts of the cluster, while the hot gas has been measured, using X-ray observations, to be in its centre.

What is currently known is that, if it exists, this DM has to be non-baryonic (i.e. unknown), cold (non-relativistic), electrically neutral and colour neutral, heavy and stable over cosmological timescales. As mentioned already, CMB precise measurements as well as many additional data (from sky surveys and structure formation analyses) not only confirm the need and the presence of DM, but also converge on the proportions with respect to baryonic matter. Finally, many models beyond the Standard Model provide promising candidates for DM particles, though so far with no robust experimental evidence. Yet, since there is not always an independent way to measure with similar accuracy the mass of the lens, alternatives to GR are still reasonable explanations to soften, if not solve, these tensions between observations and theories. Therefore, a vast amount of work is still being done on lensing in order to provide more hints on the DM scenario or on alternatives and extensions to GR, some of which are studied in what follows.

1.5 Extending General Relativity

General Relativity (GR) and the Standard Model provide a very solid background, extremely well theoretically studied and phenomenologically tested. Still, our experiences tell us that they cannot be unified as they are not complete from a high

the) potential energy. In the case of gravitational binding, one has

$$\langle\langle E_{\mathrm{K}}\rangle\rangle = -1/2\,\langle\langle E_{\mathrm{P}}\rangle\rangle \ .$$

This theorem mainly allows, in systems where the potential energy cannot be evaluated accurately, to use the knowledge of the kinetic energy, from temperature or dynamical considerations, to determine some of the binding forces parameters, such as the gravitational mass.

energy point of view. What is currently known about these two theories leads to incompatibilities and unanswered questions in cosmology. These include the initial conditions problems (inflationary scenarii can displace or reduce this issue but this is an extension), the baryon-antibaryon asymmetry, the cosmological constant problem and the dark sector issues, and the details of the formation of large scale structures in the universe.

Over the past centuries, there have been many attempts, successful or not, to broaden the scope of theories, to extend them, to unify them, to gather all natural phenomena within one unique framework. As a result, many extensions of GR have been studied in the last hundred years, the first of which being the five-dimensional attempt to reconcile Maxwell's electromagnetism with Einstein's theory. Similarly, the Standard Model arises from multiple unifications but plenty of extensions have been suggested and studied, such as supersymmetry, which relates bosonic and fermionic degrees of freedom, or additional dimensions as in string theories. Today two main sets of theories remain as possibilities for a UV completion of the laws of nature.

Unifications, these simplification processes in which *a priori* distinct phenomena are found to be linked, are built up by finding a common cause or by reducing the number of elementary bricks. Examples of the first mechanism include Newton's understanding of falling bodies and celestial mechanics using one same law, or Maxwell's description of all magnetic and electric phenomena under one set of rules. This idea used to try to unify the quantum and the relativistic worlds via the quantisation of gravitational degrees of freedom led to[23] loop quantum gravity and sister theories such as the recent group field theory. However, we will focus here on the alternative, namely string theories.

Indeed, looking for the second kind of unifications, namely the decrease in the number of elementary 'atoms' (that are, literally, unbreakable, undividable), one could go back as far as Aristotle's attempt to use the well known four elements or to the later preeminence of atomic theory, which led to Mendeleev's periodic table populated by about 60 different elements. More recently, the further developments in the 20^{th} century induced several breaking points of important reduction of the number of fundamental building blocks: the introduction of the electron, proton and neutron after the finding of many more chemical elements, then again the uncovering of the quarks following the discovery of numerous hadrons, finally resulting in the

[23]Because a naive quantum version of GR suffers non-renormalisability, one needs to develop a whole new theory in which this issue is addressed or a non-perturbative approach to quantum GR.

whole Standard Model. Today's elementary particle zoo was completed in the 2012 unearthing of the Higgs boson at the Large Hadron Collider, but many models predict an increase to come. Interestingly, sometimes the unification process leads to more fundamental elements to gather several phenomena under the same framework. Indeed, the identification of symmetries at high energy and the explanation for their low energy split come with the existence of additional particles, such as gauge bosons in the electroweak symmetry and symmetry breaking. In the same way, additional symmetries introduced in recent models might imply a larger number of elementary particles, as in supersymmetry, where at least twice as many are needed.

Simultaneously, the 1960s have seen the development of string theory — or should we say theories — in which all particles are the manifestation of a single one-dimensional object, reducing the number of elementary brick for nature to a symbolic 1 [22]. Since then, many issues and ideas came to lower and higher expectancies from this theory, which is now understood as M-theory, a $10+1$ dimensional theory populated by many objects (open and closed strings, branes of various dimension...) and whose low energy $9+1$ dimensional versions constitutes the five known superstring[24] theories. Depending on how one would lower the energy and the dimension by 1, one obtains different theories populated by different entities, providing a profusion of related models, which are all studied in various ways.

The specific features to justify our choices will not be covered in detail as this alone would require many chapters. Still, here we will focus on some peculiar manifestation of string theory where our $3+1$ universe is confined on a brane, which evolves within a $(3+d)+1$ dimensional bulk. First, our brane world cosmology leads to brane inflation and thus to a network of cosmic strings, providing with specific phenomenology, as in Chapter 2. In the second choice, the bulk is populated with point-like particles interacting with our brane universe as will be studied afterwards, in Chapter 3. In any case, Standard Model fields are open strings modes attached to the brane and thus confined to it, while the graviton is a closed string propagating in the whole bulk.

Finally, we will remind here that GR can be expressed, as any other theory, in the language of effective field theories. This implies that the theory is known to be incorrect at high energies (not UV complete) but follows known laws at low energies (namely Einstein's field equations) and some known corrections as energy increases. As shown in Section 1.2.5, Starobinsky inflation is a typical example of

[24]Indeed, supersymmetry has been a key element in the development and survival of string theories.

such framework where low curvature leads to the usual Einstein-Hilbert action and thus to GR, while larger curvatures produce correction terms which are yielding an inflationary era. Similarly, string theories often give a UV motivation for additional correction terms but until now the specifics are not fully known, which motivates an effective theory approach.

Chapter 2

Branes and strings

Cosmic strings and superstrings, even though not anymore expected to be a key component of our universe's evolution, could be the next opening towards new physics, beyond our standard models. They are believed to appear in many theories built to complement our current understanding of the universe, whether additional symmetries or more fundamental descriptions. Their evolution would leave signatures, enlightening on the specificities of the theories in which they come up. In particular, because they are highly relativistic, due to their compactness as well as their velocities, they are thought to emit gravitational waves (GWs), constantly, thus forming a stochastic background, as well as in bursts, potentially individually detectable.

In this chapter, we first present in Section 2.1, how such objects could be produced in the framework of brane world cosmologies, where our universe is not filling the whole available spacetime but is rather a smaller dimensional object, itself evolving within a larger dimensional bulk. In particular, the inflationary period that could result from brane collisions would almost generically generate a network of Cosmic (Super)Strings (C(S)S), with properties depending on the details of the model. We then discuss in Section 2.2, their properties, their evolution, the phenomenology they would lead to and the main differences between strings and superstrings. Finally, in Section 2.3 we focus on a specific setup in which a light string is stretched between two heavy, almost fixed ones, and study its periodic evolution. In particular, we evaluate the rate at which specific events, called cusps, during which a portion of the string momentarily reaches the speed of light $c = 1$, occur. They are thought to be important as they would emit large amounts of energy in the form of high frequency GWs, which themselves have been, for already more than a decade, one of the most promising new tools to study our universe.

2.1 Brane world cosmology

2.1.1 Brane inflation

Following the string theory picture, the paradigm[1] here admitted, as in Ref. [24], is that of a stack of $3+1$ dimension D-branes, one of which could play the role of our universe, on which evolve the Standard Model fields seen as various modes of open strings whose extremities lie on the branes. On the contrary, gravity and additional scalar fields (such as the dilaton) are propagated via closed string modes in the larger $(3+d)+1$ dimensional bulk, with $d = 6$. Depending on the specificities of the model, one can allow this brane either to be a solitonic field theoretic brane or a quantum state such as a D-brane, and the bulk can carry different manifold or orientifold structures. Also, Dp-branes with larger dimensions could be present at first, but the brane dynamics lead to their evaporation. In any case, the D3-branes sit on top of each other in the lowest energy state but may start more generically in any configuration.

In addition, let us denote by y_A the interbrane distance in the d bulk directions, or more basically by y either the norm of such d-vector or the distance in the one extended dimension of concern here, potentially after a rotation. We also denote by T_3 the brane tension, that is, the brane energy density regarding the 3 brane space dimensions. Furthermore, unless stated otherwise, we will assume that before the beginning of inflation, the different geometrical scalar fields are stabilised via some potential allowing a well of minimum energy, apart from the one driving inflation, obviously.

In this section, the super- or subscript (4) refers to effective $3+1$ dimensional brane realisation of some quantity[2] while (B) points to the $(3+d)+1$ dimensional whole bulk ones. When necessary, parameters of the additional d dimensions are denoted by (d).

Due to the propagation of gravity within the bulk, the effective experimental (reduced) Planck scale $M_{\rm Pl}^{(4)}$ is related to the bulk fundamental one $M_{\rm Pl}^{(\rm B)}$ by the volume of the d additional (extended) dimensions $V_{(d)} \sim R^d$ where R is the size of such dimensions, following

$$\left(M_{\rm Pl}^{(4)}\right)^2 = \left(M_{\rm Pl}^{(\rm B)}\right)^{d+2} V_{(d)} \ . \tag{2.1}$$

[1] See Ref. [23] for a full review of String Cosmology, in particular chapters 4 and 5.

[2] Later on, because we only refer to the $3+1$ dimension quantities, such as $M_{\rm Pl}$, this clarifying super- or subscript will no longer be necessary and will thus be omitted.

Similarly, one can tune the (effective $3+1$ dimension) cosmological constant $\Lambda_{(4)}$, which arises from

$$\Lambda_{(4)} = 2T_3 + \Lambda_{(\mathrm{B})} V_{(d)} + V(y) \ , \tag{2.2}$$

where $\Lambda_{(\mathrm{B})}$ is the bulk cosmological constant and $V(y)$ is a potential due to the brane-brane interactions. Several requirements are needed on the size of the additional dimensions and their stabilisation, in order not to spoil already satisfied features, such as Big Bang Nucleosynthesis (BBN), or not to overclose the universe, for instance with the overproduction of some particles after inflation, but these tend not to be very constraining [24].

From there, the evolution of the scale factor follows the Friedmann equations and the distance y is now a dynamical field which plays the role of the inflaton φ. Its energy density and pressure are, as seen in Eq. (1.29), described by the sum and difference of kinetic and potential energy terms, where the potential is here the one due to brane-brane interactions, namely $V(y) \equiv V(\varphi)$. To see that it is indeed flat apart around $\left(M_{\mathrm{Pl}}^{(\mathrm{B})}\right)^2 y \equiv \varphi = 0$, we need to consider the possible mechanisms of interactions.

First are the fields localised on the branes: when the branes are colocated, fields from different branes communicate with each other and participate in the vacuum energy; alternatively, when the branes are separated, the fields' interactions are very suppressed due to their confinement within the extremely thin (in the y direction) volume of the brane and the contribution thus decays (at least) exponentially. Because the potential is assumed attractive, we will consider that the contribution to the vacuum energy is negative; moreover, there must be some fine tuning from the additional constant terms such as the brane tension in order to realise $V(0) = 0$, which ends up being the usual cosmological constant issue, here left unresolved. This results in a zero contribution when the branes coincide, due to the cancellation of the brane tension with the negative energy from the interactions between fields located on each brane, and a positive remaining contribution from the brane tension alone when the branes are separated. This yields, denoting the effective thickness of the branes y_0, a term of the form $T_3(1 - e^{-y/y_0})$, or $T_3\left(1 - f\left(y/y_0\right)\right)$ since in place of the term e^{-y/y_0} one could have any function f of y/y_0 which decays faster for $y > y_0$.

Additionally, several processes happening in the bulk can take part in the potential. The exchange of bulk modes, whether massive or massless, induces as well an interaction which is suppressed at large distances, yielding a term of the form $e^{-my}\, y^{2-d}$ (or $\log y$ if $d = 2$) where m is the (possibly null) mass of the field con-

sidered. Finally, some strings can stretch between the branes, for instance seen as confined flux tubes, exerting a restoring force of the form ky, but this linear term can be ignored as k is proportional to the density of strings regarding the 3 dimension space brane volume, which is exponentially increasing during inflation thus washing out k.

Hence remains a potential of the form [24]

$$V(\varphi) \simeq T_3 \left[c_1 - f\Big(\frac{\varphi}{M}\Big) + \varphi^{2-d} \left(c_{2,i}\, e^{-\varphi/M_i} + c_3 \right) \right] \ , \tag{2.3}$$

where the constants c_1, $c_{2,i}$ and c_3 depend on the details of the model, as well as the explicit form of the function f as long as it decays at least exponentially; the masses M_i are related to the masses of the bulk modes m_i via $M_i = \left(M_{\rm Pl}^{(\rm B)}\right)^2 m_i^{-1}$, while M is a typical mass of the theory of the order of $T_3^{1/4}$. Deriving now the slow-roll parameters again yields constraints on the geometrical parameters of the theory which remain weak [24], thus allowing generically a successful inflationary period.

Note that the collision of the two branes considered here leads to reheating since the inflaton field, which is weakly coupled when the branes are separated, becomes increasingly coupled to the brane fields as these get closer, while it remains almost uncorrelated to the bulk fields, implying that the oscillations of the inflaton in its minimum reheat mainly the brane, as it should. In another similar kind of models where the set up is made of a brane-antibrane pair, developed after the KKLMMT model [25], it is the annihilation energy which is released and transferred to the SM particles, allowing for reheating.

Finally, it is interesting to recall that symmetries play an important role in hybrid or brane inflation scenarii. Indeed, as we mentioned, hybrid inflation is led by the inflaton field slowly rolling down a symmetry preserving (or normal phase) valley and ends when it reaches values for which a secondary field, so far lying in a false vacuum, is now out of equilibrium and rapidly shifts towards a new symmetry-breaking vacuum expectation value (ordered phase). In the brane case, the presence of two separate branes breaks the symmetry[3] of the system which is restored once the branes are overlapping. Alternatively, the gauge symmetries are present on each

[3]One can consider, for instance, either a $\mathbb{Z}_2$ symmetry on the brane, a translational invariance or, in the case of a stack of coinciding branes, the permutation between each of them. The first one means that, for an object approaching, crossing and then leaving the brane, the pre-crossing stages are symmetric to the post-crossing ones, or alternatively that the brane acts as a mirror; the existence of the other brane on one side only breaks this symmetry. The second symmetry is broken in the direction of the branes separation while the third is broken by the one brane aside.

brane as long as they remain separated, but only one symmetry group remains once the branes coincide or annihilate, yielding a symmetry-breaking scenario of the form $\mathbb{G} \times \mathbb{G} \to \mathbb{G}$ where $\mathbb{G}$ is the gauge symmetry group.

As explored in the following section, these symmetries and symmetry breaking interestingly lead to a rich phenomenology.

2.1.2 Strings formation

Phase transitions followed by Spontaneous Symmetry Breaking (SSB), occurring during the early stages of the evolution of the universe, can lead to topological defects [26]. While some, such as domain walls and monopoles, have to be avoided to fit with the observations, as they would quickly dominate the energy of the universe and spoil observations, cosmic strings, on the contrary, are not only acceptable but could even turn out useful to explain some features of the universe. Still, recall it has been shown that they cannot be the main source of anisotropies in the CMB, inflation being now thought to be the main source as it produces adiabatic ones.

Cosmic Strings (CS) are false vacuum remnants, that is solitonic extended objects containing a different phase than the rest of the universe, similarly to flux tubes in type II superconductors. The energy they carry is thus related to the energy scale of the symmetric phase, and hence of the symmetry breaking itself. They are thought to be generic [27] in supersymmetric (SUSY) Grand Unified Theories (GUT) frameworks where they are formed via the Kibble mechanism [28]. In this process, the topology of the vacuum manifold $\mathcal{M}$ is determining the presence of topological defects as well as their type.

Indeed, during a symmetry breaking of a group $\mathbb{G}$ to one of its subgroup $\mathbb{H}$, one should study the k^{th} homotopy group $\pi_k(\mathcal{M})$ of the vacuum manifold $\mathcal{M} \equiv \mathbb{G}/\mathbb{H}$, which is classifying the topologically distinct mappings between the k-sphere $\mathcal{S}^k$ and $\mathcal{M}$. Non-trivial k^{th} homotopy groups lead to $\bar{d}$-dimensional defects, where $\bar{d} = 4 - 1 - k$ (in a 4-dimensional spacetime). For instance a vacuum manifold made of disconnected elements, thus whose 0^{th} order homotopy group π_0 is not trivial, will induce 3-dimensional topological defects, namely domain walls; similarly, if $\mathcal{M}$ is not simply connected, that is if it contains loops which cannot be continuously shrunk to a point, then π_1 is not trivial and CS ($\bar{d} = 2$) form; alternatively, if $\mathcal{M}$ presents surfaces (respectively 3-spheres) which cannot be shrunk to a point, $\bar{d} = 1$ monopoles ($\bar{d} = 0$[4] defects, called textures) form.

[4] $\bar{d} = 0$ defects are punctual not only in all space directions but also in time, i.e. event-like.

It is important to remark that while we are here going to study only local CS from local, gauge symmetries, global CS can form as well. Their energy is contained in much larger distances (of the order of the horizon) and they experience long-range interactions. Besides, semi-local string interactions can lead to the formation of Y-junctions, which are of interest in the following. Finally, note that defects can be embedded in field theories with a trivial topology, but they are generally unstable and will thus be ignored too; similarly, we will not discuss further the case of superconducting strings, in which the electromagnetic gauge invariance is broken.

There exist a large variety of SUSY SSB scenarii depending on the large symmetry group $\mathbb{G}$ of the theory at high energies, which can in principle be anything as long as the Standard Model (SM) group $\mathbb{G}_{\rm SM} \equiv \mathrm{SU(3)_C} \times \mathrm{SU(2)_L} \times \mathrm{U(1)_Y}$ is satisfactorily embedded in it — that is provides the representations and the phenomenology of the SM particles. The inflationary paradigm is also contained in such scenarii since the several intermediate SSBs provide scalar fields and superpotentials, which achieve all necessary ingredients: a quasi-exponential expansion of the universe while it is in its unstable, false vacuum state; a graceful exit into the current, stable or meta-stable state; and the necessary reheating via the conversion of the false vacuum state's energy into thermal energy, to generate the particle content of today's universe.[5] Two types of hybrid inflation can be constructed, namely F-term and D-term inflations, depending on the choice of supersymmetry-breaking terms in the superpotential. While the former often leads to the so-called η-problem, where the inflaton field (as well as any scalar field) gets a mass of the order of the Hubble parameter H during inflation, the latter does not suffer from this issue but often requires the inflaton to roll on superplanckian distances, implying the need of a supergravity description. In any case, (F- or D-term) CS are generically formed at the end of inflation via the Kibble mechanism.

Alternatives are quantum string-inspired versions, namely Cosmic SuperStrings (CSS), for instance fundamental strings (F-strings) or one-dimensional Dirichlet branes (D1-branes or D-strings). Recall that in the string inspired, brane world framework, all SM particles are described as open strings ending on D3-branes[6] while the graviton and some scalar fields are closed string modes also evolving in the $d-3$ remaining dimensions (with $d=6$ for a $9+1$ dimensional bulk). As we

[5] The detailed study of such scenarii allows to either rule out or constrain them, by requiring successful inflation and production of particles with the observed properties, or by using CMB measurements such as high multipole anisotropies and non-gaussianities.

[6] Actually, the D-branes can have any $3 \leq p \leq 9$ dimension, the potential extra $\bar{p} = p-3$ one(s) being wrapped.

mentioned already, of the many scalar fields describing the geometrical features of the stack of branes (such as their distances), one can play the role of the inflaton. The field slowly rolls due to weak, long distance interactions and the annihilation or collision of the branes ends inflation.

Looking at the first case in more details, based on the explicit KKLMMT realisation [25], the production of CSS is due to what happens to the U(1) gauge symmetries present on each of the Dp-branes before such annihilation. Indeed, the process can be seen from a group point of view as a symmetry breaking $\mathrm{U}(1) \times \mathrm{U}(1) \to \mathrm{U}(1)$. The Kibble mechanism applies to the remaining U(1), which is a linear combination of the two initial U(1)'s and is coupled to the tachyonic field stretched between the branes which becomes unstable when the branes annihilate. It implies the formation of D-strings, or rather of D$(p-2)$-branes where p is the dimension of the brane-antibrane annihilating, with one of these $p - 2 = 1 + \bar{p}$ dimensions being extended, the additional $\bar{p}$ ones being wrapped. Additionally appear fundamental F-strings, which are the confined flux tubes of the U(1) symmetry which is broken, following again the Kibble mechanism. Other similar brane inflation scenarii can also lead to the formation of F- and D-strings [29, and references therein].

Finally, recall that stable bound states of F-strings and D-strings can be formed, leading to the emergence of Y-junctions [30]. As we will see in Section 2.3, these types of strings are thought to have generically cusps (points reaching temporarily the speed of light), especially in the case of a string stretched between two junctions [31].

Brane world cosmologies (via the multiple scenarii of symmetry breaking they offer, in particular at the end of brane inflation) as well as supersymmetric GUT thus suggest that one-dimensional topological defects could be a generic feature of our universe. Each specific model would lead, for the strings and their network, to peculiar properties and parameters' values, as will be explored in the next section.

2.2 Cosmic strings and cosmic superstrings

Cosmic strings or superstrings have been shown to be at least generic — if not unavoidable — features of most cosmological descriptions [27, 29, 32]. As we have seen, the former are solitonic, classical topological defects formed following the Kibble mechanism [28] during the (potentially several) Spontaneous Symmetry Breakings (SSB) which arise during the cooling history of our universe. The latter are ex-

tended quantum objects appearing in the context of supersymmetric string theories and brane inflation. Both are of interest for their genericity within some theoretical background and for the numerous phenomenological consequences on astrophysical and cosmological scales. In particular, networks of Cosmic (Super)Strings (C(S)S) participate to the energy budget of the universe, modify locally the spacetime background and thus produce lensing effects which can affect the CMB anisotropies and generate bursts of Gravitational Waves (GWs) during some specific phenomena [29, 33–40]. Their study is thus at the meeting point of cosmology and particle physics and involves such large energy scales, unreachable otherwise, giving a unique window of observations on the high energy symmetry breakings and the underlying theory of the universe.

In the following sections, we will discuss the dynamics of the C(S)S and of their network, as well as the common and different phenomenology emerging from CS and CSS.

2.2.1 The Nambu-Goto action

C(S)S are studied in the regime where their typical length scale is large compared to their thickness (but small compared to the Hubble radius) and therefore can be considered in a good approximation as one-dimensional extended objects. They thus span, through their evolution, a $1+1$ dimensional worldsheet which can be characterised by two parameters σ^a ($a = 0, 1$), with $\sigma^0 \equiv \tau$ being time-like and $\sigma^1 \equiv \sigma$ being space-like, yielding $x^\mu = X^\mu(\sigma^a) = X^\mu(\tau, \sigma)$. Note that x^μ relates to the spacetime coordinates while X^μ is a 4-vector function of the worldsheet coordinates which gives the four-dimensional equation of the worldsheet, but we might sometimes interchange one another in this chapter.

The strings follow the Nambu-Goto action [41, Chapter 6], [26] given by

$$S_{\rm NG} = -\mu \int \sqrt{-g^{\rm ind}}\, \mathrm{d}^2\sigma \ , \tag{2.4}$$

where $\mu \simeq M^2$ is the string tension (or linear mass density) and M is the energy scale of the symmetry breaking leading to the formation of strings, $g^{\rm ind} \equiv \det(g^{\rm ind}_{ab})$ with $g^{\rm ind}_{ab} \equiv g_{\mu\nu}\, x^\mu_{,a} x^\nu_{,b}$ the induced[7] metric on the worldsheet (again $a, b = 0, 1$) and $\mathrm{d}^2\sigma = \mathrm{d}\sigma^1\, \mathrm{d}\sigma^0 = \mathrm{d}\sigma\, \mathrm{d}\tau$.

Recalling that in this chapter, a dash denotes the derivative with respect to the

[7]For clarity, let us accept that $g_{\rm ind} \equiv g^{\rm ind}$ and $g_{ab\ {\rm ind}} \equiv g^{\rm ind}_{ab}$, hence $g^{-1}_{\rm ind} \equiv 1/g^{\rm ind}$.

spacelike worldsheet coordinate $X'_\mu \equiv {}^{\partial X_\mu}/_{\partial\sigma}$ while an overdot is with respect to the timelike one $\dot{X}_\mu \equiv {}^{\partial X_\mu}/_{\partial\tau}$, the determinant of the induced metric can be rewritten as

$$-g^{\text{ind}} = -(\dot{X})^2\,(X')^2 + (\dot{X}\cdot X')^2 \ , \tag{2.5}$$

where $(\dot{X})^2 \equiv \dot{X}^\mu \dot{X}_\mu$ and $\dot{X}\cdot X' \equiv \dot{X}^\mu X'_\mu$, these being 4-vectors.

Using $g_{\text{ind}}^{-1}\,\mathrm{d}g^{\text{ind}} = g_{\text{ind}}^{ab}\,\mathrm{d}g_{ab}^{\text{ind}}$, one can vary the action with respect to the spacetime coordinates $x^\mu = X^\mu(\sigma^a)$ to obtain the equation of motion for the string

$$X^\mu{}_{,a}^{\ ;a} + \Gamma^\mu_{\lambda\kappa}\, g_{\text{ind}}^{ab}\, X^\lambda_{,a} X^\kappa_{,b} = 0 \ , \tag{2.6}$$

where $\Gamma^\mu_{\lambda\kappa}$ is the Christoffel symbol[8] (from the full, four-dimensional metric). Note that here the covariant second derivative of the spacetime coordinates is

$$X^\mu{}_{,a}^{\ ;a} = \frac{1}{\sqrt{-g^{\text{ind}}}}\,\partial_a\Big(\sqrt{-g^{\text{ind}}}\, g_{\text{ind}}^{ab}\, X^\mu_{,b}\Big) \ . \tag{2.7}$$

Similarly, the string energy momentum tensor can be obtained by varying the action with respect to the metric, yielding

$$T^{\mu\nu}(x^\lambda) = \frac{\mu}{\sqrt{-g}} \int \sqrt{-g^{\text{ind}}}\, g_{\text{ind}}^{ab}\, X^\mu_{,a} X^\nu_{,b}\, \delta(x^\alpha - X^\alpha(\sigma^a))\, \mathrm{d}^2\sigma \ , \tag{2.8}$$

where δ is the (four-dimensional) Dirac function.

Choosing flat Minkowski spacetime as well as the conformal gauge

$$\dot{X}\cdot X' = 0 \qquad \text{and} \qquad (\dot{X})^2 + (X')^2 = 0 \ , \tag{2.9}$$

one can simplify the equation of motion to the two-dimensional wave equation. Additionally fixing the time gauge $\sigma^0 = t$, one can express the conformal gauge constraints and the equation of motion as a set of equations for the 3-vector position of the string, yielding

$$\dot{\mathbf{X}}\cdot\mathbf{X}' = 0 \tag{2.10a}$$

$$(\dot{\mathbf{X}})^2 + (\mathbf{X}')^2 = 1 \tag{2.10b}$$

$$\ddot{\mathbf{X}} - \mathbf{X}'' = 0 \tag{2.10c}$$

[8]The Christoffel symbols are defined following $\Gamma^\mu_{\lambda\kappa} \equiv {}^1\!/_2\, g^{\mu\alpha}\,(g_{\alpha\lambda,\kappa} + g_{\alpha\kappa,\lambda} - g_{\lambda\kappa,\alpha})$.

whose solutions are the superpositions of left- and right-moving arbitrary waves

$$\mathbf{X}(\sigma,t)=\frac{1}{2}\left(\mathbf{X}_+(\sigma_+)+\mathbf{X}_-(\sigma_-)\right)\ , \tag{2.11}$$

where we defined $\sigma_\pm\equiv\sigma\pm t$.

Note that the equations for the string can be easily interpreted as follows: the velocity and thus the movement is always perpendicular to the string itself, the (3-)velocity reaches 1 at singular points $\mathbf{X}'=0$ and in its own frame, the string acceleration is inversely proportional to the radius of curvature, meaning that a curved region of the string will tend to straighten itself. Transposed to the left- and right-movers, they imply $\left|\mathbf{X}'_+\right|^2=\left|\mathbf{X}'_-\right|^2=1$, where here the dash is the derivative with respect to the only variable, namely the lightlike $\sigma_\pm$, as in $\mathbf{X}'_\pm\equiv {}^{\mathrm{d}\mathbf{X}_\pm}\!/_{\mathrm{d}\sigma_\pm}$. Therefore, the 3-vectors $\mathbf{X}'_\pm$ lie on a unit (Kibble-Turok) sphere [42].

As we noticed already, some peculiar events might happen on the string, one of them being cusps which are points reaching momentarily the speed of light in vacuum. Indeed, $\dot{\mathbf{X}}=1$ implies as we said $\mathbf{X}'=0$, that is a null radius of curvature and thus an infinite straightening acceleration, immediately reducing the velocity below 1. In more details, one can look for the conditions for such event to occur in terms of the left- and right-movers on the string, using

$$\dot{\mathbf{X}}(\sigma,t)=\frac{1}{2}\left(\mathbf{X}'_+(\sigma_+)-\mathbf{X}'_-(\sigma_-)\right)\ . \tag{2.12}$$

Now for a loop, the periodicity of the coordinates as well as the condition $\left|\mathbf{X}'_\pm\right|^2=1$ imply that $\mathbf{X}'_+$ and $-\mathbf{X}'_-$ both describe closed loops on the unit sphere.[9] So when these two curves meet in $\mathbf{X}'_+(\sigma_+^{(\mathrm{c})})=-\mathbf{X}'_-(\sigma_-^{(\mathrm{c})})$, the velocity reaches $c=1$, following

$$\left|\dot{\mathbf{X}}(\sigma^{(\mathrm{c})},t^{(\mathrm{c})})\right|=\left|\frac{1}{2}\left(\mathbf{X}'_+(\sigma_+^{(\mathrm{c})})-\mathbf{X}'_-(\sigma_-^{(\mathrm{c})})\right)\right|=\left|\mathbf{X}'_\pm(\sigma_\pm^{(\mathrm{c})})\right|=1 \tag{2.13a}$$

$$\text{for}\quad \left(\sigma^{(\mathrm{c})},t^{(\mathrm{c})}\right)\equiv\left(\frac{1}{2}\left(\sigma_+^{(\mathrm{c})}+\sigma_-^{(\mathrm{c})}\right),\ \frac{1}{2}\left(\sigma_+^{(\mathrm{c})}-\sigma_-^{(\mathrm{c})}\right)\right)\ , \tag{2.13b}$$

where the superscript (c) refers to the cusp.

Discontinuities might also be obtained following string interactions. Indeed, even though not allowed in the zero-thickness description, field theoretic analyses, lattice

[9] As we will see further on in Section 2.3.1, additional periodicity or quasi-periodicity requirements also lead to such properties in the case of strings stretched between fixed junctions. For infinite strings, $\mathbf{X}'_\pm$ do not draw closed loops but do lie on the unit sphere.

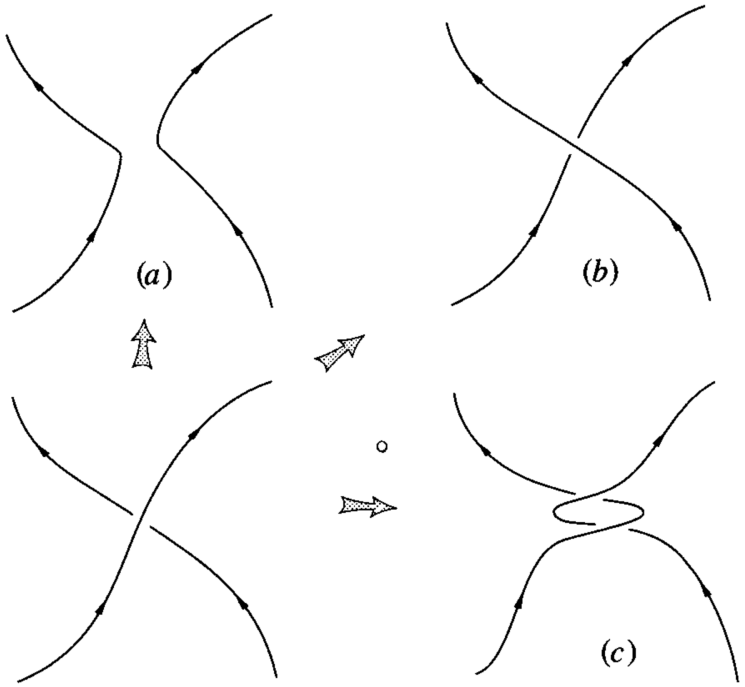

Figure 2.1: Three possible outcomes when strings intersect: (a) reconnect by exchanging legs, (b) passively pass through each other or (c) entangle. From [41, Figure 6.4].

simulations and string studies showed that under certain conditions, C(S)S of the same type have a non-null probability of exchanging legs when they intersect each other [26, 30, and references therein]. Indeed, the strings can either passively cross each other, get entangled as in some cases discussed further, or reconnect, as shown in Fig. 2.1. In the last case, the result of two strings meeting is thus two new strings with a kink, that is a discontinuity in $\dot{\mathbf{X}}$ and $\mathbf{X}'$ where the strings intersected. It is also possible to describe such event using the left and right movers description, in which a kink is a discontinuity in $\mathbf{X}'_{\pm}$ and thus leads to a gap on the curve drawn on the unit sphere. It is not actually a closed curve anymore and cusps, somewhat generic without any discontinuities [43], may become a lot easier to avoid. Note that string and superstring self-interactions lead to the production of loops, playing an important role in the evolution of the network, as well as the entanglement of two superstrings which can lead to junctions.

After giving the mathematical description of C(S)S, under the assumption that they can be treated as infinitely thin, one-dimensional objects, we will now focus on their gravitational phenomenology.

2.2.2 Phenomenology

C(S)S, because they carry an important energy density, can be substantial sources of different kinds of radiation. Most of them, such as Ultra High Energy Cosmic Rays (UHECR) and Gamma Ray Bursts (GRB), are model dependent because of the different gauge or global symmetries strings are related to, each symmetry implying different particle physics mechanisms and thus leading to different patterns in emissions. In addition, the inflationary and symmetry-breaking scenario influences the initial conditions of the network as well as its parameters, which themselves impact its evolution. This variability adds up to the complexity of the possible observations from C(S)S. However, this connection implies that any observation is shedding light on the favourable models, offering a potentially vast window on the underlying laws of nature, whether stringy or not. More importantly for us here and more generically is the gravitational emission. Indeed, because strings are relativistic, they emit GWs, whether in the form of loops or wavy long strings, in particular in high frequency bursts during three potential events: cusps, kinks, and reconnections or junctions.

First, let us recall that a straight C(S)S produces no gravitational force on its surrounding [41, Chapter 7], implying the local geometry is Minkowski, but still significantly impacts the global geometry which is conical. Indeed, there is a deficit angle in the azimuthal angle whose variations are limited from 0 to $2\pi\,(1-4G\mu)$, leading to specific lensing effects (with two similar images of a source) and discontinuous Doppler shifts (driven by the sudden deviation of the course of the source with respect to the observer as the string pass between them).

In addition, a network of strings can source the density anisotropies of the universe and hence the temperature anisotropies in the CMB, but as mentioned already, this would mainly lead to isocurvature modes, with a different structure in the power spectrum than the one observed, which favours adiabatic ones. C(S)S thus cannot be the main source of initial density anisotropies and of seeds of structure formation in the universe, while inflation has been shown to be very satisfactorily fitting the data. Still, a string network could lead to interesting polarisation patterns as well as high ℓ (that is small angular scales) contributions.

Finally, let us have a closer look at the GWs emissions from strings by first assuming that the gravitational field due to strings in motion is weak enough so that we can safely use the linearised Einstein's equations, apart in some small patches of

spacetime. Recall then that the GW equation is given by

$$\partial_\alpha \partial^\alpha h_{\mu\nu} = -16\pi G\, T_{\mu\nu} \ , \tag{2.14a}$$

whose retarded potential solution is

$$h_{\mu\nu}(\mathbf{x}, t) = 4G \int \frac{\mathrm{d}^3\tilde{\mathbf{x}}}{|\mathbf{x} - \tilde{\mathbf{x}}|}\, T_{\mu\nu}(\tilde{\mathbf{x}}, t - |\mathbf{x} - \tilde{\mathbf{x}}|) \ , \tag{2.14b}$$

while the energy momentum tensor of strings yields

$$T^{\mu\nu}(x^\lambda) = \mu \int \left(\dot{X}^\mu \dot{X}^\nu - X'^\mu X'^\nu \right) \delta(\mathbf{x} - \mathbf{X}(\sigma^a))\ \mathrm{d}\sigma \tag{2.15a}$$

$$= -\mu \int X_+^{\prime(\mu} X_-^{\prime\nu)}\, \delta(\mathbf{x} - \mathbf{X}(\sigma^a))\ \mathrm{d}\sigma \ , \tag{2.15b}$$

where the first line has been obtained using the conformal and time gauge conditions mentioned earlier in Eq. (2.9) and below, and the second one using the left- and right-movers decomposition. Note that the brackets indicate a symmetrisation in the indices, that is $X_+^{\prime(\mu} X_-^{\prime\nu)} = {}^1\!/_2 \left(X_+^{\prime\mu} X_-^{\prime\nu} + X_-^{\prime\mu} X_+^{\prime\nu} \right)$. Also, the minus sign appearing in front of the last line is consistent with positive energy density and depends on the sign convention (that is, defining the null worldsheet coordinates as $\sigma_\pm \equiv t \pm \sigma$ would have resulted in the opposite sign but the same physics).

Alternatively, using Fourier transform and Fourier decomposition [36], one can express the energy momentum tensor in momentum space as

$$T^{\mu\nu}(k^\lambda) = \frac{2\mu}{L} \int \left(\dot{X}^\mu \dot{X}^\nu - X'^\mu X'^\nu \right) e^{-ik_q \cdot X} \mathrm{d}^2\sigma \tag{2.16a}$$

$$= -\frac{2\mu}{L} \int X_+^{\prime(\mu} X_-^{\prime\nu)}\, e^{-\frac{i}{2} k_q \cdot (X_+ + X_-)} \mathrm{d}^2\sigma \ , \tag{2.16b}$$

where $L \equiv {}^E\!/_\mu$ is the average or invariant length of the (loop or piece of infinite) string, with E is its energy in its centre of mass frame and μ the tension, while we denote by $k_q^\mu \equiv (\omega_q, \mathbf{k_q}) \equiv \omega_q\,(1, \mathbf{n})$ the wave 4-vector of the plane wave in Fourier decomposition, defining the direction 4-vector $n^\mu \equiv (1, \mathbf{n})$ and the frequency $\omega_q \equiv q\,\bar{\omega} \equiv q\, {}^{4\pi}\!/_L$. Interestingly, one can separate the variables in the last formula

after a change of variables $(\sigma, t) \to (\sigma_+, \sigma_-)$, yielding

$$T^{\mu\nu}(k_q^\lambda) = T^{\mu\nu}(\omega_q, \omega_q \mathbf{n}) = \frac{\mu}{L} I_+^{(\mu} I_-^{\nu)} \tag{2.16c}$$

$$\text{with} \quad I_\pm^\mu \equiv \int X_\pm'^\mu(\sigma_\pm)\, e^{-\frac{i}{2} k_q \cdot X_\pm(\sigma_\pm)}\, \mathrm{d}\sigma_\pm \ , \tag{2.16d}$$

where we reintroduced the dependence on $\sigma_\pm$ for clarity.

Because cusps will be our main concern in terms of C(S)S phenomenology, let us apply this result to this specific case. First, one can show that the direction of highest energy emission is given by

$$l^\mu = (1, \mathbf{n}^{(\mathrm{c})}) \equiv X_+'^\mu(\sigma_+^{(\mathrm{c})}) = -X_-'^\mu(\sigma_-^{(\mathrm{c})}) \ . \tag{2.17}$$

In addition, after shifting the worldsheet coordinates origin to the cusp $\sigma_\pm^{(\mathrm{c})} \to 0$ as well as the spacetime ones to the cusp too $X^\mu(0,0) = X_\pm^\mu(0) = 0$, one can expand the left- and right-movers and their first derivative around the cusp following

$$X_\pm^\mu(\sigma_\pm) = l^\mu\, \sigma_\pm + \frac{1}{2} X_\pm''^\mu\, \sigma_\pm^2 + \frac{1}{6} X_\pm^{(3)\mu}\, \sigma_\pm^3 + \mathcal{O}(\sigma_\pm^4) \tag{2.18a}$$

$$X_\pm'^\mu(\sigma_\pm) = l^\mu + X_\pm''^\mu\, \sigma_\pm + \frac{1}{2} X_\pm^{(3)\mu}\, \sigma_\pm^2 + \mathcal{O}(\sigma_\pm^3) \tag{2.18b}$$

with higher order terms which will be ignored from now on and where the successive derivatives in the expansion $l^\mu \equiv \pm X_\pm'^\mu$, $X_\pm''^\mu$ and $X_\pm^{(3)\mu}$ are given at the cusp. The conformal gauge conditions, also called Virasoro conditions, yield $X_\pm'^2 = 0$. Differentiating this equation leads to $X_\pm' \cdot X_\pm'' = 0$ and to $X_\pm' \cdot X_\pm'^{(3)} = -X_\pm''^2$. Used to compute the exponential contraction, these give

$$l \cdot X_\pm(\sigma_\pm) = -\frac{1}{6} X_\pm''^2\, \sigma_\pm^3 \ . \tag{2.18c}$$

Finally, it can be shown that the leading term in $I_\pm^\mu$, coming from the integration of $l^\mu\, e^{-\frac{i}{2} k_q \cdot X_\pm}$, is non-physical and can be gauged away [36], so should be removed. In addition, the interesting part of the spectrum, for which the signal will not be drowned in the stochastic background emitted by each and every part of the string network [44], is the high frequency end, mainly produced by cusps[10] and highly relativistic regions of the string which are concentrated in a small patch around the

[10]Note that kinks and other specific points such as junctions, which mainly appear on CSS, can also emit high frequency GW Bursts (GWBs), but we will not consider these in details here, assuming that the cusps studied are far away from other emitting parts of the string.

cusp. It is thus possible to ignore most of the string in the integral and focus on a small interval around 0, as we will do numerically. On the contrary, one could integrate on the whole string or even on $\mathbb{R}$. These computations will anyway lead to the same behaviour in the high frequency limit, which is of interest to us here.

Considering the latter, one can analytically compute the high frequency behaviour of the energy momentum tensor carried by GWs emitted by cusps on a C(S)S and obtain [36]

$$T^{\mu\nu}(\omega_q, \omega_q \mathbf{n}^{(\mathrm{c})}) = -\frac{4^{7/3}\,\pi^2}{3^{2/3}\,\Gamma(1/3)^2}\,\frac{\mu}{L\,\omega_q^{4/3}}\,e^{i\omega_q t^{(\mathrm{c})}}\,\frac{X_+''^{(\mu}}{|X_+''|^{4/3}}\,\frac{X_-''^{\nu)}}{|X_-''|^{4/3}} \tag{2.19}$$

where Γ is Euler's function and $t^{(\mathrm{c})}$ is the arrival time of the (centre of the) burst, reintroduced by shifting the coordinate system back to the initial choice where the cusp does not lie at the origin. Most importantly, this means that the energy momentum tensor depends on the second derivative of the string position 4-vector at the cusp (again, the dependence on $\sigma_\pm^{(\mathrm{c})}$ has been hidden), on the tension and on the length, that is, on the energy of the string (as one could expect). In addition, it is proportional, for high frequencies, to the frequency to the power $-4/3$.[11]

Slower points on the string are also producing GWs but they lead to a spectrum which is suppressed in its high frequency part, compared to the cusp case. Indeed, in the exponential part of the integrals (2.16d), the linear term in the $\sigma_\pm$ expansion is cancelled due to the choice of the emission direction $k^\mu = \pm\,\omega_q\,X_\pm'^\mu(\sigma_\pm^{(\mathrm{c})})$. This can be achieved simultaneously in both integrals only if $X_+'^\mu(\sigma_+^{(\mathrm{c})}) = -X_-'^\mu(\sigma_-^{(\mathrm{c})})$, that is, at a cusp. In the case where the left- and right-movers derivatives $X_\pm'^\mu$ are not opposite to each other, one can only choose a direction of emission such that the linear term is cancelled out in the exponential of at most one of the integrals, thus leading, in the final expression for $T^{\mu\nu}$, to a power of the frequency ω_q larger (in absolute value) than $-4/3$. This means that the high frequency end of the spectrum is dominated by cusps[12] which produce Gravitational Wave Bursts (GWBs).

Still, one can wonder how the points around the cusp are participating in this burst. Indeed, physically, the region immediately surrounding the "one" point reaching the velocity of light is also highly relativistic, the left- and right-movers derivatives are there very close to satisfying $X_+'^\mu(\sigma_+^{(\mathrm{c})}) = -X_-'^\mu(\sigma_-^{(\mathrm{c})})$ and the energy released

[11] Similar analytical computations on kinks lead to a power spectrum high end proportional to the frequency to the power $-5/3$ [36].

[12] We will here ignore other peculiar points which can also lead to GWBs, namely kinks and junctions.

in high frequency GW might as well be considered as a part of the burst. Let us thus define *pseudo*cusps as points travelling at a velocity very close to 1 but not exactly, which will be present at least in the vicinity of cusps but a priori could also appear irrespectively of those. Indeed, one can imagine a situation where the curves described by $\mathbf{X}'_+$ and $-\mathbf{X}'_-$ on the unit sphere would not cross each other but rather come very close before moving apart: if they get close enough, the velocity could reach almost 1 at its local maximum and this region of the string could emit a burst, a priori weaker than an actual cusp's burst but maybe strong enough to significantly participate in the global high frequency emissions of the strings network. We will come back to this issue in the following of this chapter, in Section 2.3.

2.2.3 Differences between strings and superstrings

Now that we have looked at the common properties of C(S)S, and in particular at their common phenomenology, we will here review the main contrasting features which distinguish these objects and the consequences these have on their evolution.

Cosmic Strings (CS) are solitonic, classical objects. Their tension is set by M the energy scale of the phase transition which lead to their formation, $\mu \simeq M^2$. They can, when of the same type, exchange legs and form kinks when intersecting each other, and field theoretic computations have shown that $p_{\rm rec}^{\rm CS}$ the probability they do so is close to unity, thus yielding an approximately null probability of passively going through each other [26, 30].

In opposition, Cosmic SuperStrings (CSS) are extended, string theoretic, fully quantum objects. Their reconnection probability depends on their type as well as on the details of the model, such as the extra-dimensions compactification and moduli stabilisation schemes or the superpotentials. Still, string perturbation computations have shown that, in first approximation, these probabilities depend only upon two parameters, namely the string tension or string coupling $g_{\rm s}$, and the scale of the potential confining the strings within the extra-dimensions. For instance, fundamental strings generically reconnect with a probability $p_{\rm rec}^{\rm FF} \sim g_{\rm s}^2 \in [10^{-3}, 1]$, while D-strings reconnection probability, even though more complicated, have been evaluated to be within $p_{\rm rec}^{\rm DD} \in [10^{-1}, 1]$ [26].

In addition, CSS present several distinct types[13] which can form bound states via entanglement, as in the case (c) of Fig. 2.1. Indeed, when two superstrings of

[13] In some more complicated models, there can also be several types of CS which would present topological restrictions forbidding simple reconnections and allowing the formation of junctions.

different type meet, they cannot exchange legs but form a junction, which might then extend into a third type string. This leads to a composite (p, q)-string, made of the entanglement of p F-strings and q D-strings, joining two Y-junctions where three strings meet: the two initial strings and the new composite one. For example, a $(1, 1)$-string could be formed at a Y-junction between an F-string and D-string. More generally, a (p, q)-string meeting a (p', q')-string would form either a $(|p-p'|, |q-q'|)$-string or a $(p + p', q + q')$-string; for instance, in the specific case where say $q = q'$ and $p' = p - 1$, an F-string can be formed.

Similarly, the tension of CSS depends on the different parameters of the specific string model considered, but in first approximation it is mainly given by the Regge slope α', which is often taken to be $\alpha' \equiv M_{\rm s}^{-2}$, and by the string tension $g_{\rm s}$. For instance, in 10 flat dimensions, an F-string has roughly a tension $\mu_{\rm F} \simeq {}^{1}\!/_{2\pi\alpha'} \simeq {}^{M_s^2}\!/_{2\pi}$, a D-string presents $\mu_{\rm D} \simeq {}^{1}\!/_{2\pi\alpha' g_{\rm s}}$ while a (p, q)-string shows $\mu_{(p,q)} \simeq \mu_{\rm F}\sqrt{p^2 + {}^{q^2}\!/_{g_{\rm s}^2}}$ in first approximation [26].

These string features are important as they directly impact the way the network would evolve. A string network is allowed cosmologically (in opposition to monopoles and domain walls) thanks to reaching a scaling regime, in which it is scale invariant and can be described roughly by one parameter which grows with the horizon. This description has been extended to a three scale model [45] in which three different scales, all eventually scaling (that is growing with the horizon) are needed to describe the network: the interstring distance ξ, related to the energy density of the string network; the persistence length $\bar{\xi}$, indicating the scale of direction correlation along the string; and the small scale structure length ζ, giving the typical size of small loops produced by self-intersection and sometimes referred to as the wiggliness. The network is thus made of (eventually after a transient period) 'infinite' strings, of length larger than the horizon, and sub-horizon loops. While the energy in the first ones grows with time as their linear energy density μ is constant, the loops decay due to GWs and particle emissions and thus take away energy from the network, allowing for the system to scale. Numerical simulations[14] [46] in FLRW background have found the two first parameters to be of the same order while $\zeta \sim 10^{-2}\,\xi$, in the scaling regime in radiation and matter dominated eras, as also explored in [47] where gravitational backreaction have been considered.

The case of superstrings is somewhat similar but still more complex as the junc-

[14]Note that, unless stated otherwise, numerical simulations and even most analytical considerations neglect gravitational backreaction, which is assumed to have a limited impact on the main features of the networks and strings dynamics.

tions and the bound states influence these results. Indeed, it has first been shown by numerical simulations [48] that the CSS interstring distance scales as $\xi \propto \sqrt{p_{\rm rec}^{\rm CSS}}\, t$ and that the CSS energy density may be higher than the CS one but at most by one order of magnitude. In addition, the presence of long range interactions imposes the bound states to be short lived, leading to two almost independent networks, in which the small scale structure is enhanced by the temporary bound states. Alternatively, in the absence of these long range interactions, that is, in an only locally interacting network, the bound states play a more important role in the evolution [49]. Indeed, bound states generate another loss mechanism which is actually responsible for the scaling, as has been displayed in simulations [50]. Still, this numerical work shows that whatever the initial conditions and whether with or without bound states, the CSS network fully scales, that is, all its components (F-strings, D-strings and possible bound states) scale.

It is also worth noting that the reconnection probability influences greatly the amount of junctions and of kinks in the network. Indeed, once the scaling regime is reached, the distance between infinite strings goes like $p_{\rm rec}^{-1}$, meaning that the crossing of two strings goes like $p_{\rm rec}^{-2}$ and thus the number of successful reconnections is about $p_{\rm rec}^{-1}$. Hence more kinks but almost no junctions appear in CS networks, and few to very few kinks or reconnections but possibly many junctions form in CSS networks. In addition, as we mentioned earlier on in Section 2.2.1, the number of kinks might influence the number of cusps on a string since the former are discontinuities in the curves described by $\pm\mathbf{X}'_{\pm}$ on the unit sphere and the latter are crossing of these curves. Globally, this has an implication in the amount of GWs emitted since cusps, kinks, reconnections and junctions are important emitters of GW. Still, it has been proven that the most important of those are cusps, mainly because of the frequency dependence of the energy emitted [36], as shown for cusps in Eq. (2.19), cusps which are present on both CS and CSS. Note on that point that while it is widely acknowledged that CS generically present cusps, the question is still somehow open for CSS as details of the extra-dimensions influence may not have been perfectly understood [31, 51].

Additional thermodynamical considerations [26] have shown that this description, with infinite strings and loops, is valid for large enough energy densities in the CS network $\rho > \rho_{\rm H}$. The critical point, called the Hagedorn energy density $\rho_{\rm H}$ (related to the Hagedorn temperature), defines a phase transition where infinite strings appear. Indeed, for very low energy densities $\rho \ll \rho_{\rm H}$ (and large enough reconnec-

tion probabilities), long strings are very quickly chopped off in small sub-horizon loops of typical size $\sqrt{\mu}$ and no infinite string remains at equilibrium. Increasing ρ implies an increasing number of loops until the average distance between two of them is about their average length, that is, for $\rho \sim \rho_{\rm H} \simeq \mu^2$. Then, infinite strings become favourable at equilibrium, the energy density above $\rho_{\rm H}$ being allocated to them. Any increase in ρ leads to no more small loops but to a very slow increase in the number of long strings, which gather most of the energy density of the network.

The case of CSS is very similar as several tensions imply several Hagedorn energy densities, that is, several transitions. This can easily be understood as the light, low tension strings would be the first ones to be able, with the energy available, to form stable infinite strings and thus to perform a phase transition, while heavier, larger tension strings would remain in the gas of loops phase. Increasing the energy density further would allow forming these heavier infinite strings at a second critical point, thus allowing for all kind of strings and junctions.

After studying the formation processes of C(S)S in their different theoretical framework and before closing with their distinctive features, we looked at the (common) equations describing their evolution and phenomenology. In particular, we focused on the GW emissions from cusps, these points temporarily reaching the speed of light, highlighting the interest for these events regarding the high frequency end of the GW spectrum.

2.3 Cusps and pseudocusps on strings between Y-junctions

In this section [52],[15] we study the occurrence of cuspy events on a light string stretched between two Y-junctions with fixed heavy strings, during its periodic non-interacting evolution. We consider the specific configuration of two equal tension, heavy strings linked by a light string, which can easily be achieved for instance in the $g_{\rm s} \ll 1$ limit, where $\mu_{(1,1)} \simeq \mu_{\rm F}\sqrt{1+{}^1\!/_{g_{\rm s}^2}} \simeq {}^{\mu_{\rm F}}\!/_{g_{\rm s}} \simeq \mu_{\rm D} \gg \mu_{\rm F}$. As explained in the following, mainly in Section 2.3.1 and Appendix A, the conclusions drawn in such case can be generalised to realistic strings configurations under certain circumstances which we also discuss in such sections.

We first present an analytic study where, after looking at the periodicity requirements and symmetries on the string, in order to allow for a Fourier decomposition,

[15]The material of this section has been published in a very similar form in [52].

we give a solid criterion to discriminate between cuspy and noncuspy string configurations. Our study then draws a link between waves and cuspy phenomena on the string, where by cuspy phenomena we mean both cusps and *pseudocusps*. Recall that the former are points on the string reaching temporarily the speed of light $c = 1$. The latter are highly relativistic configurations close to cusps but reaching a velocity between 10^{-3} and 10^{-6} below c. We then describe our numerical simulation, built to draw a specific string and to subsequently compute the number of cusps and pseudocusps within a period of non-interacting evolution, in order to test our analysis. This numerical investigation allows us to look at the correlations between the string network's parameters and the occurrence of cuspy phenomena and we show that the presence of large-amplitude waves on the light string leads to cuspy events. We then relate the occurrence of cuspy events to features like the number of vibration modes on the string or the string's root-mean-square velocity.

2.3.1 General set up

Recall that stable bound states of F-strings and D1-branes (or D-strings) can be formed, leading to the emergence of Y-junctions [30]. These junctions can also appear in the context of semi-local string interactions. These types of strings are thought to have generically cusps, especially in the case of a string stretched between two junctions [31], but more details are needed, as can be understood from the open debate on this question [51]. Here, we start with a simplified and idealised version of such a configuration in order to look at the parameters influencing the occurrence and number of cusps.

The Y-junction configuration we will study is thus again made of two heavy strings connected via a light string. Hence, without loss of generality, we consider the heavy strings to be of equal tension.[16] So in what follows, we have two tensions: the tension of the heavy strings μ_h and that of the light string μ_ℓ.

We here consider the two heavy strings in the xz-plane, oriented along the z-axis and then tilted by an angle $\pm\Psi$ with respect to the z-direction (see Fig. 2.2) and spaced out by a distance Δ. The heavy strings are considered heavy enough to be at rest at least for a time longer than the time scale of the light string's movement. This implies either that the heavy string's tension is very large (at least two orders of magnitude) compared to the light string's one, or at least that the time scale of

[16]The formation of a junction depends on various parameters, such as the collision velocity and the tensions. However, once the junction is formed, the tensions will not influence the dynamics [53].

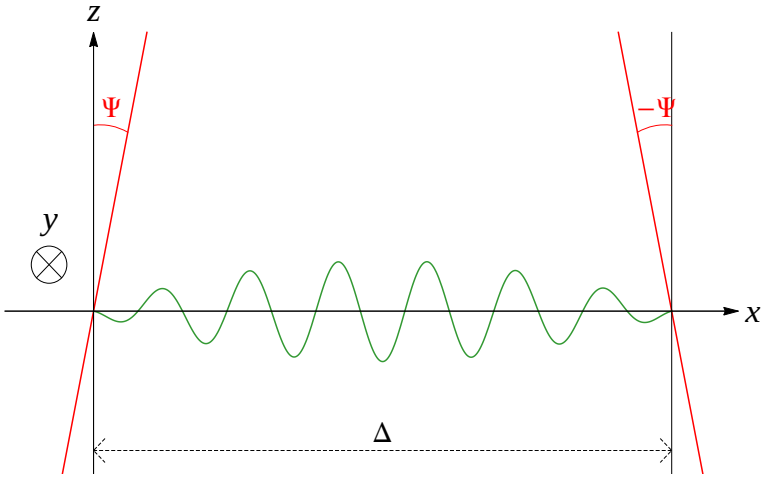

Figure 2.2: A light string stretched between two junctions with heavy strings.

the light string's movement is short compared to the ratio of the light string's length to the heavy string's velocity (with respect to the light string). In addition, since the heavy strings can be considered as straight in the vicinity of the junction and since the boundary conditions are what matter here, the heavy strings will be taken infinitely straight. Note that even though the case studied here is not generic, the conclusions are applicable to generalisations of this specific configuration as shown in Appendix A.

The boundary conditions[17] for a light string ending on two junctions with the aforementioned heavy strings are given, for any t, by

$$\dot{\mathbf{X}}_{\perp}(t,0) = \mathbf{X}'_{\parallel}(t,0) = 0 \tag{2.20a}$$

$$\dot{\mathbf{X}}_{\perp}(t,\sigma_m) = \mathbf{X}'_{\parallel}(t,\sigma_m) = 0 \ , \tag{2.20b}$$

where again $f'(\sigma,t) = \partial_\sigma f(\sigma,t)$ and $\dot{f}(\sigma,t) = \partial_t f(\sigma,t)$ while the subscript $\perp$ (respectively $\parallel$) indicates the projection along the directions orthogonal (parallel) to the (local) end string. The spacelike worldsheet coordinate σ lies within $[0,\sigma_m]$, with σ_m the parameter length of the string, that is the maximal value for σ since the minimal value is 0. Hence, projected on the space cartesian directions (x,y,z),

[17]It is important to note that while a non-null light string's tension $\mu_\ell \neq 0$ would physically lead to its length getting smaller, that is, to its centre of mass moving towards positive z (as in Fig. 2.2), our study here focuses on the movement of the light string in the limit $\mu_\ell \to 0$. Still, one can extend our results to the case $\mu_\ell \neq 0$, $\mu_\ell \ll \mu_h$, where μ_h is the heavy strings' tension.

the conditions (2.20), at any time t, read

$$\dot{X}_y(t,0) = 0 \tag{2.21a}$$
$$\dot{X}_x(t,0)\cos\Psi - \dot{X}_z(t,0)\sin\Psi = 0 \tag{2.21b}$$
$$X'_x(t,0)\sin\Psi + X'_z(t,0)\cos\Psi = 0\ , \tag{2.21c}$$

and

$$\dot{X}_y(t,\sigma_m) = 0 \tag{2.21d}$$
$$\dot{X}_x(t,\sigma_m)\cos\Psi + \dot{X}_z(t,\sigma_m)\sin\Psi = 0 \tag{2.21e}$$
$$-X'_x(t,\sigma_m)\sin\Psi + X'_z(t,\sigma_m)\cos\Psi = 0\ . \tag{2.21f}$$

Following the usual approach [36], one imposes the conformal gauge conditions $(\dot{X})^2 + (X')^2 = 0$ and $\dot{X}\cdot X' = 0$ and the temporal gauge $\sigma^0 \equiv \tau = t$, obtains the equation of motion $\mathbf{X}'' - \ddot{\mathbf{X}} = \mathbf{0}$ which is solved using the decomposition into the left- and right-movers, $\mathbf{X}_\pm(\sigma \pm t)$, as in $\mathbf{X}(\sigma,t) = \frac{1}{2}\left(\mathbf{X}_+(\sigma_+) + \mathbf{X}_-(\sigma_-)\right)$, thus leading to the system of boundary conditions

$$X'_{+y}(t) = X'_{-y}(-t) \tag{2.22a}$$
$$\left[X'_{+z}(t) - X'_{-z}(-t)\right]\tan\Psi = X'_{+x}(t) - X'_{-x}(-t) \tag{2.22b}$$
$$\left[X'_{+z}(t) + X'_{-z}(-t)\right]\frac{-1}{\tan\Psi} = X'_{+x}(t) + X'_{-x}(-t)\ , \tag{2.22c}$$

and

$$X'_{+y}(\sigma_m + t) = X'_{-y}(\sigma_m - t) \tag{2.22d}$$
$$\left[X'_{+z}(\sigma_m + t) - X'_{-z}(\sigma_m - t)\right]\tan\Psi = -X'_{+x}(\sigma_m + t) + X'_{-x}(\sigma_m - t) \tag{2.22e}$$
$$\left[X'_{+z}(\sigma_m + t) + X'_{-z}(\sigma_m - t)\right]\frac{1}{\tan\Psi} = X'_{+x}(\sigma_m + t) + X'_{-x}(\sigma_m - t)\ . \tag{2.22f}$$

Note again that in Eqs. (2.22), t is a free variable, so it can be shifted (following $t \to t + \sigma_m$) or symmetrised (as in $t \to -t$).

Periodicity requirements

Applying the transformation $t \to t - \sigma_m$ to Eq. (2.22a) and combining it with Eq. (2.22d) imply

$$X'_{+y}(-\sigma_m + t) = X'_{+y}(\sigma_m + t)\ , \tag{2.23}$$

namely that $X'_{+y}(\sigma_+)$ (and hence $X'_{-y}(\sigma_-)$) is $2\sigma_m$-periodic.

Denoting $T \equiv \tan\Psi$, the sum and the difference of Eqs. (2.22b) and (2.22c), and of Eqs. (2.22e) and (2.22f), respectively yield

$$X'_{+z}(t)\left(T-\frac{1}{T}\right) - X'_{-z}(-t)\left(T+\frac{1}{T}\right) = 2X'_{+x}(t) \tag{2.24a}$$

$$X'_{+z}(t)\left(T+\frac{1}{T}\right) - X'_{-z}(-t)\left(T-\frac{1}{T}\right) = -2X'_{-x}(-t)\ , \tag{2.24b}$$

$$X'_{+z}(\sigma_m+t)\left(T+\frac{1}{T}\right) - X'_{-z}(\sigma_m-t)\left(T-\frac{1}{T}\right) = 2X'_{-x}(\sigma_m-t) \tag{2.24c}$$

$$X'_{+z}(\sigma_m+t)\left(T-\frac{1}{T}\right) - X'_{-z}(\sigma_m-t)\left(T+\frac{1}{T}\right) = -2X'_{+x}(\sigma_m+t)\ . \tag{2.24d}$$

Redefining $t \to t-\sigma_m$ in Eq. (2.24d) and $t \to t+\sigma_m$ in Eq. (2.24c), and respectively summing them with Eqs. (2.24a) and (2.24b), lead to

$$2\left(T^2-1\right)X'_{+z}(t) = \left(T^2+1\right)\left[X'_{-z}(2\sigma_m-t) + X'_{-z}(-t)\right] \tag{2.25a}$$

$$2\left(T^2-1\right)X'_{-z}(-t) = \left(T^2+1\right)\left[X'_{+z}(2\sigma_m+t) + X'_{+z}(t)\right] \tag{2.25b}$$

Finally, one can use Eq. (2.25b) along with a version of Eq. (2.25b) where one applied the shift $t \to t-2\sigma_m$, to express the right-hand-side of Eq. (2.25a), leaving only terms of X'_{+z}. We can rearrange it and perform once more the shift $t \to t+2\sigma_m$ to get the difference equation

$$X'_{+z}(4\sigma_m+t) = \mathcal{R}X'_{+z}(2\sigma_m+t) - X'_{+z}(t)\ , \tag{2.26}$$

where

$$\mathcal{R} \equiv 4\left(\frac{\tan^2\Psi-1}{\tan^2\Psi+1}\right)^2 - 2 = 2\cos(4\Psi)\ , \tag{2.27}$$

In order to show that the solutions of this equation are periodic (or quasi-periodic), one can define $\forall n$

$$X_n(t) \equiv X'_{+z}(2n\sigma_m+t)\ , \tag{2.28}$$

and shift Eq. (2.26) by $t \to t+2n\sigma_m$, $\forall n$, so that it reads $\forall n$

$$X_{n+2}(t) = \mathcal{R}X_{n+1}(t) - X_n(t)\ , \tag{2.29}$$

with the case $n=0$ being exactly Eq. (2.26). The general solution is $(\forall t, n)$

$$X_n(t) = 2E(t)\cos(4n\Psi) + 2F(t)\sin(4n\Psi)\ , \tag{2.30}$$

where the constants (with respect to n) $E(t)$ and $F(t)$ are determined by the 'initial conditions' (with respect to n), yielding[18]

$$\begin{aligned} E(t) &= \frac{1}{2}X_0(t) \equiv \frac{1}{2}X'_{+z}(t) \\ F(t) &= \frac{1}{\sin(4\Psi)}\left(\frac{1}{2}X_1(t) - \cos(4\Psi)\,E(t)\right) \\ &= \frac{1}{2\sin(4\Psi)}\Big(X'_{+z}(2\sigma_m + t) - \cos(4\Psi)\,X'_{+z}(t)\Big)\ . \end{aligned}$$

Note that all this can be obtained for X'_{+x} as well.

If one can find $m \in \mathbb{Z}$ so that $X_m(t) = X_0(t)$, $\forall t$, then $X_n(t)$ is m-periodic (with respect to the integer index). In such case, one has $X'_{+z}(2m\sigma_m + t) = X'_{+z}(t)$, $\forall t$, implying that $X'_{+z}(t)$ is $2m\sigma_m$-periodic (with respect to the argument). So we want to determine under which conditions the function $X_n(t)$ is index-periodic, that is, find $m \in \mathbb{Z}$ such that $X_m(t) = X_0(t)$, $\forall t$. From Eq. (2.30), it is clear that this occurs for

$$4m\Psi = 2k\pi \quad \Leftrightarrow \quad m = \frac{k\pi}{2\Psi}\ , \tag{2.31}$$

where $k \in \mathbb{Z}$. In such case, the function X_n is index-periodic: $\forall t$, $X_0(t) = X_m(t) \equiv X_{k\pi/2\Psi}(t)$; that is, the function $X'_{+z}(t)$ is $(k\pi\sigma_m/\Psi)$-periodic: it satisfies, $\forall t$, $X'_{+z}(t) = X'_{+z}(t + k\pi\sigma_m/\Psi)$. Such solution m exists provided the angle Ψ can be written as

$$\Psi = \frac{\pi}{2}Q\ , \tag{2.32}$$

with $Q \in \mathbb{Q}$.[19] Thus, for a dense subset of angles in the range $\Psi \in [-\pi/2, \pi/2]$, $X'_{+x}(\sigma_+)$ and $X'_{+z}(\sigma_+)$ are $\mathcal{L}$-periodic, where we denote by $\mathcal{L} \equiv 2m\sigma_m \equiv \frac{k\pi\sigma_m}{\Psi}$ the periodicity, and hence they can be decomposed in a Fourier series to simplify the analysis.[20]

Concern over what happens for angles not satisfying Eq. (2.32) can be alleviated by noting that although the functions $X'_{+x}(\sigma_+)$, $X'_{+z}(\sigma_+)$ are not periodic, they are arbitrarily close to periodic, and this is sufficient for our requirements here, that is

[18] In the case where $\sin 4n\Psi = 0$, one has $X_n(t) = 2E(t)\cos(4n\Psi)$, $\forall n$, and $E(t) = \frac{1}{2}X_0(t) \equiv \frac{1}{2}X'_{+z}(t)$. $X_1(t) = 2E(t)\cos(4\Psi)$ is well defined and $F(t)$ does not appear.

[19] As an example, let us assume that in our setup, $\Psi = \frac{\pi}{6}$ (i.e. $Q = \frac{1}{3}$). Then, according to Eq. (2.30), $X_n(t) = 2E(t)\cos(2n\pi/3) + 2F(t)\sin(2n\pi/3)$, leading to $X_3(t) = 2E(t)\cos(2\pi) + 2F(t)\sin(2\pi) = 2E(t) = X_0(t)$, $\forall t$. X_n is 3-periodic; X'_{+z} is $6\sigma_m$-periodic.

[20] It is important to remark that, as one would naturally expect, the periodicity of $E(t)$ and $F(t)$ is a consequence and not a hypothesis here. Indeed, assuming $4m\Psi = 2k\pi$ from Eq. (2.31), one has $X_{m+n}(t) = X_m(t + 2n\sigma_m) = 2E(t + 2n\sigma_m)\cos(4m\Psi) + 2F(t + 2n\sigma_m)\sin(4m\Psi) = 2E(t + 2n\sigma_m) = X_0(t + 2n\sigma_m) \equiv X_n(t)$, $\forall t, n$, where we used Eqs. (2.30) and (2.28), and the definition of $E(t)$.

for our qualitative study. It might also be worth noting that the period can be large, which might cause problems for our approximation, namely that the end strings are static over one period — indeed, if the period is very long, the heavy strings cannot be considered static over such a large time scale anymore.

Finally, recall this specific setup is considered for its simplicity. The conclusions on the overall periodicity or quasi-periodicity, drawn from the above analysis, are thought to be generic though, since the configuration choices made here leave the string's dynamical properties unchanged. In addition, we studied in the Appendix A how these results on periodicity are modified in a more realistic and more complex strings configuration, confirming our present results.

Symmetries

To proceed, let us focus on the symmetries between the two movers on the string. Using Eqs. (2.22), we obtain

$$X'_{-x}(-t) = \frac{1}{1+\tan^2\Psi}\left(\left(1-\tan^2\Psi\right)X'_{+x}(t) - 2\tan\Psi\; X'_{+z}(t)\right) \tag{2.33a}$$

$$X'_{-z}(-t) = \frac{-1}{1+\tan^2\Psi}\left(\left(1-\tan^2\Psi\right)X'_{+z}(t) + 2\tan\Psi\; X'_{+x}(t)\right) \tag{2.33b}$$

$$X'_{-y}(-t) = X'_{+y}(t)\ . \tag{2.33c}$$

Since $\mathbf{X}'_-(\sigma - t) = \mathbf{X}'(\sigma,t) - \dot{\mathbf{X}}(\sigma,t)$ we remark that $\mathbf{X}'_-(-t) = -\mathbf{X}'_-(t)$, and then writing the above set of equations in vector notation, we get

$$\mathbf{X}'_-(t) = \mathbf{T}\,\mathbf{X}'_+(t)\ , \tag{2.34}$$

where the matrix $\mathbf{T}$ is defined by

$$\mathbf{T} = \begin{pmatrix} -\frac{1-\tan^2\Psi}{1+\tan^2\Psi} & 0 & \frac{2\tan\Psi}{1+\tan^2\Psi} \\ 0 & -1 & 0 \\ \frac{2\tan\Psi}{1+\tan^2\Psi} & 0 & \frac{1-\tan^2\Psi}{1+\tan^2\Psi} \end{pmatrix} = \begin{pmatrix} -\cos(2\Psi) & 0 & \sin(2\Psi) \\ 0 & -1 & 0 \\ \sin(2\Psi) & 0 & \cos(2\Psi) \end{pmatrix}\ . \tag{2.35}$$

This matrix is diagonalised by a change of basis, such that the z-axis is parallel to the $\sigma = 0$ end string. In this basis, we get

$$\mathbf{X}'_-(t) = \begin{pmatrix} -1 & 0 & 0 \\ 0 & -1 & 0 \\ 0 & 0 & 1 \end{pmatrix}\mathbf{X}'_+(t)\ . \tag{2.36}$$

Thus, $\mathbf{X}'_{-}(t)$ is simply given by a π-rotation of $\mathbf{X}'_{+}(t)$ with respect to the axis parallel to the end string.

Note in particular that the square velocity of the string is

$$\mathbf{v}.\mathbf{v}(t,\sigma) = \frac{1}{2}\left[1 - \mathbf{X}'_{+}(\sigma_{+}) \cdot \mathbf{X}'_{-}(\sigma_{-})\right] \tag{2.37}$$

$$= \frac{1}{2}\left[1 - \left(X'^{\parallel}_{+}(\sigma_{+})\right)^2 - \left(\mathbf{X}'^{\perp}_{+}(\sigma_{+})\right)^2\right] , \tag{2.38}$$

where $X'^{\parallel}_{+}$ and $\mathbf{X}'^{\perp}_{+}$ are the components of $\mathbf{X}'_{+}$, parallel and perpendicular to the $(\sigma = 0)$ end string, respectively.

2.3.2 The probability of cusps and pseudocusps

Let us recall that cusps appear when the two curves $\mathbf{X}'_{+}$ and $-\mathbf{X}'_{-}$ cross each other on the unit sphere — remembering that $|\mathbf{X}'_{+}| = 1 = |\mathbf{X}'_{-}|$ as a consequence of the Virasoro condition. This is equivalent to defining cusps as points reaching, for some instant t, the speed of light $c = 1$. Indeed, $\dot{\mathbf{X}}(\sigma,t) \equiv 1/2\,(\mathbf{X}'_{+}(\sigma_{+}) - \mathbf{X}'_{-}(\sigma_{-})) = \mathbf{X}'_{+}(\sigma_{+}) = -\mathbf{X}'_{-}(\sigma_{-})$ in the case of cusps.

There is a similar event we will address, and we will refer to as a *pseudo*cusp, which occurs when the two curves $\mathbf{X}'_{+}$ and $-\mathbf{X}'_{-}$ are very close (and we will see how close, for instance around Eq. (2.54) in this section's last subsection) to each other, without however intersecting, as in Fig. 2.6a. Pseudocusps have to be considered firstly because when trying to determine statistically the frequency of cusps, one might not be able to assess very accurately whether two approaching curves actually cross each other or if they are simply nearby; similarly pseudocusps can also arise if one tries to estimate the occurrence of cusps numerically because discretisation would generically generate grid approximations. In addition, being interested in Gravity Waves (GWs) emitted by the string's ongoing events such as cusps, it is important to also compute the gravitational signals emitted from any highly relativistic region of the string.

In order to investigate the occurrence of cusps and pseudocusps on the string over a periodic non-dynamical evolution and the influence of several parameters on such occurrence, we will study the average positions and standard deviation of $\mathbf{X}'_{+}$ and $-\mathbf{X}'_{-}$ on the unit sphere. We will then relate this probability to the string and network's parameters in order to determine the characteristics that can lead to cuspy events. Note that in the following, a "cusp" refers to either an actual cusp or

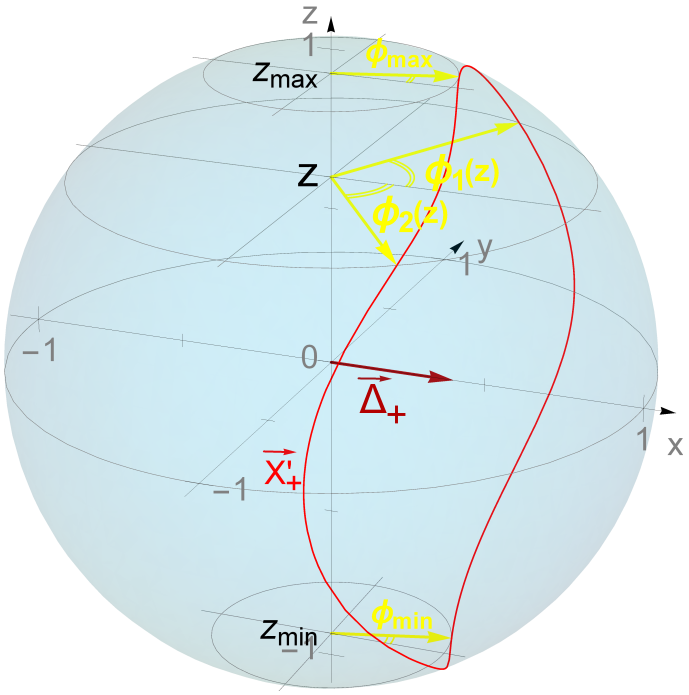

Figure 2.3: Cylindrical coordinates about the z-axis and the angles $\phi_i(z)$ for the description of $\mathbf{X}'_+$ on the unit sphere. $\mathbf{\Delta}_+ \equiv \frac{1}{\mathcal{L}} \int_{-\mathcal{L}/2}^{\mathcal{L}/2} X'_{+x}$, as in Eq. (2.51b).

a pseudocusp.

Analytical considerations

Here we define the z-axis as the axis of rotation that relates $\mathbf{X}'_+$ and $-\mathbf{X}'_-$, namely we align the z-axis with the $X'^{\parallel}_+$. Then the vectors $\mathbf{X}'_+$ can be written in cylindrical-like coordinates about this z-axis as in Fig. 2.3, and parametrised by z, yielding

$$\mathbf{X}'_+(z) = \begin{cases} \left(\sqrt{1-z^2}\,\cos\phi_1(z)\,, \sqrt{1-z^2}\,\sin\phi_1(z)\,,\; z\right) \\ \left(\sqrt{1-z^2}\,\cos\phi_2(z)\,, -\sqrt{1-z^2}\,\sin\phi_2(z)\,,\; z\right) \end{cases} \tag{2.39}$$

for $z \in [z_{\min}, z_{\max}] \subset [-1, 1]$. The coordinates $z_{\min}$ and $z_{\max}$ are defined such that the curve $\mathbf{X}'_+$ does not enter in the part of the sphere (respectively) below and above such altitudes. Note that $\forall z \in [z_{\min}, z_{\max}]$, there are at least two points on the curve $\mathbf{X}'_+$, as explicitely written in the above equation, but potentially more if the curve is not as simple. In wavier cases, as in Fig. 2.5b, one would need to define $\phi_i(z)$, $i \in \{3, 4\}$, $\forall z \in [z_{\min,2}, z_{\max,2}]$, and possibly more of such functions, so that the whole curve is parametrised by z and described by anglular functions

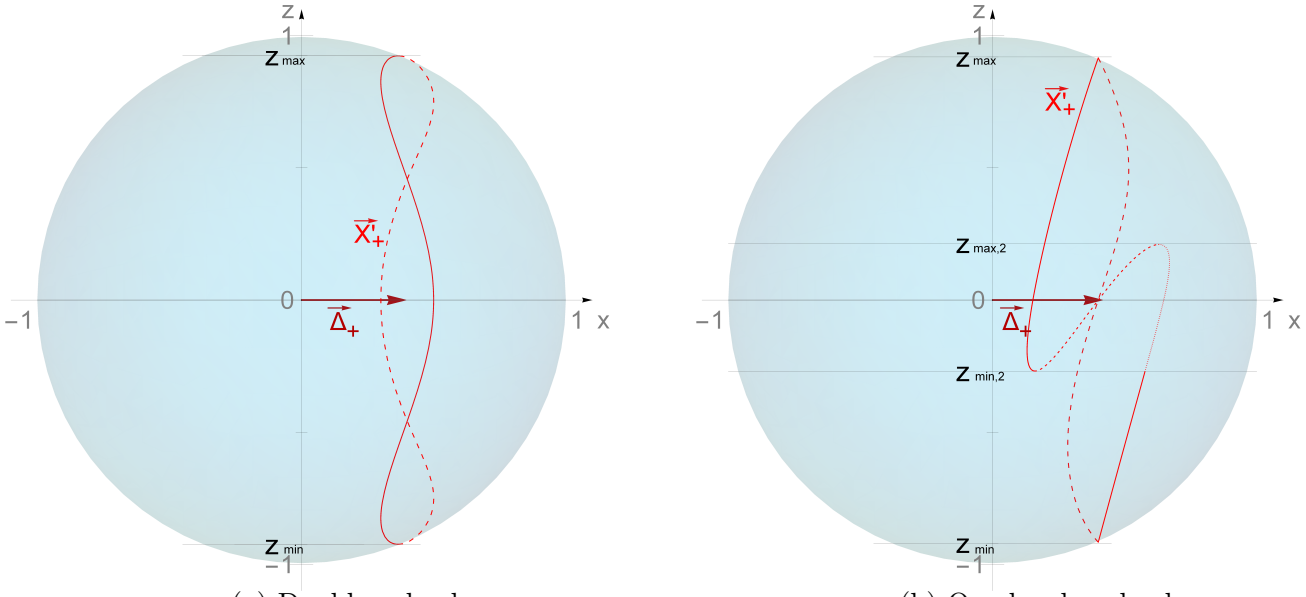

(a) Double-valued (b) Quadruple-valued

Figure 2.4: Various $\mathbf{X}'_+$ curves parametrised by z. In the simplest case (left), $\mathbf{X}'_+$ is described $\forall z \in [z_{\min}, z_{\max}]$ by a pair of angular functions $\phi_i(z)$, $i \in \{1, 2\}$, (as in Fig. 2.3); each curve (solid and large-dashed) relates to one of these functions. If the curve is wavier, one needs more functions to fully describe $\mathbf{X}'_+$, for instance (right) $\phi_i(z)$, $i \in \{3, 4\}$, $\forall z \in [z_{\min,2}, z_{\max,2}]$; each curve (solid, large-dashed, small-dashed and dotted) again relates to one of them.

$\phi_i(z)$, defined on some intervals inclued in $[-1, 1]$. Such $z_{\min,j}$ and $z_{\max,j}$ similarly bound the extension of this part of the curve. In the following of this subsection, we consider for simplicity the double-valued curve (where only $\phi_1(z)$ and $\phi_2(z)$ are needed) as in Figs. 2.3 and 2.5a, without any loss of generality.

Cusps will appear whenever $\phi_1(z) + \phi_2(z) = \pi$, as represented in Fig. 2.5, which shows a side view of the unit sphere and a top view of its upper-half. That is why this is the condition we want to investigate. One has

$$\begin{aligned}
\langle X'_{+x} \rangle_\sigma &\equiv \frac{1}{\mathcal{L}} \int_{-\mathcal{L}/2}^{\mathcal{L}/2} \mathrm{d}\sigma_+ \, X'_{+x}(\sigma_+) \\
&= \frac{1}{2\,(z_{\max} - z_{\min})} \int_{z_{\min}}^{z_{\max}} \mathrm{d}z \, \sqrt{1 - z^2} \, (\cos\phi_1 + \cos\phi_2) \qquad (2.40a) \\
\langle X'_{+y} \rangle_\sigma &\equiv \frac{1}{\mathcal{L}} \int_{-\mathcal{L}/2}^{\mathcal{L}/2} \mathrm{d}\sigma_+ \, X'_{+y}(\sigma_+) \\
&= \frac{1}{2\,(z_{\max} - z_{\min})} \int_{z_{\min}}^{z_{\max}} \mathrm{d}z \, \sqrt{1 - z^2} \, (\sin\phi_1 - \sin\phi_2) \qquad (2.40b)
\end{aligned}$$

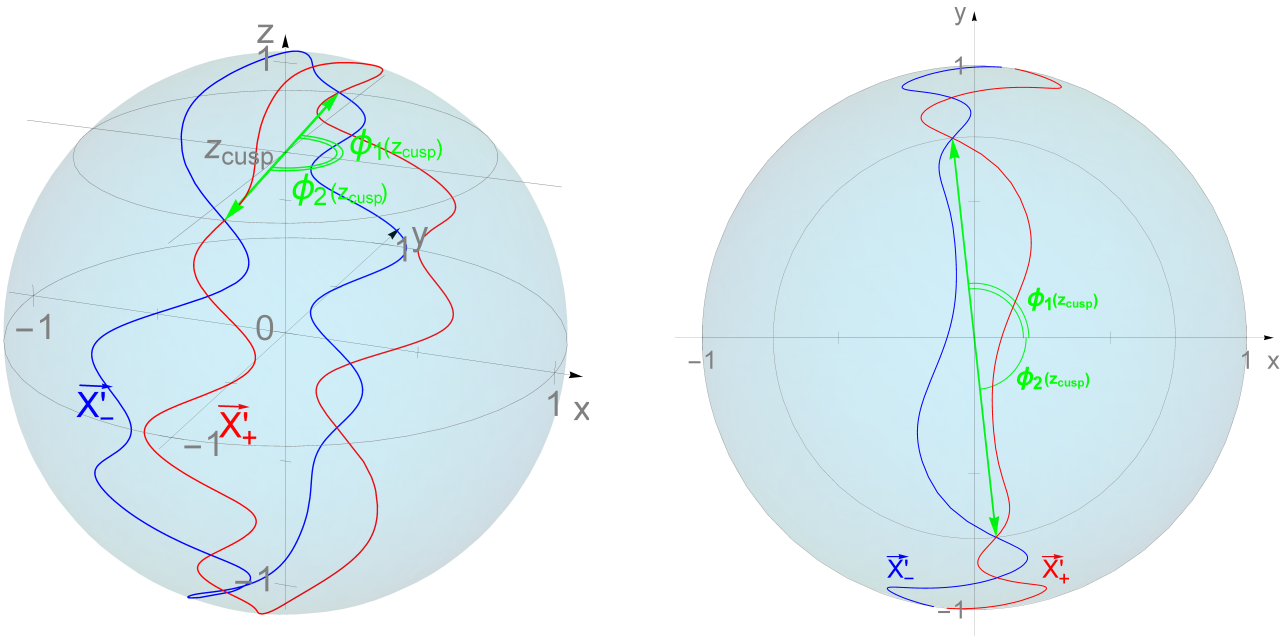

(a) Side view of the unit sphere

(b) Top view of the upper half-sphere

Figure 2.5: Various views of the $\mathbf{X}'_+$ and $\mathbf{X}'_-$ curves on the unit sphere, and the angular description $\phi_i(z)$ in the case of a cusp. The condition $\phi_1(z) + \phi_2(z) = \pi$ is satisfied at the cusp, while $\phi_1(z) + \phi_2(z) > \pi$ between two cusps.

where we used a change of coordinate, parametrising the curve with z as in Eq. (2.39), and where we have dropped the explicit dependence of ϕ_i on z for notational simplicity. Recall $\mathcal{L}$ is the periodicity of the $\mathbf{X}'_+$ loop, which needs not to be the string's invariant length $L \equiv {}^{E}/_{\mu}$ and can be different for each component.

Similarly, we can write

$$\begin{aligned}\langle X'_{+x}X'_{+x}\rangle_\sigma &\equiv \frac{1}{\mathcal{L}}\int_{-\mathcal{L}/2}^{\mathcal{L}/2} \mathrm{d}\sigma_+\, X'_{+x}(\sigma_+)X'_{+x}(\sigma_+) \\ &= \frac{1}{2\left(z_{\max}-z_{\min}\right)}\int_{z_{\min}}^{z_{\max}} \mathrm{d}z\left(1-z^2\right)\left(\cos^2\phi_1+\cos^2\phi_2\right) \qquad (2.41a)\\ \langle X'_{+y}X'_{+y}\rangle_\sigma &\equiv \frac{1}{\mathcal{L}}\int_{-\mathcal{L}/2}^{\mathcal{L}/2} \mathrm{d}\sigma_+\, X'_{+y}(\sigma_+)X'_{+y}(\sigma_+) \\ &= \frac{1}{2\left(z_{\max}-z_{\min}\right)}\int_{z_{\min}}^{z_{\max}} \mathrm{d}z\left(1-z^2\right)\left(\sin^2\phi_1+\sin^2\phi_2\right)\ . \qquad (2.41b)\end{aligned}$$

The sum of Eqs. (2.41a) and (2.41b) leads to

$$\langle X'_{+x}X'_{+x}\rangle_\sigma + \langle X'_{+y}X'_{+y}\rangle_\sigma = \frac{1}{z_{\max}-z_{\min}}\int_{z_{\min}}^{z_{\max}} \mathrm{d}z\left(1-z^2\right) = \langle 1-z^2\rangle_z\ , \qquad (2.42)$$

thus providing a direct relationship between $\langle X'_{+x}X'_{+x}\rangle_\sigma$ and $\langle X'_{+y}X'_{+y}\rangle_\sigma$. Adding Eq. (2.42) to the difference of Eqs. (2.41a) and (2.41b), we get

$$\langle X'_{+x}X'_{+x}\rangle_\sigma = \frac{1}{z_{\max}-z_{\min}}\int_{z_{\min}}^{z_{\max}} \mathrm{d}z\left(1-z^2\right)\Big[2\cos^2\left(\tfrac{\phi_1+\phi_2}{2}\right)\cos^2\left(\tfrac{\phi_1-\phi_2}{2}\right) - \cos^2\left(\tfrac{\phi_1+\phi_2}{2}\right) - \cos^2\left(\tfrac{\phi_1-\phi_2}{2}\right)+1\Big] \ . \quad (2.43)$$

Let us consider the simplifying assumption $\phi_1(z) \approx \phi_2(z)$. Note that this approximation can be easily satisfied when looking at the string with a probabilistic point of view. Indeed, one can continuously deform the curve $\mathbf{X}'_+$ to get a symmetric curve with respect to the (xz)-plane. If this transformation conserves the statistical description of the curve, it does not change significantly the probability of the curve to intersect its image under the π-rotation with respect to the z-axis. What should be conserved in the transformation is only the proportion of the curve reaching a certain distance to its mean position. It is possible to continuously deform our curve maintaining such properties, especially if we are looking at a large population of strings in which tiny variations on each string are smoothed over the number of them.

Hence, Eq. (2.40a) becomes

$$\langle X'_{+x}\rangle_\sigma \approx \frac{1}{z_{\max}-z_{\min}}\int_{z_{\min}}^{z_{\max}} \mathrm{d}z\,\sqrt{1-z^2}\,\cos\left(\frac{\phi_1+\phi_2}{2}\right) \ , \quad (2.44)$$

whilst Eq. (2.43) reads

$$\langle X'_{+x}X'_{+x}\rangle_\sigma \approx \frac{1}{z_{\max}-z_{\min}}\int_{z_{\min}}^{z_{\max}} \mathrm{d}z\left(1-z^2\right)\cos^2\left(\frac{\phi_1+\phi_2}{2}\right) \ . \quad (2.45)$$

Let us note that if the string is straight,[21] the curve described by $\mathbf{X}'_+$ is reduced to a point at the $x=1$ pole ; the further the string deviates from a straight line, the further the $\mathbf{X}'_+$ curve will deviates from this pole. Only wavy strings could thus generate a curve that spans further than the $x>0$ half-sphere, that is further than

[21] It is interesting to note that our argument here holds for strings stretched between two fixed points. In particular, a not so wavy string in such a configuration would present on the unit sphere two curves for $X'_\pm$, each one centred on a different point lying on the x-axis (in our choice of frame), such that $\langle \mathbf{X}'_+\rangle_\sigma = -\langle \mathbf{X}'_-\rangle_\sigma \neq \mathbf{0}$, meaning they can avoid each other. On the contrary, a loop must have these two curves centred on the centre of the unit sphere, with $\langle \mathbf{X}'_\pm\rangle_\sigma = \mathbf{0}$, implying that they cannot easily avoid each other as long as they remain continuous, that is as long as they are no kinks on the string. Said differently, each curve cannot lie entirely on a half sphere in the loop case [41, Chapter 6], while it can in the case studied here.

the $(\phi_1,\, \phi_2) \in [0,\, \pi/2[^2$ half-sphere. Thus, the right-hand-side of Eq. (2.44) is positive and it becomes smaller and smaller for wavier strings without changing sign. The condition we are interested in here is $(\phi_1 + \phi_2) \geq \pi$, since this would indicate that the curve described by $\mathbf{X}'_+$ on the unit sphere spans over more than a whole half-sphere, implying a crossing with $\mathbf{X}'_-$ by symmetry. Namely we would like to find the parameters for which there is a high probability that exists a $z \in [z_{\min},\, z_{\max}]$ such that $\phi_1(z) + \phi_2(z) \geq \pi$, or equivalently such that

$$\cos\left(\frac{\phi_1(z) + \phi_2(z)}{2}\right) \leq 0\ . \tag{2.46}$$

Noting that $|z_{\min}| \leq 1$ and $z_{\max} \leq 1$, we have $0 \leq 1 - z^2 \leq 1$ for all $z \in [z_{\min},\, z_{\max}]$ and hence we can rewrite the above condition as

$$\sqrt{1-z^2}\,\cos\left(\frac{\phi_1(z) + \phi_2(z)}{2}\right) \leq 0\ . \tag{2.47}$$

The average of this quantity is given by Eq. (2.44) and the fluctuations about this average are given by Eq. (2.45). In particular, the standard deviation is

$$\sigma^2_{\left(\sqrt{1-z^2}\cos((\phi_1+\phi_2)/2)\right)} \approx \langle X'_{+x} X'_{+x}\rangle_\sigma - \langle X'_{+x}\rangle^2_\sigma\ . \tag{2.48}$$

Thus, we have the average (which is positive) and the standard deviation of a quantity, for which we want to calculate the probability to be somewhere negative. This is likely to happen if the standard deviation is larger than a significant fraction of the average. This means that the probability of the quantity of interest being negative is significant when

$$\alpha\ \sigma^2_{\left(\sqrt{1-z^2}\cos((\phi_1+\phi_2)/2)\right)} \gtrsim \left\langle \sqrt{1-z^2}\,\cos\left(\,{}^{(\phi_1+\phi_2)}/_2\,\right)\right\rangle^2_x\ , \tag{2.49}$$

with α being between 1 and 5. It corresponds to a few times the standard deviation being larger than (or comparable to) the average. To illustrate the idea, let our quantity X'_{+x} follow a gaussian distribution; then, for instance $\alpha = 2$ would mean that a string should present a significant number of cusps if Eq. (2.47) was satisfied for about 2.5% of the points on the string — 2σ corresponding to a 95% confidence level.

Thus, using Eqs. (2.44) and (2.48) we find that there is a significant probability

of having cusps provided

$$\langle X'_{+x} X'_{+x} \rangle_\sigma \gtrsim \frac{1+\alpha}{\alpha} \left(\frac{|\mathbf{\Delta}|}{\sigma_m} \right)^2 = \frac{1+\alpha}{\alpha} \, \Delta_+^2 \ , \tag{2.50}$$

where we have used that $\mathbf{X}'_+$ is periodic in $\mathcal{L} \equiv 2m\sigma_m$ (from Eq. (2.31) and below), defined

$$\mathbf{\Delta} = (\Delta,\, 0,\, 0) \equiv \mathbf{X}(\sigma_m, t) - \mathbf{X}(0, t) \tag{2.51a}$$

$$\Delta_+ \equiv \frac{1}{\mathcal{L}} \int_{-\mathcal{L}/2}^{\mathcal{L}/2} \mathrm{d}\sigma_+ \, X'_{+x}(\sigma_+) \quad \text{and} \quad \Delta_- \equiv \frac{1}{\mathcal{L}} \int_{-\mathcal{L}/2}^{\mathcal{L}/2} \mathrm{d}\sigma_- \, X'_{-x}(\sigma_-) \ , \tag{2.51b}$$

and used the relations $\Delta_+ = -\Delta_-$ and $\Delta/\sigma_m = (\Delta_+ - \Delta_-)/2 = \Delta_+$. This is a key result as it gives a simple way to discriminate between cuspy and non-cuspy strings, simple in the quantities to compute and in the physical meaning behind inequality (2.50).

The prefactor $(1+\alpha)/\alpha$ lies somewhere between 1 and 2, the latter being too conservative (it corresponds to $\alpha = 1$, meaning there should be cusps only if more than 15% of the curve satisfy Eq. (2.47)) and the former not constraining enough (where $\alpha \gg 1$, that is a very small fraction of the curve satisfying Eq. (2.47) is sufficient to generate cusps along the string).

Remember that we have defined the z-axis so that the heavy string at the $\sigma = 0$ junction is aligned along this z-axis. Equation (2.50) implies a minimum distance reached by the x-component of $\mathbf{X}'_+$ (and $-\mathbf{X}'_-$) from its average circle, defined as the circle in the (yz)-plane whose center is at a distance Δ_+ from the centre of the sphere, on the x-axis. This equation can be also understood as implying a boundary on how irregular the derivatives of the two movers have to be to generate a substantial amount of cusps.

In order to make a link with the string network's and the individual string's parameters, let us first recall that Δ is the distance between the two ends of the string, stretched between the two junctions. Rescaling Δ by the parameter length of the string σ_m, this gives the distance in the unit sphere between the two average circles for $\mathbf{X}'_+$ and $-\mathbf{X}'_-$. At a fixed length, if Δ increases, the two circles are shifted away and the probability of having cusps decreases; at fixed Δ, if the length increases, the cumulated length of the curve's parts reaching the minimum distance increases too so the number of cusps becomes larger. Hence, the number of cusps is lower for straighter strings. Moreover, if the string has large-amplitude waves,

the curves $\mathbf{X}'_+$ and $-\mathbf{X}'_-$ deviate from their average position and the number of cusps increases. Therefore, strings with large waves are expected to have more cusp events. At a fixed length, if the curves have less large waves, they will exhibit a larger amplitude and thus there will be more cusps. So, a long string with large-amplitude waves should exhibit more cusps than a short straight string or a small-scale structured string.

We want to stress again this is a qualitative analysis of a non-dynamical non-interacting string with Y-junctions, whose aim is to estimate the number of cusp events. Still, it is important to identify the relevant parameters in such setups and to understand their influence. This will be done in more details in the following analysis presented mainly in Section 2.3.3 and linked to some of the usual network and string parameters [45] in its last subsection.

Pseudocusps and velocity

Let us recall that a pseudocusp is defined as a point at which the left- and right-movers' derivatives *3*-vectors $\mathbf{X}'_+$ and $\mathbf{X}'_-$ are very close to each other, enough for the point to be highly relativistic, but not exactly equal to each other. We define $\sigma^{\text{clos.}}_{\pm} = \sigma^{\text{clos.}} \pm t^{\text{clos.}}$ to be the null coordinates for which these two vectors are the closest in this neighbourhood, and denote by θ_c the angle between the two vectors at $\sigma^{\text{clos.}}_{\pm}$. We also denote

$$l^\mu = \dot{X}^\mu(\sigma^{\text{clos.}}, t^{\text{clos.}}) = {}^1\!/_2 \left(X^\mu_+(\sigma^{\text{clos.}}_+) - X^\mu_-(\sigma^{\text{clos.}}_-)\right) \tag{2.52}$$

$$\text{and} \qquad \delta^\mu = {}^1\!/_2 \left(X^\mu_+(\sigma^{\text{clos.}}_+) + X^\mu_-(\sigma^{\text{clos.}}_-)\right) \ , \tag{2.53}$$

the half-sum and the half-difference between the left- and right-movers' *4*-velocities, respectively. Note that, despite what it looks like, we here call l^μ the half-*sum* since the vectors we are interested in are X'^μ_+ and $-X'^\mu_-$.

The *4*-vector l^μ is the *4*-velocity at the point of interest and it is a null vector in the cusp case. In the case of pseudocusps, the time-component l^0 is also equal to 1, but the norm of the *3*-velocity of the string at that point $(\sigma^{\text{clos.}}_+, \sigma^{\text{clos.}}_-)$ equals

$$|l^i| = \sqrt{\frac{1+\cos(\theta_c)}{2}} \approx 1 - {}^{\theta_c^2}\!/_8 \ ; \tag{2.54}$$

however, δ^μ is space-like, with $\delta^0 = 0$ in the time gauge, and

$$|\delta^i| = \sqrt{\frac{1-\cos(\theta_c)}{2}} \approx {}^{\theta_c}\!/_2 \ . \tag{2.55}$$

The angle θ_c can be thought of as measuring the *softness* of a relativistic part of the string. The larger it is, the smaller the velocity and the softer the pseudocusp; for $\theta_c = 0$, the event is an actual cusp and the velocity reaches $c = 1$.

We would also like to roughly evaluate the number of pseudocusps statistically. The problem has to be looked at using the unit sphere description along with the mean and standard deviation of the curves drawn by $\mathbf{X}'_+$ (and $-\mathbf{X}'_-$). Let us first recall that a pseudocusp is related to the $\mathbf{X}'_+$ curve approaching its symmetric counterpart without crossing it, while a cusp is linked to the curve crossing its counterpart. One can then define for each z the angle $\theta(z) \equiv \pi - (\phi_1(z) + \phi_2(z))$ (or the appropriate $\phi_i(z)$), such that $\theta = 0$ for cusps and $\theta < 0$ between cusps. Every pair of cusps and every pseudocusp is thus related to a local minimum of the angle θ: if this minimum is positive, as in Fig. 2.6a, the string presents there a pseudocusp, and if it is negative, as in Figs. 2.6b and 2.6c, there is a pair of cusps. In addition, let us define a *narrow* pair of cusps as a pair for which the minimal angle reached between the cusps is small (in the negative values), in opposition to a *large* pair of cusps, for which the minimum reached is large (and negative). In the first case, the curves cross each other and remain close before crossing back, as shown on Fig. 2.6b, while on the second one, after the crossing, the curves spread far from each other before coming back to their natural half-sphere, as in Fig. 2.6c.

In terms of the relative occurrence of cusps and pseudocusps, a *narrow* pair of cusps should be almost as frequent as a pseudocusp, since the probability of a small, positive minimum is almost the same as that of a small, negative one. Thus, a string with cusps should also present pseudocusps. In addition, because minima are more likely to be closer to the mean value of the distance, *narrow* pairs should be more frequent than *large* ones. So one can naively think that there should be a bit more than twice as many cusps as there are pseudocusps (roughly, in addition to a few large pairs, as many narrow pairs as there are pseudocusps). Still, this highly depends on the ratio of the standard deviation by the mean of $\mathbf{X}'_+$: a large ratio leads potentially to many more large pairs of cusps than narrow ones or pseudocusps. Even more importantly, these proportions are strongly influenced by the definition of pseudocusps, namely by the velocity threshold for a piece of

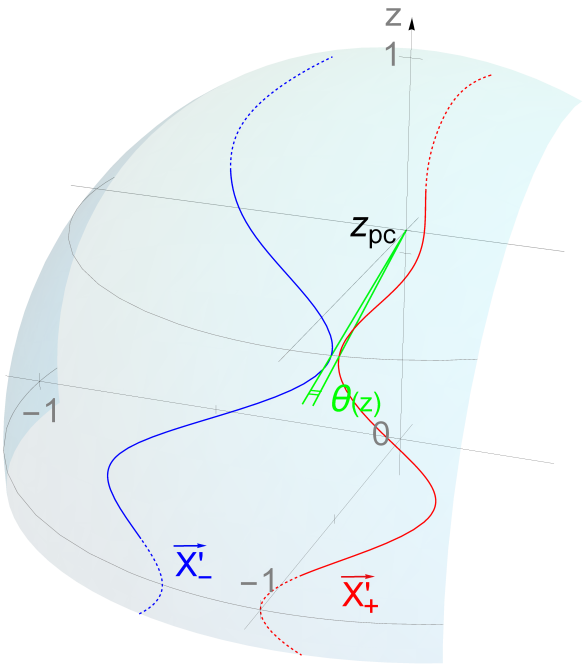

(a) Pseudocusp. $\theta \gtrsim 0$.

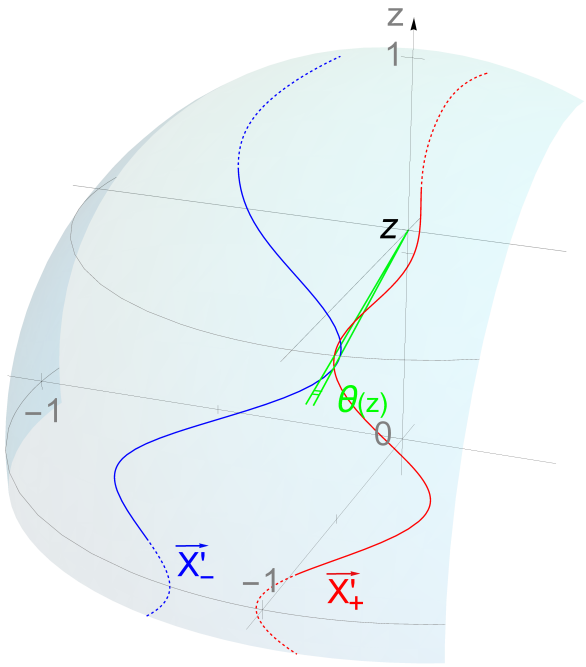

(b) Narrow pair of cusps. $\theta \lesssim 0$.

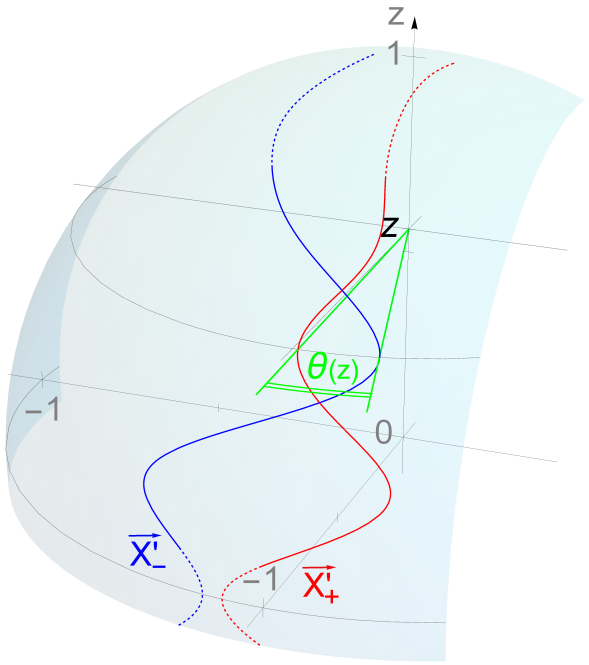

(c) Large pair of cusps. $\theta < 0$.

Figure 2.6: Different cases of cuspy events and the associated local minimum of the angle $\theta \equiv \pi - (\phi_1 + \phi_2)$ between the curves $\mathbf{X}'_+$ and $\mathbf{X}'_-$: (a) a pseudocusp, where θ 's local minimum is positive and small; (b) a narrow pair of cusps, where θ 's local minimum is negative and small; (c) a large pair of cusps, where θ 's local minimum is negative and large (in absolute value).

string to be a pseudocusp: a low threshold gives many more pseudocusps for the same number of cusps. Since our definition here is somehow arbitrary and would need additional work to fix a sensible threshold with respect to the emission of gravitational waves, no strong conclusion can be drawn from such considerations.

2.3.3 Numerical simulation

Method

We develop a simulation of the previously described configuration in order to check the considerations made and to evaluate the occurrence of cusps and pseudocusps. Our code depends on both the string network's and the individual string's parameters — namely ξ and $\bar{\xi}$ — and is based on the following assumptions. Firstly, the string's ends are fixed on the heavy strings, being themselves insensitive to the motion of the light string and to any transfer of momentum, and chosen to be parallel for simplicity. In addition, the quasi-periodic cases are neglected and the position and velocity of the string at $t = 0$ are defined by a Fourier series (i.e. by the amplitude of each mode). These amplitudes are all drawn in $[-h_m,\, h_m]$,[22] where h_m is a prefixed highest value, and the modes are the n first harmonics of the string (up to n nodes). One has thus

$$\begin{aligned}\mathbf{X}(\sigma,0) = \frac{\sigma}{\sigma_m}\,\boldsymbol{\Delta} &+ \left[\sum_{k=1}^{\bar{n}_x} c_k^x(h_m)\cos\left(\frac{2\pi k\,\sigma}{\sigma_m}\right) + s_k^x(h_m)\sin\left(\frac{2\pi k\,\sigma}{\sigma_m}\right)\right]\mathbf{e}_x \\ &+ \left[\sum_{k=1}^{\bar{n}_y} c_k^y(h_m)\cos\left(\frac{2\pi k\,\sigma}{\sigma_m}\right) + s_k^y(h_m)\sin\left(\frac{2\pi k\,\sigma}{\sigma_m}\right)\right]\mathbf{e}_y \\ &+ \left[\sum_{k=1}^{\bar{n}_z} c_k^z(h_m)\cos\left(\frac{2\pi k\,\sigma}{\sigma_m}\right)\right]\mathbf{e}_z\ , \end{aligned} \tag{2.56}$$

where $\boldsymbol{\Delta} = (\Delta,\, 0,\, 0)$, $\bar{n}_i$ are random integers uniformly drawn in $[\![1, n]\!]$ and all $c_k^i(h_m)$ and $s_k^i(h_m)$ yield random real numbers uniformly drawn in $[-h_m,\, h_m]$. n and h_m

[22] A uniform distribution in the interval $[-h_m,\, h_m]$ has been initially encoded. Note though that there is a bias: indeed, too large amplitudes can sometimes lead to velocities temporarily above $c = 1$ (depending on the amplitudes drawn). Still, the evolution equation implies that, if at $t = 0$ the velocity is well-behaved and below $c = 1$, it will remain so during the whole period. The wrongly-behaved strings are dismissed, therefore distorting a posteriori the uniform draw within the amplitude interval. It is also important to remark that this choice may affect the probability of cusps and pseudocusps, as it may favour high frequencies in comparison to, for instance, Gaussian distributions; still, this is not a problem as our goal here is to look at the influence of some parameters on the number of cuspy events and not to deliver an exact prediction of this number.

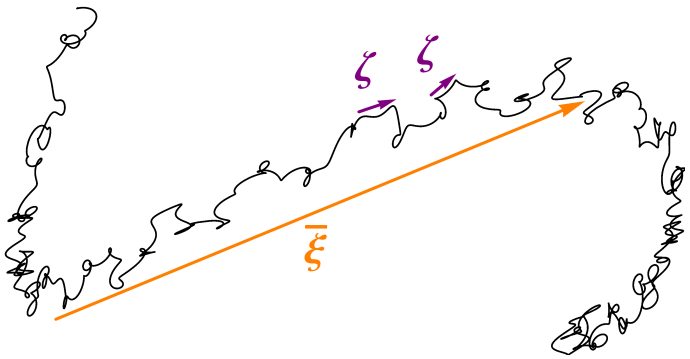

Figure 2.7: $\bar{\xi}$ and ζ, two of the network's length scales.

are input parameters of the simulation; they set up the oscillatory behaviour of the string, fixing a limit to the highest frequency and to the amplitude reached in its Fourier decomposition.

The parameter length σ_m and the interstring distance Δ are also inputs in the simulation. Indeed, to geometrically set up the system, one needs the end-to-end distance; additionally, the parameter length of the string is related to the fundamental frequency and to how wavy or wiggly the string can be. Clearly, Δ bounds σ_m, since the string cannot be shorter than the distance between its end points; one can also see that for $\sigma_m \to \Delta$ (and $\sigma_m > \Delta$), the curves $\mathbf{X}'_+$ and $-\mathbf{X}'_-$ get confined away from each other in the pole regions and ultimately shrink to a point in the case $\sigma_m = \Delta$. Since we will be mainly interested in their ratio, we chose to fix Δ by assigning to the end points invariable coordinate triplets while promoting σ_m as one of the main parameters of the code.

The network's parameters are often chosen to be ξ, $\bar{\xi}$ and ζ, representing the average interstring distance in the network, the coherence length scale (or large-scale structure) and the wiggliness (or small-scale structure) ; see for instance, Ref. [45]. Equivalently, ζ is related to small wiggles and to edgy bends on the string, while $\bar{\xi}$ characterises large-amplitude waves. We denote by *ripple* both of these variations along the string, wiggles and wiggliness being related to the small-scale structure and thus to ζ, while (large-amplitude) waves and waviness refer to the large-scale structure, that is, to $\bar{\xi}$. Fig. 2.7 gives a schematic representation of these ζ and $\bar{\xi}$ length scales.

In our simulation, Δ can be identified as the distance ξ[23] between two heavy

[23]We here consider for simplicity an overall interstring distance ξ — and generally only one set of parameters. As discussed in this section's last subsection, one can also consider that the light string and the heavy string networks have different characteristics, leading to the definition of ξ_{light}

strings, even though what matters here is the ratio Δ/σ_m. Note that this ratio could also be related to the large- and small-scale structure since a longer string has to exhibit more ripples, whatever the size of these ripples is. Here, there is no small-scale structure strictly speaking since the number of modes is quite low. So the wiggliness ζ is not defined and its influence is therefore not addressed. In addition, there is no clear input for the large-scale structure and its characteristic length $\bar{\xi}$ is to be linked with several other parameters such as the number and amplitude of the vibration modes at $t = 0$ or during a period. A crude estimation could be a fourth of a wavelength of the highest frequency mode present on the string, that is $\bar{\xi} \sim \sigma_m/2\bar{n}$, where $\bar{n}$ is the highest frequency mode on the string (and not the input n, which is only a bound on the highest possible mode). One could also consider the amplitude of the waves, for instance estimating the standard deviation of the y- and z-components of the position of the string at $t = 0$. The geometric mean of these two figures would represent even more accurately the characteristic size of a wave on the string, taking into account the two directions of extension of such large-amplitude waves.

Among the other ways to evaluate how wavy the string is, is to use the standard deviation of the x-component of the left- and right-movers' velocities, namely $\langle X'_{+x}X'_{+x}\rangle - \langle X'^2_{+x}\rangle$ (and the same with X'_{-x}) since it quantifies how far and how often the string goes away from a straight(er) position. Indeed, the straight line is represented by a constant $\mathbf{X}'_+$ and $-\mathbf{X}'_-$, while a large standard deviation from this pointlike curve means strong variations in the movers' amplitudes and smaller radii of curvature along the string.

Our simulation thus starts from these assumptions and parameters and a significant number of different string configurations is simulated. Each string's (non-interacting) evolution is then computed over a period. The string is then decomposed in a large number of points and the period is decomposed in time lapses. One can compute the norm of the velocity vector $\dot{\mathbf{X}}(\sigma, 0)$, using the tangent vector $\mathbf{X}'(\sigma, 0)$ and the Virasoro condition Eq. (2.10b) (which is thus automatically satisfied). In order to completely fix the initial conditions, that is to fix the initial velocity vector, we rotate it[24] within the plane orthogonal to the tangent vector $\mathbf{X}'$, thus satisfying by construction the Virasoro condition Eq. (2.10a). To assure continuity and periodicity, this rotation angle $\alpha(\sigma)$ is given by a Fourier decomposition: similarly to the initial position, a number of amplitudes are uniformly drawn

and ξ_{heavy}. In such a scenario, Δ would be related to ξ_{heavy} only.

[24]Before rotation, the velocity vector is such that the boundary conditions are satisfied.

in an interval $[\alpha_m, \alpha_m]$ and one gets $\alpha(\sigma) = \sum_{k=1}^{\bar{n}_\alpha} s_k^\alpha(\alpha_m) \sin\left(\frac{2\pi k\,\sigma}{\sigma_m}\right)$. One has now obtained $\mathbf{X}'(\sigma, 0)$ and $\dot{\mathbf{X}}(\sigma, 0)$, $\forall\sigma$, and the equation of motion Eq. (2.10c) leads to the decomposition $\mathbf{X}'_\pm(\sigma) = \mathbf{X}'(\sigma, 0) \pm \dot{\mathbf{X}}(\sigma, 0)$, $\forall\sigma \in [0, 2\sigma_m]$. This yields the complete (non-interacting) evolution of the string over a period of time. Note that it is checked that the various constraints, such as the Virasoro conditions, are well satisfied within the whole $(t, \sigma) \in [0, \sigma_m]^2$ plane.

The number of cusps is found by analysing the curves on the unit sphere and looking for actual crossings; the velocity is then computed and checked to reach $c = 1$ within the numerical uncertainties — which are generally[25] below 10^{-6}. The pseudocusps are all the other highly relativistic areas; here, we consider as "highly relativistic" any velocity above $0.999\,c$. Note that pseudocusps velocities are in a vast majority[26] in the range $[1 - 10^{-3}, 1 - 10^{-6}]$, helping to split between cusps ($1 - v < 10^{-6}$) and pseudocusps ($10^{-6} \leq 1 - v \leq 10^{-3}$). Finally, it is checked that pseudocusps correspond to configurations with a very small gap between the two curves on the unit sphere; the angle θ_c between the two vectors $\mathbf{X}'_+$ and $-\mathbf{X}'_-$ is computed and its minimum found (within the grid approximation).

Even though our analysis is performed within a specific setup, our qualitative results remain valid in the more realistic string configurations. The slow motion of the heavy strings can be ignored as compared to that of the light strings, whilst the periodicity can be safely considered as generic. The absence of a dynamical analysis and interaction between strings, chosen for the simplicity of the computations, should not modify the way the network parameters influence the occurrence of cusps and pseudocusps. In conclusion, our setup could represent a network of heavy and light strings interacting at a time scale which is not too small compared to the period of the light string's movement. Hence, the correlation between the network parameters and the occurrence of cuspy events should be valid independently of whether our simplifying assumptions are relaxed or not. Appendix B presents some example snapshots of a simulated string.

Description of pseudocusps

In the following, we call *computed* velocity the one from the simulation's direct evaluations, namely the highest velocity locally reached as it has been computed,

[25] About 10% of the cusps yield velocities outside a 10^{-6}-wide band around 1, and 3% outside a 10^{-5}-wide band.

[26] More than 80% of the pseudocusps' velocities lies below $1-10^{-5}$ and about 90% below $1-10^{-6}$. Figures are presented here for the computed velocity.

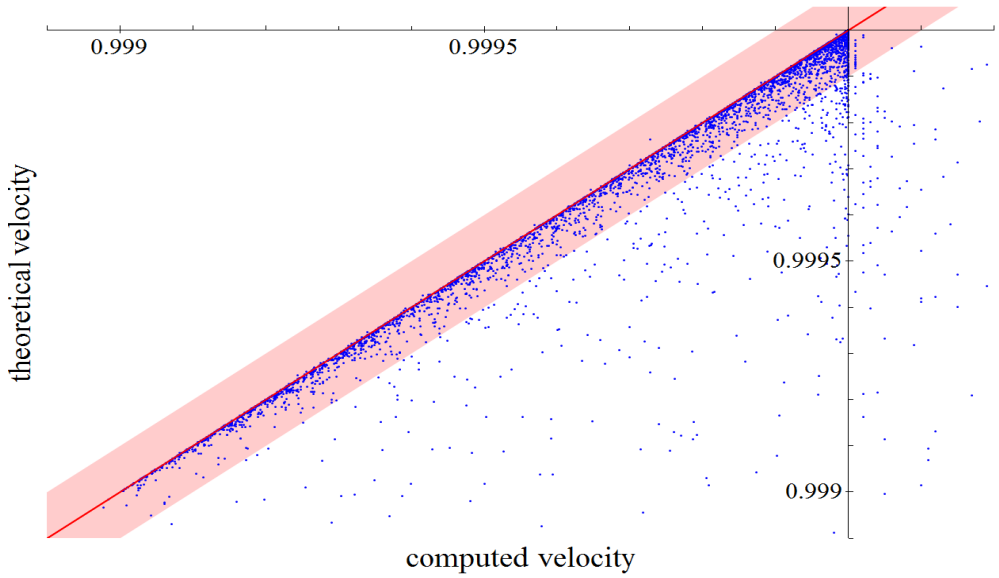

Figure 2.8: Pseudocusps: theoretically estimated velocity versus computed velocity. Note that 80% of the pseudocusps present a difference between the two velocities below 10^{-4}, meaning that it is represented here by a point in the red shaded area.

and *theoretical* velocity the value obtained using our model of pseudocusps, namely the one we got using the approximation $(1 - \theta_c^2/8 + \theta_c^4/384)$ from Eq. (2.54).[27] One can note that the latter cannot be above 1. We obtain a very good agreement between these two estimations of the strings' velocity at the pseudocusps.

Figure 2.8 shows, for almost 4300 pseudocusps[28] the computed velocity versus the theoretically estimated one. The red line draws the equality case and one can immediately note that $v_{\text{th}} \leq v_{\text{cp}}$ (except in very few cases almost not visible on this plot). This is probably due to the methods used: in the first case, the velocity has to be above 0.999 whereas in the second one it is always below 1. In addition, the computed velocity is subject to quite a lot of grid and computational uncertainties and can thus reach 1 (or even a higher value) fairly easily.[29] Finally, more than 80% present a difference between the two velocities which is below 10^{-4}.

Note though that all these discrepancies are actually gathering on the same cases. Indeed, among the 6% pseudocusps with theoretical velocity below $0.999\,c$, 80% give a computed velocity above $1-10^{-6}$. Also, almost 60% of the pseudocusps presenting velocities' discrepancies larger than 10^{-4} have either an abnormally small theoretical

[27] The approximation used here takes into account one more term, even if it is very often insignificant compared to the numerical uncertainties.

[28] About 8% of the almost 4700 pseudocusps studied here are not represented on this plot.

[29] We found almost 10% of the pseudocusps' computed velocity above $1 + 10^{-6}$. Recall that our uncertainties are generally of the order of 10^{-6}.

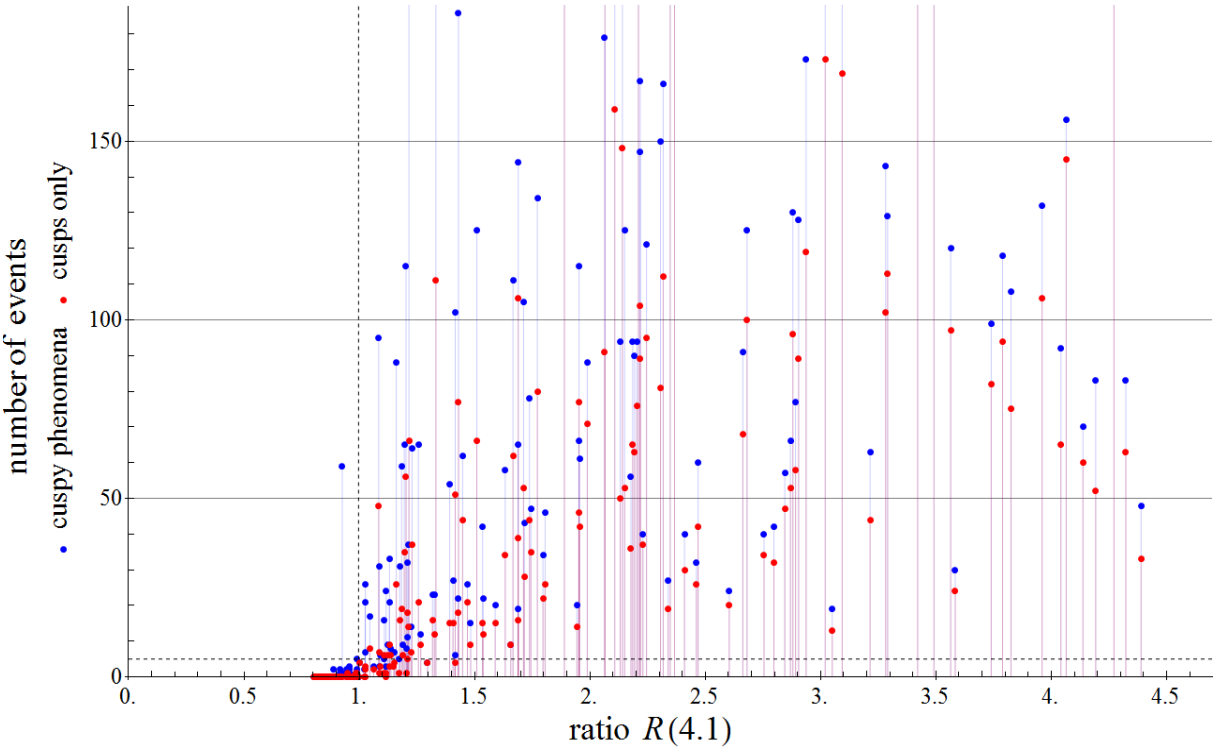

Figure 2.9: Number of cusps (red) and cuspy phenomena (blue) vs. ratio $R(4.1) = {}^{\langle X'_{+x} X'_{+x} \rangle}/_{1.24\,\Delta_+^2}$. The black dashed line standing at $R = 1$ is splitting the plane in two parts: non-cuspy strings for low ratios and cuspy strings for high ratios.

velocity or an abnormally large computed velocity.

Occurrence of cusps and pseudocusps

In order to check if the criterion set up in Eq. (2.50) is actually discriminating between configurations with cuspy phenomena and those without any cusp or pseudocusp, we simulated and studied a significant number of strings (237) within a variety of parameters. From the $\mathbf{X}'_+$ and $-\mathbf{X}'_-$ curves, we have calculated both the number of cusps and pseudocusps and the mean and standard deviation of $\mathbf{X}'_+$ in the x-direction. A very good agreement has been found between the presence of cuspy phenomena and the completion of our criterion.

On Fig. 2.9 we plot the number of cuspy phenomena versus the ratio

$$R\,(\alpha = 4.1) \equiv \left. \frac{\langle X'_{+x} X'_{+x} \rangle}{\frac{\alpha+1}{\alpha}\,\Delta_+^2} \right|_{\alpha=4.1} = \frac{\langle X'_{+x} X'_{+x} \rangle}{1.24\,\Delta_+^2}\ , \tag{2.57}$$

where the constrain parameter α can take any arbitrary value. Here it has been *a posteriori* fixed to $4.1\,^{+0.7}_{-1.6}$. Recall that once α is fitted, we are expecting to have only

strings with no cusps or pseudocusps for a ratio $R(\alpha) < 1$, and strings with cuspy phenomena for $R(\alpha) > 1$. Phrased differently, we should have neither non-cuspy strings with $R(\alpha) > 1$, nor cuspy ones with $R(\alpha) < 1$.

Note though that our statistical approach — both from the definition of the ratio $R(\alpha)$ and from the number of strings considered — will probably lead to strings in the tail of the distribution. Indeed, even with the most reliable choice of α, we are expecting to find a small range of value around 1 for which there are both strings with and without cuspy phenomena. If such an interval around 1 is not too large, this is not in contradiction with our previous analysis and does not affect the coherence of the results presented here.

Each simulated string is represented by two vertically aligned[30] dots: we use the red one to read on the vertical axis the number of cusps, and the blue one for the number of cuspy phenomena (both cusps and pseudocusps). The shaded coloured vertical lines are guides to read and have no physical meaning; it also helps to track points whose vertical coordinate is off the plotted range. The choice of the value of α and of where we divide the plane in two has to be discussed in view of the results. Before getting into the details, one can notice that the chosen value indeed fits with our set of points: on the left of the black dashed line standing at $R = 1$ are mainly non-cuspy strings, while on the right one we can almost only find cuspy strings. In addition, as we foreseen the range in which one can find both behaviours is restricted — roughly between 0.9 and 1.05. This means that strings satisfying the inequality

$$R\,(\alpha = 4.1) \gtrsim 1 \quad \Leftrightarrow \quad \langle X'_{+x} X'_{+x} \rangle \gtrsim 1.24\,\Delta_+^2 \tag{2.58}$$

would generally present cusps, and vice-versa.

To be more accurate, let us zoom on what is happening around 0.9–1.1 and let us discuss the ways to draw the limiting ratio. One may note that different rules can be set up to cut the plane in two parts (one without and another one with cusps). Firstly, one can decide to look at the highest ratio associated with a string presenting no cuspy events in order to fix the separating ratio (let's call it the *Highest with No Cuspy Events* ratio, below the HNCE). One can also consider the string with the lowest ratio and at least one cusp or pseudocusp (giving the *Lowest With Cuspy Events* ratio, or LWCE). Remark that since the HNCE is higher than the LWCE, there is a ratio interval in which we found both strings with and without cusps — again, as was expected. Alternatively, one can choose to look at cusps only and

[30]Since the two dots stand for the same string, the ratio on the horizontal axis is the same.

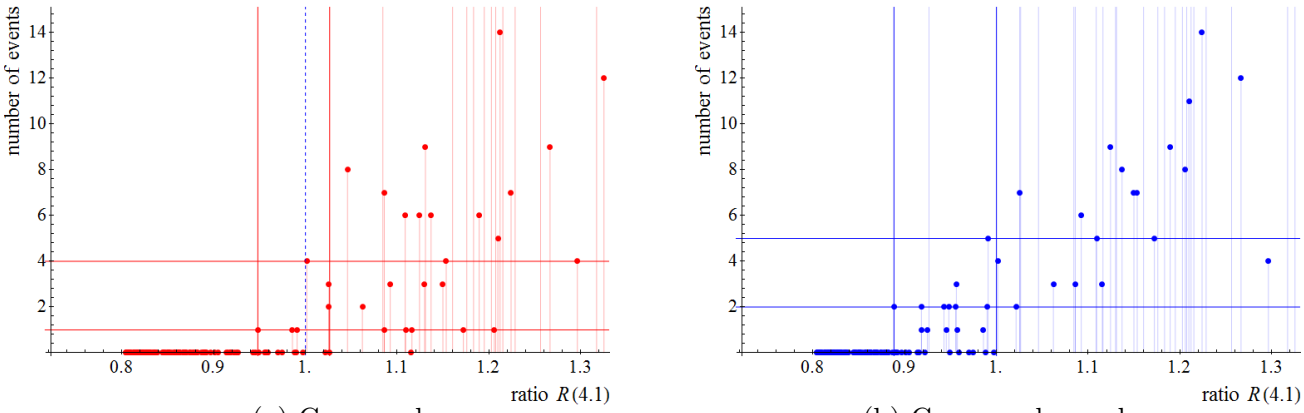

(a) Cusps only (b) Cusps and pseudocusps

Figure 2.10: Zoom around the low numbers of cuspy events. The vertical lines mark where the different splitting rules divide the plane.

follow the same method, giving two other boundary ratios (namely the HNC and the LWC, "C" standing for *Cusp(s)*). Note that these two new values are higher than their cuspy phenomena counterparts as pseudocusps are more likely to happen than cusps for borderline configurations. One thus gets four different ratio values which can equally be considered as valid turning points. One also has two intervals within which cuspy phenomena and cusps appear.

Depending on which rule one decides to apply, one gets a different line splitting the plane, giving a different value for α. Again, this does not affect our conclusions since we obtained quite close values, between 0.9 to 1.05.[31] In each of the two in-between intervals, we obtained strings with a small number of cuspy phenomena: less than 4 cusps or less than 5 pseudocusps. Also, for larger ratios, we only get very few strings presenting so few cuspy phenomena and these have all reasonably small ratios. These results confirm the expected behaviour, apart from the exceptional strings lying in the tail of the distribution and thus not giving the typical response, which are within an anticipated range.

Figure 2.10 focuses on the bottom left corner of Fig. 2.9[32] and has been divided into two plots: on the left and in red, Fig. 2.10a shows the number of cusps only versus the ratio $R(4.1)$ and on the right and in blue, Fig. 2.10b does the same for all cuspy events. On each of them, two of the four aforementioned ratios are represented

[31] We decided to neglect the two strings (over 237) presenting exceptional behaviours: one with no cusp and a quite high ratio — compared to the second-highest ratio for a string with no cusp — and one with a very large number of pseudocusps but a low ratio and no cusp. They are thought to be statistically irrelevant.

[32] Again, the shaded coloured lines connecting points are guides for reading and help to track points off the plot.

by solid coloured lines: two red lines for the LWC and the HNC on Fig. 2.10a and two blue ones for the LWCE and the HNCE on Fig. 2.10b. Note that on Fig. 2.10a is also displayed a blue dashed line marking the HNCE ratio (i.e., the highest of the two ratios for all cuspy phenomena); it is lying roughly in the middle of the interval considering cusps only (on the graph, the two solid red lines).

We would like to determine a value for the ratio which splits the plane into two regions (without and with cuspy phenomena), knowing that in a small neighbourhood around this value one should expect to find irregularities, which we hope to be sufficiently rare and small. One can see that the HNCE ratio satisfies our needs:

- on the left (i.e. for smaller ratios than the value of the HNCE) one can find only strings with no or one cusp, and strings with at most five cuspy phenomena — most of them presenting no cusp and no pseudocusp);
- on the right (i.e. for higher ratios) lies only strings with at least two cusps and pseudocusps, most of them presenting more than three cusps and five cuspy phenomena.

In addition, recall that our analytic work to find the ratio $R(\alpha)$ is identifying cusps and pseudocusps (see Section 2.3.2), so the most meaningful turning point values we found are the ones related to all cuspy phenomena (HNCE and LWCE). Hence the choice we made at the beginning to set $\alpha = 4.1$. It is important to notice that while the number of pseudocusps depends on their *a priori*, arbitrary definition, in particular on the threshold velocity $(1-10^{-3})$, the value for α does not, as can be seen from the values of the LWC and the HNC, which are within 5% of the HNCE. Also, while Eq. (2.50) gives a solid criterion, there is room around $R(\alpha) = 1$ for slightly skewed strings lying in the tail of the distribution (strings with a few cuspy events but for which $R(\alpha) \lesssim 1$ or without any cuspy event although $R(\alpha) \gtrsim 1$), but again this is due to the statistical treatment here and does not affect our main result.

While the value of α depends on the sample used to fix it, what is crucial here is that there *is* a value such that this ratio allows to discriminate between cuspy and non-cuspy strings, and that this value somehow lies within 2.5 and 5 (corresponding here roughly to choosing the threshold to be the HNC or the LWCE), whatever the sample. More strings, implying more strings in the tail of the distribution, would yield smaller LWC(E) and higher HNC(E). Still, one would fix a turning point around the same values, for instance using a combination of these limits. Again, the statistical point of view assumed here means that the tail of the distribution

populates a zone around this turning point, without limiting its interest. Its precise value is somehow arbitrary; whether it corresponds to the HNCE is not crucial, and has to be decided a posteriori anyway.

We have thus set up here a quick and efficient method to discriminate between cuspy strings and non-cuspy ones.

Number of cusps and pseudocusps

One can now try to find which parameters influence the number of cusps and pseudocusps on a string. As we have seen already, there is a strong dependence on the interstring distance $\Delta = \xi$ and the parameter length of the string σ_m — or rather on Δ/σ_m — as well as some important correlation with the mean squared x-component of the string's movers' derivatives $\langle X'_{+x} X'_{+x} \rangle$ and $\langle X'_{-x} X'_{-x} \rangle$.

A few remarks first. Recall we study how the quantity of cusps or pseudocusps is influenced by the parameters of the strings network. Therefore, we do not try to compute the number of cuspy events in a real, physically accurate system. The abundances obtained below should then be interpreted with respect to one another, and not as absolute figures. In addition, our simulation choices, in particular the spectrum of vibration modes at $t = 0$, seem to favour strings with a large number of cusps. Indeed, a uniform distribution yield higher amplitudes for high frequency modes than, say, a Gaussian distribution, thus favouring high velocity points. This might explain, at least partly, the difference between the usual, analytic (loop) modelling, with one to two cusps [43], and our simulation, with up to hundreds of cuspy events. Another explanation might also be the understandable need, in analytical derivations, for simpler strings, as well as the different physical configurations (namely loops). In fact, one could argue that this bias, yielding a whole gradation from none to many cusps, allows for a more accurate investigation of the influence of the strings network parameters.

In order to understand these relations in more detail, we first analyse the influence of the Fourier modes initially implemented in the string and found that only the x-modes[33] influence the number of cusps, both via the number of modes n and their amplitudes $A_k^{(x)}$, $k \in [\![1, n]\!]$. Indeed, the x-component of the string's initial position vector $\mathbf{X}_x(\sigma, t = 0)$ has been decomposed in n Fourier modes, with $A_k^{(x)}$ the amplitudes. On Fig. 2.11, we plot the root mean square of the amplitudes, that is

[33]The y- and z-modes are not found to be correlated to the number of cusps. The number and amplitudes of these modes are only indirectly linked to those of the x-modes via $\left|\mathbf{X}'_+\right|^2 = 1$.

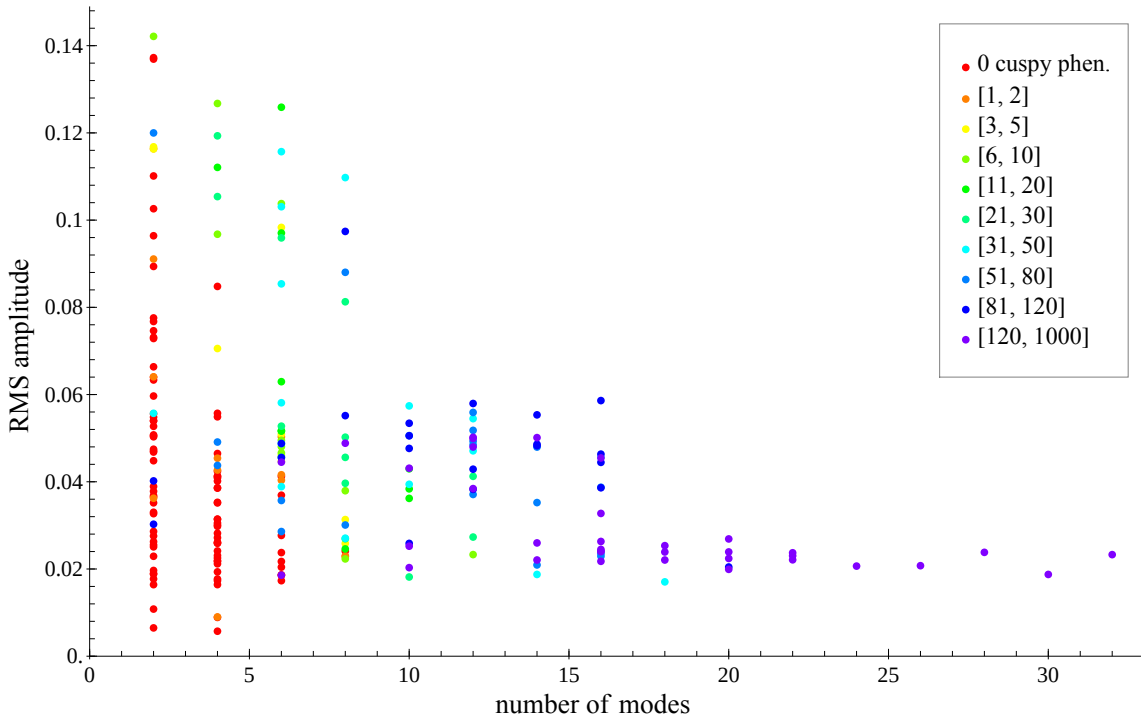

Figure 2.11: Root mean square amplitude of the x-modes versus number of x-modes. From red to purple, strings with 0 to between 120 and 1000 cuspy events.

$\sqrt{\frac{1}{n}\sum_{k=1}^{n}(A_k^{(x)})^2}$, versus the number of modes; a colour gradient is representing the strings grouped according to the number of cuspy events (from 0 in red to above 120 in purple). It is first obvious that more modes imply a lower RMS amplitude. This is due to the physical constraint to have no supraluminal points on the string.[34] In addition, one can note that a low number of x-modes imply a low number of cusps, especially for low RMS amplitudes. Also, many modes generate strings with statistically many more cusps. For a fixed number of modes, higher amplitudes are associated with strings with more cusps, whereas at a fixed RMS amplitude, more modes imply more cusps. This is to be expected for several reasons. First of all, a higher RMS amplitude as well as more modes imply more energy in the string's vibrations. More energy means a higher average energy and favours highly relativistic points. On a more specific point of view, these high amplitudes and numerous modes imply large deviations from a straighter line, both for the physical string and for the curves $\mathbf{X}'_+$ and $-\mathbf{X}'_-$. This implies a wavier string, hence more crossing on the unit sphere.

[34]This constraint is enforced during the evolution of the string but has to be carefully checked at $t = 0$.

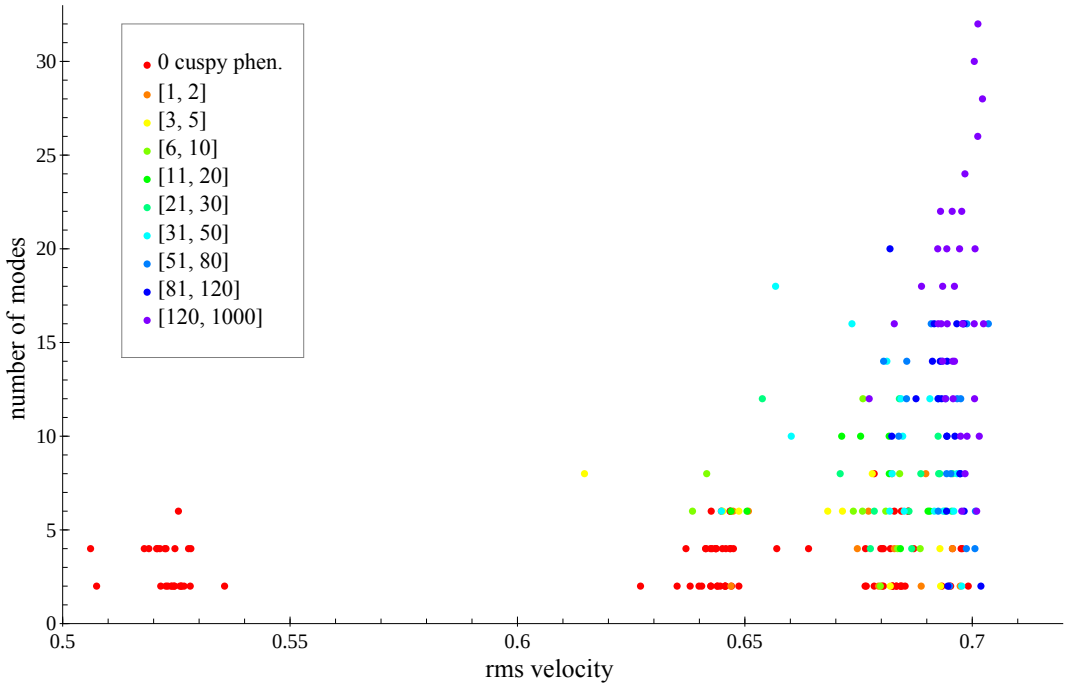

Figure 2.12: Number of x-modes versus root mean square velocity of the string. From red to purple, strings with 0 to between 120 and 1000 cuspy events.

One can then study the correlation with the RMS velocity of the string, which is related to what we just mentioned; we plot it on Fig. 2.12 the number of x-modes versus the (time-averaged) root mean square velocity (along the string).[35] Again, a colour gradient is representing the strings grouped according to the number of cuspy events (from 0 in red to above 120 in purple). One can first notice that the RMS velocity reaches a maximum around 0.7–0.71. This is due to the Virasoro and gauge conditions used on the finite string; indeed, it implies for the RMS velocity: $v_{\text{rms}}^2 \leq 1/2 \quad \Leftrightarrow \quad v_{\text{rms}} \leq \frac{1}{\sqrt{2}} \simeq 0.707$ (the equality being realised for loops).

In addition to the previously studied correlation between the number of cuspy events and the number of x-modes, there is a strong dependence on the RMS velocity of the string, as expected. One can split the set of strings into four groups according to their RMS velocity: below 0.58, between 0.58 and 0.67, between 0.67 and 0.69 and above 0.69. While the first subset of string shows no cusps or pseudocusps, the last one contains almost all the strings with more than 120 cuspy events and almost

[35] We here call 'RMS velocity' the time average of the root mean square velocity computed along the string, that is, on σ. Indeed, while one could have computed the *full* RMS velocity, as in $\langle \dot{\mathbf{X}}^2 \rangle_{\sigma,t} \sim \iint \mathrm{d}\sigma \, \mathrm{d}t \, \dot{\mathbf{X}}^2(\sigma, t)$, it made more sense to compute the time average of a quantity related to the energy of the string, that is, the time average of the RMS velocity (along the string), as in $\langle E_K \rangle_t$ where $E_K^2(t) \sim \langle \dot{\mathbf{X}}^2 \rangle_\sigma(t)$. Both are bounded by $\sqrt{1/2}$.

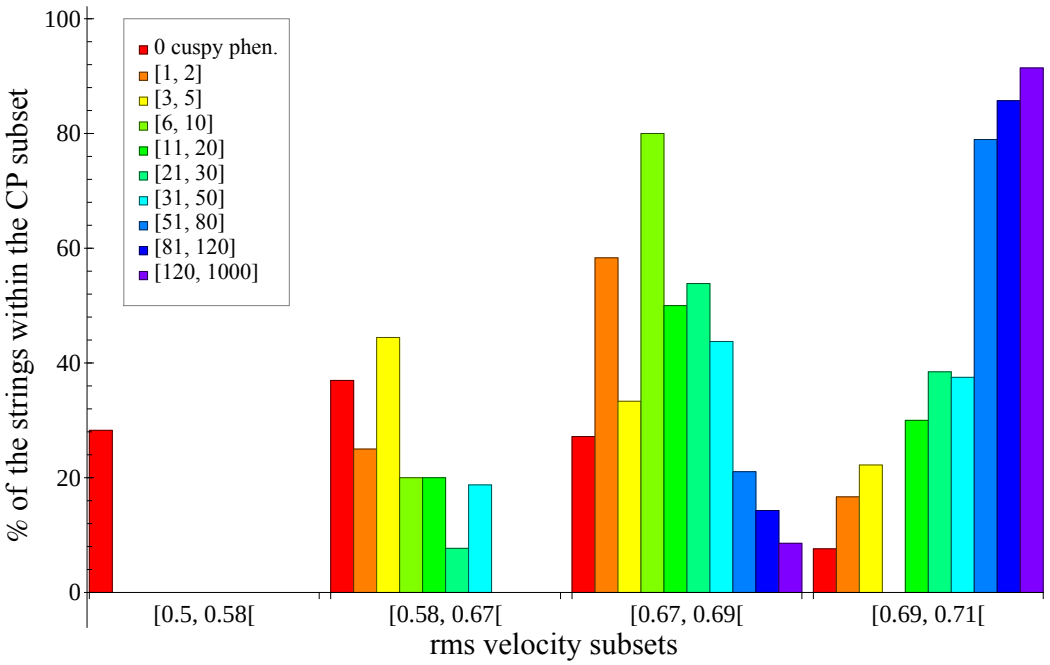

Figure 2.13: Bar chart of the percentage of the strings within a CP subset whose RMS velocity lies in each interval. Same colour representation as previously.

no string without any.

To be more explicit, for each subset of strings grouped according to the number of cuspy events, Fig. 2.13 shows the percentage of strings in each interval of RMS velocity. One can indeed notice that in the highest interval (that is for RMS velocity above 0.69) one only finds a few of the strings without cusps or pseudocusps (about 8%) but most of the strings with more than 50 cuspy events (80 to 90% of them). We also computed the average number of cuspy events in each of the four RMS velocity subsets and obtained the results given in Table 2.1. There is again an interesting

RMS velocity range	Average number of cuspy events per string
[0.50, 0.58]	$0. \pm 0.$
[0.58, 0.67]	4.3 ± 1.5
[0.67, 0.69]	21 ± 3.9
[0.69, 0.71]	130 ± 16

Table 2.1: Average number of cuspy events per string, within each range of RMS velocity.

correlation between the RMS velocity of the string, which is closely related to the energy of the string, and the number of cusps and pseudocusps.

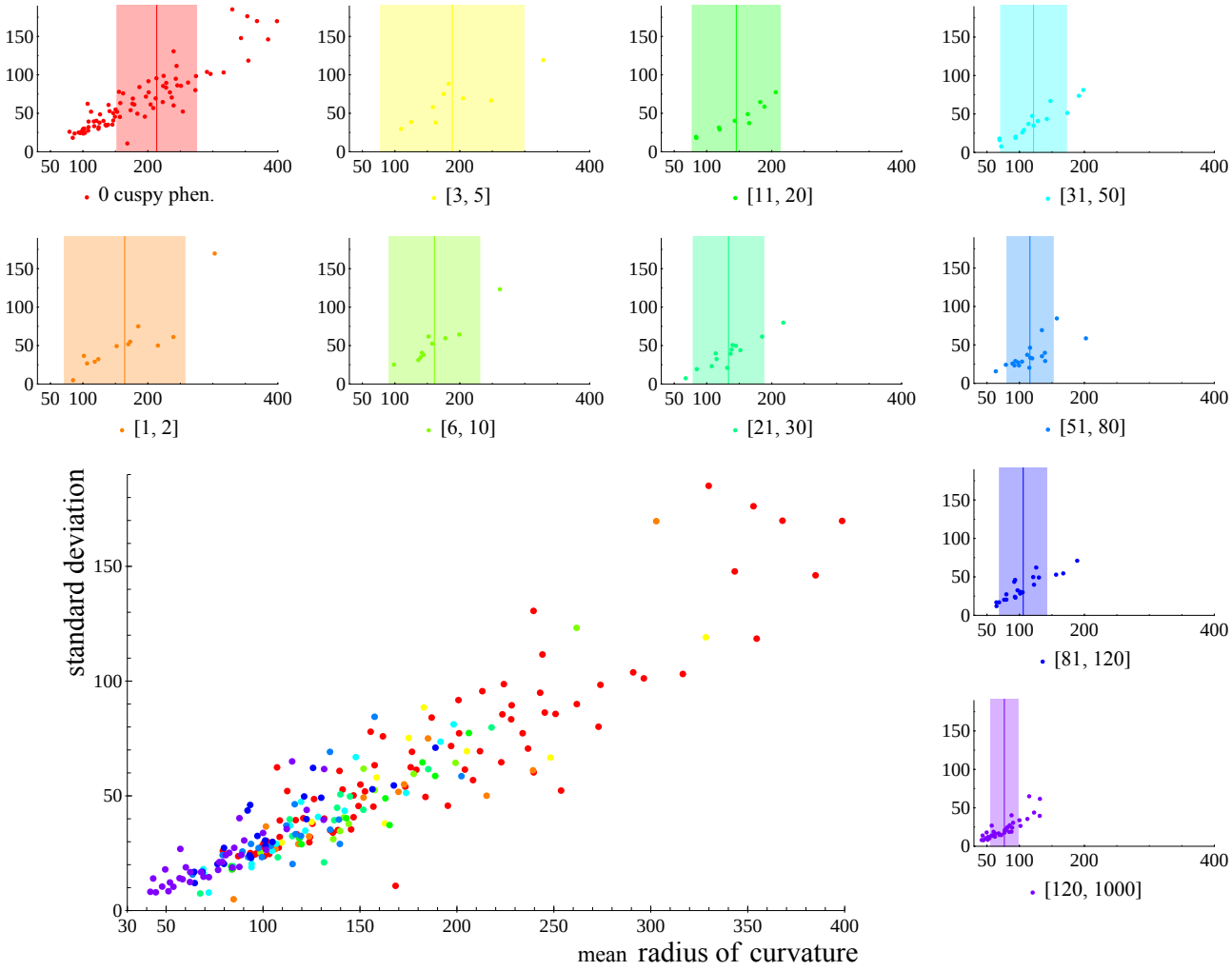

Figure 2.14: Radius of curvature and its standard deviation. Same colour representation. On each subgraph, the solid line marks the mean within the subset and the shaded area represents 5 times the standard error.

Finally, and in order to return to a previously mentioned concern, one might want to look at the correlation with the radius of curvature along the string.[36] Indeed, it can in turn be linked to the large-amplitude waves' characteristic length since it represents the average size of waves on the string; note though that it is several times larger than the characteristic length since it also takes into account the flat parts of the string between such waves.

With this in mind, we plot the standard deviation versus the (mean) radius of

[36]We are here dealing with the radius of curvature averaged along the string. For clarity, in the following we call *(mean) radius of curvature* the time average of the already space-averaged radius of curvature for each string separately; the *standard deviation* of the radius of curvature is then the deviation during a period of time from this average. We thus end up with two figures per string.

curvature for each string. We split up the set of strings according to the number of cuspy events and also draw the superposition of all the subgraphs. Figure 2.14 shows, from top to bottom and from left to right, the ten subgraphs along with the overall graph in the bottom left corner. For each separate subset has been computed the mean and the standard error[37] of the radius of curvature, showing how it evolves with the number of cuspy events. They have been added via a solid line on the mean and a coloured shaded area around it encompassing 5 times the standard error.

First of all, one can notice that the standard deviation grows almost linearly with the mean radius of curvature, albeit with some dispersion at large values. More interestingly, the radius of curvature is smaller for strings with many cusps: this shows again the foreseen correlation according to which a wavier string presents more cusps and pseudocusps. This can be seen from the overall graph, on which for instance points with a radius of curvature larger than 200 have generally less than 5 cuspy events, most of them having none. It can also be deduced from the subgraphs in Fig. 2.14. More precisely, the mean of each subset is decreasing with the number of cuspy events: from 210 for non-cuspy strings to 75 for very cuspy ones. The standard error is also decreasing, apart from the less populated subsets (for instance, subsets of strings with 1 to 5 cusps and pseudocusps have larger standard errors than the one for non-cuspy strings since the latter includes many more strings).

Correlation with the parameters of the network

As mentioned previously, we are mainly interested in two networks' parameters: the interstring distance ξ and the coherence length $\bar{\xi}$. We have defined Δ to be the distance between the junctions, hence it could be considered as the interstring distance (since it is the distance between two heavy strings) but physically, its ratio with the parameter length is more relevant. In our simulation, the end-to-end distance is fixed and the parameter length of the string plays a scaling rôle. Indeed, it turns the ratio Δ/σ_m into our length parameter since it gives the sum of the average vectors $\langle \mathbf{X}'_+ \rangle_\sigma$ and $\langle \mathbf{X}'_- \rangle_\sigma$ — which is along the x-axis — in the unit sphere description. We can thus associate the interstring distance with this simulation's parameters ratio

$$\xi \sim \frac{\Delta}{\sigma_m} \ . \tag{2.59}$$

[37]Here, the mean and the standard error are computed among the strings of the same subset on the (mean) radius of curvature, giving us two figures for each subset. Note that we define the standard error as $\frac{\sigma}{\sqrt{N_\mathrm{s}}}$ where σ is the standard deviation in the subset and N_s is the number of strings in this subset.

In the case of a *double* network consisting of both heavy and light strings, each one is associated with a set of parameters: ξ_{light}, $\bar{\xi}_{\text{light}}$ and ξ_{heavy}, $\bar{\xi}_{\text{heavy}}$. In agreement with the configuration we are studying, our analysis does not take into account the light string network's interstring distance ξ_{light} but only the heavy one's via $\xi_{\text{heavy}} \sim {}^{\Delta}/_{\sigma_m}$.

The definition of the coherence length is more subtle for several reasons. First of all, our simulation does not input directly a typical length apart from the minimal wavelength of the vibrations on the string. Instead, random numbers are drawn to define the string's structure, implying that we need to compute the length scale afterwards. In addition, in our numerical approach, one may use different ways to define the characteristic size for waves and wiggles on the string and even different definitions of large-amplitude waves.

Still, let us explore some of the possibilities, starting with the usual definition [45, 54] computing the correlation between two points along the string via

$$\bar{\xi} \equiv \int_0^{2\sigma_m} \mathrm{d}\sigma \ \langle \mathbf{X}'_+(\sigma) \cdot \mathbf{X}'_+(\sigma+\delta) \rangle_\delta \ , \tag{2.60}$$

where $\langle \dots \rangle_\delta$ is the average over $\delta \in [0, 2\sigma_m]$. However because this computation implies knowing the whole string's motion and its decomposition in left- and right-movers, it cannot be related straightforwardly to the string's parameters. It is thus of no use to us here and we need to define our persistence length differently.

In the search for different formulations, one could think of the radius of curvature. This number defines for each string a condensed typical size of all the ripples on the string during the whole period. Unfortunately, it takes into account the flat parts of the string whose radius of curvature is obviously very large. This makes the strings' radius of curvature difficult to use in order to define a specific length scale but still allows us to notice some correlation: the number of cusps and pseudocusps grows with smaller radii of curvature. This means that the information about the large-amplitude waves is, at least partially, encoded in the radius of curvature even if we cannot simply access it.

Let us use what seems to be the simplest and most reliable way to define a scale for the large-amplitude waves on the string: the vibrations' frequency. Indeed, the modes set up on the string at $t = 0$ are stable and keep the same amplitude during the evolution. Even if they can be hidden at a specific time by other frequencies and not visible when looking at the string itself (or at its radius of curvature), they are characteristic of the way the string vibrates. Moreover, this parameter can be

easily controlled by the inputs of the simulation and also evaluated once the string is drawn. The only remaining issue has to do with the number of the largest frequencies to be accounted for. Obviously, we could not only use the lowest frequency, that is, the largest wavelength, because it would not take into account the waves on the string — especially in our case where the largest wavelength is fixed and equal to twice the length of the string. We could use the highest frequency only and define the large-amplitude waves characteristic length directly according to the associated wavelength. This is not ideal though because there could be configurations where the highest frequency mode's amplitude is very small compared to that of the second highest frequency. This would indeed distort the data by increasing the highest frequency (compared to the physically relevant one), thus decreasing the interesting length scale. In general, this definition would also be too sensitive to the high frequency part of the Fourier decomposition and not enough to the whole spectrum.

One way to deal with this issue is to compute a length scale based on all the wavelengths $\lambda_k \equiv {}^{\sigma_m}/_k$, taking each one into account according to their rank k and to the associated amplitude A_k.[38] Different possibilities have been considered but what seemed to be the most accurate and the simplest one is to use the average wavelength $\bar{\lambda}$. One has to note first that in order to keep the velocity below $c = 1$ at all time, one needs to choose amplitudes such that $A_k \sim \lambda_k$ (under the simplifying assumption that all modes carry roughly the same amount of energy). Keeping this in mind, looking at $\sum \sqrt{A_k^2 + \lambda_k^2}$ is equivalent to considering $\sum \lambda_k$.

Hence, we define the coherence length in terms of the mean wavelength $\bar{\lambda} \equiv 2\,\sigma_m\, H_{\bar{n}}\,/\,\bar{n}$, giving

$$\bar{\xi} \sim \frac{\bar{\lambda}}{4} = \frac{\sigma_m\, H_{\bar{n}}}{2\,\bar{n}} \simeq \frac{\sigma_m\,(\ln(\bar{n}) + \gamma)}{2\,\bar{n}}\ , \tag{2.61}$$

where $\bar{n}$ is the highest frequency mode on the string (and again not the parameter n of the simulation) and $H_n = \sum_{k=1}^{n} {}^1/_k$ is the harmonic series. Recall $H_n \simeq \ln(n) + \gamma$ with $\gamma \simeq 0.577$ and that the difference $H_n - \ln(n) - \gamma$ is larger than 10% of H_n only for $n \leq 3$, meaning that the approximation is sufficient for our estimation as soon as $n > 3$. Finally, note that since the number of modes is quite low in our simulation (at most 16 modes are taken into account), this cannot overlap with a definition of the wiggliness ζ.

We have here estimated the two parameters of our strings' network in terms

[38] Even if the amplitudes are drawn in a symmetric interval around 0, one of them being actually null is statistically insignificant. This implies that the k^{th} wavelength is of the form ${}^{2\,\sigma_m}/_k$, recalling that the fundamental excitation has no nodes and thus has a wavelength equal to twice the string's length.

of two parameters of the simulation.[39] As foreseen, the parameter length of the string σ_m plays an important rôle, both for defining the interstring distance and the coherence length. The number of modes seems like the most obvious and accurate way to define a large waves length scale.

2.3.4 Conclusions and outlook

Gravitational waves (GWs), especially since they have been directly observed for the first time [4], are at the centre of attention. They are the next tool for cosmology and high energy astrophysics and should soon give us a stream of new data to analyse. Similarly, cosmic strings are thought to be unavoidable in most of the cosmic scenarii and should provide insight into the symmetry breaking they are remnants of or the theory to which they belong.

In this chapter, after introducing how such strings would appear in Section 2.1 and their general properties in Section 2.2, we focused on a particular configuration made of a light string stretched between two junctions with heavy strings in Section 2.3. It is important to note that even if we considered simplifying assumptions, the overall behaviour and the results should remain in more realistic configurations as long as the end points of the light string can be seen as fixed during a period of oscillation. We then looked at highly relativistic points since they are sources of high frequency bursts of GWs. Such cuspy events appear on a string when the left- and right-movers' derivatives are temporarily equal (or approximately equal), making them reasonably easy to identify. We split them into two classes: the actual cusps, resulting from crossings of the two movers' derivatives curves and hence reaching momentarily the speed of light $c = 1$, and the so-called *pseudo*cusps, resulting from a close approach between the two curves and hence reaching highly relativistic velocities, typically below $c = 1$ by 10^{-3} to 10^{-6}.

Since cuspy events emit large amounts of energy in the form of GW Bursts (GWB), to estimate the signal that could be detected in the neighbourhood of the Earth by ground- and space-based detectors, one needs to know how frequently they occur. We have here aimed to quantify this and analyse it in terms of the parameters characterising the string configuration as well as the string network, through its parameters ξ and $\bar{\xi}$ (but not ζ).

Our analytical approach allowed us to identify the symmetries of the problem.

[39] We used three parameters — Δ, σ_m and $\bar{n}$ — but in fact Δ is not a variable, leaving two actual parameters.

Indeed, because of the boundary conditions, the string moves (almost) always periodically. In addition, on the unit sphere, the left- and right-movers' derivatives are related by a π-rotation with respect to the axis parallel to the heavy strings. This simplifies the problem enough to evaluate the frequency of cusps and pseudocusps on the string with respect to a few parameters.

We found that cusps should be frequent for strings satisfying (see Eq. (2.50))

$$\langle X'_{+x} X'_{+x} \rangle_\sigma \gtrsim \frac{1+\alpha}{\alpha} \left(\frac{|\Delta|}{\sigma_m} \right)^2 ,$$

where $\mathbf{X}_+$ is the left-mover on the string and $\mathbf{X}'_+$ its first derivative (with respect to its only variable σ_+), $|\Delta|$ the end-to-end vector's norm and x its direction (the subscript x thus referring to the projection on the x-axis), σ_m the parameter length of the string and α a parameter we subsequently estimated around $\alpha = 4.1^{+0.7}_{-1.6}$. It is important to notice that such cuspy strings should present many important waves.

We then used a simulation to get a statistically important number of strings within a range of parameters, in order to check this behaviour. The set of 237 strings we obtained presents 8719 cusps and 4659 pseudocusps, i.e. slightly more than half the number of cusps. We analysed the occurrence of cuspy events with respect to several other features, confirming our analytical work and the general behaviour of such strings.

In particular, we first checked that our characterisation of pseudocusps from the minimal angle between the two curves on the unit sphere is relevant. For instance, the velocity we obtained from this description is very close to the one obtained directly from the simulation (within grid and computational inaccuracies). In addition, the presence of cusps and pseudocusps increases according to the inequality Eq. (2.50), giving us an accurate tool to discriminate between cuspy and non-cuspy strings. More importantly, it also depends on the number and amplitude of the vibration modes in the x-direction; this confirms more directly the fact that the wavier a string is, the more cuspy events it presents.

We also analysed the influence of the RMS velocity on the string: as one could expect, the more energy there is in the string, the more cusps appear. This is consistent with the fact that more vibrating modes imply more cusps, since both indicate more energy. Finally, we found the radius of curvature along the string is also correlated to the number of cusps and pseudocusps, favouring again the mentioned behaviour (a smaller radius of curvature is equivalent to more waves,

which are in turn linked to more cusps).

Expressing the usual network parameters in terms of our simulation's parameters, we refined the link between the numerical description and the way Cosmic (Super)Strings (C(S)S) networks are traditionally pictured. This should allow future work, whether on GWs or on the interacting evolution of the network, to assess, use and further continue this work.

Indeed, the next step from this work is to look at the importance of pseudocusps in terms of GWB. Indeed, as we saw, the points around a cusp also reach highly relativistic velocities and the approximations made in order to obtain the $-4/3$ slope in the high frequency end of the GW power spectrum might still hold for neighbouring points. Said differently, the whole region, around the cusp, which reaches velocities within, say, $0 < 1 - v < 10^{-5}$, might as well significantly contribute to the GWB. An important study would thus be to look at the way the slope evolves with the velocity, in order to define more pragmatically what a cusp and a pseudocusp are.[40]

In addition, one could use this method to conduct a similar analysis on other string configurations, namely loops or infinite strings — even though infinite strings have no boundary conditions, making them harder to study in the unit sphere description. The interactions of cusps with different strings features, Y-junctions and kinks for instance, could potentially modify their rate of appearance, directly or via the dynamics of the string network.

Finally, as mentioned initially, the goal is to embed this work in a general accurate prediction of the signal one could receive and detect in the Earth neighbourhood. Considering, for instance, a specific brane inflation scenario, leading to a peculiar CSS network, defined by an interstring distance ξ and a large amplitude wave scale $\bar{\xi}$, one could infer the average probability to have cusps and pseudocusps at a fixed time. Adding the network cosmological evolution and dynamics, one could compute the high frequency GWs emissions from such a network and thus the overall signal received on Earth, to be compared to observations. This would be a very interesting way to explore and constrain the underlying theory of the universe, whether string theoretic or not.

[40]We performed and will soon publish such analysis with M. Sakellariadou and M. Stott. It turns out our a priori definition of pseudocusps holds very well when considering the slope of the GWB power spectrum.

Chapter 3

Modified gravity

String theory was first developed in the late 1940s and the 1950s, to explain the behaviour of hadrons and therefore the strong force, before Quantum ChromoDynamics (QCD) emerged. Even though unsuccessful in this context, it appeared as a theory of bosons in the 1970s, until supersymmetry was included to allow for the description of fermions as well. The resulting theories were then understood, in the middle of the 1990s, as duals to one another and as limits of a more fundamental $10+1$ dimensional theory called M-theory. Despite the fact that it is still not fully formalised due to its complexity, such theory is thought and hoped, at least to shed light on the underlying laws of nature, but also to rise as a theory encompassing every mechanism of the universe. An absolute necessity is to generate a rich phenomenology from these models to demonstrate their ability to explain the known and to predict the unknown.

In this chapter, we start in Section 3.1 by looking at the interest of string-inspired models for gravity and cosmology. This is followed in Section 3.2 by an introduction on the specific model we will focus on in the following, namely the D-material universe. In particular, we present the contents of the universe and the resulting low energy action along with the formalism. The equations of motion for each field, the scalar dilaton field, the vector recoil velocity field and the graviton field, are obtained, yielding the basis of the further investigations: in Section 3.3, we assume spherical symmetry in the late Dark Energy (DE) dominated era to formulate a lensing analysis; an inflation mechanism is provided in Section 3.4, in which the field strength condensate into a slowly varying scalar field, playing the rôle of the inflaton; finally, we examine in Section 3.5 the consequences of our extra fields on the emergence of a graviton mass and on the refractive index to be considered for radiation propagation.

These tests of the theory, taking place at several length scales and during various

cosmological eras, provide multiple ways of constraining the parameters of the model, such as the string scale M_s.

3.1 String-inspired models of modified gravity

About a century ago, in November 1915, Einstein published his equations describing the entangled dynamics of the gravitational field and the curvature of spacetime on one side with the energy and matter content on the other, leading to the extremely successful General Relativity (GR) theory of gravitation. A rich history of experiments and measurements have been used to verify this paradigm, on Earth, in the Solar System and beyond, up to cosmological scales. In the recent decades, analyses based on a Friedmann-Lemaître-Robertson-Walker (FLRW) universe, which follows Einstein equations in their homogeneous and isotropic form, and on the observations of light from sources at cosmological distances from us, have given us important information on our universe, on its content, on its history. Precision measurements of the Cosmic Microwave Background (CMB) and of its anisotropies [6], of Baryon Acoustic Oscillations (BAO) and of high-redshift extragalactic type IA supernovae revealed, under such hypothesis, the energy budget of our current universe, its evolution, its properties such as its topology, down to epochs as early as inflation, which occurred sometime between 10^{-36} and 10^{-32} s after the Big Bang [10].

Nevertheless, there are still many important issues that remain open or not understood at all, such as the nature of Dark Matter (DM) and Dark Energy (DE), as well as their relative abundance, respectively 26% and 69% of the current energy budget of the universe. Furthermore, the problem of the cosmological constant's magnitude, the origin and mechanisms of inflation, or the intrinsic nature of spacetime are some of the most challenging issues of cosmology and physics in general, so far unresolved by the standard ΛCDM model. The dark sector has been attributed to (yet undiscovered) particles that may exist in extensions of the standard model, such as axions, supersymmetry, string theory, higher-dimensional field theories, etc. Even though there are stringent constraints on the DM relic abundance from direct and indirect (including collider physics) searches, there is still no concrete experimental evidence of the existence of such particles.

In the late 18^{th} century, Newton's theory of gravity was extremely well verified by both experiments on Earth and measurements of the trajectories of celestial objects, but Uranus' and Mercury's orbits presented some discrepancies with the predictions.

While the former case was resolved by Urbain Le Verrier in 1846 by introducing new content to the universe, namely Neptun, a modification of the theory was to be needed to understand the latter one, that is general relativistic corrections.

Similarly, the lack of direct experimental evidence prompted conjectures that a DM component in the universe does not exist but, instead, the assumption that the Newtonian gravitational equations describe the universe at galactic scales should be relaxed: one may have a MOdified Newtonian Dynamics (MOND) at such scales [55]. MOND theories have been embedded in relativistic modified gravitational field theories, where in addition to the graviton field, one has extra scalar and (constrained) vector modes, the so-called *Te*nsor-*Ve*ctor-*S*calar (TeVeS) theories of gravity [56]. The phenomenology of these alternative theories of gravity is, at present, controversial, in the sense that at least the simplest models of TeVeS theory proposed initially need significant amounts of DM to be compatible with some of the lensing data, which is in contradiction with their original motivation as alternatives to DM. Still, the situation of course is far from being conclusive. The cosmology of TeVeS has also been developed and some interesting links of the vector fields of such theories with large scale growth of the universe have been proposed, even though of course their phenomenology is not yet as well studied as the standard ΛCDM model. It should be noted, however, that there is no microscopic origin of the currently available modified gravity (TeVeS/MOND) models, based on some underlying fundamental physics, and this is in our opinion a major drawback of all such models.

Alternatively, endeavours to quantise gravity, perturbatively and non-perturbatively, have somehow flourished into two competing ways leading to loop quantum gravity on the one hand and string theories on the other. The latter are, so far, one of the few candidates to be the ultimate, universal, complete theory of nature [22, 23]. Due to the complexity and to the lack of a complete, formal description of string theory, an effective theory framework can be used [13] to study the low energy corrections to General Relativity, which, even though unreliable at high energy scale and thus UV incomplete, provide interesting results. These string-inspired models of modified gravity are studied in order to explain or predict the cosmological phenomenology. Indeed, as we know, the ΛCDM model completed by inflation, even though so far extremely well verified by data [57], is not the final picture. It has actually been fitted to explain the collected data with no given explanation, no fundamental mechanism. On the contrary, string theories, because they bring in supersymmetry and superpartners (candidates for DM), additional content in the

universe such as scalar fields (candidates for the inflaton or DE) or extra dimensions (possibly explaining the observed weakness of gravity with respect to the other forces), are inspiring, from a more fundamental level. They propose microphysical mechanisms from which the phenomenology we observe could emerge and their low energy realisation at least partly merges with the ΛCDM model.

We will here focus on a specific string-inspired theory, a spacetime foam model, in order to derive its phenomenology.

3.2 The D-material universe

Modified gravity models involving fundamental vector fields, but quite different from TeVeS models, may appear as the low-energy limit of certain brane theories of the type proposed in Refs. [58–60]. According to such spacetime foam models, a $3+1$ dimensional (Dirichlet) brane universe propagates in a higher-dimensional bulk punctured by populations of D0-brane (D-particle) defects, which, depending on the type of string theory considered, can be either point-like or compactified higher-dimensional 3-branes wrapped around three cycles, thus appearing from the point of view of an observer on the brane world as effectively "point-like" defects. The relative motion of the D-particles with respect to the D3-brane leads, from the brane point of view, to the former flashing "on and off" while they cross the latter, yielding a spacetime foam structure, hereby the D-foam. The D-particles are only weakly interacting among themselves, basically through gravitational interactions since they are massive with masses $M_{\rm s}/g_{\rm s}$ (with $M_{\rm s}$ the string scale and $g_{\rm s} \lesssim 1$ the weak string coupling), and thus behave more or less as a Dark Matter (DM) cosmic fluid (sometimes termed D-matter).

They may also interact via topologically nontrivial string interactions with the remaining content of the universe, namely two stacks of eight D8-branes, at rest in their lowest energy (vacuum) configuration, open strings[1] describing almost all fields of the universe and whose ends lie on the D-branes, and gravitons propagating as closed strings states in the bulk. These interactions with strings imply the splitting of the initial string, the formation of transient string states (stretched between the

[1]In type IIA theory, where our D-particles are D0-branes, conservation laws forbid interactions with electrically charged matter. In the more phenomenologically acceptable type IIB theory, where D0-branes are not allowed and D-particles are D3-branes wrapped on three cycles, electrically charged matter can interact nontrivially with D-particles but these are strongly suppressed with respect to neutral ones and can thus be ignored. In any case, the model exhibits a natural bi-metric structure.

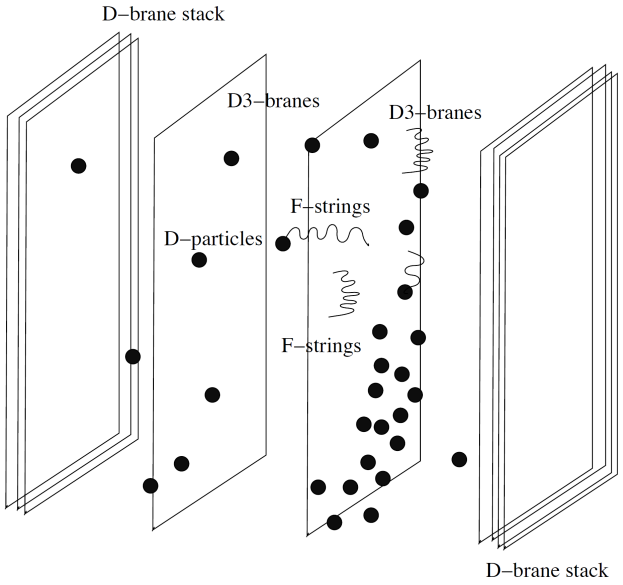

Figure 3.1: Representation of a D-particle spacetime foam model, in which our universe D3-brane interacts with effectively punctual D-particles, by way of open strings. In this particular model [58, 61], here given as an illustrative example, lies a stack of D8-branes in an orientifold structure.

D-particle and the D3-brane) and therefore the deformation of the local spacetime proportional to the momentum transfer during the non-elastic collision. Formally, this means representing the resulting recoil fluctuations as mean-field vector excitations of a stringy σ-model that describes the propagation of strings in cosmological FLRW spacetime backgrounds, punctured by populations of fluctuating D-particles (see the vertex operators Eqs. (C.9) and (C.12)). Figure 3.1 gives a schematic representation of such a brane cosmology.

The recoil velocity of the D-particles during their interactions with the stringy matter, which leads to a vector field, is thus the main ingredient responsible for the appealing features of the D-material universe. Interestingly, the non-linear Born-Infeld type dynamics of the D-matter recoil velocity vector field allows [61, 62] for the formation of scalar condensates of the corresponding field strength $\langle\langle F_{\mu\nu}\, F^{\mu\nu}\rangle\rangle$ which is viewed as a homogeneous scalar field with a mild time-dependence, virtually constant within a given cosmological era. Its value though differs in general from era to era, hence at an inflationary era, due to the dense D-particle populations as assumed in Section 3.4, the value of the condensate is much larger than the one at late-time eras, like for redshifts $z < 10$, where the lenses of our analysis and the astrophysical sources of the recently, for the first time directly, observed

Gravitational Waves (GW) [4] are located.

Interestingly, the direction given by this recoil velocity of the D-particles locally breaks Lorentz invariance, which is restored on average over small patches of the brane, that is, over large populations of D-particles, because of the zero vacuum expectation value of such velocity field. The non-zero variances would, on the contrary, lead to the interesting effects of the gauge field arising from such velocity field.

In Ref. [61] was put forward a proposal for the rôle such populations of D-particles might play in our universe, viewed as a D-brane world, in regards to large scale structure, that is, that the amount of required conventional DM is reduced. It was argued that the fluctuations of the recoil velocity of (populations of) D-particle defects, arising from their interaction with stringy matter, can provide the seeds for the formation of galaxies, provided their densities are larger than a critical value. It should be stressed that, since these models are based on string theory, their low energy effective actions may contain phenomenologically realistic extensions of the Standard Model, which include conventional DM candidates, such as neutralinos, axions, etc. The point of view in Ref. [61] as in here, is that the D-particle recoil velocity fluid may provide an additional component that play the rôle of a mixture (as evidenced from the respective equation of state) of DM and DE components, which was shown to be responsible for large-scale structure growth, in a remote analogy with the rôle of the vector fields of TeVeS models.[2] We here carry on this approach by using such an additional component to study not only how the D-particles recoil velocity field plays the rôle of DM in the late galaxy era, but also how it can influence at a deeper level the propagation of radiation, as well as a period of inflation in the absence of an inflaton field with a fine-tuned potential.

As we shall discuss in this chapter, we impose constraints on the density of the D-particles on our brane world and fine tune the cosmological constant so that the cosmic concordance model ($\Omega_{\rm m}$, Ω_Λ, Ω_k) (in a standard notation), which best fits the observations [6], is satisfied within experimental errors for the galactic era. The spatial flatness $\Omega_k = 0$ is guaranteed in our brane world model by construction (which is also consistent with our inflationary scenario), viewing our universe as a spatially flat brane. In general of course, the evolution of the D-particle universe could be very different from the standard ΛCDM model.

In the remaining of this chapter,[3] closely following results published in [63]

[2]However, we should stress that our D-brane/D-particle cosmologies are unrelated to, and in fact are very different from, TeVeS models in both their dynamics and spectra.

[3]This chapter, as we recall later on, follows closely the results and structure of Refs. [63] and [64].

and [64], we first review, in Sections 3.2.1 and 3.2.2, the relevant formalism and give the corresponding effective actions that describe the dynamics of the D-material universe. Then, in Section 3.3, we elaborate further on the results of the previous study on the galactic growth era and analyse the circumstances under which the D-particle recoil velocity fluid may "mimic" DM in galaxies, via their recoil fluctuations. A lensing phenomenology is presented for some samples of galaxies, which previously were known to provide tension for modified gravity (TeVeS) models. Then we discuss in Section 3.4 a cosmic evolution of the D-material universe by analysing the conditions under which the late eras of this universe associated with large-scale structure are connected to early epochs, where inflation takes place. We investigate on whether, and under which conditions, inflation can be induced by dense populations of D-particles in the early universe, with the rôle of the inflaton field played by the condensate of the D-particle recoil velocity fields under their interaction with relativistic stringy matter. Finally, motivated by the recent breakthrough of the direct detection of GW [4], we study their propagation in such a background in Section 3.5. The modifications of the graviton equations are studied, leading to an effective mass for the graviton. In addition, it is known [65] that the medium of D-particles may induce a competing effect, namely a superluminal refractive index, as a result of the gravitational energy of D-particles acting as a DM component. We examine the relative importance of each effect and hence constrain the graviton mass using observations. Additionally, Appendices C and D review some technical aspects and other material of our approach.

3.2.1 Low-energy effective action

As discussed in Refs. [59, 61], the following four-dimensional (low-energy) effective action expresses, in the string frame (with respect to the dilaton ϕ), the interaction of stringy matter on the brane world of three large dimensions with a medium of recoiling D-particles in the early universe[4]

$$S_{\text{eff 4D}} = \int \mathrm{d}^4x \left[-\sqrt{-g}\,\frac{1}{4}\,\mathcal{G}_{\mu\nu}\,\mathcal{G}^{\mu\nu} - \frac{T_3}{g_{\text{s0}}}\,e^{-\phi}\,\sqrt{-\det\left(g+2\pi\alpha' F\right)}\,(1-\alpha R(g)) \right.$$
$$\left. -\sqrt{-g}\,\frac{e^{-2\phi}}{\kappa_0^2}\,\tilde{\Lambda} + \sqrt{-g}\,\frac{e^{-2\phi}}{\kappa_0^2}\,R(g) + \mathcal{O}\left((\partial\phi)^2\right) \right] + S_{\text{m}}\ , \qquad (3.1)$$

[4]Recall that throughout this work, the following conventions are adopted: the metric signature is $(-,+,+,+)$, the Riemann curvature tensor is defined as $R^{\alpha}_{\ \beta\gamma\delta} = \partial_\delta\,\Gamma^{\alpha}_{\beta\gamma} + \Gamma^{\lambda}_{\beta\gamma}\,\Gamma^{\alpha}_{\lambda\delta} - (\gamma \leftrightarrow \delta)$ and the Ricci tensor as $R_{\mu\nu} = R^{\alpha}_{\ \mu\nu\alpha}$.

where the second term on the right-hand-side is the standard Dirac-Born-Infeld (DBI) action describing the dynamics of open vector fields on a D-brane world; S_m denotes the matter action, describing the dynamics of matter and radiation particles on the brane world; $\mathcal{G}_{\mu\nu}$ is a flux gauge field induced by the bulk geometry, one of the many that in general exist in brane models, which is assumed condensed ($\langle \ldots \rangle$) and whose importance will become clear later on, when discussing the cosmological constant in Eq. (3.17b) as well as in the inflation analysis of Section 3.4; T_3 is the brane tension, a priori unconstrained; $g = \det(g_{\mu\nu})$ is the determinant of the gravitational field $g_{\mu\nu}$; and g_{s0} is the string coupling for constant dilaton ϕ_0.

For our purposes, the dilaton field ϕ is assumed constant, $\phi = \phi_0$, implying that the kinetic term, here $\mathcal{O}\left((\partial\phi)^2\right)$, can be overlooked. While dilaton stabilisation can be difficult to deal with, it is not the focus of our work here, which has to do with the vector field effects. Still, the equations of motion (in particular Eq. (3.22)) will provide consistency checks on this matter. In the presence of a dilaton, the full string coupling is defined as $g_s = g_{s0}\, e^{\phi}$; for the rest of this work we assume the phenomenological value $g_{s0}^2/(4\pi) = 1/20$ that is $g_{s0} \sim 0.8$, for which string perturbation theory is valid.

The vector field A_μ (of mass dimension one, in our conventions) will denote the recoil velocity field excitation during the string-matter/D-particle interactions and has a field strength (of mass dimension two) given by

$$F_{\mu\nu} \equiv \partial_\mu A_\nu - \partial_\nu A_\mu \ . \tag{3.2}$$

We consider the recoil gauge field mainly confined on the brane world and hence its dynamics are described by the Born-Infeld square root Lagrangian on the D3-brane world, which includes a resummation over all powers of α'. Because of the physical interpretation of the vector field as a velocity field, there is an additional constraint which A_μ satisfies; as reviewed in Appendix C, see Eq. (C.18) (and discussed in Ref. [61]), it basically arises from the standard relativity relation of a four velocity $u^\mu u_\mu = -1$ where the contraction is with the metric $g_{\mu\nu}$

$$A_\mu\, A_\nu\, g^{\mu\nu} = -\frac{1}{\alpha'} \ , \tag{3.3}$$

where the right-hand-side arises from dimensional considerations. From now on, this constraint will be implemented in the action via a Lagrange multiplier λ, in order to be satisfied not only by the background configurations but also by the perturbations.

The background configurations will be discussed in the following section, mainly Eqs. (3.27) and (3.32); for more details, we refer the reader to Appendix C.

The quantity κ_0^2 is the four-dimensional bulk-induced gravitational constant defined as

$$\frac{1}{\kappa_0^2} = \frac{V_{(6)}}{g_{\rm s0}^2}\, M_{\rm s}^2 \ , \tag{3.4}$$

where $V_{(6)}$ is the compactification volume in units of the Regge slope α' of the string theory describing the excitations on the brane world and

$$\alpha = \alpha'\zeta(2) = \alpha'\,\frac{\pi^2}{6} \ , \tag{3.5}$$

in the (open string/brane) model adopted here. The cosmological constant term $\tilde{\Lambda}$ is induced in general by bulk physics [59] and it is a free parameter in the phenomenological approach we follow here. Note that in certain models, it may even be of anti-de Sitter type $\tilde{\Lambda} < 0$.

Considerations on the vacuum energy

Before proceeding, we should remark for completeness that a basic assumption [61] underlying (3.1) is that any mass contribution of the D-particle defects to the vacuum energy density is considered subleading, compared to the recoil and other terms present in (3.1). This is because, as discussed in Ref. [58], there are *mixed sign* contributions to the brane vacuum energy induced by the open strings stretched between the D-particle and the D3-brane and due to their interaction. The bulk D-particle populations at various distances, near (less than the string scale) or further (a few string lengths) away from the D3-brane world, yield, according to string perturbation theory and for adiabatic motion of the D-particles (given by Gaussian distribution in the velocities), an induced potential on the brane which is negative and inversely proportional to r^3 in the former case, and positive and proportional to r in the latter one. Therefore, the overall potential can be tuned, by choosing the (non-homogeneous) repartition of D-particles near and far from the brane, to be of the sign and amplitude needed such that it "screens" the D-particle mass contributions. Thus, while the total brane world's vacuum energy is constrained by the astrophysical data, the density of defects on the brane is not.

For future use, we also mention at this stage that the D-particle mass energy density in the Einstein frame is independent of the dilaton ϕ. To see this, let us

start from the corresponding expression in the string frame

$$\rho^{\rm string}_{\rm D-mass\ dens.} = \frac{M_{\rm s} e^{-\phi}}{g_{\rm s0}}\,\frac{\bar{N}_{\rm D}}{\mathcal{V}_{(3)}} \tag{3.6}$$

where $\bar{N}_{\rm D}/\mathcal{V}_{(3)}$ is the number three-density of D-particles on the brane world and $\mathcal{V}_{(3)}$ is the proper three-volume. Above, we took into account that, since (3.6) refers to a contribution on the brane world effective action, where open strings end, there is a $e^{-\phi}$ factor in front of the corresponding spacetime integral, which makes the effective mass of the D-particle $M_{\rm s}/g_{\rm s} = e^{-\phi}\,M_{\rm s}/g_{\rm s0}$, given that the string coupling is $g_{\rm s} = g_{\rm s0}\,e^{\phi}$. Upon passing into the Einstein frame (designated by a superscript 'E' in the appropriate quantities), that is, upon rescaling the spacetime metric by (in four dimensions)

$$g^{\rm E}_{\mu\nu} = e^{-2\phi} g_{\mu\nu} \tag{3.7}$$

the proper volume scales as $\mathcal{V}^{\rm E}_{(3)} = e^{-3\phi}\,\mathcal{V}_{(3)}$, and hence the energy density (3.6) contribution to the four-dimensional action (3.1) becomes

$$\int {\rm d}^4x\sqrt{-g}\,\rho^{\rm string}_{\rm D-mass\ dens.} = \int {\rm d}^4x\sqrt{-g^{\rm E}}\,\frac{M_{\rm s}}{g_{\rm s0}}\frac{\bar{N}_{\rm D}}{\mathcal{V}^{\rm E}_{(3)}} \equiv \int {\rm d}^4x\sqrt{-g^{\rm E}}\,\rho^{\rm E}_{\rm D-mass\ dens.} \tag{3.8}$$

that is independent of the dilaton ϕ. This will be used below, when we consider constraints on the vacuum energy imposed by using the dilaton equations of motion. Such terms escape these constraints. Note that in the Einstein frame, the mass of the D-brane is fixed to $M_{\rm s}/g_{\rm s0}$. Moreover, it is in this frame that the standard FLRW form of the universe metric is assumed, implying the scaling $\rho^{\rm E}_{\rm D-mass\ dens.} \propto a^{-3}$, where a is the scale factor, on account of the assumption of "weak- or no-force condition" among D-particles [58].[5] Thus, in general, taking into account their

[5]Numerically, if the contribution (3.8) was unscreened from bulk D-particle effects, it could play the rôle of a DM energy density component. In such a case, and under the assumption that today there are $\bar{N}^{(0)}_{\rm D}$ D-particles, in natural units, in the brane world, we would have in terms of the critical density today $\Omega_{\rm D-matter} = \frac{M^2_{\rm Pl}}{3\,H^2_0}\,\frac{M_{\rm s}}{g_{\rm s0}\,M_{\rm Pl}}\,\bar{N}^{(0)}_{\rm D}$, where H_0 is today's value of the Hubble parameter. If this were the dominant DM component, then, to avoid overclosure of the universe, we should demand that $\Omega_{\rm D-matter} \lesssim \Omega^{(0)}_{\rm m}$, where $\Omega^{(0)}_{\rm m} \sim 0.3$ is the current value of the matter density parameter, as measured by astrophysical data [6]. Thus we obtain the following upper bound for today's density of the D-particle populations on the brane world

$$\bar{N}^{(0)}_{\rm D} < 0.9\,\frac{M_{\rm Pl}}{M_{\rm D}}\,\frac{H^2_0}{M^2_{\rm Pl}}\ , \tag{3.9}$$

where $M_{\rm D} = M_{\rm s}/g_{\rm s0}$. Given that $H_0/M_{\rm Pl} \sim 10^{-60}$, and $M_{\rm s} \gtrsim 10$ TeV, phenomenologically, we observed that this bound is very stringent. However, as mentioned earlier, the presence of bulk

scaling as a^{-3}, one may absorb such subleading D-particle mass terms contributions (3.8) into the 'matter' action S_m. Throughout this work we assume that the vacuum energy is dominated until the current era by the D-particle recoil velocity effects — which were shown to scale like a^{-3} after exit from inflation, as can be seen in Eq. (3.34), or in Eq. (C.24) and the nearby discussion, as well as in Ref. [61].[6] During inflation, as was discussed in [59] and as we shall review in Section 3.4, the assumed high density of D-particles implies a constant density of D-particles on the brane, which contribute crucially to a Starobinsky-like inflation driven by strong condensate fields of the recoil velocities field strength $\langle\langle F_{\mu\nu}\, F^{\mu\nu}\rangle\rangle$.

3.2.2 Weak-field approximation and background

We next remark that the four-dimensional DBI action (on the D3-brane world) in (3.1) can be expanded in derivatives, as appropriate for a low-energy weak-field approximation[7] compared to the string scale $M_{\rm s} = 1/\sqrt{\alpha'}$, as follows

$$\det_4 (g_{\mu\nu} + 2\pi\alpha' F_{\mu\nu}) = \det_4 g \left[1 + (2\pi\alpha')^2 I_1 - (2\pi\alpha')^4 I_2^2\right] \ , \tag{3.10}$$

where

$$I_1 = \frac{1}{2}\, g^{\mu\lambda} g^{\nu\rho} F_{\mu\nu} F_{\lambda\rho} \ , \quad I_2 = -\frac{1}{4} \epsilon^{\mu\nu\lambda\rho} F_{\mu\nu} F_{\lambda\rho} \ . \tag{3.11}$$

In the approach used in Sections 3.3 and 3.4, as discussed in the following of this section, the "magnetic" field dual components for the recoil velocity field strength

D-particles, interacting via stretched open strings with the brane world, as well as the bound D-particles, screen the D-particle mass to an effective one $M_{\rm D} \ll M_{\rm s}/g_{\rm s0}$. In this case, much higher densities on the brane world are allowed, as can be seen from the above considerations.

[6] In other scenarios, even those effects may be screened by the bulk D-particle populations that accompany the D3-brane world in its travel through the bulk space, and in this way much higher densities of D-particles bound on our brane universe can be allowed without overclosing the universe. In fact, in such cases one may use the induced refractive index of the (dense) "D-foam" medium at late eras in order to explain certain observed delays of the more energetic photons compared to lower energy ones, from distant active celestial sources such as Gamma Ray Bursts or Active Galactic Nuclei [65]. On the other hand, under the assumption adopted in the current work that the recoil effects are dominant until the current era, one obtains as we shall see (in Eq. (3.50)) an upper bound for the allowed D-particle densities that is much weaker than the one required to reproduced these delays.

[7] Such derivative expansions are appropriate for weak recoil fields, which is the case characterising the galactic eras of the universe, of interest to us when one consider the rôle of the D-particles as providers of structure growth [61], as a DM component in the lensing analysis of Section 3.3 and as a medium altering the propagation of radiation as in Section 3.5. However, as we shall discuss in Section 3.4, dense D-particle populations in the early eras can condense and induce an inflationary era, which is characterised by strong recoil velocity fields. The latter necessitates keeping the Born-Infeld square-root structure intact.

are subleading, and thus for us I_2 will not be considered further. This can be easily understood once one considers a cosmological (almost homogeneous and isotropic, slowly time-dependent) vector field background, yielding $\partial_i A_j \simeq 0$, as we will explicitly see later in this section. While this is true locally for the lensing analysis and in a homogeneous universe, it is not on the cosmological scales where magnetic-like and electric-like contributions are a priori of the same order. Still, these additional contributions yield at most a factor[8] 2 and are thus ignored here. On the contrary, in the computations of Section 3.5 (see for instance Eq. (C.12)), these additional contributions are relevant because of space *and* time dependences of the vector field A_μ, and turn out playing an important role.

Upon such derivative expansions, the resulting effective action on the D3-brane universe, in the Einstein frame (3.7) (denoted by a superscript 'E'), becomes

$$S^{\rm E}_{\rm eff\ 4D} = \int {\rm d}^4x\sqrt{-g}\left[-\frac{T_3\,e^{3\phi_0}}{g_{\rm s0}} - \frac{\tilde{\Lambda}\,e^{2\phi_0}}{\kappa_0^2} - \frac{1}{4}\langle\mathcal{G}_{\mu\nu}\,\mathcal{G}^{\mu\nu}\rangle + \left(\frac{\alpha\,T_3\,e^{\phi_0}}{g_{\rm s0}} + \frac{1}{\kappa_0^2}\right)R \right.$$
$$\left. - \frac{(2\pi\alpha')^2\,T_3\,e^{3\phi_0}}{g_{\rm s0}}\,\frac{F^2}{4}\,\left(1-\alpha\,e^{-2\phi_0}\,R\right) + \lambda\left(A_\mu A^\mu + \frac{1}{\alpha'}\right)\right] + S_{\rm m}\ , \qquad (3.12)$$

where the last term corresponds to the implementation of the vector field constraint Eq. (3.3) using the Lagrange multiplier λ.

Also, from now on and throughout this chapter, we work with a constant dilaton $\phi = \phi_0$, thus removing the dilaton kinetic term. This assumption is consistent with the dilaton equation of motion Eq. (3.22) derived from the action. In such case, one may redefine the vector field A_μ so as to have canonical kinetic (Maxwell-type) term, that is

$$A_\mu \to \widetilde{A}_\mu \equiv \sqrt{\frac{(2\pi\alpha')^2\,T_3\,e^{3\phi_0}}{g_{\rm s0}}}\,A_\mu\ , \qquad (3.13)$$

which implies that the constraint (3.3) becomes

$$\widetilde{A}_\mu\,\widetilde{A}_\nu\,g^{\mu\nu} = -\frac{4\pi^2\alpha'\,T_3\,e^{3\phi_0}}{g_{\rm s0}} = -\frac{1}{\alpha'}\mathcal{J}\ , \qquad (3.14)$$

where we defined

$$\mathcal{J} \equiv \frac{(2\pi\alpha')^2\,T_3\,e^{3\phi_0}}{g_{\rm s0}}\ . \qquad (3.15)$$

[8]This influences, for instance, the order of magnitude of the energy density to avoid overclosure of the universe or the size of the condensate field leading inflation, which have no influence on the constraints given in this work.

Thus, from now on we shall be dealing with the action

$$S^{\rm E}_{\rm eff\ 4D} = \int {\rm d}^4x\sqrt{-g}\left[-\frac{T_3\,e^{3\phi_0}}{g_{\rm s0}} - \frac{\tilde{\Lambda}\,e^{2\phi_0}}{\kappa_0^2} - \frac{1}{4}\langle\mathcal{G}_{\mu\nu}\,\mathcal{G}^{\mu\nu}\rangle + \left(\frac{\alpha\,T_3\,e^{\phi_0}}{g_{\rm s0}} + \frac{1}{\kappa_0^2}\right)R \right.$$
$$\left. - \frac{\widetilde{F}^2}{4}\left(1-\alpha\,e^{-2\phi_0}\,R\right) + \lambda\left(\tilde{A}_\mu\tilde{A}^\mu + \frac{1}{\alpha'}\mathcal{J}\right)\right] + S_{\rm m}\ , \quad (3.16)$$

where $\widetilde{F}$ is the Maxwell field strength for the field $\widetilde{A}_\mu$ given in Eq. (3.13) and λ is now implementing the constraint (3.14). Notice that the first three terms on the right-hand-side of Eq. (3.16) play the rôle of a cosmological constant

$$\Lambda_0 \equiv \frac{T_3\,e^{3\phi_0}}{g_{\rm s0}} + \frac{\tilde{\Lambda}\,e^{2\phi_0}}{\kappa_0^2} \quad (3.17a)$$

$$\Lambda^{\rm vac} \equiv \Lambda_0 + \frac{1}{4}\langle\mathcal{G}_{\mu\nu}\,\mathcal{G}^{\mu\nu}\rangle\ , \quad (3.17b)$$

where Λ_0 is the non-conformal part, and bulk gauge field condensates of the form $\langle\mathcal{G}_{\mu\nu}\,\mathcal{G}^{\mu\nu}\rangle$ are conformal scalar-like constant terms. Indeed, the full action driving the dynamics of these bulk gauge fields is generically non-linear — for instance via a Born-Infeld type term — in these string theory inspired models. While for simplicity and readability we ignore the details of such dynamics, one can safely assume it consequently forms a constant condensate, as shown in Ref. [62]. Note that it can be assumed constant within a cosmological era for the same reasons our vector field strength $F_{\mu\nu}$ can, that is, due to the homogeneity of the universe on large scales. The curvature prefactor can be identified with the (reduced) Planck mass, as in

$$\frac{1}{2}M_{\rm Pl}^2 \equiv \frac{1}{16\pi\,G} = \frac{\alpha\,T_3\,e^{\phi_0}}{g_{\rm s0}} + \frac{1}{\kappa_0^2}\ . \quad (3.18)$$

A detailed study of the equations of motion and background solutions for the recoil vector field have been discussed in Ref. [61] and will be reviewed below within our approximations, as we shall need them to make our estimates of the D-particle recoil velocity fluctuation effects on the galactic dynamics. The string origin of the vector field and its construction from vertex operators, as assumed for our purposes in this chapter, are reviewed in Appendix C. A complete low-energy action, keeping all terms, as well as the equations of motion one can derive from it, are also given for completeness, along with some basic properties and order of magnitude estimates of the vector field.

The graviton equation of motion obtained from Eq. (3.16), on assuming to first approximation that terms involving $\rho_\Lambda \ll \widetilde{F}^2$ or derivatives of $\widetilde{F}^2$ can be neglected,[9] is given by

$$\left(R^\mu_{\ \nu} - \frac{\delta^\mu_{\ \nu}}{2}R\right)\left[\frac{\alpha\, T_3\, e^{\phi_0}}{g_{\rm s0}} + \frac{1}{\kappa_0^2} + \frac{\alpha e^{-2\phi_0}\,\widetilde{F}^2}{4}\right] - \frac{1}{2}\left(1 - \alpha e^{-2\phi_0}R\right)\widetilde{F}^{\mu\lambda}\widetilde{F}_{\nu\lambda} \qquad (3.19)$$
$$+ \frac{1}{8}\widetilde{F}^2\,\delta^\mu_{\ \nu} + \lambda\,\widetilde{A}^\mu\widetilde{A}_\nu - \lambda\,\frac{\delta^\mu_{\ \nu}}{2}\left(\widetilde{A}_\alpha\widetilde{A}^\alpha + \frac{1}{\alpha'}\mathcal{J}\right) + \frac{1}{2}\delta^\mu_{\ \nu}\,\Lambda^{\rm vac} = \frac{1}{2}\,T^\mu_{\ \nu}\ ,$$

where $T_{\mu\nu} = -2\frac{1}{\sqrt{-g}}\frac{\delta S_m}{\delta g^{\mu\nu}}$ is the matter stress tensor.

For future use we note that, by contracting the vector field equation of motion obtained from Eq. (3.16)

$$\left[\widetilde{F}_{\nu\mu}\left(1 - \alpha\, e^{-2\phi_0}R\right)\right]^{;\nu} + 2\lambda(x)\,\widetilde{A}_\mu = 0 \qquad (3.20)$$

(where the semicolon denotes covariant derivative) with A^μ, and then applying the constraint (3.14), we obtain the following form for the (background value) of the Lagrange multiplier field

$$\langle\lambda(x)\rangle = \frac{e^{-3\phi_0}\,g_{\rm s0}}{8\pi^2\alpha'\,|T_3|}\,\widetilde{A}^\mu\left[\widetilde{F}_{\nu\mu}\left(1 - \alpha e^{-2\phi_0}R\right)\right]^{;\nu}\ , \qquad (3.21)$$

which we shall make use in the next section when we estimate the recoil effects of the D-particles on the universe dynamics during the galactic era. An important point to note, which was the subject of discussion in Ref. [61] and which we only mention here for completeness, is that the constraint term in Eq. (3.16) is vital in coupling the recoil vector field perturbation to the density perturbations through the $\langle\lambda(x)\rangle\widetilde{A}_\mu\widetilde{A}_\nu$ term in the respective stress-energy tensor obtained from Eq. (3.16).

Finally, before we embark on an estimation of the D-particle effects on the galactic dynamics, we would like to comment on the physical importance of the constraints imposed by the dilaton equation, which should be taken into account despite the fact that the dilaton is considered to be constant in our analysis. The dilaton equation of motion, obtained by varying the effective action (3.16) with respect to the dilaton

[9] This is because spatial derivatives yield terms proportional to spatial derivatives of the metric, that is proportional to the Newtonian acceleration ζ' of a D-particle in the gravitational field of the galaxy, while temporal derivatives yield terms proportional to the Hubble parameter today H_0, which are again suppressed compared with the terms that are kept. See below, Eq. (3.33).

field ϕ and setting it to a constant value ϕ_0 at the end of the variation, reads

$$\frac{3\,T_3 e^{3\phi_0}}{g_{\rm s0}} + \frac{2\,\tilde{\Lambda}\,e^{2\phi_0}}{\kappa_0^2} - \alpha\left[\frac{T_3 e^{\phi_0}}{g_{\rm s0}} - \frac{e^{-2\phi_0}\,\widetilde{F}^2}{2}\right] R = 0\ , \tag{3.22}$$

where subleading terms, that is, dilaton kinetic terms, terms involving derivatives on $\widetilde{F}^2$ or terms proportional to the Lagrange multiplier λ, are ignored (see Appendix C for details). Taking into account [61] that for galactic scales the terms $\alpha\,\widetilde{F}^2\,R \ll \alpha\,\frac{T_3 e^{\phi_0}}{g_{\rm s0}}\,R \ll 3\,\frac{T_3 e^{3\phi_0}}{g_{\rm s0}}$, Eq. (3.22) can be well approximated by

$$\frac{T_3}{g_{\rm s0}}\,e^{3\phi_0} \simeq -\frac{2}{3}\,\frac{\tilde{\Lambda}\,e^{2\phi_0}}{\kappa_0^2}\ , \tag{3.23}$$

which justifies the hypothesis $\phi = \phi_0$ assumed of this chapter.[10] In addition, it implies that the cosmological constant on the brane world Λ_0, defined in Eq. (3.17a) with positive tension $T_3 > 0$ (as required for stability), is negative

$$\Lambda_0 \simeq -\frac{1}{2}\frac{T_3}{g_{\rm s0}}\,e^{3\phi_0} \ < \ 0\ . \tag{3.24}$$

This anti-de Sitter type cosmological constant would not be phenomenologically acceptable in the current era, as it would contradict the CMB, BAO and gravitational lensing data. This can be remedied by assuming that such terms cancel against *dilaton independent contributions* to the brane vacuum energy, coming from appropriate combinations of the mass terms of D-particles bound to the brane world [59] as in Eq. (3.8), and bulk gauge flux fields inducing condensates[11] of the form appearing in the action (3.1) — which as we shall argue in Section 3.4 play an important rôle for inflation. In this way, during the galactic era, only a *small positive cosmological constant* term survives, which plays no significant rôle on the galactic scale lensing phenomenology, in accordance to observations. This assumption will be understood in what follows in the sense that $\Lambda^{\rm vac} \equiv \Lambda_0 + \frac{1}{4}\langle \mathcal{G}_{\mu\nu}\,\mathcal{G}^{\mu\nu}\rangle + \ldots > 0$, where $\ldots$ denote potential other bulk D-particle contributions to the brane vacuum energy, here ignored. Therefore, $\Lambda^{\rm vac}$ is compatible with the bounds on the cosmological constant Λ from observations in the context of the ΛCDM model [6]. Even though this model provides several terms with opposite signs which can cancel out to leave the

[10] Using the more complete Eq. (3.22) would yield a constraint of the form $\partial_\mu\big[\widetilde{F}^2\,R\big] = 0$, which is practically satisfied since $\dot{R} \simeq 0$ even during inflation and we neglect derivatives of $\widetilde{F}^2$.

[11] These terms are thus treated as scalars in the derivation of the graviton equation of motion.

appropriate small positive cosmological constant, it does not alleviate the need for fine-tunning, and thus these effects will not be covered in more details here.

Background field

We can now discuss background field configurations which satisfy the equations of motion (3.19), (3.20) and (3.22), obtained from the actions (3.1) and (3.16). We give in Appendix C a more detailed set of equations, as well as string theory motivations for the ansatz given here.

For the cosmological time scales we are interested in, in the inflationary analysis or the graviton propagation (as in Ref. [61]), we consider the FLRW spacetime metric backgrounds, using cosmic time t or the conformal time η

$$g^{\rm FLRW}_{\alpha\beta}\mathrm{d}x^\alpha \mathrm{d}x^\beta = -\mathrm{d}t^2 + a^2(t)\left(\mathrm{d}r^2 + r^2\mathrm{d}\theta^2 + r^2\sin^2\theta\,\mathrm{d}\varphi^2\right) \tag{3.25}$$

$$= -a^2(\eta)\,\mathrm{d}\eta^2 + a(\eta)^2\left(\mathrm{d}r^2 + r^2\mathrm{d}\theta^2 + r^2\sin^2\theta\,\mathrm{d}\varphi^2\right)\ . \tag{3.26}$$

In such case, using Eq. (C.15), the dimensionful (dimension [mass]) cosmological form of the recoil vector field A_μ and its field strength $F_{\mu\nu} \equiv \partial_\mu A_\nu - \partial_\nu A_\mu$ on the D3-brane universe take the form

$$A_i \equiv -\frac{1}{\sqrt{\alpha'}}\,a^2(t)\,u_i\ , \qquad F_{0i} = -\frac{2}{\sqrt{\alpha'}}\,\dot{a}a\,u_i\ , \tag{3.27}$$

with u^i $(i = x, y, z)$ the spatial components of the D-particle recoil velocity and where the overdot denotes derivative with respect to the FLRW cosmic time t and α' is the Regge slope of the string (of dimension [length]^2).

However, when one considers local regions of spacetime, such as a galaxy, of relevance to phenomenological tests of the model via lensing analyses, discussed in Section 3.3, the spacetime background is assumed static and spherically symmetric to a good approximation, of the form

$$g_{\alpha\beta}\,\mathrm{d}x^\alpha \mathrm{d}x^\beta = -e^{\nu(r)}\mathrm{d}t^2 + e^{\zeta(r)}a^2(t)\,(\mathrm{d}r^2 + r^2\mathrm{d}\theta^2 + r^2\sin^2\theta\mathrm{d}\varphi^2)$$

$$= -e^{\nu\left(\sqrt{x^2+y^2+z^2}\right)}\mathrm{d}t^2 + e^{\zeta\left(\sqrt{x^2+y^2+z^2}\right)}\,a^2(t)(\mathrm{d}x^2 + \mathrm{d}y^2 + \mathrm{d}z^2)\ , \tag{3.28}$$

where we kept track of the (small) universe expansion at the galactic era through the dependence of the metric on the scale factor $a(t)$; here $r = r(x, y, z) = \sqrt{x^2 + y^2 + z^2}$ in terms of Cartesian coordinates.

In such metrics, following Eq. (C.13), the recoil vector field can be well approximated by[12]

$$A_i(\vec{x},t) = \frac{1}{\sqrt{\alpha'}}\, g_{ij}(\vec{x},t)\, Y^j(t)\Theta(t-t_{\rm c})\Big|_{\propto u_i} = \frac{1}{\alpha'}\, g_{ij}(\vec{x},t)\, u^j \left(t\, \frac{a(t_c)^2}{a(t)^2} - t_{\rm c} \right) \ , \quad (3.29)$$

where $t > t_{\rm c}$.

In constructing the local velocity field above, we took into account the non-clustering effects of the D-particles, by maintaining their spatial trajectories as given by the geodesics $Y^i(t)$ in the global case (C.13), but replacing the FLRW metric by the local metric (3.28) and keeping the explicit time dependence of $Y^i(t)$. However, for populations of D-particles in the neighbourhood of a galaxy, which are relevant for the lensing phenomenology of Section 3.3, the impact time $t_{\rm c}$ is of the same order of magnitude as the cosmic time t of a galaxy of given redshift z

$$t_c \sim \frac{2}{H_0\,[1+(1+z)^2]} \quad (3.30)$$

where H_0 is the present value of the Hubble constant. Because we discuss redshifts $z \ll 10$, this essentially amounts to setting $a(t_{\rm c}) \sim a_0 = 1$ in an order of magnitude, since in galactic eras the expansion of the universe is assumed small. In addition, the cosmic time t appearing there coincides with the time of observation, that is, the present time $t = t_0$.

The vector field A_μ in (3.29) also satisfies the constraint (3.3). It can then be shown after detailed computations that, on account of the constraint, any terms $\partial_i A_t$ in F_{ti} are subleading compared to $\partial_t A_i$, and thus from (3.29), (3.28) we conclude that to a very good approximation

$$F_{ti}(\vec{x},t) \simeq \frac{1}{\alpha'}\, g_{ij}(\vec{x},t)\, u^j \left(\frac{a^2(t_c)}{a^2(t)} - 2H(t)\, t_{\rm c} \right) \ , \quad (3.31)$$

where $H(t) \equiv \frac{\dot{a}(t)}{a(t)}$ is the Hubble parameter at (cosmic) time t. As already mentioned, for lensing measurements the time t is the time of observation, that is today $t = t_0$, for which $a(t_0) = 1$ in our normalisation. Thus, using Eq. (3.30) and the fact that for an expanding universe $a(t_{\rm c}) = a_0 \frac{1}{1+z}$, with z the redshift of the galaxy in the

[12]We ignore, as subleading, any term in the geodesics of the D-particle associated with the local acceleration induced by the galactic mass to only keep the fluctuations of their velocity due to their interaction with open strings representing galactic matter in our brane world. See Appendix C for more details.

neighbourhood of which we consider local populations of D-particles, we obtain from (3.31)

$$F_{ti}(\vec{x},t) \simeq \frac{1}{\alpha'}\, g_{ij}(\vec{x},t)\, u^j \left[\frac{1-3(1+z)^2}{(1+z)^2\,(1+(1+z)^2)}\right] \ . \tag{3.32}$$

In a similar manner, the "magnetic type" field strength components F_{ij} are much smaller than F_{ti} as becomes clear from the expression

$$\begin{aligned} F_{ij} &= \partial_i A_j - \partial_j A_i = \frac{1}{\alpha'}\, a^2(t) \left[t\,\frac{a^2(t_{\rm c})}{a^2(t)} - t_{\rm c}\right] \partial_{[i}\Big(e^{\zeta(r)}\Big) u_{j]} \\ &= a^2(t)\,\frac{e^{\zeta(r)}}{\alpha'}\left(u_i x^j - u_j x^i\right)\frac{\zeta'(r)}{r}\ \left[t\,\frac{a^2(t_c)}{a^2(t)} - t_{\rm c}\right] \ , \end{aligned} \tag{3.33}$$

where i,j,k,m,n denote Cartesian spatial 3-coordinates, the prime in $\zeta'(r)$ denotes derivative with respect to r and $[i...j]$ denotes antisymmetrisation in the respective indices. We now notice that $\zeta'(r) \propto -\frac{\mathcal{M}}{r^2}$, $\mathcal{M}$ being the mass of the galaxy, is the gravitational acceleration induced by the galaxy on a D-particle, which is negligible compared to the terms we keep here, thus implying (3.33) leads to suppressed contributions in the dynamics as compared to the F_{0i} terms, which we concentrate upon from now on.

For late (galaxy formation) eras of the universe, we consider populations of D-particles with fluctuating recoil velocities, which are assumed to be Gaussian stochastic for simplicity

$$\langle\langle u^m u^n \rangle\rangle = \sigma_0^2(t)\,\delta^{mn} \ , \qquad \langle\langle u^m \rangle\rangle = 0 \ , \qquad \sigma_0^2(t) = a(t)^{-3}\,|\beta| \ , \tag{3.34}$$

in order to macroscopically maintain Lorentz invariance in populations of D-particle defects. Notice that here, u^i are Cartesian coordinates, which is the reason we previously were interested in expressing the local metric fluctuations in terms of such coordinates. The transformation of the result to spherical polar coordinates is straightforward.

3.3 Lensing phenomenology

In this section, we extend further the study of such models by discussing the rôle that the D-particles can play in large structure and galaxy formation. We investigate whether their effects can "mimic" and duplicate the effect of Dark Matter (DM) and under which circumstances. Specifically, data from galactic lenses indicate a miss-

match between the observed baryonic mass content of the galaxy and the strength of the lensing it produces. This discrepancy is usually accounted for by the inclusion of DM gravitational sources, however we would like to see if D-particles can play a similar rôle. Their statistically averaged recoil velocities induce a modification to the standard gravitational relation, enhancing such effect on these scales. This mechanism might then compliment and enhance any DM component which may be present.

For the current era, of relevance for lensing (and for the graviton propagation, as in Section 3.5), the so-considered range of D-particle densities has to occur within a reasonably small window, which also ensures perturbation growth and large-scale structure but does not imply fine tuning of the model's parameters. Moreover, as we shall also study further on in Section 3.4.4, the age of the universe in our model has to match the expected one from the ΛCDM model.

To discuss the phenomenology of our D-particle universe using galactic lensing data, we use the action (3.16). We shall use the local form of the recoil vector field Eq. (3.29), averaged at the end over populations of D-particles in the neighbourhood of a galaxy. As mentioned previously, we also assume that at the local galactic level, any contribution of the four-dimensional brane world vacuum energy $\Lambda^{\rm vac}$ is small (or cancelled appropriately), of the order of the observed cosmological constant today, so that it may be safely neglected to a first approximation when considering the dynamics at galactic scales, as relevant for lensing.

3.3.1 The equations of motion

Let us now give an order of magnitude estimate of the various terms appearing in the graviton equation (3.19), setting $\Lambda^{\rm vac}$ to zero, before we proceed with the detailed lensing phenomenology. This will be useful in yielding a qualitative understanding of the order of magnitude of the quantity $|\beta|$, defined in Eq. (3.34), needed for the D-particle defects to play the rôle of DM candidates and providers of large scale growth structures [61].

To this end, we first notice that, upon using classical backgrounds, which are discussed briefly in Appendix C, the penultimate term on the left-hand-side of Eq. (3.19) will vanish identically, due to the constraint (3.14) that such backgrounds satisfy. In addition, on account of Eq. (3.21), the term on the stress tensor proportional to the Lagrange multiplier λ yields terms proportional to derivatives of the field strength, which are suppressed compared to the remaining contributions from

the vector field (however the reader should bear in mind the aforementioned important rôle of this term in coupling the perturbations of the vector field to the density perturbations [61], thus leading to the growth of structure).

Moreover, as we discussed above, any spatial ("magnetic" type) components of the field strength are locally subleading compared to the "electric" type ones F_{0i}, which, on account of (3.31), implies

$$\widetilde{F}^{t\rho}\widetilde{F}_{t\rho} = -\,a^2(t)\,e^{\zeta(r)-\nu(r)}\,\delta_{jk}u^j u^k\,\frac{\mathcal{J}}{\alpha'^2}\left(\frac{a^2(t_c)}{a^2(t)} - 2H(t)\,t_c\right)^2 \,, \tag{3.35}$$

where the local metric that contracts the velocities is given by Eq. (3.28). For a lensing galaxy at redshift z, we apply Eq. (3.32) for today's observational time ($t = t_0$, $a(t_0) = 1$)

$$\widetilde{F}^{t\rho}\widetilde{F}_{t\rho} = -\,e^{\zeta(r)-\nu(r)}\,\delta_{jk}u^j u^k\,\frac{\mathcal{J}}{\alpha'^2}\,\mathcal{H}(z)^2 \,, \tag{3.36}$$

with $\mathcal{H}(z) = \left[\frac{1-3(1+z)^2}{(1+z)^2\,(1+(1+z)^2)}\right]$.

At this point we can take the statistical average of the velocities over populations of D-particles in the neighbourhood of galaxies, as given in Eqs. (3.34), (C.24), which yields

$$\langle\!\langle \widetilde{F}^{t\rho}\widetilde{F}_{t\rho}\rangle\!\rangle = -\mathcal{J}\,\frac{3\,\sigma_0(t)^2}{\alpha'^2}\,e^{\zeta(r)-\nu(r)}\,\mathcal{H}(z)^2 \,. \tag{3.37}$$

We also have, in Cartesian coordinates too, the other components

$$\langle\!\langle \widetilde{F}_\mu{}^\rho\widetilde{F}_{\nu\rho}\rangle\!\rangle = \mathcal{J}\,\frac{\sigma_0^2}{\alpha'^2}\begin{bmatrix} -3e^{\zeta-\nu} & \dots & \dots & \dots \\ \dots & -e^{\zeta-\nu} & \dots & \dots \\ \dots & \dots & -e^{\zeta-\nu} & \dots \\ \dots & \dots & \dots & -e^{\zeta-\nu} \end{bmatrix}\mathcal{H}(z)^2 \,, \tag{3.38}$$

where the $\dots$ denote subleading terms of order either $x^i\frac{\zeta'}{r}\,\mathcal{H}(z)$, or $x^ix^j\frac{\zeta'^2}{r^2}\,\mathcal{H}(z)^2$, which are ignored to a first approximation.

Einstein's equations for the lensing system are best described in spherical polar coordinates (t, r, θ, ϕ) to which the above quantities easily transform to. When investigating the modified Einstein's equations, the two components we will use to find the differential equation system that defines $\zeta(r)$ and $\nu(r)$ will be the tt and $\theta\theta$ components. In fact, the symmetry of the system we are analysing allows us to set

$\theta = \frac{\pi}{2}$. Thus, the $\theta\theta$ component of $\widetilde{F}^{\mu\rho}\widetilde{F}_{\nu\rho}$ will be given by

$$\langle\!\langle \widetilde{F}^{\theta\rho}\widetilde{F}_{\theta\rho}\rangle\!\rangle = -\mathcal{J}\,\frac{\sigma_0^2}{\alpha'^2}\,e^{\zeta(r)-\nu(r)}\,\mathcal{H}(z)^2\ , \qquad \text{with} \quad T^{\theta}_{\ \theta} = T^{z}_{\ z} \quad \text{when} \quad \theta = \frac{\pi}{2}\ . \tag{3.39}$$

Hence, the components we will use in Eq. (3.19) will assume the form

$$\begin{aligned}
\langle\!\langle \widetilde{F}^{\alpha\beta}\widetilde{F}_{\alpha\beta}\rangle\!\rangle &\simeq -6\,\mathcal{J}\,\frac{\sigma_0^2}{\alpha'^2}\,e^{\zeta(r)-\nu(r)}\,\mathcal{H}(z)^2\ ,\\
\langle\!\langle \widetilde{F}^{t\rho}\widetilde{F}_{t\rho}\rangle\!\rangle &\simeq -3\,\mathcal{J}\,\frac{\sigma_0^2}{\alpha'^2}\,e^{\zeta(r)-\nu(r)}\,\mathcal{H}(z)^2\ ,\\
\langle\!\langle \widetilde{F}^{\theta\rho}\widetilde{F}_{\theta\rho}\rangle\!\rangle &\simeq -\mathcal{J}\,\frac{\sigma_0^2}{\alpha'^2}\,e^{\zeta(r)-\nu(r)}\,\mathcal{H}(z)^2\ ,
\end{aligned} \tag{3.40}$$

with $\sigma_0^2(t_0) \simeq |\beta|$ (cf. Eq. (3.34)).

Moreover, non-minimal terms in Eq. (3.19) of the form $\widetilde{F}^2 R$ are also suppressed and ignored in our leading order estimates below. Taking the above considerations into account and concentrating on the tt component of the graviton equation (3.19) after taking statistical averages as in Eq. (3.34) and using Eq. (3.40), we approximate it as follows (the observation time is set to today $t = t_0$ with $a(t_0) = 1$)

$$\begin{aligned}
&\left[\frac{1}{\kappa_0^2} + \frac{\alpha\,T_3\,e^{\phi_0}}{g_{\rm s0}} + \frac{\alpha\,e^{-2\phi_0}\,\langle\!\langle \widetilde{F}^2\rangle\!\rangle}{4}\right]\left(R^{t}_{\ t} - \frac{1}{2}\,R\right)\\
&\qquad\qquad + \frac{1}{8}\,\langle\!\langle \widetilde{F}^2\rangle\!\rangle - \frac{1}{2}\,\langle\!\langle \widetilde{F}^{t\rho}\widetilde{F}_{t\rho}\rangle\!\rangle + \ldots = \frac{1}{2}\,T^{t}_{\ t}\\
\Rightarrow\quad &\left[\frac{1}{\kappa_0^2} + \mathcal{J}\,\frac{e^{-2\phi_0}}{24\,\alpha'}\left(1 - 6\pi^2\,|\beta|\,\mathcal{H}(z)^2\right)\right]\left(R^{t}_{\ t} - \frac{1}{2}\,R\right)\\
&\qquad\qquad + \frac{3}{4\,\alpha'^2}\,\mathcal{J}\,|\beta|\,\mathcal{H}(z)^2 + \ldots \simeq \frac{1}{2}\,T^{t}_{\ t}\ ,
\end{aligned} \tag{3.41}$$

where the $\ldots$ denote subleading terms, such as $\alpha e^{-2\phi_0}\,\langle\!\langle \widetilde{F}^{t\rho}\,\widetilde{F}_{t\rho}\rangle\!\rangle\,R$ and terms containing derivatives on $\widetilde{F}$. For ease of presentation above we also took into account that for the lensing data $e^{\zeta(r)-\nu(r)} = \mathcal{O}(1)$, however for the full numerical calculation presented in Tables 3.1 and 3.2, these terms were computed explicitly.

To model the lensing systems we shall be looking at, we take the energy momentum tensor to describe an ideal pressureless fluid, thus

$$T^{t}_{\ t} = -\rho(r)\ , \qquad T^{i}_{\ j} = 0\ . \tag{3.42}$$

We hence observe from the right-hand-side of Eq. (3.41) that the recoil velocity

field contribution to the tt component of the stress tensor has the right sign to be interpreted as a positive energy density contribution.

The quantity

$$\frac{1}{\kappa_{\rm eff}^2} \equiv \frac{1}{\kappa_0^2} + \mathcal{J}\,\frac{e^{-2\phi_0}}{24\,\alpha'}\left(1 - 6\pi^2\,|\beta|\,\mathcal{H}(z)^2\right) \tag{3.43}$$

plays the rôle of an effective inverse gravitational constant, which thus depends on the statistical variance of the recoil field $|\beta|$. For the lensing analysis, $|\beta|$ is determined from Eq. (C.25) and $M_{\rm s}$ (the string mass) can take any value such that $M_{\rm s} \lesssim 10^{18}$ GeV; however the assumption of non observation of large extra dimensions in current particle accelerators (including the run II of LHC) means that $M_{\rm s} \gtrsim 10^4$ GeV.

For concreteness, from now on we set the constant dilaton value to zero $\phi_0 = 0$. We also note at this stage that, in the analysis of Ref. [61], the brane tension was taken to satisfy

$$\frac{(2\pi\alpha')^2\,T_3}{g_{\rm s0}} = 1\ . \tag{3.44}$$

In such a case, $\mathcal{J} = 1$ in Eq. (3.15). However, as we shall see in section 3.4, one cannot obtain consistent inflation for brane tensions for which Eq. (3.44) is adopted. On the contrary, for the case of consistent inflation (that is when we have large fields, compared to the Planck mass scale) in which the D-material universe evolution connects smoothly the galactic structure era to the inflationary era, one needs $\mathcal{J} \gg 1$. This will be the case of interest to us in the present study. Again for concreteness, we consider for the remainder of the section that the brane tension and the parameter κ_0 (which is phenomenological in our construction) satisfy

$$\kappa_0^{-2} \sim \frac{1}{2}\,M_{\rm Pl}^2 \sim \frac{\mathcal{J}}{24}\,M_{\rm s}^2\ . \tag{3.45}$$

The identification of the parameter κ_0^{-2} with half of the (square of the) four-dimensional reduced Planck mass, $M_{\rm Pl}^2 = (16\pi G)^{-1}$, was chosen so as, on account of Eq. (3.43), to have

$$\kappa_{\rm eff}^{-2} \simeq M_{\rm Pl}^2\ , \tag{3.46}$$

given that the term proportional to β on the right-hand-side of Eq. (3.43) is relatively suppressed for $|\beta| \ll 1$ (which is the case in late eras). This is desirable from the point of view of not having significant variations of the gravitational constant, due to the unobserved (so far) violations of the weak equivalence principle. The reader should also notice that the choice Eq. (3.45) necessitates low string mass scales,

$M_{\rm s} \ll M_{\rm Pl}$, as assumed in Ref. [61], if one requires $\mathcal{J} \gg 1$ in order to satisfy the criterion for a smooth connection of this era with inflation.[13]

Using Eq. (3.42), demanding the recoil vector field contributions to the stress tensor to be *at most* of the same order of magnitude as the mass terms, and considering typical values of the mass density $\rho(r)$ for lenses to be of order $\rho(r) \sim 10^{-119}\, M_{\rm Pl}^4$ (cf. Table 3.4 below), we obtain from Eq. (3.41) the following *upper bound* on the parameter $|\beta|$

$$|\beta| \leq \frac{4}{3}\,\mathcal{J}^{-1}\,10^{-119}\,(\mathcal{H})^{-2}\left(\frac{M_{\rm Pl}}{M_{\rm s}}\right)^4 \sim 10^{-120}\,(\mathcal{H})^{-2}\left(\frac{M_{\rm Pl}}{M_{\rm s}}\right)^2\,, \tag{3.47}$$

on account of Eq. (3.45). For e.g. $M_{\rm s} \simeq 10^4$ GeV (used as a concrete case in Ref. [61]) and taking into account that $\mathcal{H} \in [-1, {}^{-1}\!/_3]$, i.e. of $\mathcal{O}(1)$, for a redshift range of interest $z \in [0, 2]$, we observe from Eq. (3.47) that $|\beta| \leq 10^{-92}$.

However, as discussed in Ref. [61], there is a *minimum* $|\beta|$, i.e. a minimum density of D-particles, that guarantees the existence of a growing model. The reader should bear in mind that the normalisation of $|\beta|$ in Ref. [61] was different from the one used in the present study, since in there a dimensionless factor $t_{\rm c}/\sqrt{\alpha'}$, where $t_{\rm c}$ is the time of contact of the string matter with the D-particle defect, had been absorbed in the definition of the recoil velocity. More precisely, the relation between the recoil velocity $v^{\rm MSY}$ used in Ref. [61] and the dimensionless recoil velocity u used here is

$$v^{{\rm MSY}\,i} = u^i\,\frac{t_c}{\sqrt{\alpha'}}\,.$$

For the galactic era, of interest to us here, $t_{\rm c} \sim t_0 \sim H_0^{-1}$ and thus the relation between the two $|\beta|$ parameters, defined through Eq. (3.34) for the respective recoil velocities, is given by

$$|\beta| \sim \alpha' H_0^2\,|\beta^{\rm MSY}|\,, \tag{3.48}$$

with again the notation $|\beta^{\rm MSY}|$ referring to definitions used in Ref. [61].

It was shown in Ref. [61] that, for $M_{\rm s} \sim 10^4$ GeV, $g_{\rm s0} \sim 0.1$, growth of structure due to the recoil velocity field is possible for

$$|\beta^{\rm MSY}| \geq 10^{-3}\,,$$

[13] If the latter is relaxed, one may consider more general cases, in which the string scale can be as large as $M_{\rm Pl}$ [61] (in such a case the first two terms in Eq. (3.43) contribute more or less equally, but the last one is still suppressed for small $|\beta|$).

a value which is largely insensitive to the value of $M_s \in [10^4, 10^{18}]$ GeV. This implies (for the $|\beta|$ used here)

$$|\beta| \geq 10^{-3} \left(\frac{H_0}{M_s}\right)^2 \sim 10^{-123} \left(\frac{M_{Pl}}{M_s}\right)^2 \sim 10^{-95} , \tag{3.49}$$

taking into account that $H_0 \sim 10^{-60}\ M_{Pl}$.

The analysis in Ref. [61] assumed a brane tension satisfying Eq. (3.44). As we shall discuss in the next section, inflation can only be driven by large D-particle recoil velocity condensates which occur for relatively large brane tensions T_3 compared to those satisfying Eq. (3.44). It would be therefore essential to repeat the growth-of-structure analysis of Ref. [61] for such large values of T_3.

Indeed, relaxing this condition and considering a wider range of values for the tension does not affect the value that β^{MSY} needs to take in order to ensure the growth of structure. This is because the dominant terms in the equation governing the growth of vector perturbations in Ref. [61] have a simple relationship with the tension T_3, such that it appears only as a scaling term. Thus, the vector field associated with the D-particle recoil velocity excitation always enters a growing mode for $\beta^{MSY} \gtrsim 10^{-3}$, and T_3 simply scales the result. As a consequence, by appropriately scaling the initial size of the vector perturbations in the early universe, any value of T_3 can be made compatible with the growth of structure.

Using Eqs. (C.25), (C.26) in our semi-microscopic model for estimating $|\beta|$, we obtain the allowed range of $|\beta|$ and densities of D-particles. Denoting by $N_D^{(0)}$ and $N_\gamma^{(0)}$ the current (dimensionful) number densities of D-particles and photons, respectively, and considering $M_s \sim 10^4$ GeV,[14] we get

$$10^{-95} \leq |\beta| \leq 10^{-92} \quad \Rightarrow \quad 10^{-62}\, \widetilde{\xi}_0^{-2} \leq \frac{N_D^{(0)}}{N_\gamma^{(0)}} \leq 10^{-59}\, \widetilde{\xi}_0^{-2} , \qquad \widetilde{\xi}_0 < 1 , \tag{3.50}$$

which serves as an indicative order of magnitude for the required densities so that the D-matter recoil velocity fluid in this stringy universe can "mimic" DM in galaxies, in the sense that its contribution to the energy density is of the same order as the mass density of a galaxy. Upon comparing (3.50) with the upper bounds on the number density of D-particles (3.9), obtained in the case where the screening of their mass effects by the D-particles neighbouring the D3-brane world did not occur, the alert

[14] While the left-hand-side of the bound on $|\beta|$ is independent of the string scale, the right-hand-side is quadratic in M_{Pl}/M_s; but because the same dependence appears in Eq. (C.25), the right-hand-side of the bound on $N_D^{(0)}/N_\gamma^{(0)}$ is string scale independent.

reader can appreciate the significant increase in the allowed densities in our case, without overclosing the universe.

In this latter respect some remarks are in order at this point. Although the rest mass contributions of D-particles have been assumed to be neutralised to a large extent by repulsive contributions from populations of D-particles in the neighbourhood of the brane world [61], it is worth mentioning that if the above upper bounds on the present-era density of D-particles of (rest) mass $M_{\rm s}/g_{\rm s0}$ are satisfied, then the corresponding contributions to the brane's vacuum energy (as seen by a comoving observer, and assuming the D-particles bound on the brane and comoving with its expansion) would be $\rho_{\rm D-mass} \sim N_{\rm D}^{(0)}\, M_{\rm s}/g_{\rm s0}$. Now, assuming that $N_\gamma^{(0)} = 10^9\, N_{\rm b}^{(0)}$, where $N_{\rm b}^{(0)}$ is the current number density of baryons in the universe, and estimating the baryon density by considering a common proton mass $m_{\rm p}$ for all species of order 1 GeV, we obtain $\rho_{\rm D-mass} \sim 10^{-48}\, \rho_{\rm b}^{(0)}\, M_{\rm s}/(g_{\rm s0}\, m_{\rm p})$, with $\rho_{\rm b}^{(0)}$ the energy density of the baryons in the present universe. For masses of $M_{\rm s}/g_{\rm s0} \in [10^4, 10^{18}]$ GeV, we obtain that $\rho_{\rm D-mass} \in [10^{-44}, 10^{-30}]\, \rho_{\rm b}^{(0)}$, which means that the overclosing of the universe is in fact not a problem at all.

3.3.2 The lensing system

After the above generic estimates, we now proceed with the detailed lensing phenomenology. There are two spherical mass profiles which we use for the lensing analysis. First, there is the Hernquist mass profile, which is used to model the baryonic mass profiles of the galaxies we are looking at. It is described by

$$M_{\rm H}(\hat{r}) = \frac{M\hat{r}^2}{(\hat{r}+r_h)^2}\ . \tag{3.51}$$

This definition uses the standard Schwarzschild radius parameter, $\hat{r}$, which is related to the radius parameter which appears in the metric system defined in Eq. (3.28) through $\hat{r} = e^{\zeta(r)/2}\, r$. There is also a parameter, r_h, which defines a scale for the core of the mass distribution. This scale is derived from the observable half mass radius R_e. M denotes the total mass of the galaxy.

Second we use the Navarro-Frenk-White (NFW) profile [66], which is usually applied to model the total DM and luminous matter contributions to a galaxy. It is

described by

$$M_{\rm NFW}(\hat{r}) = \frac{M}{\Gamma}\left[\ln\left(1+\frac{\mathcal{C}\hat{r}}{r_{\rm vir}}\right) - \frac{\mathcal{C}\hat{r}}{r_{\rm vir}+\hat{r}}\right] \ , \tag{3.52}$$

where $\Gamma = \ln(1+\mathcal{C}) - \frac{\mathcal{C}}{1+\mathcal{C}}$, $\mathcal{C}$ is a concentration parameter, usually taken to be around 10 based on computer simulations, and $r_{\rm vir}$ is the virial radius, related once again to the observable half mass radius R_e.

The above mass profiles are used in the equations describing the deflection of light in our system. The deflection of light in our metric (3.28) is given by

$$\Delta\varphi = 2\int_{r_0}^{\infty} \frac{1}{r}\frac{\mathrm{d}r}{\sqrt{e^{\zeta(r)-\nu(r)}\,\frac{r_0^2}{b^2}-1}} - \pi \ , \tag{3.53}$$

where r_0 is the point of closest approach for the light ray and b is the observable impact parameter of the light ray. They are related to each other through

$$b^2 = e^{\zeta(r_0)-\nu(r_0)}\, r_0^2 \ . \tag{3.54}$$

The mass profiles implicitly appear in the above equations through the dependence of $\zeta(r)$ and $\nu(r)$ on the density profile $\rho(r)$, which is derived from the mass profiles. Similarly, the tt and $\theta\theta$ equations of the graviton equation of motion Eq. (3.19), after using Eqs. (3.34) and (3.40) but keeping the non-minimal terms of the form $\widetilde{F}^2 R$ and the exact exponential structure $e^{\nu(r)-\zeta(r)}$, and after some mixing and manipulations, yield

$$\begin{aligned} -\zeta''(r) = \frac{4\pi G}{\alpha'}\left[e^{-2\phi_0}\,8\pi^3 G\,\rho(r) + \frac{3}{\alpha'}\right]\mathcal{J}|\beta|\mathcal{H}(z)^2\, e^{2\zeta(r)-\nu(r)} \\ + 8\pi G\,\rho(r)\,e^{\zeta(r)} + \frac{2}{r}\,\zeta'(r) + \frac{1}{4}\,\zeta'(r)^2 \end{aligned} \tag{3.55}$$

$$\begin{aligned} \nu''(r) = \frac{4\pi G}{\alpha'}\left[e^{-2\phi_0}\,8\pi^3 G\,\rho(r) + \frac{5}{\alpha'}\right]\mathcal{J}|\beta|\mathcal{H}(z)^2\, e^{2\zeta(r)-\nu(r)} \\ + 8\pi G\,\rho(r)\,e^{\zeta(r)} + \frac{1}{r}\left[\zeta'(r)-\nu'(r)\right] + \frac{1}{4}\left[\zeta'(r)^2 - 2\nu'(r)^2\right] \ , \end{aligned} \tag{3.56}$$

where any information about the mass profile lies in $\rho(r)$. The limit $\beta \to 0$ naturally gives back the General Relativity equations. Solving these and using the data we have for our lenses, for instance Q0142-100, yields the metric coefficients of Fig. 3.2. We here give the deviation from ± 1, that is, flat spacetime, which is naturally

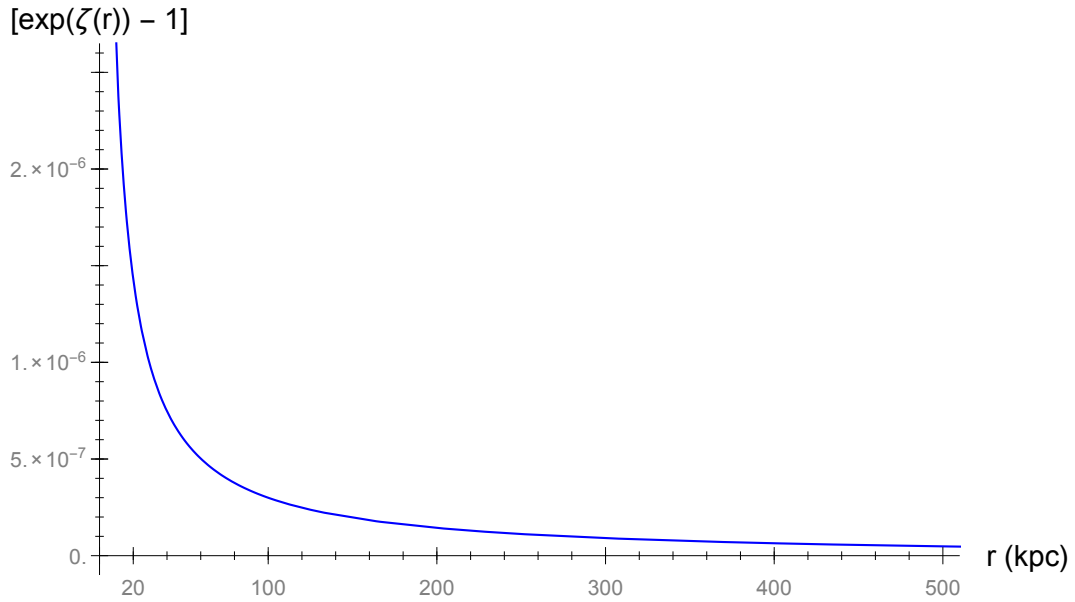

Figure 3.2: Profile of the deviation from 1 of the metric coefficients, $(-e^{\nu(r)}+1) \simeq (e^{\zeta(r)}-1)$, for one of our lens, namely Q0142-100.

retrieved at sufficiently large distances.

Finally, the lensing system is described by the thin lens equation, that is

$$\hat{\beta} = \theta - \Delta\varphi(\theta, M, b)\frac{D_{\rm ds}}{D_{\rm s}} \ , \tag{3.57}$$

where $\hat{\beta}$ is the unknown true angular position of the source galaxy, θ is the observable angular position of the source, $D_{\rm ds}$ is the angular distance from the source to the lens and $D_{\rm s}$ is the angular distance to the source. There are two unknowns in the above equation, the deflection angle $\Delta\varphi$ and $\hat{\beta}$, thus two images of the source are needed and the data from both are combined to constrain the true values of these parameters. Note that here we use a concordance cosmological model $(\Omega_{\rm m}, \Omega_\Lambda, \Omega_k) = (0.3, 0.7, 0)$, since departures from it lead only to insignificant changes in our lensing analysis.[15] The lensing equation (3.57) is applied independently to the multiple images of the background source, and solving it we obtain the actual position $\hat{\beta}$ of the source and the mass M of the lens.

To estimate the amount of DM in the system, the lensing mass is compared to

[15] As we have seen above, the density of D-particles can be constrained appropriately so that the $\Omega_{\rm m}$ parameter lies within its best-fit value today. The cosmological "constant" contribution can also be made small as we discussed previously, below Eq. (3.24). The flatness is of course guaranteed by our brane-world construction.

		Salpeter IMF		Chabrier IMF	
Lens	$z_{\rm l}$	% DM in GR	$T_3\beta$ for no DM ($\times 10^{-121} M_{\rm Pl}^4$)	% DM in GR	$T_3\beta$ for no DM ($\times 10^{-121} M_{\rm Pl}^4$)
Q0142-100	0.49	0.4 ± 5.7	0.0072 ± 0.0960	47.9 ± 3.0	0.81 ± 0.05
HS0812+123	0.39	37.8 ± 2.2	0.66 ± 0.04	67.6 ± 1.3	1.2 ± 0.02
BRI0952-012	0.63	-6.3 ± 4.5	–	48.6 ± 1.8	0.73 ± 0.03
LBQS1009-025	0.88	64.7 ± 2.3	1.2 ± 0.04	81.7 ± 1.2	1.5 ± 0.2
B1030+071	0.60	59.7 ± 2.1	1.3 ± 0.04	78.5 ± 1.3	1.7 ± 0.3
HE1104-181	0.73	63.2 ± 1.6	1.1 ± 0.03	81.9 ± 0.8	1.5 ± 0.1
B1152+200	0.44	25.1 ± 3.5	0.63 ± 0.09	61.0 ± 1.2	1.5 ± 0.3
SBS1520+530	0.71	41.1 ± 3.4	0.83 ± 0.07	67.5 ± 1.8	1.4 ± 0.4
B1600+434	0.42	61.4 ± 1.3	1.2 ± 0.03	78.9 ± 0.5	1.6 ± 0.09
HE2149-275	0.60	60.7 ± 1.7	1.1 ± 0.03	79.7 ± 0.9	1.5 ± 0.2
Q0957+561A	0.36	76.7 ± 0.5	1.6 ± 0.01	86.9 ± 0.3	1.8 ± 0.06
Q0957+561B	0.36	77.4 ± 0.5	1.6 ± 0.01	87.3 ± 0.3	1.9 ± 0.06

Table 3.1: The best fit values of $T_3\beta$ to get near zero Dark Matter (DM) for a galaxy using the Hernquist mass profile. Here $M_{\rm s} = 15$ TeV and $z_{\rm l}$ is the redshift of the lensing galaxy. The DM requirements in standard GR gravity when comparing the lensing mass to the stellar mass is also given. Error estimates arise from errors on the stellar mass content of the galaxies, as presented in [70].

the stellar mass content of the galaxies. The stellar mass is calculated assuming both a Salpeter [67] Initial Mass Function (IMF) and a Chabrier [68] IMF.[16] The IMF is defined as the distribution of stellar masses at birth, and for our purposes it is relevant as it dominates the conversion of light into mass. It is usually assumed to be a universal function, although there is some discussion about the exact form of the IMF. For this reason our analysis presents two choices of IMF, a classical Salpeter function, which consists of a single power law, therefore along the lines of a claimed excess of low-mass stars; and a Chabrier IMF, which truncates the power law with a lognormal distribution at the low mass end, resulting in systematic lower values of the mass to light ratio. The stellar mass estimates for the two cases were based on the results presented in Ref. [69]. The stellar mass is measured out to some aperture radius, and the lensing total mass is truncated to this radius when comparing the two values.

Comparing the lensing mass and the luminous mass of the galaxies allows us to estimate the DM content of the galaxies. We can then alter the value of the key parameter in the D-particle model, that is $T_3\beta$, to give the best fit value of $T_3\beta$ for

[16]For details about the different IMFs used here and their meaning, we refer the reader to Ref. [61].

		Salpeter IMF		Chabrier IMF	
Lens	z_l	% DM in GR	$T_3\beta$ for no DM ($\times 10^{-121} M_{\rm Pl}^4$)	% DM in GR	$T_3\beta$ for no DM ($\times 10^{-121} M_{\rm Pl}^4$)
Q0142-100	0.49	-2.9 ± 5.8	–	46.2 ± 3.1	0.78 ± 0.05
HS0812+123	0.39	30.2 ± 2.5	0.53 ± 0.04	63.6 ± 1.4	1.1 ± 0.03
BRI0952-012	0.63	-3.0 ± 4.3	–	50.3 ± 1.7	0.75 ± 0.03
LBQS1009-025	0.88	66.9 ± 2.2	1.2 ± 0.04	82.8 ± 1.1	1.5 ± 0.02
B1030+071	0.60	61.3 ± 2.0	1.3 ± 0.04	79.4 ± 1.3	1.7 ± 0.03
HE1104-181	0.73	54.5 ± 2.0	0.99 ± 0.04	77.6 ± 1.0	1.4 ± 0.02
B1152+200	0.44	23.2 ± 3.6	0.58 ± 0.09	60.0 ± 1.3	1.5 ± 0.03
SBS1520+530	0.71	43.8 ± 3.3	0.88 ± 0.06	69.0 ± 1.7	1.4 ± 0.04
B1600+434	0.42	64.2 ± 1.2	1.3 ± 0.02	80.4 ± 0.4	1.6 ± 0.008
HE2149-275	0.60	58.8 ± 1.8	1.1 ± 0.03	78.7 ± 0.9	1.4 ± 0.02
Q0957+561A	0.36	74.9 ± 0.5	1.6 ± 0.01	85.8 ± 0.3	1.8 ± 0.006
Q0957+561B	0.36	74.3 ± 0.5	1.6 ± 0.01	85.5 ± 0.3	1.8 ± 0.006

Table 3.2: As Table 3.1, now with the NFW profile.

no DM to be required in these systems. Note that the purpose of this analysis is not to show the lensing can be explained in the absence of DM, as DM candidates come naturally with the string model we are working with. However, the results for $T_3\beta$ shown in Table 3.1 and 3.2 represent the upper bound on the value of $T_3\beta$ in these systems.

We examine a selection of lensing galaxies from the CfA-Arizona Space Telescope Survey (CASTLES) [71] database. Given our 1-D lensing analysis, we are restricted to only studying those lenses with 2 images only, as systems with quad images require accounting for the ellipticity of the lens. We are also restricted to looking at those galaxies for which there was high quality data for the luminous mass content. We thus get the list of 11 galaxies for which we present results below. Note that Q0957+561A and Q0957+561B are both a special case for which one galaxy was lensing two separate sources simultaneously. The results for the Hernquist profile are presented in Table 3.1 and the results for the NFW profile are given in Table 3.2.

Note that in the results, using the Salpeter IMF leads to a negative estimate for the DM content of two galaxies, namely BRI0952-012 for the Hernquist and NFW profile, and Q0142-100 for the NFW profile. This is a result of the form of the IMF, which tends to systematically overestimate the contribution of low mass stars when calculating the stellar mass of galaxies. We include both IMF's for completeness and also to show the weak dependence of our results on the specific IMF chosen, but the Chabrier case is widely considered to be the most evidentially robust for

precisely this reason [69]. In addition, as shown in [69, 70], one can note that the errors given are due to the errors in the astrophysical data (namely, in the evaluation of the stellar mass) and are, in the vast majority, within 10%. The numerical code does not amplify nor reduce these errors. Finally, we would like to recall once more that one can safely assume, between different lenses, a 10% variation of β due to a slight inhomogeneity in the D-particles distribution.

Thus, given the allowed range of values for β in Eq. (3.50) for $M_{\rm s} = 15$ TeV, we would expect T_3 to be approximately in the range $10^{-60}\, M_{\rm Pl}^4 \lesssim T_3 \lesssim 10^{-57}\, M_{\rm Pl}^4$. This result is actually largely insensitive to the value of the string mass scale $M_{\rm s}$. The corresponding range of $\mathcal{J}$ (cf. (3.15)), for $\phi_0 = 0$, $M_{\rm s} = 15\,$TeV and phenomenologically relevant values of the string coupling ${}^{8\pi^2}/_{g_{\rm s0}} = \mathcal{O}(10^2)$ is then $1 \ll 10^9 \lesssim \mathcal{J} \lesssim 10^{12}$.

3.3.3 Numerical estimates of the modified contributions

We shall now examine some numerical results for different contributions of the graviton equation of motion, to allow a more intuitive understanding of the different contributions arising from our model.

$\frac{1}{2\kappa_0^2} + \frac{\alpha T_3 e^{\phi_0}}{2 g_{\rm s0}} \quad (M_{\rm Pl}^2)$	$\frac{\alpha e^{-2\phi_0} \langle\!\langle \widetilde{F}^{\alpha\beta} \widetilde{F}_{\alpha\beta} \rangle\!\rangle}{4} \quad (M_{\rm Pl}^{-2})$
4.0×10^{-2}	$-5.8\, T_3 \beta \times 10^{31}$

Table 3.3: Comparison of the values for the different contributions to $\kappa_{\rm eff}^{-2}$, defined in Eq. (3.43). Note that the units in the second column are $M_{\rm Pl}^{-2}$ since $[T_3] = M_{\rm Pl}^4$.

$\left(R^{\mu}{}_{\nu} - \frac{1}{2}\, g^{\mu}{}_{\nu} R\right) \frac{1}{\kappa_0^2} \quad (M_{\rm Pl}^4)$	$\rho(r) \quad (M_{\rm Pl}^4)$	$\frac{1}{8} \langle\!\langle \widetilde{F}^2 \rangle\!\rangle - \frac{1}{2} \langle\!\langle \widetilde{F}^{t\rho} \widetilde{F}_{t\rho} \rangle\!\rangle$
-4.9×10^{-120}	1.6×10^{-119}	$5.8\ T_3 \beta \times 10^3$

Table 3.4: Comparison of the values for the different contributions to the tt component of the metric Eqs. (3.41), (3.42); evaluated for the lens HS0818+123, at a distance of 15 kpc. Note that the final column is given in dimensionless form since $[T_3] = M_{\rm Pl}^4$.

Table 3.3 shows the values of the different contributions to $\kappa_{\rm eff}^{-2}$. The second term will be of the same order as $1/8\pi G$ when $T_3 \beta = 10^{-33}\, M_{\rm Pl}^4$. Thus, in order to ensure that there is a negligible contribution from our model to the value of the effective gravitational constant, we get an upper limit on $T_3\beta$ of $10^{-33}\, M_{\rm Pl}^4$, which is satisfied considering our above estimates. However, more stringent upper limits on this value come from other considerations, as shown in Eq. (3.50).

In Table 3.4 we show the values of the standard GR terms and the modifications coming from our model. The following can be seen: looking at the last item in the table we can see that this will be of the same order as the GR contribution only when $T_3\beta \simeq 10^{-123}\, M_{\rm Pl}^4$. Note that the above analysis can only provide a rough understanding of the relative sizes of the contributions coming from different parts of the model; a more accurate numerical analysis presented in Table 3.1 does not make the same simplifications as the ones that have been taken here, and this accounts for the difference in the calculated value of $T_3\beta$ and the one estimated above.

3.4 Inflation induced by D-particles

Another important aspect of D-particles outlined in Ref. [59] is the fact that they may induce (slow-roll) inflation consistent with the latest cosmological data such as the Planck survey [10], through condensation of their recoil velocity field. There are two physically relevant cases, which depend crucially on the size of the string scale involved. One pertains to large condensate fields, which may arise in the case of very dense populations in the early universe, and we ensure a smooth connection, in the sense of a cosmic evolution, between the weak condensates of the recoil velocity field at late epochs of the universe relevant for galaxy and large-scale structure formation, with the strong condensates induced by dense D-particle populations in the early universe. This case, which we shall study in second in Section 3.4.3, is appropriate for low string mass scales $M_{\rm s}$ compared to the Hubble scale. The first case pertains to weak condensates, which are associated with string scales large compared to the Hubble inflationary scale and will be studied in Section 3.4.2. We investigate to see whether both cases can lead to consistent inflation, compatible with the Planck data [6], before exploring the connection of successful inflationary period with the late eras in the final Section 3.4.4 and after some common formalism.

3.4.1 Formalism

Before going to the specifics, it is useful to first introduce the reader to the pertinent formalism. For the inflationary metric, the background recoil vector field assumes the form (3.29) but with the term $t_{\rm c}$ being dominant over the term $(t\, a(t_{\rm c})/a(t))^2$ as a result of the exponential expansion of the universe and the fact that $t_{\rm c}$ is of order

of a few string time scales $t_c \sim \sqrt{\alpha'}$. The relevant background vector field is

$$A_i(t) \simeq \frac{1}{\alpha'}\, g_{ij}(t)\, u^j \left(\frac{a(t_c)^2}{a(t)^2}\, t - t_c \right)$$
$$\simeq -\frac{1}{\alpha'}\, g_{ij}(t)\, u^j\, t_c \sim -\frac{1}{\sqrt{\alpha'}}\, g_{ij}(t)\, u^j \ , \qquad t > t_c \sim \sqrt{\alpha'} \ , \tag{3.58}$$

and the metric $g_{\mu\nu}(t)$ is just the homogeneous and isotropic de Sitter FLRW metric (3.25) with $a(t) = a_0\, e^{H_I t}$ and H_I the Hubble scale during inflation, which is assumed constant and of the following order of magnitude $H_I \sim 10^{-5}\ M_{\rm Pl} \gg H_0$ [6]. Thus the recoil vector field is assumed homogenoeus and isotropic in agreement with standard cosmology. This is a feature consistent with the assumption of dense populations of D-particles in the early universe. As discussed previously, we can covariantise the background, using Eq. (C.15), which satisfies the constraint (C.18). The "electric" field strength corresponding to this case is given by Eq. (C.19) in Appendix C. Due to the time dependence only of the (cosmological) background there are no "magnetic" field components, $F_{ij} = 0$.

We shall adopt a mean field approach, that is, a coarse-grained approximation, in which we shall consider appropriate distribution functions over the D-particle recoil velocities, thus treating the ensemble of particles and their properties (such as their velocities) over a small patch of the universe. We consider distributions of the stochastic Gaussian type (3.34), which preserve the rotational symmetry and isotropy and homogeneity of spacetime (and are thus consistent with the cosmological principle).

As we study later on in Section 3.4.3, inflation may be induced in case there are very dense populations of D-particles in the early universe, leading to large condensates of the respective velocity fields. In such a case, the full structure of the Born-Infeld action (3.1) needs to be kept to describe inflation. Using Eq. (3.10) we do observe that in the Minkowski spacetime, there is an upper bound on the allowed value of the condensate of the "electric" field $\langle\langle F_{\mu\nu}\, F^{\mu\nu} \rangle\rangle = -\langle\langle \mathbf{E}^2 a^2(t) \rangle\rangle$, with $F^{0i} \equiv E^i$, otherwise the integrand of the square root becomes imaginary. This is the problem of the *maximal electric field* in the Minkowskian Born-Infeld theory. However, when we consider the dynamics of inflation, we necessarily work in a finite temperature formalism, that is a Euclidean time, in order to account for the (observer dependent) de Sitter temperature characterising the inflationary scenario. In this case, the Euclidean Born-Infeld action does not have a bounded "electric" field. Analytic continuation back to Minkowski spacetime can be performed at the

end of the computations.

From Eq. (3.2), one can define a dimensionless covariant condensate in the FLRW spacetime background described by the FLRW metric g_{ij} (3.25)

$$\mathcal{C}(t) \equiv (2\pi\alpha')^2 \langle\langle F_{\mu\nu} F^{\mu\nu} \rangle\rangle = (2\pi\alpha')^2 \, 2 \, \langle\langle F_{0i} \, F_{0j} \, g^{00} \, g^{ij} \rangle\rangle = -8\pi^2 \alpha'^2 \, \langle\langle F_{0i} \, F_{0j} \, \frac{1}{a^2} \, \delta^{ij} \rangle\rangle$$
$$= -32\pi^2 \left(\frac{H(t)}{M_{\rm s}} \right)^2 \langle\langle u_i^{\rm phys} u_j^{\rm phys} \, \delta^{ij} \rangle\rangle = -96\pi^2 \left(\frac{H(t)}{M_{\rm s}} \right)^2 \sigma_0^2 \, , \tag{3.59}$$

where $u_i^{\rm phys} = a \, u_i$ is the D-particle recoil velocity in the comoving frame.

During inflation (approximately de Sitter spacetime background), there is a temperature associated with this frame, the so-called Hawking-Gibbons temperature of a de Sitter spacetime [72]

$$T = \frac{H}{2\pi} \, , \tag{3.60}$$

associated with the observer dependent horizon of the de Sitter spacetime.

Depending on the relative magnitude of this temperature, we may have a relativistic or non-relativistic "thermal" motion of the D-particle ensemble. If $M_{\rm D} = M_{\rm s}/g_{\rm s0}$ is the mass of the D-particle, set by the string scale $M_{\rm s} = 1/\sqrt{\alpha'}$, then, for the case where $H \simeq H_{\rm I} \gg M_{\rm D}$, that is when the string scale $M_{\rm s} \ll H_{\rm I} \simeq 10^{14}$ GeV, we have $T/M_{\rm D} \gg 1$ and the thermal motion of D-particles may be considered relativistic. In such a case, and again considering the properties of an ensemble of D-particles within a small patch of the universe, that is, using a coarse-grained approximation, a Boltzman distribution of the form

$$\int {\rm d}^3 p \, f(p) \sim \int {\rm d}^3 p \, e^{-p/T} = 4\pi \int {\rm d}p \, p^2 \, e^{-p/T} \, , \quad p \equiv |\mathbf{p}| \gg M_{\rm D} \, , \tag{3.61}$$

may be assumed without loss of generality.

The physical velocity $u_i^{\rm phys} = p_i^{\rm phys}/M_{\rm D} = g_{\rm s0} \, p_i/M_{\rm s}$ is now assumed to undergo this thermal distribution, because it is only in the physical (cosmological observer's) frame that such a (observer dependent) temperature can be defined, as explained above. Thus, over such a patch, the variance $\langle\langle u_i^{\rm phys} u_j^{\rm phys} \rangle\rangle$ (since $\langle\langle u_i^{\rm phys} \rangle\rangle = 0$) can

then be computed on the basis of Eq. (3.61) to be of order

$$\langle\!\langle u_i^{\rm phys} u_j^{\rm phys} \delta^{ij} \rangle\!\rangle = \frac{1}{M_{\rm D}^2} \langle\!\langle p_i^{\rm phys} p_j^{\rm phys} \delta^{ij} \rangle\!\rangle = \frac{g_{\rm s0}^2}{M_{\rm s}^2} \frac{\int {\rm d}p\, p^4\, e^{-p/T}}{\int {\rm d}p\, p^2\, e^{-p/T}}$$
$$\sim\, 12\, g_{\rm s0}^2 \left(\frac{T}{M_{\rm s}}\right)^2 \sim\, 12\, g_{\rm s0}^2 \left(\frac{H_{\rm I}}{2\pi M_{\rm s}}\right)^2 , \qquad |p| \ll T \ , \tag{3.62}$$

during inflation, and that it is approximately constant, decreasing with $H_{\rm I}$.

In the nonrelativistic case, that is, when the string scale $M_{\rm s}$ is much higher than the inflationary scale $H_{\rm I}$, one has, still using the coarse-grained approximation, a Maxwell distribution (Gaussian in the velocities) instead, with

$$\int {\rm d}^3 p\, f(p) \sim\, 4\pi \int {\rm d}p\, p^3\, e^{-p^2/TM_{\rm D}} \ , \tag{3.63}$$

$$\langle\!\langle u_i^{\rm phys} u_j^{\rm phys} \delta^{ij} \rangle\!\rangle = \frac{g_{\rm s0}^2}{M_{\rm s}^2} \frac{\int {\rm d}p\, p^5\, e^{-p^2/TM_{\rm D}}}{\int {\rm d}p\, p^3\, e^{-p^2/TM_{\rm D}}}$$
$$\sim\, 2\, g_{\rm s0} \left(\frac{T}{M_{\rm s}}\right) \sim\, 2\, g_{\rm s0} \left(\frac{H_I}{2\pi M_{\rm s}}\right) \ll 1 \ . \tag{3.64}$$

It is important to notice that the correct treatment of a thermal distribution of recoil velocities requires a Euclideanised spacetime, stemming from the replacement of the time coordinate with a Wick rotated one, $x^0 \to i\tau$, which is then identified with the inverse temperature. In this sense, the (dimensionless) condensate of the field strengths (3.59) then assumes the following form in an order of magnitude estimate

$$\begin{aligned} \mathcal{C}^{\mathcal{E}}(t) &\sim 96\, (H_{\rm I}/M_{\rm s})^4\, g_{\rm s0}^2 \qquad \text{for} \quad M_{\rm s} \ll H_{\rm I} \quad \text{(relativistic)} \\ &\sim 32\pi (H_{\rm I}/M_{\rm s})^3\, g_{\rm s0} \qquad \text{for} \quad M_{\rm s} \gg H_{\rm I} \quad \text{(non-relativistic)}, \end{aligned} \tag{3.65}$$

and notice that this Euclideanised condensate (indicated with the superscript '$\mathcal{E}$') is *positive definite*, so large values (much larger than one) are allowed, which would otherwise have been excluded on the basis of the reality of the argument of the square root of the Minkowskian Born-Infeld Lagrangian. This Euclidean path integral was adopted by Hawking in his treatment of the thermal properties of the black-hole horizon [73], and by Gibbons and Hawking [72] when discussed the de Sitter temperature, which is of interest to us here.

3.4.2 The fate of inflationary scenarii for small condensates

We next proceed to consider the possibility of D-particle recoil-induced inflation in the case where the condensate is a weak field (that is, much smaller than 1), which pertains either to the case when $M_{\rm s} \gg H_{\rm I}$ in Eq. (3.65) or to the case of arbitrary string scales but with the brane tension satisfying Eq. (3.44), which was dismissed in the lensing analysis.[17] Weak condensates characterise the galaxy growth era [61], and such situations cannot lead to inflation driven by the recoil velocity, as we will try to demonstrate here. Nevertheless, in such a case, other moduli fields in string theory, such as the dilaton (for large negative values), can drive a Starobinsky-type inflation, as discussed in Ref. [59] and reviewed briefly in Appendix D.

The dynamics of small condensates is described by an appropriate weak-field expansion of the Born-Infeld square root action of (3.1). For our purposes, it suffices to keep terms up to quadratic order in the recoil field strength F^2, leading to the effective action (3.12). The reader should also recall that we have fixed the brane tension to (3.44) for convenience, which results in a canonical Maxwell kinetic term for the recoil vector field. The latter satisfies the constraint (C.18). We also set the dilaton field to zero $\phi_0 = 0$, since our primary purpose here is to examine the possibility of a D-particle recoil driven inflation.

Using the condensation field

$$\langle\langle F^2 \rangle\rangle = -24\,\sigma_0^2\,\dot{a}^2\,\alpha' = -24\,\sigma_0^2\,H_I^2\,M_{\rm s}^2 \equiv \mathcal{C}_{\rm M4}\ , \tag{3.66}$$

(where $\mathcal{C}_{\rm M4} \equiv {}^1\!/_{(2\pi\alpha')^2}\,\mathcal{C}(t)$ has dimension [mass]^4, $\mathcal{C}(t)$ being defined in Eq. (3.59)) and ignoring any matter during the inflationary era, the effective action we shall make use from now on reads

$$S_{\rm eff\ 4D} = \int {\rm d}^4x\,\sqrt{-g}\left[-\Lambda_0 - \frac{1}{4}\,\langle \mathcal{G}^2\rangle - \frac{1}{4}\,\mathcal{C}_{\rm M4} + \left(\frac{1}{\kappa_0^2} + \frac{\alpha T_3}{g_{\rm s0}} + \frac{\alpha}{4}\,\mathcal{C}_{\rm M4}\right) R\right]\ . \tag{3.67}$$

Recall that even though $C_{\rm M4}$ is here treated as a time-dependent scalar field in a first approximation, it hides in fact a more complex (space- and time-dependent) vector field structure, which turns out to be the kinetic term of our vector field A_μ. As usual in inflationary considerations, we only consider the vacuum expectation values of the fields, in order to derive their cosmological evolution and ignoring local variations or quantum fluctuations. Any term containing derivatives of F^2 included

[17] See the discussion around Eq. (3.86) in the next subsection.

at this level would end up subleading and can thus be, here again, safely ignored.

We define then the following constants

$$\frac{1}{\kappa_{\rm eff}^2} = \frac{1}{\kappa_0^2} + \frac{\alpha\, T_3}{g_{\rm s0}}\ , \qquad \Lambda_0 = \frac{T_3}{g_{\rm s0}} + \frac{\tilde{\Lambda}}{\kappa_0^2} \simeq \frac{1}{3}\,\frac{\tilde{\Lambda}}{\kappa_0^2} = f_\kappa\,\frac{\tilde{\Lambda}}{\kappa_{\rm eff}^2} < 0 \tag{3.68}$$

where for the (non-conformal) cosmological constant we used Eqs. (3.17a) and (3.23) and defined $f_\kappa \equiv \frac{1}{3}\,\frac{\kappa_{\rm eff}^2}{\kappa_0^2}$. We also define the scalar field

$$\sigma \equiv \frac{1}{4}\,\alpha\,\kappa_{\rm eff}^2\,\mathcal{C}_{\rm M4} \tag{3.69}$$

and we obtain

$$S_{\rm eff\ 4D} = \int {\rm d}^4x\,\sqrt{-g}\,\frac{1}{\kappa_{\rm eff}^2}\left[-f_\kappa\,\tilde{\Lambda} - \widetilde{\mathcal{D}} - \frac{\sigma}{\alpha} + (1+\sigma)\,R\right]\ , \tag{3.70}$$

where the constant term of dimension [mass]^2, $\widetilde{\mathcal{D}} \equiv \kappa_{\rm eff}^2\,\mathcal{D} \equiv {}^1\!/_4\,\kappa_{\rm eff}^2\,\langle\!\langle \mathcal{G}_{\mu\nu}\,\mathcal{G}^{\mu\nu}\rangle\!\rangle$, corresponds to a flux field condensate[18] as well as potentially other dilaton-independent terms such as the rest mass contributions of a population of D-particles on the brane world to the vacuum energy density [59].[19]

Since we are concentrating here on the case of small fields $\sigma \ll 1$, this yields

$$\sigma = \frac{1}{4}\,\frac{\pi^2}{6}\frac{1}{M_{\rm s}^2}\,\kappa_{\rm eff}^2\left[24\,\sigma_0^2\,H_{\rm I}^2\,M_{\rm s}^2\right] \simeq \pi^2\,\sigma_0^2\left(\frac{H_{\rm I}}{M_{\rm Pl}}\right)^2 \ll 1\ , \tag{3.71}$$

where we used $\alpha = \frac{\pi^2}{6}\frac{1}{M_{\rm s}^2}$ and $\frac{1}{\kappa_{\rm eff}^2} \simeq M_{\rm Pl}^2$. Recalling $H_I \simeq 10^{-5}\,M_{\rm Pl}$, one has

$$\sigma_0^2 \ll \frac{10^{10}}{\pi^2} \simeq 10^9\ . \tag{3.72}$$

Changing the metric $g_{\mu\nu} \to g_{\mu\nu}^{\rm E} \equiv (1+\sigma)\,g_{\mu\nu}$ and defining

$$\varphi \equiv \sqrt{\frac{3}{2}}\,\ln(1+\sigma) \tag{3.73}$$
$$\partial_\mu\varphi = \sqrt{\frac{3}{2}}\,\frac{\partial_\mu\sigma}{1+\sigma}$$

[18] See Eq. (3.17b) and recall these flux gauge field condense due to the generic non-linearity of their bulk dynamics, as in Ref. [62].

[19] See Eq. (3.8) as well as Eq. (D.10) in Appendix D.

leads to the following

$$R = (1+\sigma)\left[R^{\rm E} + (\partial_\rho\varphi\,\partial^\rho\varphi)\right] \tag{3.74}$$

$$\sqrt{-g} = \frac{1}{(1+\sigma)^2}\sqrt{-g^{\rm E}}\,. \tag{3.75}$$

We hence get the action

$$S^{\rm E}_{\rm eff\ 4D} = \int {\rm d}^4x\,\sqrt{-g^{\rm E}}\,\frac{1}{\kappa^2_{\rm eff}}\left[R^{\rm E} + (\partial\varphi)^2 - V(\varphi)\right]\,,$$

$$\text{with}\quad V(\varphi) \equiv \widetilde{\mathcal{D}} + \frac{e^{-\sqrt{\frac{2}{3}}\varphi}}{\alpha} + \left(f_\kappa\,\tilde{\Lambda} - \frac{1}{\alpha}\right)e^{-\sqrt{\frac{8}{3}}\varphi}\,, \tag{3.76}$$

where the flux gauge term $\widetilde{\mathcal{D}}$ is conformal in four spacetime dimensions and thus remains constant upon the change of frame. We note that, as in the large condensate case of the following section, it is this field that drives inflation but the fluctuations of the recoil velocity inflaton field φ are what leads to exit from it. In addition, one can see the appearance from the curvature term of a kinetic term for our inflaton field, confirming that it is a dynamic field even though it was not explicit previously in actions (3.67) and (3.69).

Assuming $\sigma \ll 1$, then $\varphi \simeq \sqrt{1.5}\,\sigma \ll 1$ and thus the field φ is also small. Taylor expanding the exponentials around $\varphi \sim 0$, one obtains that the effective (inflationary) potential for small $\varphi \ll 1$ reads

$$\begin{aligned} V(\varphi) \simeq\ & \left[\widetilde{\mathcal{D}} + \frac{1}{\alpha}\left(1 - \sqrt{\frac{2}{3}}\,\varphi + \frac{1}{3}\,\varphi^2 + \mathcal{O}(\varphi^3)\right)\right. \\ & \left. + \left(f_\kappa\,\tilde{\Lambda} - \frac{1}{\alpha}\right)\left(1 - \sqrt{\frac{8}{3}}\,\varphi + \frac{4}{3}\,\varphi^2 + \mathcal{O}(\varphi^3)\right)\right] \\ \simeq\ & \left[\widetilde{\mathcal{D}} + f_\kappa\,\tilde{\Lambda} + \sqrt{\frac{2}{3}}\left(\frac{1}{\alpha} - 2f_\kappa\,\tilde{\Lambda}\right)\varphi\right. \\ & \left. + \frac{1}{3}\left(-\frac{3}{\alpha} + 4f_\kappa\,\tilde{\Lambda}\right)\varphi^2 + \mathcal{O}(\varphi^3)\right]\,. \end{aligned} \tag{3.77}$$

We shall now proceed to demonstrate that a purely D-particle recoil driven slow-roll inflation is impossible, in the case of weak condensate fields. To this end, one needs to study the slow-roll conditions and the WMAP imposed constraints [5, 10]. More precisely, the slow-roll parameters ϵ, η, ξ, the number N of e-folds, the spectral

index $n_{\rm s}$ and the WMAP normalisation [5, 10] read

$$\epsilon \equiv \frac{1}{2}\, M_{\rm Pl}^2 \left(\frac{V'}{V}\right)^2 \ll 1 \ , \tag{3.78a}$$

$$\eta \equiv M_{\rm Pl}^2 \left(\frac{V''}{V}\right) \ll 1 \ , \tag{3.78b}$$

$$\xi \equiv M_{\rm Pl}^4 \left(\frac{V''' V'}{V^2}\right) \ll 1 \ , \tag{3.78c}$$

$$N \equiv -\int_{\varphi_i}^{\varphi_e} \frac{V}{V'}\, {\rm d}\varphi \simeq 60 \ , \tag{3.78d}$$

$$n_{\rm s} \equiv 1 - 6\epsilon + 2\eta \simeq 0.96 \ , \tag{3.78e}$$

$$\left(\frac{\frac{1}{\kappa_{\rm eff}^2} V}{\epsilon}\right)^{1/4} = 0.0275\ M_{\rm Pl} \ . \tag{3.78f}$$

We note first that, as a result of the dilaton equation, the condition Eq. (3.24) is imposed, implying that $\tilde{\Lambda}$ is negative and the coefficients of the linear and quadratic terms in φ that are present in Eq. (3.77) are non-zero. This leads to nontrivial slow-roll parameters, yielding

$$N = \frac{V}{V'}\,\Delta\varphi \qquad \Rightarrow \qquad \epsilon = \frac{(\Delta\varphi)^2}{2\,N^2} \ , \qquad \eta = \frac{V''}{V'}\frac{\Delta\varphi}{N} \ ,$$

which, combined with the definition of $n_{\rm s}$, leads to

$$n_{\rm s} = 1 - 6\,\frac{(\Delta\varphi)^2}{2\,N^2} + 2\,\frac{V''}{V'}\frac{\Delta\varphi}{N} \qquad \Leftrightarrow \qquad \frac{V''}{V'} = \frac{3}{2}\frac{\Delta\varphi}{N} - \frac{N}{\Delta\varphi}\,\frac{1-n_{\rm s}}{2} \ . \tag{3.79}$$

Since $N \sim 60$ and $\Delta\varphi \ll 1$, one has $(1-n_{\rm s})\,N/\Delta\varphi \gg 1$ and $\Delta\varphi/N \ll 1$. Hence, to a good approximation, it gives

$$\frac{V''}{V'} \simeq -\frac{N}{\Delta\varphi}\,\frac{1-n_{\rm s}}{2} \quad \Leftrightarrow \quad \frac{\frac{2}{3}\left(-\frac{3}{\alpha} + 4 f_\kappa\,\tilde{\Lambda}\right)}{\sqrt{\frac{2}{3}}\left(\frac{1}{\alpha} - 2 f_\kappa\,\tilde{\Lambda}\right)} \simeq -\frac{N}{\Delta\varphi}\,\frac{1-n_{\rm s}}{2}$$

$$\Leftrightarrow \qquad \frac{1}{\alpha}\left(-3 + \sqrt{\frac{3}{2}}\,\frac{N}{\Delta\varphi}\,\frac{1-n_{\rm s}}{2}\right) \simeq -2 f_\kappa\,\tilde{\Lambda}\left(2 - \sqrt{\frac{3}{2}}\frac{N}{\Delta\varphi}\,\frac{1-n_{\rm s}}{2}\right) \ . \tag{3.80}$$

Since $\sqrt{\frac{3}{8}}\,N\,(1-n_{\rm s}) \sim 1.5$ and $\Delta\varphi \ll 1$, the constant term in each bracket in the

above equation is small and can be neglected. This yields

$$\frac{1}{\alpha}\left(\frac{1.5}{\Delta\varphi}\right) \simeq 2 f_\kappa \tilde{\Lambda}\left(\frac{1.5}{\Delta\varphi}\right) \quad \Leftrightarrow \quad \frac{1}{\alpha} \simeq 2 f_\kappa \tilde{\Lambda} \simeq 2\,\kappa_{\rm eff}^2\,\Lambda_0 \ , \tag{3.81}$$

leading to a positive Λ_0, incompatible with Eq. (3.24), which is required by the dilaton equation.

One is then led to the conclusion that no valid scenario exists for small field inflation induced by D-particles alone.

3.4.3 Inflation for large recoil velocity condensate fields

Let us now concentrate on the low string scale case, where the condensate (3.65) is large

$$M_{\rm s} \ll H_I \sim 10^{-5}\, M_{\rm Pl} \ll M_{\rm Pl} \ , \tag{3.82}$$

where we used that the Planck data [6] point towards the fact that $H_I \simeq 10^{-5}\, M_{\rm Pl}$. In this case, one cannot expand the square root of the Born-Infeld action, but one can approximate it by ignoring the constant inside, that is the (*Euclideanised* spacetime) action (3.1) becomes (setting $\phi_0 = 0$ from now on)

$$S_{\rm eff\ 4D} \simeq \int {\rm d}^4x\,\sqrt{g}\left[-\frac{1}{4}\,\mathcal{G}_{\mu\nu}\mathcal{G}^{\mu\nu} - \frac{T_3}{g_{\rm s0}}\sqrt{\frac{\mathcal{C}^{\mathcal{E}}}{2}} - \frac{\tilde{\Lambda}}{\kappa_0^2} + \frac{1}{\kappa_0^2}\left(1+\kappa_0^2\,\frac{\alpha\,T_3}{g_{\rm s0}}\sqrt{\frac{\mathcal{C}^{\mathcal{E}}}{2}}\right)R(g)\right] \ , \tag{3.83}$$

where α is given by Eq. (3.5) and the condensate is positive. Let us define the dimensionless field

$$\sigma(t) \equiv \kappa_0^2\,\frac{\alpha\,T_3}{g_{\rm s0}}\sqrt{\frac{\mathcal{C}^{\mathcal{E}}(t)}{2}} \ > 0 \ , \tag{3.84}$$

by means of which the action (3.83) becomes

$$S_{\rm eff\ 4D} \simeq \int {\rm d}^4x\,\sqrt{g}\,\frac{1}{\kappa_0^2}\left[-\frac{\kappa_0^2}{4}\,\mathcal{G}_{\mu\nu}\,\mathcal{G}^{\mu\nu} - \tilde{\Lambda} - \frac{\sigma}{\alpha} + (1+\sigma)\,R(g)\right] \ . \tag{3.85}$$

Before going further, we should make some remarks regarding the magnitude of the condensate field (3.84). First of all we observe that, if we were to follow the structure formation analysis [61] mentioned in Section 3.3 using brane tensions that satisfy

Eq. (3.44), the condensate field would be small $\sigma(t) \ll 1$ since

$$\sigma(t) \simeq \frac{g_{\rm s0}}{2\sqrt{3}} \left(\frac{H_I}{M_{\rm Pl}}\right)^2 \ll 1 \ , \tag{3.86}$$

where we have used Eqs. (3.65) and (3.43) and the fact that $M_{\rm s} \ll M_{\rm Pl}$ (cf. Eq. (3.82)) to approximate $M_{\rm Pl}^2 \simeq \kappa_0^{-2}$. As we saw in subsection 3.4.2, such weak condensates cannot lead to slow-roll inflation.

Here we are interested in large field inflation, which, as we try to demonstrate here, can be induced by large recoil velocity condensate fields $\sigma(t) \gg 1$. The latter condition may be achieved if we relax again Eq. (3.44) and use large brane tensions, namely

$$\frac{(2\pi\alpha')^2\, T_3}{g_{\rm s0}} \equiv \mathcal{J} \gg 1 \ . \tag{3.87}$$

The reader should recall Eq. (3.15) where the parameter $\mathcal{J}$ was first defined. In such a case, we obtain from Eq. (3.84)

$$\sigma(t) \simeq \frac{g_{\rm s0}}{2\sqrt{3}}\, \mathcal{J}\, \kappa_0^2\, H_I^2 \simeq \frac{g_{\rm s0}}{\sqrt{3}}\, \mathcal{J} \left(\frac{H_I}{M_{\rm Pl}}\right)^2 \ , \tag{3.88}$$

which can be much larger than one. In this case from Eq. (3.43) we obtain that $M_{\rm Pl}^2 = \frac{1}{\kappa_0^2} + \frac{\mathcal{J}}{24}\, M_{\rm s}^2$ and κ_0^2 is a parameter independent from $M_{\rm Pl}$. Without loss of generality one can simply assume the relation (3.45), used in the previous section for the lensing analysis, which is consistent with Eq. (3.82). In such a case one obtains

$$\sigma(t) \sim 8\sqrt{3}\, g_{\rm s0} \left(\frac{H_{\rm I}}{M_{\rm s}}\right)^2 \gg 1 \ , \tag{3.89}$$

during inflation. In the remainder of this subsection we shall stick to this case.

We now proceed to discuss how inflation is induced by such large condensates and how one can show the induced inflation is of Starobinsky-type [59]. We first redefine the metric in Eq. (3.85) as

$$g_{\mu\nu} \to \tilde{g}_{\mu\nu} = (1+\sigma) g_{\mu\nu} \ . \tag{3.90}$$

We also define a canonically normalised scalar field

$$\varphi(t) = \sqrt{\frac{3}{2}} \ln\Big(1+\sigma(t)\Big) \ , \tag{3.91}$$

in terms of which the action (3.85) becomes

$$S_{\rm eff\ 4D} \simeq \int {\rm d}^4x\sqrt{\tilde{g}}\,\frac{1}{\kappa_0^2}\left[R(\tilde{g}) + \frac{1}{2}\,\partial_\mu\varphi\,\partial^\mu\varphi - \frac{\kappa_0^2}{4}\,\mathcal{G}_{\mu\nu}\mathcal{G}^{\mu\nu} - \frac{e^{-\sqrt{\frac{2}{3}}\,\varphi}}{\alpha} - \left(\tilde{\Lambda} - \frac{1}{\alpha}\right)e^{-2\sqrt{\frac{2}{3}}\,\varphi}\right]\,, \tag{3.92}$$

where we took into account the conformal nature of the flux gauge term in four spacetime dimensions. We may assume now that the flux field condenses into a constant one, because of the non-linearity of its dynamics, as in Ref. [62], and contributes to the vacuum energy as

$$\frac{1}{4}\langle\langle\mathcal{G}_{\mu\nu}\,\mathcal{G}^{\mu\nu}\rangle\rangle \equiv \mathcal{D}\,, \tag{3.93}$$

as in the previous case. The last three terms in the Euclidean effective action (3.92) define the *Euclideanised* (superscript '$\mathcal{E}$') effective potential of the φ field in the region of large values (defined with dimensions of $[mass]^2$)

$$V^{\mathcal{E}} = -\kappa_0^2\,\mathcal{D} - \frac{e^{-\sqrt{\frac{2}{3}}\,\varphi}}{\alpha} - \left(\tilde{\Lambda} - \frac{1}{\alpha}\right)e^{-2\sqrt{\frac{2}{3}}\,\varphi}\,. \tag{3.94}$$

The reader should take notice of the relative sign of the potential compared to the kinetic term of the scalar field in (3.92), as appropriate for a euclidean effective action, which is just the effective Hamiltonian of the system. We should now *analytically* continue (3.94) back to the Minkowski spacetime. This implies that, apart from the time being rendered a Minkowskian signature, $x^0 \to it$, the field φ acquires an imaginary part

$$\sqrt{\frac{2}{3}}\,\varphi \to \ln(i|\sigma|) = \ln|\sigma| + i\frac{\pi}{2} = \sqrt{\frac{2}{3}}\,\tilde{\varphi} + i\frac{\pi}{2}\,, \tag{3.95}$$

where now the field $\tilde{\varphi}$ is real.

Thus, from Eq. (3.94), and assuming that the flux condensate $\mathcal{D}$ is of "electric" type so that under analytic continuation to Minkowski spacetime one has $\mathcal{D} \to -\mathcal{D}$, the potential acquires an imaginary part and is approximated by

$$V(\varphi) \simeq \kappa_0^2\,\mathcal{D} + \left(\tilde{\Lambda} - \frac{1}{\alpha}\right)e^{-2\sqrt{\frac{2}{3}}\,\tilde{\varphi}} + i\,\frac{e^{-\sqrt{\frac{2}{3}}\,\tilde{\varphi}}}{\alpha}\,. \tag{3.96}$$

Notice that the imaginary part of the potential is the only one appearing in the analytically-continued effective action (3.92), given that the kinetic terms are real, since the imaginary part of the φ field is constant in spacetime.

The presence of an imaginary part indicates an instability of the de Sitter inflationary vacuum which is not an unwelcome fact. The field will roll down towards smaller values of H^2. Eventually, the condensate (3.65) will become smaller than the Born-Infeld critical field and hence the imaginary part will disappear. In this regime, one may expand the square root of the Born-Infeld action, as done in Ref. [61], to obtain the effective action relevant for the radiation and matter eras.

The imaginary part of the potential gives by definition the width, or equivalently, the inverse of the lifetime of the de Sitter vacuum, namely

$$\tau = \hbar\,\Gamma^{-1} \sim \kappa_0^{-1}\,\alpha\, e^{\sqrt{\frac{2}{3}}\,\tilde{\varphi}} \tag{3.97}$$

which is sufficiently long (as compared to the reduced Planck time κ_0) for any positive value of $\tilde{\varphi} \sim \sqrt{6}\,\ln(H_{\rm I}/M_{\rm s})$.

The real part of the effective potential (3.96)

$$\mathrm{Re}\,V(\tilde{\varphi}) = \tilde{\mathcal{D}} + \left(\tilde{\Lambda} - \frac{1}{\alpha}\right) e^{-2\sqrt{\frac{2}{3}}\,\tilde{\varphi}}\ , \quad \tilde{\mathcal{D}} \equiv \kappa_0^2\,\mathcal{D}\ , \tag{3.98}$$

is of Starobinsky type, provided one can tune the flux-field condensate to be $\tilde{\mathcal{D}} > 0$ and such that the minimum of the potential occurs for the field value $\tilde{\varphi} = 0$ and corresponds to zero potential. The quantity $\tilde{\Lambda}$ is negative, as a consequence of the dilaton equation of motion, and in fact can be tuned to the value given by Eq. (3.23) in order to ensure continuity of the inflation phase with the growth era. Hence, the coefficient of the $e^{-2\sqrt{\frac{2}{3}}\,\tilde{\varphi}}$ term is negative relative to $\tilde{\mathcal{D}}$. Again, an *important feature* of the approach here is that it is the gauge field flux condensate $\langle \mathcal{G}_{\mu\nu}\mathcal{G}^{\mu\nu}\rangle$ that induces a de Sitter phase (positive, almost constant, vacuum energy), and hence inflation, but it is the recoiling D-particles velocity vector field that induces a slowly rolling scalar degree of freedom that allows exit from inflation.

Now, let us see how one can get slow-roll inflation in this case by evaluating the conditions (3.78). For large condensate σ, one has

$$\begin{aligned} &V(\tilde{\varphi}) = \tilde{\mathcal{D}} + \left(\tilde{\Lambda} - \frac{1}{\alpha}\right) e^{-2\sqrt{\frac{2}{3}}\,\tilde{\varphi}} = \tilde{\mathcal{D}} - A\, e^{-B\tilde{\varphi}}\ , \\ &V'(\tilde{\varphi}) = AB\, e^{-B\tilde{\varphi}}\ , \qquad V''(\tilde{\varphi}) = -AB^2\, e^{-B\tilde{\varphi}}\ , \qquad V'''(\tilde{\varphi}) = AB^3\, e^{-B\tilde{\varphi}}\ , \end{aligned} \tag{3.99}$$

where we defined the constants $A \equiv -\left(|\tilde{\Lambda}| + \frac{1}{\alpha}\right) > 0$ and $B \equiv 2\sqrt{\frac{2}{3}} \simeq 1.15$. Hence

$$N \simeq \frac{\tilde{\mathcal{D}}}{AB^2}\, e^{B\tilde{\varphi}} \tag{3.100a}$$

$$\epsilon \simeq \frac{A^2B^2}{2\tilde{\mathcal{D}}^2}\, e^{-2B\tilde{\varphi}} = \frac{1}{2B^2N^2} \quad \text{and} \quad \eta \simeq -\frac{AB^2}{\tilde{\mathcal{D}}}\, e^{-B\tilde{\varphi}} = -\frac{1}{N} \tag{3.100b}$$

$$\Rightarrow \quad 1 - n_{\rm s} = 6\epsilon - 2\eta = \frac{3}{B^2N^2} + \frac{2}{N} \tag{3.100c}$$

$$\xi \simeq \frac{A^2B^4}{\tilde{\mathcal{D}}^2}\, e^{-2B\tilde{\varphi}} = \frac{1}{N^2} \tag{3.100d}$$

$$\left(\frac{{}^1\!/_{\kappa_0^2}\, V}{\epsilon}\right)^{\frac{1}{4}} \simeq \left(\frac{\tilde{\mathcal{D}}}{\epsilon}\right)^{\frac{1}{4}} = 0.0275\; M_{\rm Pl} \tag{3.100e}$$

$$\Rightarrow \quad \tilde{\mathcal{D}} \simeq (0.0275)^4\; \epsilon\, M_{\rm Pl}^4 \simeq \frac{5.7\times 10^{-7}}{2B^2N^2}\, M_{\rm Pl}^4 \tag{3.100f}$$

where the last equation comes from the WMAP constraint [5, 10]. So, as is standard in Starobinsky-type inflation, the constant A is not constrained by the slow-roll conditions (in our microscopic model, as we have already mentioned, we may tune it to the value determined by Eq. (3.23) by demanding continuity of the inflationary epoch to the galactic-growth era of the string universe). Thus, fixing $n_{\rm s}$ fixes N (and vice-versa). Indeed, one gets (from solving the second degree trinomial in N from Eq. (3.100c) and choosing the positive solution)

$$N = \frac{1}{1-n_{\rm s}}\left(1 + \sqrt{1 + \frac{3\,(1-n_{\rm s})}{B^2}}\right)\ . \tag{3.101}$$

Planck 2015 analysis [10] gives $n_{\rm s} = 0.968 \pm 0.006$ (68% CL, PlanckTT+LowP) which is shifted towards higher values compared to earlier results, that gave a central value $n_{\rm s} = 0.965$. The solid black line in Figure 3.3 shows N as a function of $n_{\rm s}$ for $B = 2\sqrt{{}^2\!/_3}$. The vertical blue shaded area corresponds to the 68% CL interval for $n_{\rm s}$ corresponding to the two central values $n_{\rm s} = 0.965$ and $n_{\rm s} = 0.968$, while the horizontal shaded area in red shows the relevant interval for N. The black dashed lines highlight the central values for $n_{\rm s}$ and the corresponding values for N. One notes the excellent fitting of the predictions of the model to the data.

If we adopt $n_{\rm s} = 0.965$, we get $N = 57.7$, leading to

$$\epsilon \simeq 5.6\times 10^{-5} \ll 1\ , \quad \eta \simeq -1.7\times 10^{-2} \ll 1\ , \quad \xi \simeq 3.0\times 10^{-4} \ll 1 \tag{3.102a}$$

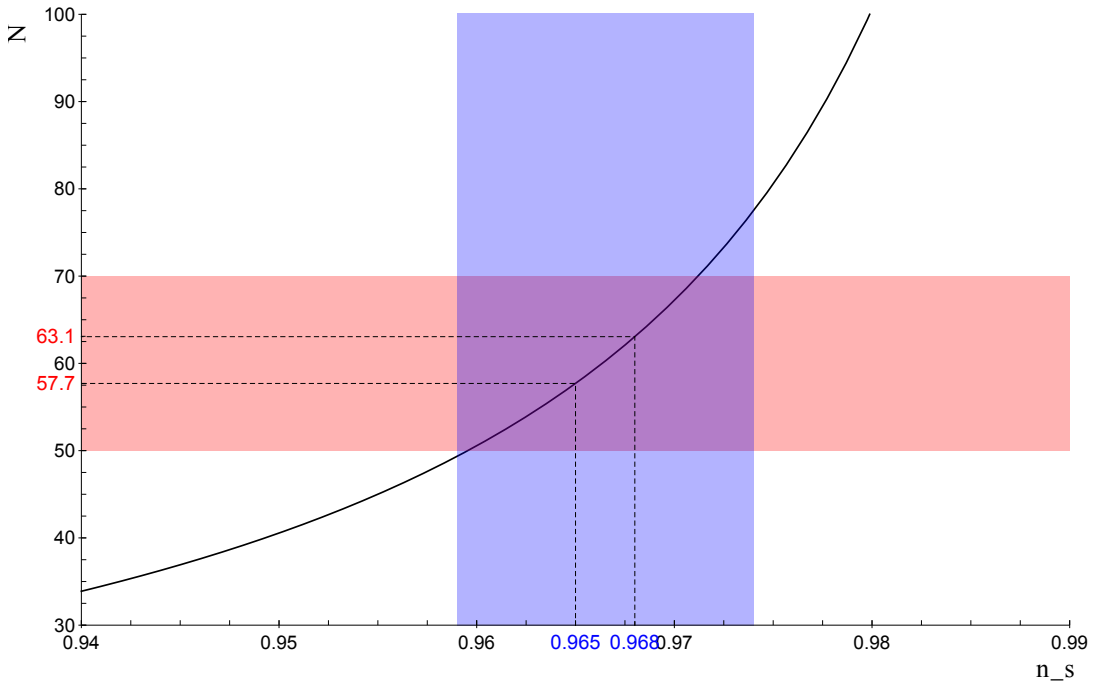

Figure 3.3: N as a function of n_s from the potential 3.98. The vertical blue shaded area corresponds to the 68% CL interval for n_s around the central values $n_\mathrm{s} = 0.965$ and $n_\mathrm{s} = 0.968$, while the horizontal red shaded area shows the relevant interval for N. The black dashed lines highlight the central values for n_s and the corresponding values for N.

and

$$\mathcal{D} \simeq 3.2 \times 10^{-11}\ M_{\mathrm{Pl}}^4 \qquad \Leftrightarrow \qquad \tilde{\mathcal{D}} \simeq 3.2 \times 10^{-11}\ M_{\mathrm{Pl}}^2\ , \tag{3.102b}$$

showing that every constraint related to the slow-roll conditions is satisfied: $N \sim 60$, $\epsilon \ll 1$, $\eta \ll 1$, $\xi \ll 1$, while the WMAP constraint on V/ϵ gives constraints on the size of the potential.

The constant A and the value of the field $\tilde{\varphi}$ are not constrained at all so far except in that their combination $A\, e^{-B\tilde{\varphi}}$ must satisfy

$$\tilde{\mathcal{D}} \gg A\, e^{-B\tilde{\varphi}}\ , \tag{3.103}$$

in order to ensure slow-roll. From Eq. (3.100a), we know

$$A\, e^{-B\tilde{\varphi}} = \frac{\tilde{\mathcal{D}}}{B^2 N} \simeq \frac{\tilde{\mathcal{D}}}{1.5 \times 10^2} \ll \tilde{\mathcal{D}}\ , \tag{3.104}$$

which confirms the consistency of our model.

Note that this result is not very sensitive to the value of B, especially to larger

B. Indeed, even with B a hundred times larger, the curve is shifted down by less than 1 unit meaning that N decreases by 1 e-fold. Lowering B would modify a bit more our results but not much either, since with a B twice as small, N increases by less than 2 e-folds while with a B four times smaller, N increases by less than 8 e-folds (reaching about 70 for $n_{\rm s} = 0.968$).

At this point it is worth making a few important remarks. The considerations leading to Eq. (3.98) indicate the possibility of inflationary scenarios for the redefined metric $\tilde{g}_{\mu\nu}$ through Eq. (3.90). Nevertheless, for a slowly rolling condensate $\sigma(t)$, as required during inflation, the original metric is also inflationary, up to a time coordinate change. Indeed, let us denote by $\tilde{t}$ the cosmic time coordinate in the $\tilde{g}$-metric. The latter during inflation corresponds to a line-element of the form

$$\begin{aligned} {\rm d}\tilde{s}^2 &= {\rm d}\bar{t}^2 - \tilde{a}(\bar{t})^2 h_{ij}(x^k)\,{\rm d}x^i{\rm d}x^j \\ &= (1+\sigma(t))\,{\rm d}t^2 - (1+\sigma(t))\,a(t)^2 h_{ij}(x^k)\,{\rm d}x^i{\rm d}x^j \ , \end{aligned} \tag{3.105}$$

in a standard FLRW notation, with $\sigma \gg 1$, and where

$${\rm d}\tilde{t} = \sqrt{(1+\sigma(t))}\,{\rm d}t \simeq \sqrt{\sigma}\,{\rm d}t \ , \qquad \tilde{a}(\tilde{t}) = \sqrt{(1+\sigma(t))}\,a(t) \simeq \sqrt{\sigma}\,a(t) \ . \tag{3.106}$$

For a slowly moving σ field (almost constant), the two metrics differ by an overal scale factor, and the corresponding Hubble parameters are related as follows (quantities with a tilde pertain to the metric (3.90) and the coordinates (3.106))

$$\tilde{H} \equiv \frac{1}{\tilde{a}(\tilde{t})}\frac{\rm d}{{\rm d}\tilde{t}}\tilde{a}(\tilde{t}) = \frac{1}{\sqrt{\sigma}}\left(\frac{\dot{\sigma}}{\sigma} + \frac{\dot{a}}{a}\right) \simeq \frac{1}{\sqrt{\sigma}}\,H \ , \tag{3.107}$$

since during inflation $\dot{\sigma}/\sigma \ll 1$ and can be neglected in front of the $H = \dot{a}/a$ term (the overdot denotes time derivatives with respect to the cosmic time pertaining to the initial metric $g_{\mu\nu}$).

Taking into account (3.89) as a concrete example, for $M_{\rm s} \ll H_I$, we can estimate

$$\tilde{H} \equiv H_I \sim \frac{1}{\sqrt{8\sqrt{3}\,g_{\rm s0}}}\,\frac{M_{\rm s}}{H_{\rm I}}\,H \ , \tag{3.108}$$

from which it follows that the inflationary scale of the original metric is much higher than $H_{\rm I}$, of order

$$H \sim \sqrt{8\sqrt{3}\,g_{\rm s0}}\,\frac{H_{\rm I}^2}{M_{\rm s}} \gg H_I \ , \qquad M_{\rm s} \ll H_{\rm I} \ . \tag{3.109}$$

The reader should bear in mind that above we matched the cosmological observations [6] on inflation with predictions made by the conformal rescaled metric $\tilde{g}_{\mu\nu}$ (3.90), and therefore it is the scale $\tilde{H}$ that we call the "physical" Hubble scale $H_{\rm I} \sim 10^{-5}\, M_{\rm Pl}$ used in observations [6]. For a smooth connection with the galaxy data in this case we should use the action (3.92) with the metric (3.90), after the inflaton decays, that is we should couple it to matter and radiation. At the end of inflation the condensate of D-particles vanishes $\sigma \to 0$ and the two metrics coincide. At the radiation era that succeeds the exit from inflation, the condensate field σ is replaced by the weak field $\widetilde{F}_{\mu\nu}\widetilde{F}^{\mu\nu}$ and the action (3.16) describes now the dynamics. Note that in the discussion in Section 3.3, the possibility of large brane tension Eq. (3.87), which replaces Eq. (3.44), has been taken into account as shown in Eqs. (3.45) and (3.47).[20]

Another important aspect is that the condensate $\sigma(t)$ defined in Eq. (3.84), upon the redefinition of the metric (3.90), can be expressed in terms of $\tilde{g}_{\mu\nu}$ as follows

$$\sigma = (1+\sigma)^2\tilde{\sigma} \tag{3.110}$$

where $\tilde{\sigma}$ is the condensate $\langle\langle F_{\mu\nu}F_{\alpha\beta}\,\tilde{g}^{\mu\alpha}\,\tilde{g}^{\nu\beta}\rangle\rangle$, which, because it is a scalar, will assume the same value if one passes onto the coordinates (3.106). For large $\sigma \gg 1$ one obtains from (3.110) $\sigma \sim 1/\tilde{\sigma} \gg 1$. In terms of the $\tilde{\sigma}$ field, the canonically normalised inflaton field defined in Eq. (3.91) reads $\varphi \sim -\ln(\tilde{\sigma})$.

Finally, before closing this section, it is important to comment on the order of magnitude of the statistical parameter $\sigma_0^2 \equiv \sigma_{0,\rm infl}^2$ (3.66) during the large-condensate inflationary era with $M_{\rm s} \ll M_{\rm Pl} = \kappa_{\rm eff}^{-1}$. As we have already mentioned, this parameter is assumed constant during inflation, due to the fact that during that epoch the brane world moves in a bulk region which is densely populated by D-particle defects, in such a way that there is a large incoming flux of D-particles from the bulk onto the brane compensating any potential dilution of their population on the brane due to the brane-universe expansion. From Eqs. (3.62), (3.89) we estimate

$$\frac{\sigma_{0,\rm infl}^2}{\sigma_{\rm slow-roll}} \simeq \frac{g_{\rm s0}}{8\pi^2\sqrt{3}}\,, \tag{3.111}$$

[20]Otherwise, it would have quantitative consequences in the allowed range of the β parameter and hence in the density of D-particles relevant in late eras. Therefore, one would need to consider the parameter $\mathcal{J}\,|\beta|$ to match the DM in a galaxy — see for instance Eqs. (3.41) or (3.47) — thus leading to much smaller upper bounds for the density of D-particles in order for them to mimic DM through their recoil velocity field fluctuations.

where $\sigma_{\rm slow-roll} = 8\sqrt{3}\, g_{s0}\, (H_I/M_s)^2$. For $M_s = \mathcal{O}(10^4)$ GeV, we obtain $\sigma^2_{0,\rm infl} = \mathcal{O}(10^{16})$.[21]

3.4.4 Estimates of the age of the D-material universe

Before closing this section we would like to make some crude estimates of the age of the D-material universe t_0 in the case where inflation is driven by strong condensates of D-particle recoil velocities. It goes without saying that, without detailed microscopic models it is not possible to find a precise connection of the value of $\sigma^2_0 \simeq |\beta|$ during the galactic era with $\sigma^2_{0,\rm infl}$, which would allow for a precise estimate of t_0. Indeed, this would require knowledge of the bulk distribution of D-particles from the moment of the exit from inflation until the current era. In our complicated dynamical system, the equation of state of the pertinent cosmic fluid is not a constant and depends on many factors, including the density profile of the bulk and brane D-particles at any given era. Nevertheless, one can make some simplifying assumptions, which allow us to make some estimates of the age of the D-material universe in a phenomenological context.

To this end, we first recall that in the case of complete dominance of the classical recoil velocity condensates, based on statistical populations of D-particles whose dynamics is governed by a Born-Infeld action of the vector field alone, the equation of state of the recoil velocity fluid would be $w = -1/3$ [61]. This is the limiting case (from above) for which acceleration of the universe occurs. From the corresponding Friedmann equation, that would lead to a linearly expanding universe with the cosmic time, $a(t) \sim t$, which is not physical. However, the D-material universe's Lagrangian is much more complicated than a simple Born-Infeld fluid. The presence of matter as well as non-minimal couplings of the Born-Infeld factors with spacetime curvature (cf. Eq. (3.1)), alter the situation drastically and one expects, as already mentioned, a time (redshift) dependent equation of state for the total fluid, D-particles and matter strings, $w_{\rm tot}(z)$, whose form is currently difficult to estimate without detailed knowledge of the density profile of the bulk D-particles.

Matter domination era in our case includes contributions to the stress tensor coming from the recoil velocities of the D-particles bound on the brane world, as a consequence of their interactions with string matter. Matter dominance, therefore, does not exclude the possibility that the contributions of the recoil velocity fluid to the total energy density of the universe are of the same order of magnitude as the

[21] Notice that for large condensates the restriction (3.72) does not apply.

corresponding matter energy density during the galaxy formation era, that is with redshifts $z \gtrsim 1$, which corresponds to the upper bound in the inequality (3.47). On the other hand, for the current era, i.e. redshifts $z \lesssim 10^{-2}$, current data indicate a cosmological constant dominance, $w_{\rm tot}(z \simeq 0) = -1$. If we make the (considerable) simplification that there is a depletion of bulk D-particles from the exit of inflation era until the galaxy formation era, and if we assume a *simple* power scaling of the energy density of the total fluid $\rho_{\rm total}$ with the scale factor of the universe as

$$\rho_{\rm total} \sim a^{-3(1+w_{\rm tot})} \tag{3.112}$$

with $w_{\rm tot}$ approximately constant, then, from the Friedmann equation, we would obtain the following time dependence of the scale factor on the cosmic time

$$a(t)_{\rm m\,+\,D-part.\ rec.\ fl.} \sim t^{\frac{2}{3(1+w_{\rm tot})}} \ . \tag{3.113}$$

Then, assuming that Eq. (3.34) is valid from the galactic era all the way back to the exit from inflation epoch, we obtain that, for a given moment t in the history of the D-material universe, the statistical variance of the D-particle recoil velocities behaves as

$$\langle\langle u_i u^i \rangle\rangle \equiv \sigma_0^2(t) = \frac{|\beta|}{\left({}^{a(t)}\!/_{a_0}\right)^3} \tag{3.114}$$

where $a_0 \equiv a(t_0)$, with t_0 the universe age, is today's value of the scale factor, which is re-instated here to be linked with and allow the estimation of t_0.

At the exit from inflation, at cosmic times $t = t_{\rm infl}$, the variance is assumed to have the value $\sigma^2_{0,{\rm infl}}$. Since we are interested in an order of magnitude estimate of the universe age, we are at liberty to ignore the short duration of the late de Sitter accelerating phase of the universe, and assume the scaling (3.112) for the statistical fluctuations of the recoil velocities from the inflationary era until practically today $t = t_0$. Then, from Eq. (3.114), we obtain

$$\sigma^2_{0,{\rm infl}}\, a(t_{\rm infl})^3 \sim |\beta|\, a_0^3 \ . \tag{3.115}$$

Using the upper and lower bounds for $|\beta|$ given in Eqs. (3.47) and (3.49), so that the recoil velocity fluid either mimics the DM in galaxies (upper bound) or at least is responsible for inducing growth of structures in the universe (lower bound), we

obtain the following allowed range for the D-material universe age

$$\left(10^{60}\,\frac{g_{s0}}{\pi}\,\frac{H_{\rm I}}{M_{\rm Pl}}\,\mathcal{H}\right)^{1+w_{\rm tot}} \lesssim \frac{t_0}{t_{\rm infl}} \lesssim \left(10^{61.5}\,\frac{g_{s0}}{\pi}\,\frac{H_{\rm I}}{M_{\rm Pl}}\right)^{1+w_{\rm tot}}$$
$$\Rightarrow \quad 10^{54.5\,(1+w_{\rm tot})} \lesssim \frac{t_0}{t_{\rm infl}} \lesssim 10^{56\,(1+w_{\rm tot})}\ , \tag{3.116}$$

where in the last line we used that $H_{\rm I} \simeq 10^{-5} M_{\rm Pl}$, $g_{s0} \sim 0.8$, $\pi \sim 10^{0.5}$ and $\mathcal{H} = \mathcal{O}(1)$. Using that in conventional cosmology one estimates that exit from inflation occurs at times $t_{\rm infl} \sim 10^{12}\, t_{\rm Pl}$, where $t_{\rm Pl}$ is the Planck time (10^{-45} s), we observe that the age of the universe in units of Planck time is estimated to be

$$10^{66.5\,(1+w_{\rm tot})} \lesssim \frac{t_0}{t_{\rm Pl}} \lesssim 10^{68\,(1+w_{\rm tot})}\ . \tag{3.117}$$

If we insist that the age of the D-material universe t_0 is in agreement with the corresponding ΛCDM model estimates from Planck data [6], i.e. $t_0 \sim 10^{60}\, t_{\rm Pl}$, then in case the upper bound (3.47) is satisfied — that is when the D-particle recoil velocity fluid mimics DM in the galaxies, as far as lensing is concerned — we obtain for the equation of state $w_{\rm tot} = -0.095$. On the other hand, for the lower bound case (3.49) to be satisfied — that is when the fluid of recoiling D-particles induces growth of structures in the universe, but falls short of reproducing the lensing effects of DM in galaxies — one obtains $w_{\rm tot} = -0.115$.

These values are not far from the pure Born-Infeld equation of state $w = -1/3$ for classical condensates [61]. However, given that $w = -1/3$ is the maximum value for inducing acceleration in an Einstein universe, that satisfies the positive energy conditions, i.e. $w > -1$, we observe that in the matter dominated era the D-material universe decelerates, as it should be. As discussed in Refs. [61, 62], quantum fluctuations of the recoil velocity condensates that satisfy Born-Infeld dynamics, when they are dominant, can lead to an accelerating almost de Sitter phase, with an equation of state near to $p \simeq -\rho$. To match with the current universe phenomenology, according to which the universe today appears to be in a de Sitter-like phase, one is led to the conclusion that quantum fluctuations of the weak condensates, that characterise the current era, dominate over the classical statistical effects. This is plausible in the low temperatures of the current universe.

3.5 Gravitational radiation

The Gravitational Wave (GW) signals — GW150914 and GW151226 — detected by Advanced LIGO (aLIGO) [4], based on the effects of the distortion of spacetime on the arms of the 4-km-wide interferometric devices, opened a new window on the universe and thus on fundamental laws governing it. The foreseen extended network of terrestrial interferometers combined with eLISA, the first GW observatory in space, may eventually detect even quantum aspects of gravity, or at least falsify quantum gravity models which entail Lorentz Invariance Violation (LIV) for which there are already stringent restrictions from various sources.

The D-material universe [58, 60] is one microscopic LIV model which evades such constraints. The interaction, for instance of a photon with the population of such D-particles, crossing or being confined on our brane-world, leads to time delays proportional to the energy of the incident photon. This effectively yields a linear modification of the corresponding dispersion relation, suppressed though, not by the Planck scale but by an effective mass scale inversely proportional to the linear density $N_{\rm D}^{\rm lin}(z)$ of the defects encountered in the path of the photon [65]

$$E = p\left(1 - \frac{p}{M_{\rm QG}}\right) \quad \text{where} \quad M_{\rm QG} = \frac{M_{\rm Pl}}{N_{\rm D}^{\rm lin}(z)} \,, \tag{3.118}$$

$M_{\rm Pl} = 2.4 \times 10^{18}$ GeV is the four-dimensional (reduced) Planck scale and z is the cosmic redshift. Notice that the dispersion relation (3.118) is always *subluminal* for specifically stringy reasons. The bound $M_{\rm QG} \geq 1.22\, M_{\rm Pl}$ on the Quantum Gravity (QG) scale can be thus interpreted as an upper bound on the linear density of defects $N_{\rm D}^{\rm lin}(z)$, which, in an inhomogeneous D-material universe, depends in general on the redshift.

In the presence of D-particle ensembles, both the pattern of emission and the propagation of GW will in principle be modified. The modification of the GW emission pattern due to the presence of D-particles in the region of the collapsing black holes may be expected to be negligible in the sense that the ensemble of massive D-particles will behave as matter in the presence of the spiralling black hole system, and the gravitational pull they will exert on the black holes will be very weak to affect the formation of the giant black hole and the subsequent emission of GW.

However, this is not the case for the velocity of propagation of gravitons in the medium, far away from the black hole source, which will be affected in two ways,

discussed in the following. Firstly, the propagation speed of GW will be reduced as compared to the massless case (*subluminal* propagation), due to the development of a mass, as a result of the (gravitational) interaction with the recoil velocity condensate field. Secondly, the presence of Dark Energy (DE) density in the universe, either as a result of the recoil kinetic energy of the D-particles or due to additional Dark Matter (DM) species in the universe (that may co-exist with the D-particles), will also induce a *superluminal* contribution to the group velocity of gravitons. Current observations, including GW interferometry, can provide restrictions to such effects in a way that will be the topic of our discussion here.

In the following, we first discuss the effect of the induced graviton mass due to the D-matter "medium", then we look at the refractive index effects as a result of the finite energy density of D-particles and other species of DM in the universe, and finally we study the phenomenology of these effects using results from the recent aLIGO GW detection and observations involving Ultra High Energy Cosmic Rays (UHECR). Our analysis leads to constraints on the parameters of the model, in particular lowering significantly the maximal allowed magnitude of the string scale itself, under some natural assumptions.

3.5.1 Induced graviton mass

One of the most important rôle of the D-matter recoil field condensate arises from its effects on the graviton equation of motion where, along with a modification in the gravitational constant in the string frame description, it contributes to a mass term for the graviton, leading to an additional polarisation mode. We shall discuss this issue next, while later on in this section we shall discuss the implications of the current bounds on the graviton mass in terms of the D-particle density and mass $M_{\rm s}/g_{\rm s}$ that enter the respective formulae.

Theoretical considerations

Our discussion starts with the effective (low-energy) action of Eq. (3.16), describing the interaction of the vector recoil velocity field A_μ with the graviton, in the Einstein frame, after considering $\phi = \phi_0$ and weak recoil fields $\sqrt{\alpha'}\, A_\mu \ll 1$ as appropriate

for late eras of the universe. Recall it yields

$$S^{\rm E}_{\rm eff\ 4D} = \int {\rm d}^4x\sqrt{-g}\left[-\Lambda_0 - \frac{1}{4}\langle \mathcal{G}_{\mu\nu}\,\mathcal{G}^{\mu\nu}\rangle + \left(\frac{1}{2}M_{\rm Pl}^2 + \frac{\alpha e^{-2\phi_0}\,\widetilde{F}_{\mu\nu}\widetilde{F}^{\mu\nu}}{4}\right)R \right.$$
$$\left. -\frac{1}{4}\,\widetilde{F}_{\mu\nu}\widetilde{F}^{\mu\nu} + \lambda\left(\tilde{A}_\mu\tilde{A}^\mu + \frac{1}{\alpha'}\mathcal{J}\right)\right] + S_{\rm m}\ , \qquad (3.119)$$

with, in particular

$$\mathcal{J} \equiv \frac{(2\pi\alpha')^2\,T_3\,e^{3\phi_0}}{g_{\rm s0}}\ , \quad \frac{1}{2}M_{\rm Pl}^2 \equiv \frac{\alpha\,T_3\,e^{\phi_0}}{g_{\rm s0}} + \frac{1}{\kappa_0^2}\ , \quad \Lambda_0 \equiv \frac{T_3\,e^{3\phi_0}}{g_{\rm s0}} + \frac{\tilde{\Lambda}\,e^{2\phi_0}}{\kappa_0^2}\ . \quad (3.120)$$

Moreover, the reader should recall that, under the appropriate assumptions, the dilaton equation of motion leads to $\Lambda_0 < 0$, which is an anti-de Sitter type cosmological constant and is thus not phenomenologically acceptable in the current era. To remedy this fact we assume that contributions from the bulk, such as $\frac{1}{4}\langle \mathcal{G}_{\mu\nu}\,\mathcal{G}^{\mu\nu}\rangle$, fine tunes the negative cosmological constant to an acceptably small positive one $\Lambda^{\rm vac}$ in the current era, as in Eq. (3.17b).

As mentioned in previous sections and discussed in detail in Appendix C (see also Ref. [61] and references therein), the vector field excitation describing the D-particle recoil presents two types of contributions:

(i) "Electric type", associated with the linear recoil momentum excitations, described by Eq. (C.9). They correspond, in our later era cosmological background, to vector field excitations $\tilde{A}_i$ with a target-spacetime field strength (after the impact) of the form

$$\widetilde{F}_{0i} = E_i = M_{\rm s}^2\,g_{ij}u^j\ , \qquad (3.121)$$

where E_i denotes the "electric" field, as given in Eq. (C.20).

(ii) "Magnetic type", associated with non-zero angular momentum of the recoiling D-particles, described by Eq. (C.12). These here imply a target-space field strength with spatial components

$$\widetilde{F}^{ij} = -\epsilon^{ijk}\,B_k = M_{\rm s}^2\epsilon^{ijk}g_{k\ell}\,u^\ell \ \Rightarrow\ B_k = M_{\rm s}^2\,g_{k\ell}\,u^\ell\ , \qquad (3.122)$$

where B_i denotes the "magnetic" field, as in Eq. (C.21).

Although in the gravitational lensing analysis of Section 3.3 we have ignored the angular momentum contributions, which as we show again, for instance in Eq. (3.127) or below Eq. (3.130), would not change the order of magnitude of our

conclusions, nevertheless for the purpose of our present analysis, which is to study GW propagation in the D-material universe in the (low-temperature, compared to the inflationary epoch) galactic era, such contributions shall play an important rôle for the stability of the vacuum. Recall for the (unstable) inflationary high-temperature phase, such contributions are negligible as found in Section 3.4 and thus the conclusions obtained above remain valid.

The graviton equation of motion obtained from the action (3.119) reads

$$\left(R_{\mu\nu} - \frac{g_{\mu\nu}}{2}R\right)\left[\frac{1}{2}M_{\rm Pl}^2 + \frac{\alpha e^{-2\phi_0}\,\widetilde{F}^2}{4}\right] = \frac{1}{2}\,T^{\rm rec}_{\mu\nu} - \frac{1}{2}\,g_{\mu\nu}\,\Lambda^{\rm vac} + \frac{1}{2}\,T^{\rm m}_{\mu\nu}\ , \qquad (3.123)$$

where from now on we use the short-hand notation $\widetilde{F}^2 = \widetilde{F}_{\mu\nu}\widetilde{F}^{\mu\nu}$. Note that $T^{\rm m}_{\mu\nu}$ denotes the stress tensor of conventional matter, including DM other than D-particles, and $T^{\rm rec}_{\mu\nu}$ is the recoil velocity contribution

$$T^{\rm rec}_{\mu\nu} = \widetilde{F}_{\mu\alpha}\,\widetilde{F}_{\nu}^{\ \alpha} - g_{\mu\nu}\,\frac{\widetilde{F}^2}{4}\ . \qquad (3.124)$$

The latter resembles of course the corresponding stress tensor of electrodynamics, but here the vector field $\tilde{A}_\mu$ is the recoil velocity field, which satisfies the constraint[22]

$$\tilde{A}_\alpha\tilde{A}^\alpha + \frac{1}{\alpha'}\mathcal{J} = 0\ .$$

A few remarks are in order here. Recall the dynamics of the vector recoil field $\tilde{A}_\mu$ in the action (3.119) is much more complicated than the lowest-order weak-field expansion given above. Actually, as discussed in Ref. [61], detailed string theory considerations imply that there is a Born-Infeld term, whose perturbative expansion yields the Maxwell kinetic term in the action (3.119). Such non-linear square root interactions may be responsible for the formation of condensates of the recoil velocity field, following the discussion in Ref. [62], which was adapted to the D-matter case so far. Therefore, as we assumed so far, $\widetilde{F}^2$ can condense, forming a scalar-like field,

[22]This is the only effect of the Lagrange multiplier field λ. Indeed, as the analysis of earlier sections and of Ref. [61] has demonstrated, any terms in the equations of motion involving the field λ become — upon its expression, via the equations of motion, in terms of the other fields in the Lagrangian — proportional to terms with gravitational-covariant derivatives acting on $\widetilde{F}$, which are negligible under our assumptions here.

which is at most time-dependent at cosmological scales. In addition, we have

$$\sigma_F(t) \equiv \langle \widetilde{F}^2 \rangle = \langle\!\langle \widetilde{F}^2 \rangle\!\rangle + \langle \widetilde{F}^2 \rangle_{\rm q} \ , \tag{3.125}$$

where $\langle\!\langle \ldots \rangle\!\rangle$ denote *classical* condensates, due to the statistical nature of the recoil velocity field in macroscopic D-particle populations in the universe, whose magnitude has been estimated above, while $\langle \ldots \rangle_{\rm q}$ denotes *quantum vacuum* effects [62], associated with the full Born-Infeld dynamics of the vector field, which cannot be computed at present. Since our point here is to study GW propagation from sources at redshifts $z < 10$, as is the situation characterising the recent discovery reported in Ref. [4], where $z \sim 0.09$, we consider short enough scales for which $\sigma_{\rm F}$ is practically constant, thus suppressing all its derivatives. Of course between cosmological eras the value of σ_F changes, in particular at the inflationary era, where strong condensates of the field σ_F are needed to drive inflation. For the matter-dominated era, of interest to us here, σ_F can be safely assumed to be weak.

In a mean-field approximation, one may first consider (3.123) with the stress tensor of the recoil field averaged in the sense of (3.125). If we consider *equal strength* electric and magnetic contributions, given respectively by (3.121) and (3.122), then we get

$$\sigma_F = \langle \widetilde{F}^2 \rangle = 2 \, \langle \widetilde{F}_{0i} \, \widetilde{F}_{0j} \rangle \, g^{00} g^{jk} + \langle \widetilde{F}_{ik} \, \widetilde{F}_{j\ell} \rangle \, g^{ij} g^{k\ell} \ . \tag{3.126}$$

For the classical statistical averages, we have

$$\begin{aligned} \langle\!\langle \widetilde{F}_{0i} \, \widetilde{F}_{0j} \, g^{ij} \rangle\!\rangle &= M_{\rm s}^4 \, \langle\!\langle u^i u^j g_{ij} \rangle\!\rangle > 0 \ , \\ \langle\!\langle \widetilde{F}_{0i} \, \widetilde{F}_{0j} \, g^{00} g^{ij} \rangle\!\rangle &= -M_{\rm s}^4 \, \langle\!\langle u^i u^j g_{ij} \rangle\!\rangle < 0 \ , \\ \langle\!\langle \widetilde{F}_{ik} \, \widetilde{F}_{j\ell} \, g^{ij} g^{k\ell} \rangle\!\rangle &= 2 M_{\rm s}^4 \, \langle\!\langle u^i u^j g_{ij} \rangle\!\rangle > 0 \ , \end{aligned} \tag{3.127}$$

and hence, on account of (3.126), we recover the equipartition theorem for the classical condensates of the vector field we are familiar with from ordinary electrodynamics, according to which the classical condensate *vanishes*, namely

$$\langle\!\langle \widetilde{F}^2 \rangle\!\rangle = 0 \ . \tag{3.128}$$

Note again that this is neither happening in the lensing framework, where the metric form implies subleading "magnetic" type field with respect to the "electric" one, nor in the inflation regime, where the cosmological principle (homogeneity and isotropy, hence a space-independent metric) implies no "magnetic" field. We thus have for

the appropriately averaged recoil stress tensor (3.124)

$$\langle\langle T^{\rm rec}_{\mu\nu}\rangle\rangle = \langle\langle \widetilde{F}_{\mu\alpha}\,\widetilde{F}_{\nu}{}^{\alpha}\rangle\rangle - \frac{1}{4}\,g_{\mu\nu}\,\langle\langle \widetilde{F}^2\rangle\rangle \ , \tag{3.129}$$

which, on account of Eqs. (3.127), (3.128), leads to

$$\langle\langle T^{\rm rec}_{00}\rangle\rangle \equiv \rho^{\rm class}_{\rm rec} = \frac{1}{2}\,\langle\langle E_i E^i\rangle\rangle + \frac{1}{2}\,\langle\langle B_i B^i\rangle\rangle = \frac{M_{\rm s}^4}{a^2(t)}\,\langle\langle u^i u^j \delta_{ij}\rangle\rangle \ , \tag{3.130}$$

The reader should notice that $\rho^{\rm class}_{\rm rec}$ is of the same order of magnitude as the recoil energy density considered Section 3.3, where only "electric" type E_i fields were considered (the result is larger by a factor of 2) and hence the lensing phenomenology conclusions remain unchanged whether these "magnetic" contributions are included or not.

The quantum fluctuations of the recoil velocity field are significant in the low temperature, galactic eras and for those we have, as dictated by the isometry structure of the FLRW cosmological spacetime [62]

$$\begin{aligned}
\langle \widetilde{F}_{0\alpha}\,\widetilde{F}_{0}{}^{\alpha}\rangle_{\rm q} &= \frac{\tilde{a}_t(t)}{4}\,g_{00} \ , \\
\langle \widetilde{F}_{i\alpha}\,\widetilde{F}_{j}{}^{\alpha}\rangle_{\rm q} &= \frac{\tilde{a}_{\rm s}(t)}{4}\,g_{ij} \ , \\
\sigma_F = \tilde{a} = \langle \widetilde{F}^2\rangle_{\rm q} &= \frac{1}{4}\,(\tilde{a}_{\rm t} + 3\,\tilde{a}_{\rm s}) > 0 \ ,
\end{aligned} \tag{3.131}$$

where $\tilde{a}_{\rm t} = \tilde{a}_{\rm t}(t)$ and $\tilde{a}_{\rm s} = \tilde{a}_{\rm s}(t)$. Note that we assume the positivity of the quantum condensate $\tilde{a}$, so as to be able to use such condensates as providers of zero-point (vacuum) energy of de Sitter type [61, 62]. The corresponding contribution to the recoil stress tensor is then

$$\begin{aligned}
\langle T^{\rm rec}_{00}\rangle_{\rm q} &= -\frac{1}{4}\,(\tilde{a} - \tilde{a}_{\rm t})\,g_{00} \ , \\
\langle T^{\rm rec}_{ij}\rangle_{\rm q} &= \frac{1}{12}\,(\tilde{a} - \tilde{a}_{\rm t})\,g_{ij} \ .
\end{aligned} \tag{3.132}$$

Another important point we wish to make is that in the current work we view any vacuum energy contribution, including those obtained from the bulk dynamics, as microscopic, due to the (quantum) dynamics of fields of the underlying string theory, and hence related to the stress tensor (right-hand-side of the (low energy) Einstein equations (3.123)), rather than geometric in origin thereby related to the left-hand-

side. In the latter case one would have to deal with (anti) de Sitter spacetimes, since those are the maximally symmetric spacetimes about which one expands, in which case the concepts of the graviton mass and the refractive index, upon which we shall concentrate here, become more complicated. For our purposes in the current analysis we take the point of view that there should be always a flat limit of the left-hand-side of the Einstein's equations, since the result of any cosmological constant type term is due to some sort of condensate (either bulk field or recoil D-particle fluctuations). This allows for a conventional definition of GW and massive graviton effects in the GW propagation, which will be the focus of our attention in what follows.

With the above in mind, one can then expand the metric around its (non-flat[23]) unperturbed cosmological value $g_{\mu\nu} = g^{(0)}_{\mu\nu} + h_{\mu\nu}$, where the background $g^{(0)}_{\mu\nu}$ takes into account the presence of a (space-independent, field-induced) "cosmological constant type" vacuum energy and $|h_{\mu\nu}| \ll 1$. Working, as appropriate for GW analysis, in the transverse traceless (TT) gauge, for which

$$\partial_\mu h^\mu{}_\nu = 0 \ , \quad h^\alpha{}_\alpha = 0 \ , \quad h_{\mu 0} = 0 \ , \tag{3.133}$$

the perturbed Einstein tensor becomes[24]

$$R_{\mu\nu} - \frac{1}{2}\, g_{\mu\nu} R = -\frac{1}{2}\, \partial^2 h_{\mu\nu} \ . \tag{3.134}$$

In the TT gauge, the only non-zero contributions to the recoil stress tensor to first order in the metric expansion (indicated by the superscript '(1)') are the spatial ones

$$\begin{aligned} \langle\!\langle \widetilde{F}_{i\alpha}\, \widetilde{F}_j^{\ \alpha} \rangle\!\rangle^{(1)} &= \langle\!\langle \widetilde{F}_{ik}\, \widetilde{F}_{j\ell}\, h^{k\ell} \rangle\!\rangle = M_{\rm s}^4\, \epsilon_{ikm} \epsilon_{j\ell n}\, \langle\!\langle u^m\, u^n \rangle\!\rangle\, h^{k\ell} \\ &= \delta_{j[i}\, \delta_{k]\ell}\, \frac{1}{3}\, \sigma_0^2\, h^{k\ell} = -\frac{1}{3}\, \sigma_0^2\, h_{ij} \ , \end{aligned} \tag{3.135}$$

where we used $h_{ij} = h_{ji}$ and $\sigma_0^2 = M_{\rm s}^4\, \langle\!\langle u^m u^n g^{(0)}_{mn} \rangle\!\rangle$, as well as [61]

$$M_{\rm s}^4\, \langle\!\langle u_m u_n \rangle\!\rangle = \frac{1}{3}\, \sigma_0^2\, g^{(0)}_{mn} \simeq \frac{1}{3}\, \sigma_0^2\, \delta_{mn} \ ,$$

[23]The expanding four-dimensional metric is not flat, even though the space slicing is flat.

[24]Our conventions are $(-,+,+,+)$ for the signature of the metric, and $R_{\mu\nu} \equiv R^\alpha{}_{\mu\nu\alpha} \equiv \partial_\alpha \Gamma^\alpha_{\nu\mu} - \partial_\nu \Gamma^\alpha_{\alpha\mu} + \Gamma^\alpha_{\alpha\beta}\Gamma^\beta_{\nu\mu} - \Gamma^\alpha_{\nu\beta}\Gamma^\beta_{\alpha\mu}$.

since for the galactic era $g^{(0)}_{mn} = a^2(t)\,\delta_{mn} \simeq \delta_{mn}$.

Recalling that the zeroth order (in the metric expansion) equation of motion is satisfied and taking into account Eqs. (3.124), (3.127), (3.128), (3.131) and (3.135), one obtains a first-order equation of motion for the spatial perturbations h_{ij} in the TT gauge (3.133) of the form

$$\partial^2 h_{ij} - \kappa^2_{\rm eff}\left[\frac{1}{3}\,M_{\rm s}^4\,\langle\!\langle u^m u^n\, g^{(0)}_{mn}\rangle\!\rangle - \frac{1}{12}\,(\tilde{a}-\tilde{a}_{\rm t}) + \Lambda^{\rm vac}\right] h_{ij} = 0\ ,$$
$$\text{where}\quad \frac{1}{\kappa^2_{\rm eff}} \equiv \frac{1}{\kappa_0^2} + \frac{\alpha\, T_3\, e^{\phi_0}}{g_{\rm s0}} + \frac{\alpha e^{-2\phi_0}\,\sigma_{\rm F}}{4}\ . \tag{3.136}$$

Assuming that the condensate σ_F is small and that $\Lambda^{\rm vac}$ is also small as compared to $M^4_{\rm Pl}$, then to leading order in σ_F and $\Lambda^{\rm vac}$, one may replace from now on $\kappa^2_{\rm eff}$ by $2\,M_{\rm Pl}^{-2}$. Hence, Eq. (3.136) is just the equation of motion of a *massive* graviton, with mass squared

$$m^2_{\rm G}(t) \simeq M_{\rm Pl}^{-2}\left[\frac{2}{3}\,M_{\rm s}^4\,\langle\!\langle u^m u^n \delta_{mn}\rangle\!\rangle - \frac{1}{6}\,(\tilde{a}-\tilde{a}_{\rm t}) + 2\rho_{\Lambda^{\rm vac}}\right]\ , \tag{3.137}$$

where $\rho_{\Lambda^{\rm vac}} \equiv \Lambda^{\rm vac}$.[25]

One can remark that should we explicitly write perturbations for the vector field, of the form $A_\mu + \delta A_\mu$ with $|\delta A_\mu| \ll |A_\mu|$, or similarly $u_\mu + \delta u_\mu$ with $|\delta u_\mu| \ll |u_\mu|$, the first additional term in Eq. (3.136) would be of the form $\langle\!\langle u^m\,\delta u_m\rangle\!\rangle = 0$ since $\langle\!\langle u_\mu\rangle\!\rangle = 0$ as in Eq. (3.34) (and u and δu are completely uncorrelated), while the next one would read $\langle\!\langle \delta u^m\,\delta u_m\rangle\!\rangle$ which is subleading and can thus safely be ignored. There is therefore no doubt concerning the physical interpretation of Eq. (3.136) as a true graviton mass.

The mass is real, provided the right-hand-side of Eq. (3.137) is positive, otherwise the graviton would appear tachyonic.[26] Fortunately, this can be easily guaranteed by assuming either small quantum corrections compared to the statistical classical terms or that the condensates $\tilde{a}$ and $\tilde{a}_{\rm t}$ are both positive. The latter assumption is in line with attempts [62], in the context of Born-Infeld electrodynamics, to associate such quantum condensates with positive (de Sitter type) contributions to the vacuum energy. We shall thus make this assumption in what follows.

[25]Note indeed that our $\Lambda^{\rm vac}$ is of dimension of an energy density, as one can see in the action (3.119) or in the definition given below in Eq. (3.120).

[26]Causality is defined with respect to the front velocity so is not in jeopardy. In addition, our theory is embedded in a UV complete, causally valid theory.

In this latter respect, from Eqs. (3.127) and (3.132), we observe that the recoil energy density, including quantum condensate contributions, reads

$$\rho_{\rm rec}^{\rm full} = M_{\rm s}^4 \left\langle\!\left\langle u_i u_j \delta^{ij} \right\rangle\!\right\rangle + \frac{\tilde{a} - \tilde{a}_{\rm t}}{4} > 0 \ . \tag{3.138}$$

We now impose the requirement that the upper bound of $\rho_{\rm rec}^{\rm full}$ should *not* exceed the matter energy density $\rho_{\rm m}^{\Lambda{\rm CDM}}$ of the ΛCDM model. For the value of $\rho_{\rm m}^{\Lambda{\rm CDM}}$ we take here the benchmark point [6]

$$\rho_{\rm m}^{\Lambda{\rm CDM}} = 0.3\,\rho_{\rm c}^0 = 0.9\,H_0^2\,M_{\rm Pl}^2 = 9 \times 10^{-121}\ M_{\rm Pl}^4 \ , \tag{3.139}$$

with $\rho_{\rm c}^0$ the current-era critical density and $H_0 \sim 10^{-60}\,M_{\rm Pl}$ the present-day Hubble rate. Hence we obtain

$$0 < \rho_{\rm m} \equiv \rho_{\rm rec}^{\rm full} + \rho_{\rm DM+b} \sim \rho_{\rm m}^{\Lambda{\rm CDM}} \ , \tag{3.140}$$

and

$$\frac{M_{\rm s}^4}{a^2(t)} \left\langle\!\left\langle u_i u_j \delta^{ij} \right\rangle\!\right\rangle + \frac{\tilde{a} - \tilde{a}_{\rm t}}{4} \lesssim \rho_{\rm m}^{\Lambda{\rm CDM}} \ , \tag{3.141}$$

where $\rho_{\rm m}$ is the total matter energy density of the universe, including D-matter as well as (conventional) DM and baryonic matter (denoted together as $\rho_{\rm DM+b}$) contributions, which, according to Section 3.3, would imply that the recoil velocity contributions in the D-material universe would be compatible with the ΛCDM model.

If the upper bound in the inequality of (3.141) is saturated, then D-matter provides the dominant component of DM. The reader should recall though that the Born-Infeld form of the recoil velocity vector field $\tilde{A}_\mu$ studied so far in this work and in Ref. [61] provide a dark fluid which also contributes to DE, hence recoiling D-matter should be viewed as a *mixed* DE/DM model.

In this respect, the condition (3.140) also ensures that the total energy density of the D-material universe, including vacuum energy contributions

$$\rho_{\rm total} = \rho_{\rm m} + \rho_{\Lambda^{\rm vac}} \ , \tag{3.142}$$

is of the order dictated by the current data [6], i.e. close to the critical density. Thus, the conclusions of Section 3.3 that D-matter can play the rôle of DM in galactic lensing measurements remain valid, given that the order of magnitude of

the contributions to the recoil energy density does not change by the inclusion of "magnetic" field (3.122) components in the Born-Infeld fluid describing the recoil excitations of the D-particles.

Let us make a short remark on the order of magnitude of the allowed density of D-particles in the D-material universe [61]. We recall that in the galactic era, following Eq. (C.24), one has the following estimate for the statistical (classical) component of the recoil velocity condensate

$$\langle\langle u_i u_j \delta^{ij} \rangle\rangle \sim \frac{N_{\rm D}^{(0)}}{N_\gamma^{(0)}} \frac{\widetilde{\xi}_0^2 \, |\mathbf{p}_{\rm phys}|^2}{M_{\rm s}^2} \, g_{\rm s0}^2 \ , \tag{3.143}$$

with $\tilde{\xi}_0 < 1$ an order $\mathcal{O}(1)$ parameter, that describes the momentum transfer during the scattering of a D-particle with an open string representing radiation (which is assumed to be the dominant species with which the D-particles interact). The quantity $\mathbf{p}_{\rm phys}$ is the "physical" average 3-momentum of a photon as observed by a comoving cosmological observer in the FLRW universe, assumed to be a thermalised CMB photon at $T = 2.7$ K, hence $|\mathbf{p}_{\rm phys}| \simeq 3k_{\rm B}\, T \simeq 7.2 \times 10^{-4}$ eV $\simeq 3 \times 10^{-31}\, M_{\rm Pl}$. By $N_{\rm D}^{(0)}$ and $N_\gamma^{(0)}$ we denote the (dimensionful) number densities of D-particles and photons, respectively, in the current era of the universe; note that $N_\gamma^{(0)} = 4 \times 10^{-97}\, M_{\rm Pl}^3$ [6]. In deriving (3.143) we assumed $N_\gamma^{(0)} \gg N_{\rm D}^{(0)}$, so that $N_{\rm D}^{(0)}/(N_\gamma^{(0)} + N_{\rm D}^{(0)}) \simeq N_{\rm D}^{(0)}/N_\gamma^{(0)}$ is the probability of interaction of D-particles with the CMB photons that constitute the most dominant species for the recoil of D-particles in the medium.

We also note that the analysis of Ref. [61] and of Section 3.3 implied a lower limit to the density of D-particles, as a result of the requirement that the D-matter can enhance the growth of large-scale structure in the universe. In fact, if we ignore (assuming them as subleading) the quantum corrections in Eq. (3.138), then, in view of the inequality (3.141), we get the following bounds on the statistical condensate $\langle\langle u_i u_j \delta^{ij} \rangle\rangle$ defined in (3.143)

$$10^{-123}\, \frac{M_{\rm Pl}^2}{M_{\rm s}^2} \lesssim \langle\langle u_i u_j \, \delta^{ij} \rangle\rangle \lesssim 10^{-120}\, \frac{M_{\rm Pl}^2}{M_{\rm s}^2} \ , \tag{3.144}$$

which lead to the following bounds on the D-particle density $N_{\rm D}^{(0)}$

$$10^{-123}\, \frac{M_{\rm Pl}^2}{g_{\rm s0}^2\, \widetilde{\xi}_0^2 \, |\mathbf{p}_{\rm phys}|^2} \lesssim \frac{N_{\rm D}^{(0)}}{N_\gamma^{(0)}} \lesssim 10^{-120}\, \frac{M_{\rm Pl}^2}{g_{\rm s0}^2\, \widetilde{\xi}_0^2 \, |\mathbf{p}_{\rm phys}|^2} \ , \tag{3.145}$$

which turn out to be independent of $M_{\rm s}$

$$6\times 10^{-159}\,\widetilde{\xi}_0^{-2}\,M_{\rm Pl}^3 \lesssim N_{\rm D}^{(0)} \lesssim 6\times 10^{-156}\,\widetilde{\xi}_0^{-2}\,M_{\rm Pl}^3\,. \tag{3.146}$$

These estimates are affected if the quantum fluctuations $\tilde{a}$, $\tilde{a}_t$ to the condensate σ_F are included. Unfortunately, lacking a microscopic theory of stringy D-particles we cannot estimate the magnitude of the quantum condensates $\tilde{a}$, $\tilde{a}_t$ entering the mass (3.137) and hence we can only discuss below some phenomenological bounds coming from experimental constraints on the graviton mass. At any rate for the galactic eras of relevance to us today we assume that the quantum fluctuations are of the same order as the statistical condensate.

Phenomenological constraints on induced graviton mass and implications for the D-material universe

To discuss effects of matter in the GW propagation, let us first remark that the relativistic dispersion formula for *massive* gravitons $\omega^2 = k^2 + m_{\rm G}^2$ (in natural units), leads to the subluminal group velocity (denoted by a subscript 'g')

$$v_{\rm g}^{\rm mass} = \frac{\partial\omega}{\partial k} = \frac{k}{\omega} = \frac{1}{v_{\rm p}^{\rm mass}} = n_{\rm G}^{\rm mass} \simeq 1 - \frac{m_{\rm G}^2}{2\,\omega^2}\,, \tag{3.147}$$

assuming $m_{\rm G} \ll \omega$, where $n_{\rm G}^{\rm mass}$ denotes the index of refraction of GW due to the graviton mass and $v_{\rm p}^{\rm mass}$ is the corresponding phase velocity (which is larger than unity, without conflict with causality, as the phase of the wave does not carry out any physical information). For two gravitons with frequencies ω and ω', the difference in group velocities is thus

$$\Delta v_{\rm g}^{\rm mass} = \frac{m_{\rm G}^2}{2}\left|\frac{1}{\omega^2} - \frac{1}{\omega'^2}\right|\,. \tag{3.148}$$

The induced dispersion in the GW, taking into account the cosmic expansion (redshift z) of a standard ΛCDM universe, leads to differences in the observation times of GW components of two different (low) frequencies ω and ω', emitted with a time difference $\Delta t_{\rm e}$ at the source [74]

$$\Delta t_{\rm o}^{\rm mass} = (1+z)\left[\Delta t_{\rm e} + (1+z)\,\mathcal{D}\,\frac{m_{\rm G}^2}{2}\left(\frac{1}{\omega^2} - \frac{1}{\omega'^2}\right)\right]\,, \tag{3.149a}$$

where

$$\mathcal{D} = \int_{z_o}^{z_e} \mathrm{d}\tilde{z}\, \frac{1}{H_0} \frac{(1+\tilde{z})^{-2}}{\sqrt{\Omega_m (1+\tilde{z})^3 + \Omega_\Lambda}} \ , \tag{3.149b}$$

with $D \equiv (1+z)\,\mathcal{D} = (1+z)\int_{t_e}^{t_o} a(t)\,\mathrm{d}t$ the proper distance, $a(t)$ the scale factor (in units where today $a_0 = a(t_o) = 1$) and where the subscipt o (e) pertains to observation (emission) quantities. In the standard ΛCDM fiducial cosmology [6], which we assume here again, we have $(\Omega_m, \Omega_\Lambda, \Omega_k) = (0.3, 0.7, 0)$.

Assuming for simplicity that the two gravitons where emitted simultaneously ($\Delta t_e \simeq 0$) one may get from (3.149a) a lower bound for the graviton mass to be *detectable* by interferometric GW devices with time-difference sensitivity Δt_s and $\omega' = \xi\,\omega$, given by

$$m_G^2 \ \geq\ \frac{\xi^2}{|1-\xi^2|}\, \frac{2\,\Delta t_s\, \omega^2}{(1+z)^2\,\mathcal{D}} \ . \tag{3.150}$$

The aLIGO measurements [4] achieve a very good time-frequency coverage for a broad range of signal morphologies by having the analysis repeated with seven frequency resolutions ranging from 1 Hz to 64 Hz in steps of powers of two, corresponding to time resolutions

$$\Delta t_s^{\mathrm{aLIGO}} = {}^1\!/_2\,(\Delta\omega_s^{\mathrm{aLIGO}})^{-1} \ \in [7.8\times10^{-3},\, 5\times10^{-1}]\ \mathrm{s}\ . \tag{3.151}$$

The clusters at different resolutions overlapping in time and frequency are then combined into a trigger that provides a multi-resolution representation of the excess power event recorded by the detectors. The minimum of the right-hand-side of the inequality (3.150) is obtained for the minimum value of the time resolution possible, that is in our case $\Delta t_s^{\mathrm{aLIGO}} \sim 7.8\times10^{-3}$ s, and the minimum value of ξ. Theoretically, if $\Delta\omega = 0$ could be measured experimentally, then the experiment would have infinite sensitivity to measure the graviton mass; however the minimum possible detectable frequency difference is the frequency resolution given by Eq. (3.151), which for the lower limit on Δt_s considered, leads to $\Delta\omega_s^{\mathrm{aLIGO}} \simeq 64$ Hz. With these values, for gravitons in the aLIGO frequency detection range[27] $\omega \simeq 100$ Hz $\simeq 4\times10^{-13}$ eV $\simeq 1.7\times10^{-40}\ M_{\mathrm{Pl}}$ emitted at a distance of 410 to 440 Mpc (corresponding to a redshift $z \simeq 0.09$ and hence $\mathcal{D} = 0.08\,H_0^{-1}$ [4], with $H_0 \simeq 10^{-60}\,M_{\mathrm{Pl}}$), we get

$$m_G \gtrsim 4.6\times10^{-50}\ M_{\mathrm{Pl}} \simeq 1.1\times10^{-22}\ \mathrm{eV}\ , \tag{3.152}$$

[27] While the two available detections allow us to constrain gravitons with frequencies $\omega \simeq 100$ Hz and $\omega \simeq 400$ Hz, we use here the former because it yields stronger bounds. In any case, considering the latter would only slightly change the numerics and not the qualitative conclusions of this work.

in order for the graviton mass to be observable by aLIGO. If the time and frequency resolution improves in future interferometric networks, leading to improvements of the signal to noise ratio $\omega\,\Delta t$ smaller than 1/10, value which characterises aLIGO [4], then the sensitivity to the graviton mass will increase.

Assuming a standard ΛCDM cosmology, the LIGO collaboration performed a detailed statistical analysis [4] during the observation of GW by the black-hole merger event GW150914, and found no significant signal up to Compton wavelengths of order $\lambda_{\rm q}^{\rm aLIGO} = h/m_{\rm G}^{\rm aLIGO} > 10^{13}$ km , implying an upper bound on the graviton mass

$$m_{\rm G}^{\rm aLIGO} < 1.2 \times 10^{-22}\ {\rm eV} \simeq 5.0 \times 10^{-50}\ M_{\rm Pl} \quad ({\rm aLIGO})\ , \tag{3.153}$$

which is in perfect agreement with the analytical bound (3.152). It can be used in our model to bound the condensate effects responsible for the induced graviton mass (3.137).

Before doing so, let us discuss first some additional effects of the D-particle "medium" on the propagation of GW in the D-material universe. As we shall argue in the next section, D-matter may induce a refractive index for graviton propagation, which leads to additional constraints, beyond the ones discussed due to the induced graviton mass.

3.5.2 Other effects on graviton propagation in the D-material universe

In addition to the mass induced effects, graviton propagation in the D-material universe (which includes also conventional DM components) is also affected by refractive index effects in the medium of D-particles. Given the low-frequency regime ($\omega \sim 100$ Hz) of GW of relevance to the LIGO observations, we expect (and shall verify explicitly below) that any stringy effect of the D-foam on the GW propagation — in general expected to increase with frequency, being proportional to some positive power of it — is negligible. This leaves the low-energy point-like field theory interactions of GW with the environment of matter (including DM) scatterers in the universe as the dominant source of induced refraction for low-frequencies.

Refractive index of gravitons

If GWs propagate in a medium of matter scatterers with density $\rho_{\rm m}$, then they will experience an induced refractive index, arising from the coordinate dependent

gravitational potential corrections to the Newtonian metric, as demonstrated long ago in Ref. [75]. To estimate such effects, it suffices to consider the approximate situation in which all matter is assumed to be concentrated in a "thin" spatial layer of thickness Δz, through which GW pass. Such layers modify the gravitational Newtonian potential felt by GW. To lowest order in ω, for *massless* gravitons, the index of refraction is larger than unity for $\rho_{\rm m} > 0$ and of the form

$$0 < n_{\rm G}^{\rm DM} - 1 \simeq \frac{2\pi\, G\, \rho_{\rm m}}{\omega^2} = \frac{\rho_{\rm m}}{4\, M_{\rm Pl}^2\, \omega^2} \ll 1 \ , \tag{3.154}$$

to linear order in the gravitational potential induced by matter. Here, $\rho_{\rm m}$ is the (4-dimensional) matter density (including DM and D-matter) (see Eq. (3.139)); we took that the (4-dimensional) gravitational constant is $8\pi\, G = M_{\rm Pl}^{-2}$ and the frequency range which we are interested in is $\omega \simeq 100$ Hz. In our case, the recoil contribution of the D-material universe is included in $\rho_{\rm m}$ which is then expressed as in Eq. (3.140).

Equation (3.154) implies that the phase velocity of GWs, $v_{\rm p}^{\rm DM} = 1/n$, is *subluminal* while the group velocity, $v_{\rm g}^{\rm DM}$, is *superluminal* for low ω. Indeed, to obtain the latter, one can use the derivative of the refractive index with respect to ω

$$\frac{1}{v_{\rm g}} = n + \omega\, \frac{{\rm d}n}{{\rm d}\omega} \ , \tag{3.155}$$

which, in the case of a medium with refractive index given by $n - 1 = \chi\omega^{-2}$ with χ a constant (as we have here), leads to

$$\frac{1}{v_{\rm g}} = n - 2\,\chi\omega^{-2} = 1 - \chi\,\omega^{-2} \quad \Rightarrow \quad v_{\rm g} \simeq 1 + \chi\omega^{-2} > 1 \ , \tag{3.156}$$

if $\chi\omega^{-2} \ll 1$. Hence, the *superluminal* group velocity for *massless* gravitons propagating in the DM and D-matter medium, yields here

$$v_{\rm g}^{\rm DM} \simeq 1 + \frac{\rho_{\rm m}}{4\, M_{\rm Pl}^2\, \omega^2} \simeq 1 + 10^{-41} \ , \tag{3.157}$$

where we considered again $\omega \simeq 1.7 \times 10^{-40}\ M_{\rm Pl}$.

This will lead to time differences in the arrival times of two gravitons with frequencies ω and ω', using Eq. (3.149a) and replacing the term $1/2\ m_{\rm G}^2$ by $\rho_{\rm m}/4\, M_{\rm Pl}^2$,

yielding

$$\Delta t_{\rm o}^{\rm DM} = -(1+z)\left[\Delta t_{\rm e} + (1+z)\,\mathcal{D}\,\frac{\rho_{\rm m}}{4\,M_{\rm Pl}^2}\left(\frac{1}{\omega^2}-\frac{1}{\omega'^2}\right)\right]\ , \tag{3.158}$$

with $(1+z)\,\mathcal{D}$ the proper distance from the GW source to the observer as in Eq. (3.149b). Note that the relative minus sign in Eq. (3.158), as compared to Eq. (3.149a), is due to the fact that $\Delta t_{\rm o}^{\rm DM}$ now denotes an advance rather than a delay due to the superluminal nature of the graviton group velocity.

Some comments are in order here regarding the superluminal nature of the group velocity (3.157). This was to be expected by the corresponding case for light propagation in a nontrivial vacuum. The graviton excitations find themselves in a *negative* (as compared to the trivial flat spacetime empty vacuum) gravitational energy density $\rho = -\rho_{\rm m} < 0$ environment (as a result of the attractive gravitational potential of the scatterers exerted on the graviton "particles"). Indeed, in such nontrivial vacuum with an energy density ρ, the group velocity of massless photons or gravitons, after taking into account vacuum polarisation effects, deviates from 1 by an amount $v_{\rm g} - 1 \propto -\rho = +\rho_{\rm m} > 0$. The (low-frequency) superluminal GW velocity is not in conflict with causality, since no physical (i.e. observer independent) information can be transmitted, given that the results pertain to a specific frame (Robertson Walker); moreover, it is the high-frequency limit that would be of relevance.

Refractive index of photons

It should be remarked at this point that (3.157) is similar in form to the refractive index of a photon in Quantum ElectroDynamics (QED) passing through a gas of charged particles, upon making the substitutions that yield the gravitational inverse square law from the corresponding Coulomb force law. More precisely, one must replace the charge density by the mass density of scatterers, set the charge per unit mass equal to 1 and replace the constant $1/4\pi\epsilon_0$ (where ϵ_0 is the permeability of the vacuum) by *the opposite of* the gravitational constant, namely $-G$. Note that this minus sign is crucial, in that it implies a subluminal group velocity for photons due to vacuum polarisation effects.

Thus, for photons in a flat spacetime, scattered of a density of free (non-interacting) charged particles, we may write the induced index of refraction (in natural

units where $\epsilon_0 = 1$) as[28]

$$n_\gamma^{\text{vac. pol.}} = 1 - \frac{q^2 e^2 \,\tilde{\rho}}{2\, m^2\, \omega^2} + \dots \tag{3.159}$$

with respectively $\tilde{\rho} > 0$, m and qe the mass density, mass and charge of the charged particles. The ... indicate subleading positive contributions coming from polarisability of the scatterer, which are either constant or proportional to positive powers of ω^2.

It should be noted that the expression (3.159) is generic and may incorporate milli-charged DM candidates that may exist in some models of particle physics but not in the majority of phenomenologically relevant ones. If we ignore such milli-charged DM candidates, then it becomes clear that the photon polarisation refractive index effects are subleading compared to the ones induced by the scattering of photons off (neutral) DM, which is the dominant candidate by several orders of magnitude. For instance, the dominant source of charged scatterers in the universe are protons, for which the corresponding cosmic energy density, that is the baryon density, is two orders of magnitude smaller than the DM density; the ΛCDM parameters today read $\Omega_{\rm b}/\Omega_{\rm DM} \simeq 2.2 \times 10^{-2}$ [6].

Hence, for all practical purposes, we only consider the effects on the photon refraction of the weak gravitational potential induced by the matter density $\rho_{\rm m}$, which, according to Ref. [75], are negligible. That is, to linear order in the weak gravitational potential at hand, the refractive index of photons with low-frequencies should be considered as that of the vacuum

$$n_\gamma^{\rm DM} \simeq 1 \ , \tag{3.160}$$

[28]This is obtained from the standard expression following the optical theorem, according to which the index of refraction is expressed in terms of the coherent forward scattering amplitude for a photon with polarisation λ as

$$n(\omega) = 1 + \frac{2\pi\, N}{k^2} f_{\lambda\lambda}(0) \ ,$$

where N is the number density of the scatterers, m denotes their mass, k is the wave-vector of light (equivalently k may be replaced by the frequency ω of photons assumed massless) and in the framework of a quantum field theory model

$$f_{\lambda\lambda}(0) = \frac{1}{8\pi m}\, \mathcal{M}_{\lambda\lambda}(k, k' \to k, k') \ ,$$

with the overall phase of the field theory amplitude $\mathcal{M}_{\lambda\lambda}$ fixed by the optical theorem, relating the total scattering cross section to the imaginary part of $f_{\lambda\lambda}(0)$.

upon ignoring vacuum polarisation effects. In this sense, at the low-frequency regime we are interested in, the photons behave as light-like particles.

Purely stringy effects of D-matter

We should remark at this point that, in the context of the D-particles foam, there are also terms in the refractive index that scale linearly with the frequency ω, which arise from the nontrivial interactions of the D-particles with the photons, viewed as open strings, that can be captured by the D-matter defects. Such terms stem from the stringy uncertainty principle, $\Delta t\,\Delta x \geq \alpha'$, and can be computed by considering string scattering amplitudes of open strings, representing the photons, off a D-particle background [65]. Taking into account the cosmic expansion, the induced delays of photons with observed frequencies ω due to these purely stringy effects are of the form

$$\Delta t_{\rm o}^{\rm D-foam} \simeq \int_0^z {\rm d}\tilde{z}\, C\, \frac{(N_{\rm D}^{(0)})^{1/3}}{M_{\rm s}^2}\, \frac{\omega}{H_0}\, \frac{(1+\tilde{z})}{\sqrt{\Omega_{\rm m}(1+\tilde{z})^3+\Omega_\Lambda}}\ , \tag{3.161}$$

where $C < 1$ is some fudge factor, entailing information on the momentum transfer of the incident string on a D-particle during the scattering, while $N_{\rm D}^{(0)}$ is again today's D-particle number three-volume density, which in principle should read $N_{\rm D}(z)$ and depend on the redshift for inhomogeneous D-particle foam models, but for our purposes here is considered z-independent for small $z < 10$ and thus is identified with today's value. Note that this effect is also valid, in a first approximation, for closed strings such as gravitons which, by hitting the D-particle, would open and attach to the brane and thus act in a similar way. This computation is thus applicable to the case of gravitons.

3.5.3 Gravity wave phenomenology of the D-material universe

In this section we shall compare the various refractive index effects (3.149a), (3.158) and (3.161) against the current GW phenomenology. The aim is to derive constraints on the string scale within the context of the D-material universe.

It can be readily seen that the stringy delays (3.161) are subleading (by at several orders of magnitude, thus negligible) compared to the ω^{-2} terms in (3.158), for the low frequencies we are interested in this work and the very small D-particle number

densities $N_{\rm D}^{(0)}$ (3.144) required so that the D-matter fluid acts as DM in the universe, as in Section 3.3. Indeed, one has

$$\Delta t_{\rm o}^{\rm D-foam} \lesssim 1.4 \times 10^{-1}\ M_{\rm Pl}^{-1} \ll |\Delta t_{\rm o}^{\rm DM}| = 8.4 \times 10^{14}\ M_{\rm Pl}^{-1}\ , \tag{3.162}$$

as can be seen from (3.158) for GW frequencies of order of 100 Hz and where we used Eq. (3.146) to get $N_{\rm D}^{(0)} \lesssim 6 \times 10^{-156}\, \widetilde{\xi}_0^{-2}\ M_{\rm Pl}^3 \lesssim 6 \times 10^{-154}\ M_{\rm Pl}^3$ with say $\widetilde{\xi}_0 \sim 0.1$, and $M_{\rm s} \gtrsim 10^{-15}\ M_{\rm Pl}$.

Constraining the condensate using experimental bounds on the graviton mass

Once the stringy effects are ignored, one is left with two competing effects on GW propagation: (i) *delays* (compared to the propagation in vacuum) due to the induced graviton mass (3.149a) and (ii) *advances* due to the propagation of gravitons in the weak gravitational potentials induced by D-matter and DM distributions (3.158). In principle, as already mentioned, the above effects (3.149a) and (3.158) will lead to a modification of the pattern of the GW signal, due to induced dephasings of the various frequency components comprising the signal. We shall here discuss the conditions under which the mass effects are dominant, in which the graviton group velocity would be *subluminal*.

By comparing the two cases (3.149a) and (3.158), we conclude that the graviton would have a *subluminal* propagation velocity if and only if its mass is larger than a critical minimal value

$$m_{\rm G} \geq m_{\rm G}^{\rm c} = \sqrt{\frac{\rho_{\rm m}}{2\, M_{\rm Pl}^2}} \simeq 7 \times 10^{-62}\ M_{\rm Pl} \simeq 2 \times 10^{-34}\ {\rm eV}\ , \tag{3.163}$$

where we assume the ΛCDM value given in (3.139) [6] for the matter density.

Equations (3.137), (3.138), (3.141) and (3.157) lead to the following remarks:

- (A) If quantum fluctuations are sub-dominant as compared to statistical effects, mass effects dominate over the energy density induced refraction, and *subluminal* graviton velocities in the D-material universe are attained. In such a case, the induced mass of the graviton is (in units of $M_{\rm Pl}$) of the order of the critical density of the universe, which in the current era is by several orders of magnitude smaller than the sensitivity of aLIGO/Virgo, or even pulsar timing experiments [76] which give the strongest limit to date (cf. Eq. (3.169) below).

- (B) If recoil quantum fluctuations are taken into account, much larger graviton masses are allowed.[29] Indeed, in such a case, the refractive effects of Eq. (3.154) due to a medium of matter scatterers with density $\rho_{\rm m}$ reduce the *effective* mass of the graviton, to be constrained by experiments, to

$$0 < (m_{\rm G}^{\rm eff})^2 \equiv m_{\rm G}^2 - \frac{\rho_{\rm m}}{2\,M_{\rm Pl}^2} \tag{3.164}$$
$$= \frac{1}{M_{\rm Pl}^2}\left[\frac{1}{6}\,M_{\rm s}^4\,\langle\!\langle u_i u_j \delta^{ij}\rangle\!\rangle + 2\rho_{\Lambda^{\rm vac}} - \frac{\rho_{\rm DM+b}}{2} - \frac{7}{24}\,(\tilde{a}-\tilde{a}_t)\right]\,,$$

  where we remind the reader that $\rho_{\rm DM+b}$ denotes any conventional matter content of the D-material universe, including both (ordinary) baryonic matter and (conventional) DM. Equation (3.164) is a *necessary* and *sufficient* condition for positivity of $(m_{\rm G}^{\rm eff})^2$ (that is a condition for dominance of mass effects over the refractive index ones). The reader should bear in mind that in (3.164), $2\rho_{\Lambda^{\rm vac}} - \frac{1}{2}\,\rho_{\rm DM+b} > 0$, as a result of the ΛCDM cosmic concordance in the current era.

Now, in what follows, we shall make the assumption (as a special but quite indicative case), that $0 < \tilde{a} < \tilde{a}_t$, which is required for consistency of (3.141) if one assumes, as we do here, that

$$M_{\rm s}^4\,\langle\!\langle u_i u_j \delta^{ij}\rangle\!\rangle \gg \rho_{\rm m}^{\Lambda{\rm CDM}}\,. \tag{3.165}$$

The positivity of the condensates is a mild assumption we make, following Ref. [62], where such quantum condensates have been argued to provide DE contributions. Thus, the importance of non-zero quantum condensates lies on the fact that their presence allows a much larger induced graviton mass than the critical density of the universe. Indeed, on requiring further

$$\tilde{a}_{\rm t} \sim \tilde{a} + 4M_{\rm s}^4\,\langle\!\langle u_i u_j \delta^{ij}\rangle\!\rangle\,, \tag{3.166}$$

we see that (3.141) is guaranteed even with the assumption (3.165), and hence the conclusions of Section 3.3 remain unchanged.

Note that the presence of the symbol $\sim$ instead of equality in (3.166) indicates a small but non-zero difference between the left- and right-hand-sides of the above

[29] Nevertheless, the stringy effects (3.161), that grow linearly with the GW frequency ω, are still subleading, for the very low-energies we consider here, compared with the mass and refractive index effects, that are inversely proportional to the square of ω.

equation of order of the critical density of the universe, which is the same order as the total (observed) energy density today $\rho_{\rm total}$ as in Eq. (3.142). One may solve Eq. (3.166) by assuming (as an indicative example) that in the current era of the universe

$$\tilde{a} \sim M_{\rm s}^4 \langle\!\langle u_i u_j \, \delta^{ij} \rangle\!\rangle \quad \Rightarrow \quad \tilde{a}_{\rm t} \sim 5\tilde{a} \ , \tag{3.167}$$

implying that the induced effective mass of the gravitons (3.164) can be much larger than the total energy density of the D-material fluid, namely

$$\begin{aligned} (m_{\rm G}^{\rm eff})^2 \, M_{\rm Pl}^2 \simeq \frac{4}{3}\,\tilde{a} + 2\rho_{\Lambda^{\rm vac}} - \frac{\rho_{\rm DM+b}}{2} \sim \frac{4}{3}\, M_{\rm s}^4 \, \langle\!\langle u_i u_j \delta^{ij} \rangle\!\rangle \\ \gg \{\rho_{\Lambda^{\rm vac}}, \, \rho_{\rm DM+b}\} \ , \end{aligned} \tag{3.168}$$

for $\tilde{a} \gg \{\rho_{\Lambda^{\rm vac}}, \rho_{\rm DM+b}\}$, assumed in Eqs. (3.165) and (3.167). Thus, in this example, the effective mass of the graviton is of the same order as the mass (3.137) induced by the dominant "magnetic" field condensates. It is important to remark that here one should no longer assume the range (3.144), since the quantum effects are the ones responsible for ensuring the satisfaction of the upper bound (3.141).

The most stringent current bounds on the mass of the graviton are given by pulsar timing experiments [76], which are stronger than the bound (3.153) from aLIGO's direct detection of GW [4]. They give

$$\begin{aligned} m_{\rm G}^{\rm eff} &< 8.5 \times 10^{-24} \ {\rm eV} = 3.5 \times 10^{-51} \ M_{\rm Pl} \quad \text{(pulsar)} \\ m_{\rm G}^{\rm eff} &< 1.2 \times 10^{-22} \ {\rm eV} = 5.0 \times 10^{-50} \ M_{\rm Pl} \quad \text{(aLIGO)} \ . \end{aligned} \tag{3.169}$$

If quantum effects are ignored, in case (A) above, the induced mass is of the order of the current critical density of the universe and hence cannot be constrained by the current limits. However, in case (B), assuming for concreteness example (3.167), then (3.168), (3.169) imply

$$\begin{aligned} \tilde{a} &< 9.2 \times 10^{-102} \ M_{\rm Pl}^4 \quad \text{(pulsar)} \\ \tilde{a} &< 1.9 \times 10^{-99} \ M_{\rm Pl}^4 \quad \text{(aLIGO)} \ , \end{aligned} \tag{3.170}$$

namely the upper bounds are much larger values (by several orders of magnitude) than the ΛCDM critical density.

Gravitational Cherenkov radiation

The subluminal nature of the graviton in the case considered above implies other effects, independent of the GW aLIGO observations, which may constrain further the string scale in our model. We will thus investigate gravitational Cherenkov radiation [77], namely the emission of a graviton from a highly relativistic particle, propagating with a velocity almost equal to that of the speed of light *in vacuum*. Such a process is kinematically allowed, provided the graviton group velocity is less than the speed of light *in vacuum*. We will therefore examine under what conditions, if at all, such an effect exists in the D-material universe. In the affirmative case, following Ref. [77] and using Ultra High Energy Cosmic Rays (UHECR), we shall impose constraints on the lower allowed bound of the graviton propagation speed.

For electrically charged particles, the D-matter medium looks transparent [65], on account of gauge invariance properties. This is the case of the UHECR, which therefore can propagate in the D-matter medium, for which (3.163) is satisfied, with a speed higher than that of (low-frequency) gravitons, and therefore gravitational Cherenkov radiation is kinematically allowed [77]. As a result, cosmic rays will lose energy. The observation of the most energetic cosmic rays, with energies 10^{20} eV, implies then stringent constraints on the lower bound of the propagation velocity of such subluminal low-frequency gravitons. According to the analysis in Ref. [77] and depending on the assumptions on the origin (galactic or extragalactic) of the UHECR, one obtains the bounds

$$\begin{aligned} &0 < 1 - v_{\rm g} < 2 \times 10^{-15} \qquad \text{for UHECR of galactic origin} \\ &0 < 1 - v_{\rm g} < 2 \times 10^{-19} \qquad \text{for UHECR of extragalactic origin} \end{aligned} \tag{3.171}$$

in units of the speed of light in vacuum. From (3.147), upon substituting $m_{\rm G}$ by $m_{\rm G}^{\rm eff}$ (3.164), we then obtain the bounds

$$\begin{aligned} &(m_{\rm G}^{\rm eff})^2 < 4 \times 10^{-15}\, \omega^2 \qquad \text{for UHECR of galactic origin} \\ &(m_{\rm G}^{\rm eff})^2 < 4 \times 10^{-19}\, \omega^2 \qquad \text{for UHECR of extragalactic origin} \end{aligned} \tag{3.172}$$

which, in the example (3.167) leading to (3.168) and for the frequency range of the

GW of aLIGO [4], that is $\omega \simeq 100$ Hz $\simeq 1.7 \times 10^{-40}\ M_{\rm Pl}$, yields

$$\begin{aligned} &\tilde{a} < 8.7 \times 10^{-95}\ M_{\rm Pl}^4 \quad \text{for UHECR of galactic origin} \\ &\tilde{a} < 8.7 \times 10^{-99}\ M_{\rm Pl}^4 \quad \text{for UHECR of extragalactic origin .} \end{aligned} \tag{3.173}$$

Thus, if UHECR are of extragalactic origin, then the bounds on the minimal value of the (subluminal) graviton propagation speed obtained as a consequence of the gravitational Cherenkov radiation, are at best of the same order of magnitude as the bounds (3.169), otherwise (namely, for UHECR of galactic origin) the corresponding bounds are several orders of magnitude weaker.

3.6 Conclusions and outlook

In this work we built upon previous discussions on the potential rôle of the recoil velocity fluctuations of D-particle (effectively point-like) defects in brane universes, by presenting a cosmic evolution of the so-called D-material universe. The latter is a brane world which is punctured by populations of D-particles and propagates in a bulk space with varying densities of such defects. Their string interactions, with (open and closed) string modes representing matter and radiation on the brane world, generate a recoil velocity, which can be promoted to a dynamic field once related to the local spacetime deformations. In the early stages of the universe, one may encounter dense populations of bulk D-particles, which imply a dense population of D-particles bound to the brane world. For low string scales $M_{\rm s}$ compared to the Hubble scale and for sufficiently large brane tensions compared to $M_{\rm s}^4$, the recoil velocity fluctuations lead to the formation of large condensate scalar fields which can safely be assumed homogeneous and slowly time varying. The careful analysis of the potential emerging from our model shows that such large scalar field can drive slow-roll Starobinsky-like inflation and yield a successful exit. In the case of large string scales compared to the Hubble scale, or smaller brane tensions of the order of $M_{\rm s}^4$, the resulting condensates are small and cannot drive inflation. In such, inflation might be induced by other mechanisms, for instance it may be driven by large negative values of a slowly rolling dilaton field.

As (the cosmic) time lapses, the universe exits from a bulk region of such dense D-particle populations, inflation ends and the universe enters a radiation dominated era, with power-law expansion of the scale factor in cosmic time. In such a case, the

recoil velocity fluctuations of the D-particle diminish with the inverse cubic power of the scale factor. The pertinent condensates are weak. At such late eras of the universe, it has been shown that the recoil velocity fluctuation fluid may "mimic" Dark Matter (DM) in a way compatible with lensing phenomenology. Of course, given that the underlying string theory contains its own particle DM candidates, our findings here should be interpreted only as suggesting that the recoil velocity component might be the dominant one in agreement with current lensing data. Certainly, given that this assumption implies only upper bounds for the pertinent densities of D-particles, the picture of a multicomponent DM where both conventional particle and D-particle candidates might play an equal rôle in DM composition cannot be excluded at present. The density of D-particles at a given era in the history of the D-material universe is in a sense a free parameter in our low-energy treatment, although this can be actually controlled by performing numerical simulations of the evolution of a dense population of D-particles in colliding brane scenarios (whereby the collision implies the initial Big-Bang-like cosmically catastrophic event [58]). This is not feasible at present.

In addition, we considered the effects of the recoiling D-particles on the propagation of GW. For the low-energy regime of interest for GWs observed by aLIGO, which was the focus of our attention here, the main effect is an induced effective mass for the graviton, given by (3.137), which, depending on the magnitude of the D-particle recoil velocity fluctuations, can be much larger than the vacuum energy and DM density, and hence can be bounded by pulsar timing or aLIGO measurements. As the magnitude of such quantum fluctuations cannot be determined theoretically at present, due to uncertainties in the underlying dynamics of the collection of D-particle defects that require going beyond the current perturbative analysis in brane/string theory, such studies can only be phenomenological at present, and this is what we concentrated upon in this work.

One of the most important features of a massive graviton is that it is *subluminal* as compared to photons, due to a negligible refractive index effect for the low-energy regime of interest to us here. In that case, gravitational Cherenkov radiation may impose additional constraints, in particular if one considers Ultra High Energy Cosmic Rays (UHECR) of an extragalactic origin. As we have shown, one gets upper bounds on graviton masses comparable (in order of magnitude) to those obtained from aLIGO interferometric measurements of GW, but still weaker than those obtained from pulsar timing data. Certainly, Cherenkov radiation bounds may improve

in the future (once higher energies can be probed). Of course, if Lorentz violation due to the D-particle populations is significant, then the optical transparency of the high-energy universe may be further affected, modifying the above discussed bounds.

We feel stressing once more the point of view taken in this part of our work as far as the effects of recoil velocity condensates on the GW propagation are concerned. Any such effects contribute to the so-called vacuum energy and in the context of our D-material universe, such contributions were assumed as being due to the stress tensor of string matter rather than the geometry. This allowed us to treat any such effect as corrections on top of a virtually flat spacetime FLRW background, where a mass for the graviton can be defined. We hope that the D-material universe as a concept is an interesting one, especially because it seems that the model is capable of passing all of the current phenomenological challenges, including the effects of the medium on the GW, but also lensing phenomenology on challenging sources and a consistent, successful inflationary era.

Before closing, we should point out that there are some important predictions of the D-material universe, given that the refractive indices of the D-particle medium are dominantly affecting photons and gravitons. In the early universe, where the density of D-particles is significantly higher than that of the current era, one expects that such Lorentz-violating effects of the D-foam impact significantly the propagation of primordial GWs. In our inflationary phenomenology above we assumed standard analysis of the cosmological perturbations in order to match the slow-roll parameters to the data, and in particular the tensor-to-scalar ratio. In the actual situation, where the dynamics of the densely populated medium of D-particles is properly taken into account, one may have non-trivial effects on this ratio, which might lead to observational signatures. This is an open issue that would be interesting to pursue in the future.

A final comment concerns the production of D-particles, in case their masses are less than 7 TeV, in the run II of the Large Hadron Collider (LHC) and their potential detection. The production of neutral D-$\overline{\text{D}}$ pairs, from decays of (for instance) highly-energetic off-shell Z^0-bosons, is a rare but possible event at LHC. The neutral defect pairs should manifest themselves in a way similar to ordinary particle/antiparticle DM pairs at colliders. However, the D-particles have an additional peculiar property, which implies non conventional ways of detection since their presence results in a deficit angle in the neighbouring spacetime. Once therefore a D-particle is produced

(in a pair with its antiparticle) in a collider, the colliding Standard Model particles in the beam will find themselves in the environment of a spacetime with a deficit angle, leading to locally maximal scattering amplitudes under some circumstances and thus to peculiar scattering patterns ("*Newton-like* rings") around the trajectory of the defect. This specificity makes the detection of such pair possible in ATLAS and CMS LHC experiments, or even in the MoEDAL LHC experiment [78], which is the seventh LHC recognised experiment, dedicated to the detection of highly ionising avatars of new physics, including the aforementioned D-matter. In view of the interesting cosmological properties of D-matter, outlined in the present work, producing it at LHC, if it exists and is sufficiently light, would further enhance the opportunities of studying its peculiar properties and unravel its brany structure. This in turn, may result in a better understanding of fundamental properties of brane theory itself.

Chapter 4

Conclusions and perspectives

Studies of our universe have revealed it to be extremely homogeneous and isotropic (up to a part in 10^5), very flat (within a 0.4% margin) and currently in accelerated expansion (for at least 3 to 4 billion years) [6]. Still, the mechanisms leading to such a state are not fully understood. Inflation explains why it is so uniform and flat but a plethora of models compete to deliver the most sensible and accurate inflationary era. The energy budget of the universe is mainly divided into three components: about 70% Dark Energy (DE), 30% matter (out of which a seventh is conventional baryonic matter while the rest is made of Dark Matter (DM)) and a pinch of highly relativistic species (mostly photons and neutrinos). However, the nature of the dark sector (DM and DE) is not completely understood and again a large variety of models describes possible origins, compositions and behaviours for such fluids.

Moreover, the standard ΛCDM model as well as the theories on which it is constructed — such as General Relativity (GR) and the Standard Model of particle physics — are all effective theories, known to be valid only at low energy densities. A UV complete description which would encompass all phenomena of nature is still to be written. Two candidates which are currently being most seriously considered are non-perturbative quantum gravity and string theory. Still, many corrections, either *ad hoc* or suggested by a higher energy picture, can be added to the known models. The study of their self-consistency, as well as a comparison with the available (or foreseeable) data, yield information about the favoured models and their parameter space.

Detailed analysis of the Cosmic Microwave Background (CMB) and statistical studies of surrounding sources in the whole electromagnetic spectrum have led us to our present state of understanding. New advances will be achieved by reaching ever greater precision in such investigations but also through the use of additional tools

such as Gravitational Waves (GWs). While their existence was long inferred by indirect effects, the first direct detections occurred only very recently [4] and complementary data should soon be available to explore as yet unreachable phenomena. For instance, isolated events are shedding light on compact objects binaries, collapsing supernovae and other extremely violent processes. Knowledge of their inner mechanisms and their abundance, as well as of the properties of GWs themselves, could emerge from such studies. On the other hand, investigations of the GW background, similar to the CMB, could enlighten us about the nature of inflation and the very early universe. Likewise, the stochastic superposition of individual signals from the multiplicity of local sources could reveal additional cosmological and astrophysical information.

With this in mind, our work here has focused on two specific models and their phenomenological consequences. In Chapter 2, we studied peculiar events producing GW Bursts (GWB) in a network of cosmic strings. As presented in Section 2.1, these networks are thought to be generic in many scenarii which include some Spontaneous Symmetry Breaking (SSB) and/or certain types of supersymmetric or string theory inflation. Indeed, the Kibble mechanism [28] is responsible for the creation of topological defects, which are confined regions in which the normal phase survives in an ordered phase background. Under certain circumstances regarding the symmetries, these defects can be linear, namely Cosmic Strings (CS). Alternatively, some string-inspired models, in which our universe is a brane evolving within a larger-dimensional bulk and where inflation is related to brane collisions, can also lead to the quantum equivalent, namely Cosmic SuperStrings (CSS). The properties and parameters of such strings depend on the model they emerge from, but can be studied, as we do in Section 2.2, from an effectively one-dimensional perspective, that is, following the Nambu-Goto action given in Eq. (2.4). It is interesting to notice this common framework for CS and CSS, even though their formation, and thus some of their parameters and their evolutions, might be different.

One exciting feature of such linear objects is called a cusp, and this corresponds to a region of the C(S)S momentarily reaching the speed of light $c = 1$. The interest in such events lies in the GWB emitted at that point, whose high frequency spectrum has been analytically examined [36]. Our work in Section 2.3 focused on such events from a light string stretched between two heavy, almost fixed strings, as could appears in C(S)S networks. We investigated in particular the rate of such phenomena. Doing so numerically, we also saw some potentially important relatives

to cusps emerging, called *pseudo*cusps, where the velocity reached was very close to 1 but still a bit (say 10^{-5}) below. An analytical criterion allowing us to discriminate between cuspy and non-cuspy strings was found, Eq. (2.50), and compared to our simulations, confirming several of our intuitions. For instance, we found that the wavier a C(S)S is, the cuspier it will be, and that there could be on average as many pseudocusps as they are cusps, in order of magnitude. The actual number of cusps being very model- and parameter-dependent, and our setup being specific even though quite realistic, we can only give the overall trends and not definite rates of occurrence.

Still, we would like to stress that our study led not only to a better understanding of cuspy events with respect to their GWs emissions, but also of the frequency of such phenomena and their occurrence rates relative to the main parameters of string networks [45]. This opens up possibilities for future work on several fronts. Firstly, the GW spectrum of pseudocusps could be studied in order to derive the dependence of the high frequency behaviour on the local velocity. This would provide a more informed choice for the relevant points regarding GWBs (as the threshold used here was somewhat arbitrary and mainly motivated by the limits on numerical accuracy). The incidence of cusps and pseudocusps could also be studied for additional string configurations, such as loops, strings between moving junctions or strings with kinks. Once this is determined, dynamical evolutions of C(S)Ss and networks could be simulated, taking into account properties such as the expansion of the universe and the scaling of the network, the string interactions, and the local features (for instance kinks, junctions, and zipping). Such model dependent analyses would refine our knowledge of the number of cuspy events on a more realistic, complete network. We could thus obtain multiple predictions of the high frequency GW signal one could expect on Earth. We believe that this would allow a better understanding of future detections, both stochastic backgrounds and potential single events, in addition to providing more accurate constraints on a large range of high energy models.

We discussed in Chapter 3 a specific (string inspired) brane world scenario, that is, a model where our lower-dimensional universe evolves in a larger-dimensional bulk. The graviton is seen as a closed string and is also located in the bulk, while other fields are open strings whose extremities end on the branes. The key feature of this model, as detailed in Section 3.2, is the presence of a foam of effectively point-like D-particles in the bulk, either as D0-branes or as three-times-compactified D3-branes, depending on the string background. Their interactions with our uni-

verse brane and its contents, namely open strings, generate a vector recoil velocity field. This influences the graviton equations of motion, Eq. (3.19), mainly via extra content terms due to the squared field strength. These can be interpreted differently depending on the hypotheses adopted and were shown to lead to various astrophysical and cosmological consequences.

As we showed in Section 3.3, this recoil velocity field can form a condensate in late eras of the universe and act as a DM fluid, thus reducing the need for other types of DM, although it generically appears in such string-inspired models. We detailed under which circumstances this condensate can fully replace the need for alternative DM, relying on a lensing analysis and relating our constraints to the ones previously obtained in the context of large scale structure growth [61]. We would emphasise, once more, however, that we do not seek via this model to eliminate the need for DM, but rather to partially relax the current bounds. Looking back to the early universe in Section 3.4, we then studied the inflationary era and produced a successful scenario in which the condensate, which is homogeneous and slowly varying in time, plays the rôle of the inflaton scalar field. Two limits are studied, one in which the condensate is weak (in the case of large string scale with respect to the Hubble scale during this era) which turns out to be unsatisfactory, and the second where it is large (with small string scale) which fulfils all the requirements for inflation. The constraints of this scenario were then tested with respect to the late era limits, and the age of the universe was computed for overall consistency. An alternative scenario for the former, deficient case was also given, where the dilaton field induces the inflationary era. Finally, driven again by the late direct detections [4], we studied in Section 3.5 the propagation of GW in such a modified theory and obtained a mass for the graviton. Additional effects, such as refractive ones, both on the graviton and the photon, were studied and compared, in order to constrain the parameters of our model. It is important to note that for such analysis, the so far neglected "magnetic" type field strength of our vector recoil velocity field plays an important rôle, as well as the quantum fluctuations of the condensate. Still, this is consistent with the previous sections; each setup implies different hypotheses such as homogeneity or time independence, leading to different leading and subleading terms in the equations and thus to different physical effects.

Our analysis provides multiple tests of this D-material universe model, spanning several eras as well as several space scales, which consistently fits the current data and solves several outstanding problems of the ΛCDM model. Let us stress that this

scenario provides microphysical interpretations for the introduction of additional terms in the equations, and thus proves to be not only experimentally successful but also theoretically well motivated. Still, the lack of a better string theoretic understanding limited our ability to produce a detailed analysis of the quantum fluctuations of the condensate. These are necessary to relax some assumptions, refine the underlying mechanisms and further constrain the model. In addition, a full comparison to the CMB temperature and polarisation anisotropies, regarding the GW and photon propagations, could yield additional limits on the model parameters. Our inflationary era could produce specific signatures, such as GW signals or effects on the tensor-to-scalar ratio, distinguishing foam models from other brane world scenarii. Finally, the presence of D-particles in our immediate surroundings could be indirectly observed in particle detectors such as the Large Hadron Collider (LHC), for example, by the spacetime angle deficit they create locally.

Finally, a word on the theories which were investigated. For us, their appeal lay in the fact that they provide immediate phenomenological consequences, as well as being strongly theoretically motivated. The link between hypothesis and observable outcome is unambiguous, allowing us to disprove a theory, however beautiful, and whatever the amount of time and energy that has been spent to develop it. This is at the heart of the necessary and productive conversation between theoretical and experimental research. The following famous quote from Richard Feynman [79, Chapter 7, p. 156] conveys well these views, as well as the tough truth about the theorist's task:

> In general we look for a new law by the following process. First we guess it. Then we compute the consequences of the guess to see what would be implied if this law that we guessed is right. Then we compare the result of the computation to nature, with experiment or experience, compare it directly with observation, to see if it works. If it disagrees with experiment it is wrong. In that simple statement is the key to science. It does not make any difference how beautiful your guess is. It does not make any difference how smart you are, who made the guess, or what his name is – if it disagrees with experiment it is wrong. That is all there is to it.

The true goal is to fail one's own theory, to force it to confront the reality of observations, to constrain it, until there is no parameter space left.

With these ideas in mind, this thesis has sought to push further on the limits of the theories it presents. It is hoped that future work will build upon this one, in

cosmic strings, in dark matter, in the early universe, in such a way as to carry on this fruitful dialogue between theory and reality.

Appendix A

Generalised configuration of strings between Y-junctions

We here extend our initial strings' configuration detailed in Section 2.3.1, in order to show that the quasi-periodicity of the movement of the light string is indeed generic.

A.1 Coplanar heavy strings with various angles

In this section, we choose different angles at the two junctions and denote Ψ_0 (respectively Ψ_m) the angle between the z-axis and the heavy string at the $\sigma = 0$ (respectively $\sigma = \sigma_m$) junction. In addition, by setting the upper half-plane to be the symmetric of the lower half-plane, one forms a $(\pi - 2\Psi_0)$ (respectively $(\pi - 2\Psi_m)$) angle along the heavy string. Note that here, the two heavy strings remain coplanar and orthogonal to the y-axis, as shown in Fig. A.1.

One can then define $S_0 = \text{sign}(X'_z(0,t))$ and $S_m = \text{sign}(X'_z(\sigma_m,t))$ the signs of the z-component of the light string's velocity at each end. These both take the value ± 1 depending on whether we consider the $z \lessgtr 0$ half-plane, respectively. They allow us to write in a compact way all the boundary conditions coming from Eqs. (2.20), giving

$$\dot{X}_y\,(t,0) = 0 \tag{A.1a}$$

$$\dot{X}_x\,(t,0) - S_0 \tan(\Psi_0)\,\dot{X}_z\,(t,0) = 0 \tag{A.1b}$$

$$S_0 \tan(\Psi_0)\,X'_x\,(t,0) + X'_z\,(t,0) = 0\ , \tag{A.1c}$$

and

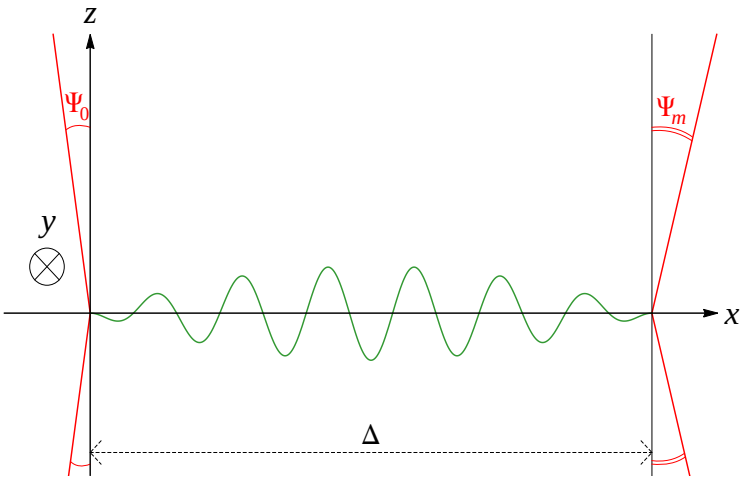

Figure A.1: A light string stretched between two junctions with heavy strings. Here the upper-half plane is symmetric to the lower-half plane and each heavy string forms a different angle with the z-axis. The heavy strings are coplanar.

$$\dot{X}_y\left(t,\sigma_m\right)=0 \tag{A.1d}$$

$$\dot{X}_x\left(t,\sigma_m\right)+S_m\tan(\Psi_m)\,\dot{X}_z\left(t,\sigma_m\right)=0 \tag{A.1e}$$

$$S_m\tan(\Psi_m)\,X'_x\left(t,\sigma_m\right)-X'_z\left(t,\sigma_m\right)=0\ , \tag{A.1f}$$

leading to the system of equations

$$X'_{+y}\left(t\right)=X'_{-y}\left(-t\right) \tag{A.2a}$$

$$\left[X'_{+z}\left(t\right)-X'_{-z}\left(-t\right)\right]S_0\tan\Psi_0=X'_{+x}\left(t\right)-X'_{-x}\left(-t\right) \tag{A.2b}$$

$$X'_{+z}\left(t\right)+X'_{-z}\left(-t\right)=-\left[X'_{+x}\left(t\right)+X'_{-x}\left(-t\right)\right]S_0\tan\Psi_0\ , \tag{A.2c}$$

and

$$X'_{+y}\left(2\sigma_m+t\right)=X'_{-y}\left(-t\right) \tag{A.2d}$$

$$\left[X'_{+z}\left(2\sigma_m+t\right)-X'_{-z}\left(-t\right)\right]S_m\tan\Psi_m=-X'_{+x}\left(2\sigma_m+t\right)+X'_{-x}\left(-t\right) \tag{A.2e}$$

$$X'_{+z}\left(2\sigma_m+t\right)+X'_{-z}\left(-t\right)=\left[X'_{+x}\left(2\sigma_m+t\right)+X'_{-x}\left(-t\right)\right]S_m\tan\Psi_m \tag{A.2f}$$

replacing Eqs. (2.22). Manipulating Eqs. (A.2b) and (A.2c) allows us to express $X'_{+x}(t)$ and $X'_{-x}(-t)$ in terms of $X'_{+z}(t)$, $X'_{-z}(-t)$ and polynomials of $(S_0\tan\Psi_0)$, and thus $X'_{+x}(2\sigma_m+t)$ after a shift $t\to 2\sigma_m+t$. Replacing in Eqs. (A.2e) and (A.2f), one gets two equations involving $X'_{+z}(2\sigma_m+t)$, $X'_{+z}(t)$, $X'_{-z}(-2\sigma_m-t)$ and $X'_{-z}(-t)$, and combination of $(S_0\tan\Psi_0)$ and $(S_m\tan\Psi_m)$.

Shifting the variable $t \to 2\sigma_m + t$, one gets four equations involving six variables: $X'_{+z}(4\sigma_m + t)$, $X'_{+z}(2\sigma_m + t)$, $X'_{+z}(t)$, $X'_{-z}(-4\sigma_m - t)$, $X'_{-z}(-2\sigma_m - t)$ and $X'_{-z}(-t)$. One can then use three of them to eliminate the three X'_{-z} variables — namely $X'_{-z}(-4\sigma_m - t)$, $X'_{-z}(-2\sigma_m - t)$ and $X'_{-z}(-t)$ — to obtain an expression similar to Eq. (2.26)

$$X'_{+z}(t) = -\mathcal{R} X'_{+z}(-2\sigma_m + t) - X'_{+z}(-4\sigma_m + t) \ , \tag{A.3}$$

where

$$\mathcal{R} \equiv -2\cos(2S_0\Psi_0 + 2S_m\Psi_m) \ , \tag{A.4}$$

and similarly for X'_{+x}.

This expression is very similar to the one we obtained in the initial setting, which we can retrieve by setting $S_m = 1 = S_0$ and $\Psi_0 = \Psi_m$. In addition, this equation also reveals that the functions X'_{+x} and X'_{+z} are periodic for a dense subset of angles, otherwise quasi-periodic; one simply needs to replace 2Ψ by $\Psi_0 \pm \Psi_m$. This justifies our initial simpler choice.

A.2 Non-coplanar heavy strings

In this section, we choose to modify the initial configuration by rotating the σ_m-end string in the plane containing the y-axis, as shown on Fig. A.2. In other words, one rotates the string around the axis which is perpendicular both to the initial position of the string and to the y-axis, that is the axis directed by the vector $(\cos\Psi,\, 0\,,\, \sin\Psi)$.

This rotation generates a coupling between X'_{+y} and the other components of $\mathbf{X}'_+$, namely X'_{+x} and X'_{+z}, contrarily to previous cases. Indeed, the boundary conditions at $\sigma = 0$ remain the same while the ones at $\sigma = \sigma_m$ become

$$\begin{aligned}
-\sin\Psi\,\sin\Phi\left[X'_{+x}(2\sigma_m + t) - X'_{-x}(-t)\right] + \cos\Phi\left[X'_{+y}(2\sigma_m + t) - X'_{-y}(-t)\right] \\
+ \cos\Psi\,\sin\Phi\left[X'_{+z}(2\sigma_m + t) - X'_{-z}(-t)\right] = 0 \quad \text{(A.5a)} \\
\left[X'_{+x}(2\sigma_m + t) - X'_{-x}(-t)\right] + \tan\Psi\left[X'_{+z}(2\sigma_m + t) - X'_{-z}(-t)\right] = 0 \quad \text{(A.5b)} \\
\sin\Psi\,\cos\Phi\left[X'_{+x}(2\sigma_m + t) + X'_{-x}(-t)\right] + \sin\Phi\left[X'_{+y}(2\sigma_m + t) + X'_{-y}(-t)\right] \\
- \cos\Psi\,\cos\Phi\left[X'_{+z}(2\sigma_m + t) + X'_{-z}(-t)\right] = 0 \quad \text{(A.5c)}
\end{aligned}$$

replacing Eqs. (2.22d) to (2.22f). These are significantly more complicated than previously and imply that one needs to manipulate more equations to obtain a

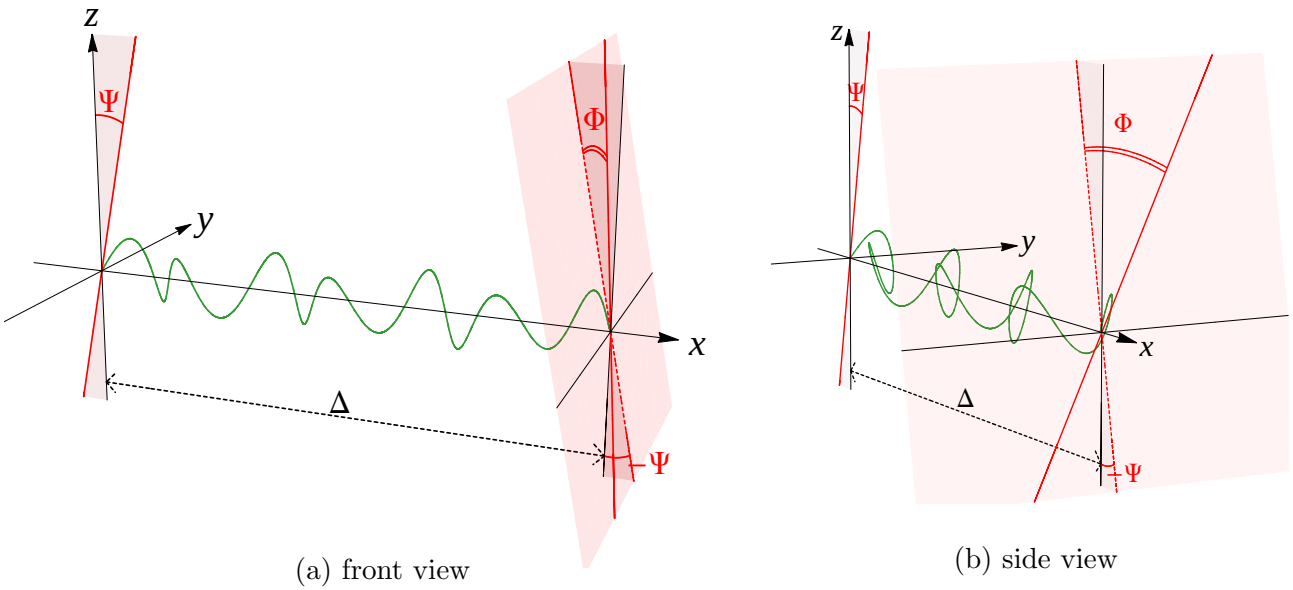

(a) front view (b) side view

Figure A.2: A light string stretched between two junctions with heavy strings. Here the $\sigma = \sigma_m$ end string has been rotated in the plane containing the y-axis by an angle Φ. The two heavy strings are no longer coplanar.

relationship similar to Eq. (2.26). In the end, this coupling generates a 3rd order equation for X'_{+x} and X'_{+z} instead of the 2nd order one that is Eq. (2.26).

We believe that the conclusion on the periodicity, obtained in the previous string configurations, is still valid in this general setup, basically since the energy density per unit length remains constant (no emission has been incorporated). Indeed, the energy being constant implies that any damping or amplification in one of the components of the signal along the string is linked to some compensation somewhere else in the system.

In the previous situations, if, for instance, the energy of the y-component was null at the beginning, it remained that way; similarly, an energy loss in the x-component would be balanced by a gain in the z-component, and vice versa. In our non-coplanar situation, one needs to take into account all three components in a very entangled and more complex way. This suggests that a loss of energy in, say, the z-component can be balanced by an amplification in the y-component, for instance. Indeed, at the $\sigma = \sigma_m$ junction, this kind of transfer can happen since all three modes are coupled. In addition, it is believed that the damping in the z-direction could be seen as a source term in the x- and y-directions, linked to a general conservation of energy density and implying a globally periodic movement.

More precisely, the 3rd order equation is of the form

$$X_{+,n+3} - \bar{\mathcal{R}}\, X_{+,n+2} + \bar{\mathcal{R}}\, X_{+,n+1} - X_{+,n} = 0 \ , \tag{A.6}$$

where $\bar{\mathcal{R}}$ depends solely on the angles; it gives solutions of the form

$$X_{+,n} = A\, e^n + e^{un}\left(B\cos vn + C\sin vn\right) \ , \tag{A.7}$$

where A, B and C are constants depending on the initial conditions (i.e. on $X_{+,0}$, $X_{+,1}$ and $X_{+,2}$) and u and v depend directly and solely on $\bar{\mathcal{R}}$. Taking A to be non-zero gives unphysical solutions since one needs to keep in mind that $X'_{+y} = \pm\sqrt{1-(X'_{+x})^2-(X'_{+z})^2}$.[1] One would get large values for X'_{+x} and X'_{+z} as n grows, giving a negative value for $(1-(X'_{+x})^2-(X'_{+z})^2)$. Similarly, one cannot understand physically the exponential prefactor e^{un} unless there is a mechanism to either suppress this factor or reverse it after some time. Indeed, let us divide this in three cases: if u is null, one obtains a periodic motion; if $u > 0$, we find ourselves in the case described previously, that is unphysical complex values for X'_{+y}; finally, if $u < 0$, one would have a situation where $X'_{+z} = 0 = X'_{+x}$ and all the energy lies in X'_{+y}, which is unrealistic as well. A mechanism suppressing or reversing this prefactor would imply a balance between each component through time, which again makes sense physically.

Generally, it is believed that the rotation of the $\sigma = \sigma_m$ string should not change the global understanding of the movement of the light string, meaning that what was considered as consistent in the coplanar case should remain valid here.

[1] Indeed, recall $\mathbf{X}'^2_+ = 1 = (X'_{+x})^2 + (X'_{+y})^2 + (X'_{+z})^2$.

Appendix B

Snapshots of the strings simulation

We present in Fig. B.1 some snapshots of a string simulated using our code. The chosen parameters here are such that $\zeta \sim {}^{\Delta}/_{\sigma_m} = 0.25$ and $\bar{\zeta} \sim 2$ since 4 modes have been implemented on the string. Finally, we use here a rescaled time $t' \equiv {}^{t}/_{\sigma_m}$, meaning that $t' = 1$ after a half of the period. Note though that using symmetries, one can deduce how the string is behaving in the second half of the period from the string's position during the first half. Finally, note that $\Psi = 0$.

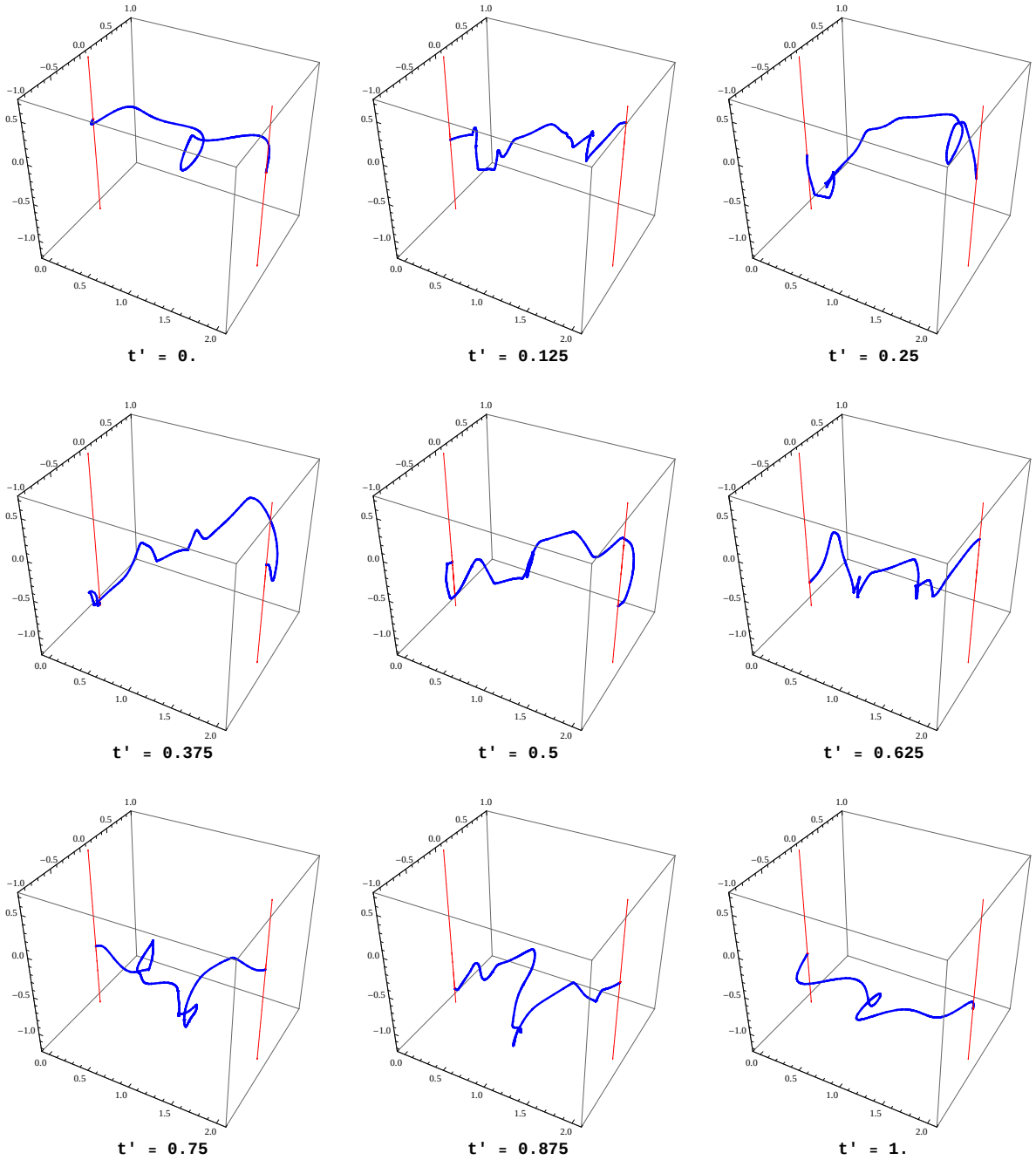

Figure B.1: Snapshots of a simulated light string (in blue) stretched between two junctions with fixed heavy strings (in red). $t' = {}^{t}/_{\sigma_m}$ is the rescaled time. $\zeta \sim {}^{\Delta}/_{\sigma_m} = 0.25$ and $\bar{\zeta} \sim 2$.

Appendix C

Background field considerations in the D-material universe

Here, we discuss background field considerations which satisfy equations of motion obtained from the actions (3.1) and (3.16).

Equations of motion

Let us first give the detailed equations of motion one gets from the low-energy, weak-field[1] action in which we include a dilaton kinetic term as well as derivatives of the vector field strength. The action, in such case, yields [61]

$$S^{E}_{\text{eff }4\text{D}} = \int \mathrm{d}^4x\sqrt{-g}\left[-\frac{T_3\,e^{3\phi_0}}{g_{s0}} - \frac{\tilde{\Lambda}\,e^{2\phi_0}}{\kappa_0^2} - \frac{1}{4}\langle\mathcal{G}_{\mu\nu}\,\mathcal{G}^{\mu\nu}\rangle + \left(\frac{\alpha\,T_3\,e^{\phi_0}}{g_{s0}} + \frac{1}{\kappa_0^2}\right)R \right.$$
$$- \frac{\widetilde{F}^2}{4}\left(1-\alpha e^{-2\phi_0}R\right) + \lambda\left(\widetilde{A}_\mu\widetilde{A}^\mu + \frac{1}{\alpha'}\mathcal{J}\right)$$
$$\left. -\frac{3\alpha\,e^{-2\phi_0}}{2}\,g^{\mu\nu}\,\partial_\mu\widetilde{F}^2\,\partial_\nu\phi + \mathcal{O}\left((\partial\phi)^2\right)\right] + S_m\ , \tag{C.1}$$

where the last two terms are the ones ignored in Eq. (3.16) and in our main computations. The first term contains derivatives of the dilaton and of the squared field strength, and leads to an additional set of terms in the graviton equation of motion, of the form

$$\left(\frac{3\alpha\,e^{-2\phi}}{4}\right)\left[\frac{g_{\mu\nu}}{2}\,\nabla^2\widetilde{F}^2 - \nabla_\mu\nabla_\nu\widetilde{F}^2 - 2\,\nabla^2\left[\widetilde{F}_\mu{}^\lambda\widetilde{F}_{\nu\lambda}\right]\right]\ . \tag{C.2}$$

[1] As in action (3.16), we use here the renormalised vector field $\widetilde{A}_\mu$, following Eq. (3.13).

Hence the full graviton equation of motion reads[2]

$$\left(R_{\mu\nu}-\frac{g_{\mu\nu}}{2}R\right)\left[\frac{\alpha\,T_3\,e^{\phi_0}}{g_{s0}}+\frac{1}{\kappa_0^2}+\frac{\alpha e^{-2\phi_0}\,\widetilde{F}^2}{4}\right]+\frac{g_{\mu\nu}}{2}\,\Lambda^{\rm vac} \tag{C.3}$$
$$+\frac{g_{\mu\nu}}{8}\,\widetilde{F}^2-\frac{1}{2}\left(1-\alpha e^{-2\phi_0}R\right)\widetilde{F}_\mu{}^\lambda\widetilde{F}_{\nu\lambda}-\frac{g_{\mu\nu}}{2}\,\lambda\left(A_\alpha A^\alpha+\frac{1}{\alpha'}\mathcal{J}\right)+\lambda\,\widetilde{A}_\mu\widetilde{A}_\nu$$
$$+\frac{3\alpha\,e^{-2\phi_0}}{4}\left[\frac{g_{\mu\nu}}{2}\,\nabla^2\widetilde{F}^2-\nabla_\mu\nabla_\nu\widetilde{F}^2-2\,\nabla^2\left[\widetilde{F}_\mu{}^\lambda\widetilde{F}_{\nu\lambda}\right]\right]=\frac{1}{2}\,T^m_{\mu\nu}\ .$$

Again, assuming the squared field strength is almost constant (homogeneous and isotropic on cosmological scales, and slowly time varying) leads to Eq. (3.19).

In the vector equation of motion, extra terms would be proportional to derivatives of the dilaton field ϕ, which is taken (exactly) constant. Unlike the approximation $\nabla\widetilde{F}^2\simeq 0$, the assumption $\phi=\phi_0$ is considered to be exact, meaning that terms of the form $\partial_\mu\phi$ or $\nabla^2\phi$ are negligible in front of any other kind of subleading term. The vector equation of motion thus gives, as already stated in (3.20)

$$\left[\widetilde{F}_{\nu\mu}\left(1-\alpha\,e^{-2\phi_0}R\right)\right]^{;\nu}+2\lambda(x)\,\widetilde{A}_\mu=0\ , \tag{C.4}$$

where again the semicolon denotes covariant derivative. Note that the Lagrange multiplier, obtained by contracting the above equation by $\widetilde{A}^\mu$ and using the constraint (3.14), is given in Eq. (3.21) as

$$\langle\lambda(x)\rangle=\frac{e^{-3\phi_0}\,g_{s0}}{8\pi^2\alpha'\,|T_3|}\,\widetilde{A}^\mu\left[\widetilde{F}_{\nu\mu}\left(1-\alpha e^{-2\phi_0}R\right)\right]^{;\nu}\ . \tag{C.5}$$

It is subleading as it yields derivatives of $\widetilde{F}_{\mu\nu}$ and R.

Finally, the dilaton equation of motion is affected by both additional terms in the action above. While the kinetic term $\mathcal{O}\left((\partial\phi)^2\right)$ is ignored in the end, we feel the need to give some details on the computations arising from the first additional term of the action. Denoting

$$S_{F\phi}\equiv\int\mathrm{d}^4x\sqrt{-g}\left[-\frac{3\alpha\,e^{-2\phi_0}}{2}\,\partial^\mu\widetilde{F}^2\,\partial_\mu\phi\right]\ , \tag{C.6}$$

[2]Once more, we assumed the condensate of bulk gauge fields of the form $\langle\mathcal{G}^{\mu\nu}\mathcal{G}_{\mu\nu}\rangle$ to be scalar-like when deriving this equation of motion.

which we vary with respect to the dilaton field, we obtain

$$\begin{aligned}\delta S_{F\phi} &= \int \mathrm{d}^4x\sqrt{-g}\left(-\frac{3}{2}\,\alpha\right)\left[e^{-2\phi}\,\partial^\mu\widetilde{F}^2\,\partial_\mu(\delta\phi) - 2\,\delta\phi\,e^{-2\phi}\,\partial^\mu\widetilde{F}^2\,\partial_\mu\phi\right] \\ &= \int \mathrm{d}^4x\sqrt{-g}\left(-\frac{3}{2}\,\alpha\right)\left[e^{-2\phi}\,\partial^\mu\widetilde{F}^2\,\partial_\mu(\delta\phi) - e^{-2\phi}\left(\delta\phi\,\nabla^2\widetilde{F}^2 + \partial^\mu\widetilde{F}^2\,\partial_\mu(\delta\phi)\right)\right] \\ &= \int \mathrm{d}^4x\sqrt{-g}\left[\frac{+3\alpha\,e^{-2\phi}}{2}\,\nabla^2\widetilde{F}^2\right]\delta\phi\ , \end{aligned} \tag{C.7}$$

where, between the first and the the second line, we used an integration by part on the second term.[3] The dilaton equation of motion (once we assumed $\phi = \phi_0$, only removing the kinetic term) thus yields[4]

$$\begin{aligned}\frac{3\,T_3 e^{3\phi_0}}{g_{\rm s0}} + \frac{2\,\tilde{\Lambda}\,e^{2\phi_0}}{\kappa_0^2} - \alpha\left[\frac{T_3 e^{\phi_0}}{g_{\rm s0}} - \frac{e^{-2\phi_0}\,\widetilde{F}^2}{2}\right]R \\ -\frac{3\alpha\,e^{-2\phi_0}}{2}\,\nabla^2\widetilde{F}^2 + \lambda\,\frac{3}{\alpha'}\mathcal{J} = 0\ , \end{aligned} \tag{C.8}$$

which, assuming again $\nabla_\lambda\widetilde{F}_{\mu\nu} \simeq 0$ (and hence $\lambda \simeq 0$), gives back Eq. (3.22).

Vertex operators

As discussed in detail in Ref. [61] and references therein, the D-particle recoil fluctuations are in general represented by a vector mean-field excitation of a stringy σ-model that describes the propagation of strings in cosmological FLRW spacetime backgrounds, punctured by populations of fluctuating D-particles, with two types of contributions:

(i) "Electric type", associated with the linear recoil momentum excitations, described by σ-model world-sheet boundary ($\partial\Sigma$) deformations of the form

$$\begin{aligned}V_{\text{lin. mom.}} &= \frac{1}{2\pi\alpha'}\int_{\partial\Sigma}\mathrm{d}\tau\,g_{ik}\,Y^k(\tau)\,\Theta_\epsilon(X^0)\,\partial_n X^i \\ &= \frac{1}{2\pi\alpha'}\int_{\partial\Sigma}\mathrm{d}\tau\,g_{ik}\,u^k\,X^0\,\Theta_\epsilon(X^0)\,\partial_n X^i\ , \end{aligned} \tag{C.9}$$

with $\Theta_\epsilon(X^0)$ a regularised Heaviside function, describing the impact (and impulse) of the matter string on the D-particle at a time $X^0 = 0$ and $\partial_n X^i$ the normal world-

[3] Using the notation $\int uv' = [uv] - \int u'v$, we here chose $u = \delta\phi\,\partial^\mu\widetilde{F}^2$ and $v' = -2\,e^{-2\phi}\,\partial_\mu\phi$.

[4] Recall the definition of $\mathcal{J}$ in Eq. (3.15). It leads to the (subleading) term containing the Lagrange multiplier.

sheet derivative, where X^i are σ-model fields obeying Dirichlet boundary conditions on the world sheet, and τ is a σ-model field obeying Neumann boundary conditions on the world-sheet, whose zero mode is the cosmic target time. The path $Y^i(\tau)$ may be identified with the geodesic equation of a massive D-particle in the spacetime described by the metric g_{ij}. One can rewrite $X_0 = t - t_c$ and use cosmic time t, t_c being the impact time. The quantity u^i is the D-particle recoil velocity emerging from the inelastic interactions and $g_{ij} = a^2(t)\delta_{ij}$ are the spatial components of the metric for a (spatially flat) Friedmann-Lemaître-Robertson-Walker (FLRW) universe, with scale factor $a(t)$, we assume here, as dictated by the current astrophysical/cosmological data [6]. For the galactic eras we are interested in in the lensing analysis of Section 3.3) and in the graviton propagation study of Section 3.5, one can assume $a(t) \sim 1$. The vertex operators (C.9) satisfy a (logarithmic) conformal algebra[5] on the world-sheet, hence they are consistent string deformations.

Upon a T-duality transformation (which exchanges Neumann and Dirichlet boundary conditions), assuming it to be an exact symmetry of the underlying string theory, we observe that the "impulse" vertex operator on $\partial\Sigma$ (C.9) corresponds to that of a covariant vector (gauge) field[6]

$$V_{\text{lin. mom.}} = \frac{1}{2\pi\sqrt{\alpha'}} \int_{\partial\Sigma} \mathrm{d}\tau \, A_\mu \, \partial_\tau X^\mu \ , \tag{C.10}$$

where ∂_τ denotes tangential world-sheet derivative. The vector field has spatial components [61]

$$A_i = \frac{1}{\sqrt{\alpha'}} \, g_{ik} \, Y^k(t) \, \Theta_\epsilon(t - t_c) \ . \tag{C.11}$$

(ii) "Magnetic type", associated with σ-model deformations corresponding to non-zero angular momentum of the recoiling D-particles, described by the world-sheet boundary vertex operators

$$V_{\text{ang. mom.}} = \frac{1}{2\pi\alpha'} \int_{\partial\Sigma} \mathrm{d}\tau \, \epsilon_{ijk} \, u^k \, X^j \Theta_\epsilon(X^0) \, \partial_n X^i \ , \tag{C.12}$$

[5]From a world-sheet viewpoint, the Heaviside function is an operator, which is such that the impulse/recoil operator (C.9) satisfies a logarithmic conformal algebra on the world-sheet of the string, which is the limiting case between conformal theories and general renormalisable two-dimensional theories, that can be classified by conformal blocks. For the purposes of this work, we shall work with $X_0 > 0$, that is, $t > t_c$, so that the Heaviside function can be set safely to one.

[6]There is an Abelian gauge symmetry associated with the vertex (C.10) due to the fact that, upon a $U(1)$ target-space gauge transformation, with parameter $\theta(X^\alpha(\sigma, \tau))$, under which $A_\mu \to A_\mu + \partial_\mu\theta(X)$, the vertex remains unchanged, since $\oint_{\partial\Sigma} \partial_\mu\theta(X) \, \partial_\tau X^\mu = \oint_{\partial\Sigma} \frac{\mathrm{d}}{\mathrm{d}\tau}\theta = 0$, recalling the boundary of a boundary is zero by construction.

with ϵ_{ijk} the antisymmetric symbol in three-space dimensions. As is the case of the "impulse" linear momentum vertex operators (C.9), the operators (C.12) also satisfy a (logarithmic) conformal algebra on the world-sheet of the string.

These "magnetic type" contributions are either subleading, due to symmetric metric conditions used in some parts of the lensing analysis of Section 3.3 or in the homogeneous isotropic cosmological background of the inflationary era in Section 3.4. Alternatively, they can be of the same order than the "electric type" ones, for instance in the galactic scales of the matter dominated era, as used in the graviton propagation analysis of Section 3.5. Still, they have been sometimes ignored for simplicity in our estimates as they would at most add a factor 2, thus not changing our conclusions.

Background configurations

Let us now look in more details at the form the vector field takes. For a FLRW background with a power-law scale factor $a(t) \sim t^p$ relevant for the matter dominated era we are interested in some parts of this work (see as well [61]), and for times large compared to the moment of impact t_c for any given D-particle, one has

$$Y^i(t) \simeq \frac{v^i}{1-2p}\left(t\,\frac{a^2(t_c)}{a^2(t)} - t_c\right) + \ldots \simeq -\frac{v^i}{1-2p}\,t_c \qquad t \gg t_0 \ , \tag{C.13}$$

which, on account of Eq. (C.11), implies the cosmological form of the recoil vector field A_μ and its field strength $F_{\mu\nu}$ on the D-brane given in Eq. (3.27), that is

$$A_i \equiv -\frac{1}{\sqrt{\alpha'}}\,a^2(t)\,u_i \ , \qquad F_{0i} = -\frac{2}{\sqrt{\alpha'}}\,\dot{a}a\,u_i \ , \tag{C.14}$$

having absorbed irrelevant numerical factors into the definition of the recoil velocity and restored the correct dimensionality via appropriate powers of $\sqrt{\alpha'}$.

The temporal component of the covariant vector field A_0 cannot be fixed in this approach, given that the target time coordinate satisfies Neumann boundary conditions on the world-sheet, and as such $\partial_n t(\sigma) = 0$ and thus does not appear in the original vertex (C.9) in the Dirichlet picture. As in Ref. [61], and for the case of cosmological spacetimes *only*, we have covariantised the vector background by considering the temporal component of the (T-dual) vector field to be such that the

four-vector field A_μ (of mass dimension one) assumes the form

$$A_\mu = -\frac{1}{\sqrt{\alpha'}}\, g_{\mu\nu}(t)\, u^\nu \ , \tag{C.15}$$

where $u^\mu = \mathrm{d}x^\mu/\mathrm{d}\tau$ is a (dimensionless) four-velocity, thus satisfying the time-like constraint (in our convention)

$$u^\mu\, u^\nu\, g_{\mu\nu} = -1 \ . \tag{C.16}$$

Recall that in this approach, the recoil velocity field u_μ is elevated to a dynamical one, as a part of a dynamical gauge background field in the D-particle recoil process. That is to say, upon T-duality, the vertex operator (C.9) is related to the gauge potential deformation $A_i = u_i X^0\, \Theta(X^0)$ (where one can assume, without any loss of generality, the time axial gauge $A_0 = 0$). The interaction of neutral matter with the background of the recoiling D-particle is described in average by such new dynamical vector field degrees of freedom, associated with the back reaction of the D-matter on spacetime.

The cosmological FLRW spacetime have the conformally flat form (in conformal time η coordinates, cf. (3.26))

$$g_{\mu\nu} = a^2(\eta)\, \eta_{\mu\nu} \ , \tag{C.17}$$

where $a(\eta)$ is the scale factor as a function of the conformal frame. In view of Eqs. (C.16) and (C.17), the vector field (C.15) appears to satisfy the constraint

$$A_\mu\, A_\nu\, g^{\mu\nu} = -\frac{1}{\alpha'} \ , \tag{C.18}$$

since $g^{\mu\nu} = a^{-2}(\eta)\, \eta^{\mu\nu}$ for the FLRW metric in conformal time frame. Since the left-hand-side of (C.18) is coordinate-frame independent, the constraint (C.18) also characterises the FLRW time frame (3.25). Note that in conformal time η, the prime here meaning derivation with respect to η, the field strength (C.14) becomes

$$F_{0i} = -\frac{2}{\sqrt{\alpha'}}\, a'\, u_i \ . \tag{C.19}$$

Thus, the cosmological background appears to break (spontaneously) the stringy gauge symmetry, leading to a massive vector field. This has been taken into account

in this work (as in Ref. [61]), whenever the global (cosmological) background (C.15) is used, like, for instance, in the Section 3.4 where we shall consider its role in an inflationary era of this string/fluctuating-D-particle universe.

Under such conditions, the vertex operators (C.9) correspond to vector field excitations $\widetilde{A}_i$ with a target-spacetime field strength (after the impact, that is, for $t > t_c$) of the form

$$\widetilde{F}_{0i} = E_i = M_s^2 \, g_{ij} u^j \ , \tag{C.20}$$

where E_i denotes the "electric" field, while the vertex operators (C.12) imply a target-space field strength with spatial components

$$\widetilde{F}^{ij} = -\epsilon^{ijk} \, B_k = M_s^2 \epsilon^{ijk} g_{k\ell} \, u^\ell \ \Rightarrow \ B_k = M_s^2 \, g_{k\ell} \, u^\ell \ , \tag{C.21}$$

where B_i denotes the "magnetic" field. This leads to the form of the field strength in the cosmological picture of the late eras, as considered in the graviton propagation of Section 3.5.

Numerical estimations

The reader is invited at this stage to notice the presence of the (inverse cube of the) scale factor in Eq. (3.34), which plays a rôle in the cosmological evolution between eras (see Section 3.4.4) and arises from the fact that the statistical fluctuations are proportional to the cosmic density of defects at a global scale [61], with $a(t)^3$ denoting the proper volume in a FLRW universe. In a semi-microscopic treatment, this scaling of σ_0 can be justified by noting that essentially

$$\langle\langle u_i u_j g^{ij} \rangle\rangle(t) \sim V_{\mathcal{D}}^{-1} \int_{\mathcal{D}} \mathcal{P} \, \overline{u}_i \overline{u}_j \, g^{ij} \ , \tag{C.22}$$

where $g_{ij}(\vec{x}, t)$ is the metric (3.28), $\mathcal{D}$ is a *spatial* domain (with (proper) three-volume $V_{\mathcal{D}}$) upon which the (statistical) average over D-particle populations is considered at any given moment in cosmic time t, and $\mathcal{P} = \frac{N_D}{N_\gamma}$ is a probability of recoil of a D-particle under its interaction with low-energy cosmic photons, assumed to be the main contribution for the generation of the recoil field, with N_D, N_γ the corresponding number densities of D-particles and photons respectively. The quantity $\overline{u}_i$ is the spatial recoil velocity arising from a single scattering event of a photon with a

D-particle. It is proportional to Δp_i the momentum transfer during the scattering

$$\overline{u}_i = \frac{\Delta p_i}{M_{\rm s}}\, g_{\rm s0} = \frac{\widetilde{\xi}_0\, p_i}{M_{\rm s}}\, g_{\rm s0} = \frac{\widetilde{\xi}_0\, p_i^{\rm phys}}{a(t)\, M_{\rm s}}\, g_{\rm s0} \tag{C.23}$$

with $\widetilde{\xi}_0 < 1$ is a spacetime local constant "fudge" factor (hence independent of the universe's expansion), characteristic of the microscopic theory, and $\mathbf{p}_{\rm phys}$ denotes the "physical" momentum observed by a cosmological observer who is comoving with the Hubble flow for an expanding universe with scale factor $a(t)$. The quantity $M_{\rm s}/g_{\rm s0}$ is the mass of a D-particle, with $M_{\rm s} = 1/\sqrt{\alpha'}$ the string scale and $g_{\rm s0} \lesssim 1$ the string coupling, assumed weak so that string loop perturbation theory (and thus world-sheet formalism of recoil) is valid. From Eqs. (3.28), (C.22) and (C.23), and taking into account the scaling with the scale factor $a(t)$ of the densities of the (non interacting among themselves) D-particles, $N_{\rm D} = N_{\rm D}^{(0)} a^{-3}(t)$, and the photons (radiation) $N_\gamma = N_\gamma^{(0)}\, a^{-4}(t)$, with the superscript (0) denoting present-day quantities, we obtain

$$\langle\!\langle u_i u_j g^{ij} \rangle\!\rangle(t) \sim \frac{1}{a^3(t)}\, \frac{N_{\rm D}^{(0)}}{N_\gamma^{(0)}}\, \frac{\widetilde{\xi}_0^2\, |\mathbf{p}_{\rm phys}|^2}{M_{\rm s}^2}\, g_{\rm s0}^2 \ , \tag{C.24}$$

with $|\mathbf{p}_{\rm phys}|^2$ the square of the amplitude of the physical spatial momenta, computed with the time-independent part of the spatial metric (3.28) with $a^2(t)$ factored out. Comparing (C.24) with (3.34) we obtain an estimate for $|\beta|$ at late (galactic) epochs of the universe

$$|\beta| \sim \frac{1}{3}\, \frac{N_{\rm D}^{(0)}}{N_\gamma^{(0)}}\, \frac{\widetilde{\xi}_0^2\, |\mathbf{p}_{\rm phys}|^2}{M_{\rm s}^2}\, g_{\rm s0}^2 \ . \tag{C.25}$$

We remind the reader that Eq. (C.25) relies on the assumption that the dominant contributions to the recoil velocity field and its statistical fluctuations come from scatterings of D-particles with the abundant background of cosmic photons, taken for concreteness to be mostly CMB for the galactic era. In this case $|\mathbf{p}_{\rm phys}|$ denotes an average energy $\bar{E}$ of such photons as observed in the present day, i.e. $\bar{E}({\rm eV}) = 1.24/\lambda(\mu{\rm m})$, with $\lambda(\mu{\rm m})$ a typical wavelength of the CMB photon, $\lambda \sim 1.9\,{\rm mm}$. This yields

$$\bar{E}^{\rm CMB} = \sqrt{|\mathbf{p}_{\rm phys}^{\rm CMB}|^2} \sim 7 \times 10^{-4}\ {\rm eV} \ . \tag{C.26}$$

We now remark that the $a(t)^{-3}$ dependence of σ_0 in (3.34) is over and above any inhomogeneities that may characterise local populations of D-particles in the neighbourhood of galaxies we shall concentrate upon in our lensing analysis. The latter may be incorporated in a mild dependence of σ_0 from galaxy to galaxy, which, as we

show in Section 3.3, may arise from uncertainties in cosmological measurements. It is also understood that the statistical averages above, leading to Eqs. (3.34), (C.25) and (C.26) are only applied at the end of the pertinent computations.

At this point, we should make the following remark. The quantum fluctuations about such averaged quantities over populations of D-particles can be described in terms of the low-energy string effective action Eq. (3.1). The nonlinear Born-Infeld dynamics encoded in this action might then be responsible [62] for the formation of *quantum condensates* of the recoil velocity field that characterise the early universe epoch, which are distinct from the statistical averages (3.34) that correspond to the classical part of a condensate $\langle\langle F_{\mu\nu} F^{\mu\nu} \rangle\rangle$ of the D-particle recoil velocity field. In our considerations in this work, the inflationary epoch of Section 3.4 is characterised by very dense populations of D-particles, and as such one may consider the classical, statistical effects as dominant, while the quantum fluctuations are explicitly expressed and necessary in our graviton propagation analysis of Section 3.5.

Appendix D

Inflation for small condensates of the D-material universe

Although small condensate inflation induced by the D-particle population alone, with a zero dilaton, is not a viable scenario, as we have seen above, nevertheless one may [59] obtain Starobinsky-type inflation induced by the dilaton in a slow-rolling regime where the dilaton assumed large negative values. In this case, a crucial rôle is played by the D-particle small condensates in assisting this inflation in the sense of providing the means for a potential minimum towards which the dilaton field (which plays here the rôle of an inflaton) rolls slowly. The details have been presented in Ref. [59] and will not be repeated here, however, for completeness, we shall outline below the main features.

In the case of a non trivial dilaton ϕ, a convenient starting point is the σ-model-frame effective action (3.1), expanded (for small condensate fields) up to quadratic order in F^2 recoil field strength

$$S_{\rm eff\ 4dim} \simeq \int {\rm d}^4x\,\sqrt{-g}\left[-\frac{T_3\,e^{-\phi}}{g_{\rm s0}} - \frac{\tilde{\Lambda}\,e^{-2\phi}}{\kappa_0^2} - \mathcal{D} - \mathcal{A}_s + \left(\frac{\alpha\,T_3\,e^{-\phi}}{g_{\rm s0}} + \frac{e^{-2\phi}}{\kappa_0^2}\right)R(g) \right.$$
$$\left. - \frac{(2\pi\alpha')^2\,T_3\,e^{-\phi}}{g_{\rm s0}}\frac{F^2}{4}\left(1-\alpha R(g)\right) + \mathcal{O}\left((\partial\phi)^2\right)\right]\,, \qquad \text{(D.1)}$$

where $\mathcal{D}$ are dilaton independent flux condensates in the brane, defined previously (cf. (3.93)), and

$$\mathcal{A}_{\rm s} \equiv \frac{M_{\rm s}}{g_{\rm s0}}\,e^{-\phi}\,N_{\rm D}^{\rm str}\,, \qquad \text{(D.2)}$$

with $N_{\rm D}^{\rm str}$ the (dimensionfull) proper space density of D-particles in the string frame, is a contribution to the brane vacuum energy due to the (rest) mass of the D-particles

(cf. Eq. (3.6)).

Upon considering vacuum condensates in a Hartree-Fock approximation, i.e. replacing $F_{\mu\nu}F^{\mu\nu}$ by the condensate field in the presence of a dilaton $\langle\langle F_{\mu\nu}F^{\mu\nu}\rangle\rangle \sim \mathcal{C}_{\rm M4}(t)$, such that one can define the dimensionless condensate field $\sigma(t,x)$

$$\sigma(t,x) \equiv \frac{1}{4}\,\alpha\kappa^2_{\rm eff}\left(e^{-2\phi}\mathcal{J}\right)\mathcal{C}_{\rm M4}(t)\ , \tag{D.3}$$

where one recalls the definition of $\mathcal{J}$ as in Eq. (3.15), the effective ation (D.1) becomes [59]

$$S_{\rm eff\ 4dim} \simeq \int {\rm d}^4x\,\sqrt{-g}\,\frac{e^{-2\phi}}{2\kappa^2_{\rm eff}}\Big[\,(1+2\sigma(x^\mu))\,R - \frac{2}{\alpha}\,\sigma(x^\mu) \\ - 2\kappa^2_{\rm eff}\left(2\bar{\mathcal{B}} + e^{2\phi}\mathcal{D}\right)\Big] + \ldots \tag{D.4}$$

where $\alpha = {}^{\pi^2}\!/_6\,\alpha'$ as before, the $\ldots$ denote dilaton derivatives, which are subleading terms in the slow-roll inflationary phase we are interested in here, and where we have defined $\frac{1}{2\kappa^2_{\rm eff}} \equiv \left(\frac{\alpha\,T_3 e^\phi}{g_{\rm s0}} + \frac{1}{\kappa_0^2}\right) \simeq \frac{1}{2}\,M^2_{\rm Pl}$ along with

$$2\bar{\mathcal{B}} \equiv \frac{T_3\,e^\phi}{g_{\rm s0}} - \frac{|\tilde{\Lambda}|}{\kappa_0^2} + e^{2\phi}\mathcal{A}_{\rm s}\ , \tag{D.5}$$

which is an effective vacuum energy and is almost a cosmological constant for slowly rolling $\phi(t) \simeq \phi_0$ large and negative. The reader should recall at this stage that the dilaton equation imposes the condition (3.23), which allows us to express the parameter $|\tilde{\Lambda}|$ in terms of the brane tension $T_3 > 0$.

We next pass into the Einstein frame, denoted by a supersctipt E, by redefining the metric [59]

$$g_{\mu\nu} \to g^{\rm E}_{\mu\nu} = (1+2\sigma(t,x))\ e^{-2\phi_0}\,g_{\mu\nu}\ , \tag{D.6}$$

in which case the field $\sigma(t,x)$ becomes a dynamical scalar degree of freedom. We define a canonically-normalised scalar field $\varphi(t,x)$

$$\varphi(t,x) \equiv \sqrt{\frac{3}{2}}\ln\left(1+2\sigma(t,x)\right)\ , \tag{D.7}$$

so that the action (D.4) becomes

$$S^{\rm E}_{\rm eff\ 4dim} = \frac{1}{2\kappa^2_{\rm eff}} \int {\rm d}^4x\sqrt{-g^{\rm E}}\left[R^{\rm E} + g^{{\rm E}\,\mu\nu}\partial_\mu\varphi\,\partial_\nu\varphi - V\left(\varphi\right)\right] + \mathcal{O}\Big(g^{{\rm E}\,\mu\nu}\partial_\mu\varphi\,\partial_\nu\phi_0,\, g^{{\rm E}\,\mu\nu}\partial_\mu\phi_0\,\partial_\nu\phi_0\Big)\ , \tag{D.8}$$

with the effective potential $V(\varphi)$ in the inflationary regime of *large negative values* of ϕ_0 given approximately by [59]

$$V(\varphi) \simeq \left[\frac{1}{\alpha}\left(e^{\sqrt{\frac{2}{3}}\varphi} - 1\right) + 4\kappa^2_{\rm eff}\bar{\mathcal{B}}^{\rm E}\right] e^{2\phi_0}\, e^{-\sqrt{\frac{8}{3}}\varphi} + 2\kappa^2_{\rm eff}\,\mathcal{D}\ , \tag{D.9a}$$

$$\text{where}\quad 2\bar{\mathcal{B}}^{\rm E} \simeq -\frac{T_3\, e^{\phi_0}}{2\, g_{\rm s0}} + e^{2\phi_0}\,\mathcal{A}^{\rm E}\ , \tag{D.9b}$$

with $\mathcal{A}^{\rm E}$ the Einstein frame (D.6) (dilaton-independent) vacuum energy corresponding to the σ-model-frame quantity $\mathcal{A}_s$ (D.2) (cf. Eq. (3.8))

$$\mathcal{A}^{\rm E} \sim \frac{M_{\rm s}}{g_{\rm s0}}\, e^{-\phi_0}\, N_{\rm D}\, M^3_{\rm Pl} \tag{D.10}$$

where $N_{\rm D}$ is the number density of D-particles per (reduced) Planck three-volume on the brane world (assumed more or less constant during inflation [59]).

It is important to note that, in order to arrive at Eq. (D.9a), we took into account the conformal nature of the flux condensate term in the four-dimensional spacetime action $\int d^4x\sqrt{g}\,\mathcal{D}$ (under rescalings of the form (D.6)), and have ignored terms that are more than quadratic in the vector potential. Moreover, as already emphasised, for our purposes here we concentrate on the slow-roll phase of the dilaton field ϕ_0, so any potential-like terms with dilaton time-derivative factors are ignored. In this approximation, we do not need to worry about the cross-kinetic terms $\partial_\mu\phi_0\partial^\mu\varphi$, which can, in any case, be eliminated by a further redefinition (mixing) of the fields φ and ϕ_0 [59].

From the discussion in Ref. [59], an extra factor $\sqrt{2}$ needs to be absorbed into the dilaton normalisation in order to obtain a canonical kinetic term for this field, yielding finally

$$\frac{1}{2\kappa^2_{\rm eff}}\, V(\varphi) = \frac{1}{\alpha\, 2\kappa^2_{\rm eff}}\left(e^{\sqrt{\frac{2}{3}}\varphi} - 1\right) e^{-\sqrt{\frac{8}{3}}\varphi}\, e^{\sqrt{2}\phi_0} - \frac{T_3}{2g_{\rm s0}}\, e^{-\sqrt{\frac{8}{3}}\varphi}\, e^{\frac{3}{\sqrt{2}}\phi_0} + \mathcal{A}^{\rm E}\, e^{-\sqrt{\frac{8}{3}}\varphi}\, e^{2\sqrt{2}\phi_0} + \mathcal{D}\ . \tag{D.11}$$

For weak condensates $\varphi \ll 1$, where the approximations in this work hold, and large negative values of the dilaton ϕ_0, the reader will recognise in (D.11) the Starobinsky-like form of the effective potential for the dilaton-driven inflation provided $\mathcal{A}+\mathcal{D} > 0$. This can fit the Planck data [6] due to the very small value of the tensor-to-scalar ratio r predicted by this class of theories.

By minimising the effective potential (D.11) with respect to the condensate field, for fixed large negative values of the dilaton ϕ_0, we observe that the minimum occurs for $\varphi \simeq 0$ (as required for consistency) provided that

$$\mathcal{A}^{\rm E} \simeq \frac{T_3}{2g_{\rm s0}}\left[\frac{3g_{\rm s0}}{\pi^2}\frac{M_{\rm s}^2\,M_{\rm Pl}^2}{T_3}\,e^{-\frac{1}{\sqrt{2}}\phi_0}+1\right]e^{-\frac{1}{\sqrt{2}}\phi_0}\ . \tag{D.12}$$

Taking into account (D.10) with the rescaled dilaton $\phi_0 \to {}^{\phi_0}/_{\sqrt{2}}$, we have from (D.12)

$$\bar{N}_{\rm D} \sim \frac{T_3}{2\,M_{\rm s}\,M_{\rm Pl}^3}\left[\frac{3g_{\rm s0}}{\pi^2}\frac{M_{\rm s}^2\,M_{\rm Pl}^2}{T_3}\,e^{-\frac{1}{\sqrt{2}}\phi_0}+1\right] \tag{D.13}$$

for the (dimensionless) number of D-particles on the brane world during the dilaton-driven inflation area.

If we adopt the standard relation (used in Ref. [61]) $(2\pi\alpha')^2\,T_3 = 1$, that is $4\pi^2\,T_3 = M_{\rm s}^4$, which is consistent with weak condensate fields φ, as we have seen previously, then one obtains

$$\bar{N}_{\rm D} \sim \frac{1}{8\pi^2}\left(\frac{M_{\rm s}}{M_{\rm Pl}}\right)^3\left[12\,g_{\rm s0}\left(\frac{M_{\rm Pl}}{M_{\rm s}}\right)^2 e^{-\frac{1}{\sqrt{2}}\phi_0}+1\right]\ . \tag{D.14}$$

Now for $M_{\rm s} \sim 10^{16}$ GeV $\gg H_I \sim 10^{13}$ GeV, $g_{\rm s0} \sim 0.8$ and nominal values of the dilaton field in the range $|\phi_0| \in [1,\,10]$ (with $\phi_0 < 0$), we obtain $\bar{N}_{\rm D} \in [10^{-4},\,10^{-1}]$. Higher densities can be obtained for larger brane tensions T_3. Thus, we observe that, even for the weak recoil velocity condensate fields case, during slowly-rolling dilaton-driven inflation, the density of D-particle defects must be much higher than then corresponding one in the galactic era. This is a rather generic feature of the D-material universe.

Bibliography

[1] G. Lemaître. *Un univers homogène de masse constant et de rayon croissant rendant compte de la vitesse radiale des nébuleuses extra-galactiques.* Annales de la Société Scientifique de Bruxelles, **47** (1927) 49 (See pp. 2, 6)

[2] E. Hubble. *A relation between distance and radial velocity among extra-galactic nebulae.* Proceedings of the National Academy of Sciences of the United States of America, **15** 3 (1929) 168 (See pp. 2, 6)

[3] Planck Collaboration (P. A. R. Ade *et al.*) *Planck 2013 results. I. Overview.* Astronomy and Astrophysics (2013) (See pp. 2, 8)

[4] LIGO Scientific Collaboration and Virgo Collaboration (B. P. Abbott *et al.*) *Observation of Gravitational Waves from a Binary Black Hole Merger.* Physical Review Letters, **116** 6 (2016) 061102;
——. *GW151226: Observation of Gravitational Waves from a 22-Solar-Mass Binary Black Hole Coalescence.* Physical Review Letters, **116** 24 (2016) 241103;
(See pp. 3, 27, 99, 107, 108, 151, 155, 162, 163, 170, 172, 177, 179)

[5] WMAP Collaboration (G. Hinshaw *et al.*) *Nine-year Wilkinson Microwave Anisotropy Probe (WMAP) observations: cosmological parameter results.* The Astrophysical Journal Supplement Series, **208** 2 (2013) 19 (See pp. 6, 7, 11, 21, 138, 139, 144)

[6] Planck Collaboration (P. A. R. Ade *et al.*) *Planck 2015 results. XIII. Cosmological parameters.* Astronomy and Astrophysics (2015) (See pp. 6–9, 11, 21, 103, 107, 111, 116, 132, 133, 140, 147, 150, 159, 160, 162, 166, 168, 176, 192, 201)

[7] Planck Collaboration (P. A. R. Ade *et al.*) *Planck 2013 results. XVI. Cosmological parameters.* Astronomy and Astrophysics (2013) (See p. 9)

[8] V. F. Mukhanov. *Physical Fundations of Cosmology.* Cambridge University Press, 2005 (See p. 12)

[9] A. R. Liddle and D. H. Lyth. *COBE, gravitational waves, inflation and extended inflation.* Physics Letters B, **291** 4 (1992) 391;
——. *The cold dark matter density perturbation.* Physics Reports, **231** 1-2 (1993) 1;
(See p. 19)

[10] Planck Collaboration (P. A. R. Ade *et al.*) *Planck 2015 results. XX. Constraints on inflation.* Astronomy and Astrophysics (2015) (See pp. 21, 103, 132, 138, 139, 144)

[11] WMAP Collaboration (E. Komatsu *et al.*) *Seven-year Wilkinson Microwave Anisotropy Probe (WMAP) observations: cosmological interpretation.* The Astrophysical Journal Supplement Series, **192** 2 (2011) 18 (See p. 21)

[12] A. H. Guth. *Inflationary universe: A possible solution to the horizon and flatness problems.* Physical Review D, **23** 2 (1981) 347 (See p. 22)

[13] J. F. Donoghue. *Introduction to the Effective Field Theory Description of Gravity* (1995) 217 (See pp. 22, 104)

[14] A. de Felice and S. Tsujikawa. *f(R) theories.* Living Reviews in Relativity, **13** 03 (2010) (See p. 23)

[15] A. A. Starobinsky. *A new type of isotropic cosmological models without singularity.* Physics Letters B, **91** 01 (1980) 99 (See p. 23)

[16] A. Kehagias, A. M. Dizgah, and A. Riotto. *Comments on the Starobinsky Model of Inflation and its Descendants.* Physical Review D, **89** 4 (2014) 043527 (See p. 23)

[17] N. Makino and M. Sasaki. *The Density Perturbation in the Chaotic Inflation with Non-Minimal Coupling.* Progress of Theoretical Physics, **86** 1 (1991) 103 (See p. 24)

[18] D. I. Kaiser. *Primordial Spectral Indices from Generalized Einstein Theories.* Physical Review D, **52** 8 (1995) 4295 (See p. 24)

[19] A. Linde. *Hybrid inflation.* Physical Review D, **49** 2 (1994) 748 (See p. 25)

[20] R. A. Hulse and J. H. Taylor. *Discovery of a pulsar in a binary system.* The Astrophysical Journal, **195** (1974) 51;
J. M. Weisberg and J. H. Taylor. *Relativistic Binary Pulsar B1913+16: Thirty Years of Observations and Analysis.* Binary Radio Pulsars, ASP Conference Series, **328** (2005) 25;

J. M. Weisberg, D. J. Nice, and J. H. Taylor. *Timing measurements of the relativistic binary pulsar PSR 1913+16.* The Astrophysical Journal, **722** (2010) 1030;
(See p. 27)

[21] S. Weinberg. *Gravitation and Cosmology: Principles and Applications of the General Theory of Relativity.* John Wiley & Sons, Inc., 1972 (See p. 27)

[22] D. McMahon. *String Theory Demystified.* McGraw-Hill, 2009 (See pp. 45, 104)

[23] D. Baumann and L. McAllister. *Inflation and String Theory.* Cambridge Monographs on Mathematical Physics, Cambridge University Press, 2015 (See pp. 48, 104)

[24] G. Dvali and S.-H. H. Tye. *Brane inflation.* Physics Letters B, **450** (1999) 72 (See pp. 48–50)

[25] S. Kachru, R. Kallosh, A. Linde, J. Maldacena, L. McAllister, and S. P. Trivedi. *Towards Inflation in String Theory.* Journal of Cosmology and Astroparticle Physics, **03** 10 (2003) 013 (See pp. 50, 53)

[26] Sakellariadou M. *Cosmic Strings and Cosmic Superstrings.* Nuclear Physics Proceedings Supplements, **192-193** 10 (2009) 68 (See pp. 51, 54, 57, 62–64)

[27] Jeannerot R., Rocher J., and Sakellariadou M. *How generic is cosmic string formation in supersymmetric grand unified theories.* Physical Review D, **68** 10 (2003) 103514 (See pp. 51, 53)

[28] T. W. B. Kibble. *Topology of cosmic domains and strings.* Journal of Physics A, **9** 8 (1976) 1387 (See pp. 51, 53, 177)

[29] J. Polchinski. *Introduction to Cosmic F- and D-Strings.* **208** (2006) 229 (See pp. 53, 54)

[30] E. J. Copeland, R. C. Myers, and J. Polchinski. *Cosmic F- and D-strings.* Journal of High Energy Physics, **04** 06 (2004) 013 (See pp. 53, 57, 62, 66)

[31] A.-C. Davis, W. Nelson, S. Rajamanoharan, and M. Sakellariadou. *Cusps on cosmic superstrings with junctions.* Journal of Cosmology and Astroparticle Physics, **08** 11 (2008) 022 (See pp. 53, 64, 66)

[32] S. Sarangi and S.-H. H. Tye. *Cosmic string production towards the end of brane inflation.* Physics Letters B, **536** 3-4 (2002) 185 (See p. 53)

[33] E. J. Copeland, L. Pogosian, and T. Vachaspati. *Seeking string theory in the cosmos.* Classical and Quantum Gravity, **28** 20 (2011) 204009 (See p. 54)

[34] T. Vachaspati and A. Vilenkin. *Gravitational radiation from cosmic strings.* Physical Review D, **31** 12 (1985) 3052 (See p. 54)

[35] M. Sakellariadou. *Gravitational waves emitted from infinite strings.* Physical Review D, **42** 02 (1990) 354;
——. *Erratum: Gravitational waves emitted from infinite strings.* Physical Review D, **43** 12 (1991) 4150;
(See p. 54)

[36] T. Damour and A. Vilenkin. *Gravitational wave bursts from cusps and kinks on cosmic strings.* Physical Review D, **64** 06 (2001) 064008 (See pp. 54, 59–61, 64, 68, 177)

[37] T. Damour and A. Vilenkin. *Gravitational Wave Bursts from Cosmic Strings.* Physical Review Letters, **85** 18 (2001) 3761 (See p. 54)

[38] R. Brandenberger, H. Firouzjahi, J. Karouby, and S. Khosravi. *Gravitational radiation by cosmic strings in a junction.* Journal of Cosmology and Astroparticle Physics, **09** 01 (2009) 008 (See p. 54)

[39] LIGO Scientific Collaboration (B. P. Abbott *et al.*) *First LIGO search for gravitational wave bursts from cosmic (super)strings.* Physical Review D, **80** 06 (2009) 062002 (See p. 54)

[40] S. Ölmez, V. Mandic, and X. Siemens. *Gravitational-wave stochastic background from kinks and cusps on cosmic strings.* Physical Review D, **81** 10 (2010) 104028 (See p. 54)

[41] A. Vilenkin and E. P. S. Shellard. *Cosmic Strings and Other Topological Defects.* Cambridge University Press, 1994 (See pp. 54, 57, 58, 76)

[42] T. W. B. Kibble and N. Turok. *Self-intersection of cosmic strings.* Physics Letters B, **116** 2-3 (1982) 141 (See p. 56)

[43] N. Turok. *Grand unified strings and galaxy formation.* Nuclear Physics B, **242** (1984) 520 (See pp. 57, 91)

[44] C. J. Burden. *Gravitational radiation from a particular class of cosmic strings.* Physics Letters B, **164** 4-6 (1985) 277 (See p. 60)

[45] D. Austin, E. J. Copeland, and T. W. B. Kibble. *Evolution of cosmic string configurations.* Physical Review D, **48** 12 (1993) 5594 (See pp. 63, 79, 83, 97, 178)

[46] C. Ringeval, M. Sakellariadou, and F. R. Bouchet. *Cosmological evolution of cosmic string loops.* Journal of Cosmology and Astroparticle Physics, **07** 02 (2007) 023 (See p. 63)

[47] L. Lorenz, C. Ringeval, and M. Sakellariadou. *Cosmic string loop distribution on all length scales and at any redshift.* Journal of Cosmology and Astroparticle Physics, **10** 10 (2010) 003 (See p. 63)

[48] M. Sakellariadou. *A note on the evolution of cosmic string/superstring networks.* Journal of Cosmology and Astroparticle Physics, **05** 04 (2005) 003 (See p. 64)

[49] A. Rajantie, M. Sakellariadou, and H. Stoica. *Numerical experiments with p F-strings and q D-strings: the formation of (p, q) bound states.* Journal of Cosmology and Astroparticle Physics, **07** 11 (2007) 021 (See p. 64)

[50] M. Sakellariadou and H. Stoica. *Dynamics of F/D networks: the role of bound states.* Journal of Cosmology and Astroparticle Physics, **08** 08 (2008) 038 (See p. 64)

[51] E. O'Callaghan, S. Chadburn, G. Geshnizjani, R. Gregory, and I. Zavala. *On detection of extra dimensions with gravitational waves from cosmic strings.* Physical Review Letters, **105** 08 (2010) 081602 (See pp. 64, 66)

[52] T. Elghozi, W. Nelson, and M. Sakellariadou. *Cusps and pseudocusps in strings with Y-junctions.* Physical Review D, **90** 12 (2014) 123517 (See p. 65)

[53] E. J. Copeland, T. W. B. Kibble, and D. A. Steer. *Constraints on string networks with junctions.* Physical Review D, **75** 06 (2007) 065024 (See p. 66)

[54] G. R. Vincent, M. Hindmarsh, and M. Sakellariadou. *Scaling and small scale structure in cosmic string networks.* Physical Review D, **56** 02 (1997) 637 (See p. 97)

[55] M. Milgrom. *A Modification of the Newtonian dynamics as a possible alternative to the hidden mass hypothesis.* The Astrophysical Journal, **270** (1983) 365;

——. *A Modification of the Newtonian dynamics: Implications for galaxies.*

The Astrophysical Journal, **270** (1983) 371;
(See p. 104)

[56] J. D. Bekenstein. *Relativistic gravitation theory for the MOND paradigm.* Physical Review D, **70** 08 (2004) 083509 (See p. 104)

[57] Planck Collaboration (P. A. R. Ade *et al.*) *Planck 2015 results. XIV. Dark energy and modified gravity.* Astronomy and Astrophysics (2015) (See p. 104)

[58] J. R. Ellis, N. E. Mavromatos, and M. Westmuckett. *A Supersymmetric D-brane model of space-time foam.* Physical Review D, **70** 04 (2004) 044036;
——. *Potentials between D-branes in a supersymmetric model of space-time foam.* Physical Review D, **71** 10 (2005) 106006;
(See pp. 105, 106, 110, 111, 151, 173)

[59] J. R. Ellis, N. E. Mavromatos, and D. V. Nanopoulos. *Starobinsky-Like Inflation in Dilaton-Brane Cosmology.* Physics Letters B, **732** (2014) 380;
——. *D-Flation.* Journal of Cosmology and Astroparticle Physics, **14** 11 (2014) 014;
(See pp. 105, 108, 110, 112, 116, 132, 136, 137, 141, 198–200)

[60] N. E. Mavromatos and M. Sakellariadou. *Relativistic modified Newtonian dynamics from string theory?* Physics Letters B, **652** 2-3 (2007) 97 (See pp. 105, 151)

[61] N. E. Mavromatos, M. Sakellariadou, and M. F. Yusaf. *Stringy models of modified gravity: space-time defects and structure formation.* Journal of Cosmology and Astroparticle Physics, **13** 03 (2013) 015 (See pp. 106–110, 112, 114–117, 120, 121, 123–126, 129, 136, 140, 143, 148, 150, 153, 154, 156, 157, 159, 160, 179, 189, 191–193, 195, 201)

[62] E. Elizalde, J. E. Lidsey, S. Nojiri, and S. D. Odintsov. *Born-Infeld quantum condensate as dark energy in the universe.* Physics Letters B, **574** 1-2 (2003) 1 (See pp. 106, 114, 137, 142, 150, 154–156, 158, 169, 197)

[63] T. Elghozi, N. E. Mavromatos, M. Sakellariadou, and M. F. Yusaf. *The D-material universe.* Journal of Cosmology and Astroparticle Physics, **16** 02 (2016) 060 (See p. 107)

[64] T. Elghozi, N. E. Mavromatos, and M. Sakellariadou. *Graviton propagation within the context of the D-material universe.* http://arxiv.org/abs/1605.02680 Submitted for publication (See pp. 107, 108)

[65] J. R. Ellis, N. E. Mavromatos, and D. V. Nanopoulos. *Derivation of a Vacuum Refractive Index in a Stringy Space-Time Foam Model.* Physics Letters B, **665** 5 (2008) 412;
——. *D-Foam Phenomenology: Dark Energy, the Velocity of Light and a Possible D-Void.* International Journal of Modern Physics A, **26** 13 (2011) 2243;
T. Li, N. E. Mavromatos, D. V. Nanopoulos, and D. Xie. *Time Delays of Strings in D-particle Backgrounds and Vacuum Refractive Indices.* Physics Letters B, **679** 4 (2009) 407;
(See pp. 108, 112, 151, 167, 171)

[66] J. F. Navarro, C. S. Frenk, and S. D. M. White. *The Structure of Cold Dark Matter Halos.* The Astrophysical Journal, **462** (1996) 563 (See p. 126)

[67] E. E. Salpeter. *The Luminosity Function and Stellar Evolution.* The Astrophysical Journal, **121** (1955) 161 (See p. 129)

[68] G. Chabrier. *Galactic Stellar and Substellar Initial Mass Function.* Publications of the Astronomical Society of the Pacific, **115** 809 (2003) 763 (See p. 129)

[69] D. Leier, I. Ferreras, P. Saha, and E. E. Falco. *Resolving the Baryon-fraction Profile in Lensing Galaxies.* The Astrophysical Journal, **740** 2 (2011) 97 (See pp. 129, 131)

[70] I. Ferreras, N. E. Mavromatos, M. Sakellariadou, and M. F. Yusaf. *Incompatibility of rotation curves with gravitational lensing for TeVeS theory.* Physical Review D, **80** 10 (2009) 103506;
——. *Confronting MOND and TeVeS with strong gravitational lensing over galactic scales: An extended survey.* Physical Review D, **86** 08 (2012) 083507;
(See pp. 129, 131)

[71] D. Rusin, C. S. Kochanek, E. E. Falco, C. R. Keeton, B. A. McLeod, C. D. Impey, J. Lehár, J. A. Muñoz, C. Y. Peng, and H.-W. Rix. *The Evolution of a Mass-Selected Sample of Early-Type Field Galaxies.* The Astrophysical Journal, **587** 1 (2003) 143 (See p. 130)

[72] G. W. Gibbons and S. W. Hawking. *Cosmological Event Horizons, Thermodynamics, and Particle Creation.* Physical Review D, **15** 10 (1977) 2738 (See pp. 134, 135)

[73] S. W. Hawking. *Particle Creation by Black Holes.* Communications in Mathematical Physics, **43** 3 (1975) 199 (See p. 135)

[74] C. M. Will. *Bounding the mass of the graviton using gravitational wave observations of inspiralling compact binaries.* Physical Review D, **57** 4 (1998) 2061 (See p. 161)

[75] P. C. Peters. *Index of refraction for scalar, electromagnetic, and gravitational waves in weak gravitational fields.* Physical Review D, **9** 8 (1974) 2207 (See pp. 164, 166)

[76] D. Baskaran, A. G. Polnarev, M. S. Pshirkov, and K. A. Postnov. *Limits on the speed of gravitational waves from pulsar timing.* Physical Review D, **78** 04 (2008) 044018 (See pp. 168, 170)

[77] G. D. Moore and A. E. Nelson. *Lower bound on the propagation speed of gravity from gravitational Cherenkov radiation.* Journal of High Energy Physics, **01** 09 (2001) 023 (See p. 171)

[78] MoEDAL Collaboration (B. Acharya *et al.*) *The physics programme of the MoEDAL experiment at the LHC.* International Journal of Modern Physics A, **29** 23 (2014) 1430050 (See p. 175)

[79] R. P. Feynman. *The Character of Physical Law.* The M.I.T. Press, 1985 (See p. 180)